



HAL
open science

Polymer-Metal Organic Frameworks (MOFs) Mixed Matrix Membranes For Gas Separation Applications

Salman Shahid

► **To cite this version:**

Salman Shahid. Polymer-Metal Organic Frameworks (MOFs) Mixed Matrix Membranes For Gas Separation Applications. Other. Université Montpellier; Universiteit Twente (Enschede, Nederland), 2015. English. NNT: 2015MONTTS141 . tel-01994803

HAL Id: tel-01994803

<https://theses.hal.science/tel-01994803>

Submitted on 25 Jan 2019

HAL is a multi-disciplinary open access archive for the deposit and dissemination of scientific research documents, whether they are published or not. The documents may come from teaching and research institutions in France or abroad, or from public or private research centers.

L'archive ouverte pluridisciplinaire **HAL**, est destinée au dépôt et à la diffusion de documents scientifiques de niveau recherche, publiés ou non, émanant des établissements d'enseignement et de recherche français ou étrangers, des laboratoires publics ou privés.

THÈSE

Pour obtenir le grade de
Docteur

Délivré par **l'Université de Montpellier**

Préparée au sein de l'école doctorale
Sciences Chimiques Balard

Et de l'unité de recherche
Institut Européen des Membranes

Spécialité : **Chimie et Physicochimie des
matériaux**

Présentée par **Salman SHAHID**

**Membranes à matrice mixte
Polymère- Réseaux métallo-
organiques (MOF) pour des
applications en séparation des gaz**

Soutenue le 05/02/2015 devant le jury composé de

| | |
|--|----------------------------------|
| M. Richard D. NOBLE, Prof., Université du Colorado | Rapporteur, Président du jury |
| Mme. Christine KIRSCHHOCK, Prof., Université KU Leuven | Rapporteur |
| M. Jeroen J.L.M. CORNELISSE, Prof., Université de Twente | Examineur |
| M. Arian NIJMEIJER, Prof., Université de Twente | Examineur |
| M. Damien QUEMENER, MCF, Université de Montpellier | Examineur |
| Mme. Dorothea C. NIJMEIJER, Prof., Université de Twente | Directeur de thèse |
| M. Ivo VANKELECOM, Prof., Université KU Leuven | Co-directeur |
| M. André DERATANI, Prof., Université de Montpellier | Co-directeur |



Polymer-Metal Organic Frameworks (MOFs) Mixed Matrix Membranes For Gas Separation Applications

by

Salman Shahid

Promoter: Prof. Dr. Ir. D.C. Nijmeijer¹

Prof. Ivo Vankelecom²

Co-Promoter: A/Prof. Damien Quemener³

¹*Membrane Science & Technology, University of Twente, The Netherlands.*

²*IEM (Institut Europeen des Membranes), Universite Montpellier 2, France.*

³*Centre of Surface Chemistry and Catalysis, KU Leuven, Belgium.*

Table of Contents

| | |
|---|------------|
| Chapter 1: Introduction | 1 |
| Chapter 2: High pressure gas separation performance of mixed-matrix polymer membranes containing mesoporous Fe(BTC) | 23 |
| Chapter 3: Performance and plasticization behavior of polymer-MOF membranes for gas separation at elevated pressures | 59 |
| Appendix 1. Supporting information chapter 3 | 91 |
| Chapter 4: Matrimid®/polysulfone blend mixed matrix membranes containing ZIF-8 nanoparticles for high pressure natural gas separation | 97 |
| Chapter 5: MOF-mixed matrix membranes: precise dispersion of MOF particles with better compatibility via a particle fusion approach for enhanced gas separation properties | 127 |
| Appendix 2. Supporting information chapter 5 | 157 |
| Chapter 6: Reflections and outlook | 169 |
| Summary | 183 |

Chapter 1

Introduction

1.1 Membranes for gas separation

Membrane based processes are useful in many industrial gas separations [1]. Gas separations currently comprise a membrane market of over four hundred million dollars per year, which constitutes 24 % of the total membrane market [1]. Membranes result in preferential separation of one or more components from a feed mixture based on size, shape and physiochemical properties of the components in the feed mixture. Inorganic, polymeric as well as composite membranes have been used and studied for gas separation over the last few decades [2, 3]. Inorganic membranes e.g. alumina, zeolite, carbon etc. generally have exceptional separation efficiency compared to polymer membranes as well as higher chemical and thermal stability, but their brittleness (poor mechanical properties), difficult processing and high cost make them less attractive [4, 5]. The majority of gas separation membranes used in the recent years in industry are polymeric membranes, because of their inherent advantages such as low cost, easy processing and reasonable gas separation properties [6]. Some of the principal applications of gas separations using membrane technology are natural gas treatment (removal of CO₂), hydrogen recovery, oxygen enrichment from air (medical devices) and nitrogen enrichment from air (used as protecting atmosphere for oxygen sensitive compounds) [7-9].

Natural gas is one of the cleanest and efficient burning fuels. The worldwide demand of natural gas is increasing constantly with the global increase in population. The global consumption of natural gas is expected to increase to 182 trillion cubic feet by 2030 [10]. Although methane is the main component of natural gas, it also contains considerable concentrations of various impurities including water, carbon dioxide, hydrogen sulphide and other hydrocarbons. The focus of natural gas treatment is typically on acid gas removal [11]. For fuel applications, natural gas sweetening is essential to (1) increase the calorific value, (2) reduce pipeline corrosion within the gas distribution network and (3) prevent atmospheric pollution [11-13].

Air separation to generate nitrogen-enriched streams from air is another main application of membrane gas separation and is predicted to cover 49 % of the gas separation membrane market by 2020 [14]. Nitrogen and oxygen are the third and fifth largest bulk chemicals produced worldwide [15]. Nitrogen-enriched streams (purity 98-

99%) are used as inert blanketing for fuel storage tanks and pipelines to minimize fire hazards and to reduce oxidation during various heating operations. Oxygen-enriched air (30-40% O₂) is relatively a less explored application of membranes. Oxygen-enriched streams are most commonly used in power plants to increase the efficiency of combustion processes [15].

Hydrogen recovery was among the first large scale commercial applications of gas separation membranes [16]. The main sources of hydrogen gas are steam reforming of natural gas, petroleum hydrocarbon purge streams, or electrolysis of water. Major use of recovered hydrogen is in the petroleum and chemical industries. The largest application of H₂ is for the processing ("upgrading") of fossil fuels, and in the production of ammonia and methanol, hydrogenation of oils and fats and also as coolant in power station generators [2, 4].

1.2 Gas transport theory

The utility of membranes in gas separation processes depends on the permeability through the membrane and the selectivity towards the different components in the mixtures [8, 9]. The permeability for component A, P_A, is the intrinsic ability of a membrane material to control the rate at which gas molecules are allowed to permeate through the membrane. It equals the penetrant diffusive flux (J_A) through the membrane normalized by the change in partial pressure across the membrane, Δp_A (cmHg), multiplied by the thickness of the membrane, l (cm):

$$P_A = \frac{J_A \cdot l}{\Delta p_A} \quad \text{Eq. 1.1}$$

Permeability is given in units of Barrer, defined as:

$$1 \text{ Barrer} = 1 \cdot 10^{-10} \frac{\text{cm}^3(\text{STP}) \cdot \text{cm}}{\text{cm}^2 \cdot \text{s} \cdot \text{cmHg}} \quad \text{Eq. 1.2}$$

Generally gas molecules are transported through a polymeric membrane by the solution-diffusion mechanism [17]. Through Fick's first law, eq. 1.1 can be rearranged so that permeability is expressed as a product of the solubility coefficient, S (cm³(STP)/cm³·cmHg) and the diffusivity coefficient, D (cm²/s) of penetrant A [8]:

$$P_A = D_A \cdot S_A \quad \text{Eq. 1.3}$$

The solubility coefficient through a membrane can be expressed as [18]:

$$S_A = \frac{C_A}{p_A} \quad \text{Eq. 1.4}$$

where S_A is the solubility coefficient of component 'A' in the membrane, C_A is the upstream concentration of component 'A' sorbed into the membrane, and p_A is the corresponding partial pressure [8]. For glassy polymers, the sorption of molecules is usually described by the dual mode sorption model, which consist of two types of sorption sites e.g. a Henry's site (solution) and a Langmuir site (hole filling) [19].

Diffusion of a penetrant through a polymeric membrane can be described by a series of diffusional jumps through temporary cavities created by the constantly vibrating polymer chains. Thus, the diffusion coefficient of component 'A', D_A , is a function of the frequency of the diffusive "jumps" made by gas molecules in the polymer matrix ' f_A ', and the jump length λ_A . The diffusion coefficient for a given gas penetrant 'A' can be given as [20]:

$$D_A = \frac{f_A \cdot \lambda_A^2}{6} \quad \text{Eq. 1.5}$$

The selectivity of a membrane for a gas pair A and B is the ratio of the permeability of component 'A' over the permeability of component 'B'.

$$\alpha_{A/B} = \frac{P_A}{P_B} \quad \text{Eq. 1.6}$$

The above equation is used when the individual permeabilities of the two pure components in a gas pair are known, which are typically estimated from pure gas experiments. Above equation can be extended when combined with Eq.3.

$$\alpha_{A/B} = \frac{P_A}{P_B} = \frac{D_A}{D_B} \cdot \frac{S_A}{S_B} \quad \text{Eq. 1.7}$$

where S_A/S_B is the solubility selectivity and D_A/D_B is the diffusion selectivity. For a mixed gas feed, the composition of the feed needs to be take into account and the separation factor can be calculated as,

$$\alpha_{A/B} = \frac{y_A / y_B}{x_A / x_B} \quad \text{Eq. 1.8}$$

where y_A and y_B are the mole fractions of the components (A and B) produced in the permeate, while x_A and x_B are their corresponding mole fractions in the feed [21].

In the solution-diffusion model, the gas molecules absorb on the feed side of the membrane and then diffuse through the membrane through the free volume between the polymer chains, driven towards the downstream side by, for example a concentration or pressure gradient and desorb at the permeate side. The thermodynamic parameter solubility is dependent on the condensability of the penetrant gas, which is directly influenced by the critical temperature of the gas (defined as the temperature at or above which the gas molecules cannot be liquefied whatever the pressure). Generally, gas molecules with a higher critical temperature (T_c) possess a higher polymer solubility than the ones with a lower T_c [1]. Solubility is also influenced by the size and chemical affinity of the penetrant with the polymer. As the size of the penetrant increases, the solubility usually increases. Similarly, polar gases have higher solubility in polymers [22].

In contrast, the diffusivity of a gas in a polymer is a kinetic parameter and depends on the penetrant size and shape [18]. Smaller molecules diffuse faster through a polymeric membrane. The shape of the molecule is also important as linear molecules can diffuse faster than spherical molecules because of their ability to diffuse along their smallest dimension [18]. However, both high solubility and diffusion are important to have higher permeabilities.

Table 1.1. General properties of gases CO₂, N₂ and CH₄ [23].

| Gas | Molecular mass (g/mol) | Critical temperature (K) | Kinetic diameter (nm) |
|-----------------|------------------------|--------------------------|-----------------------|
| CO ₂ | 44 | 304 | 0.33 |
| N ₂ | 28 | 126 | 0.36 |
| CH ₄ | 16 | 190 | 0.38 |

As shown in Table 1.1, CO₂ has a smaller kinetic diameter and much higher critical temperature compared to N₂ and CH₄. The smaller kinetic diameter and high critical

temperature (higher condensability) of CO₂ aids in higher diffusion and solubility coefficients and hence the higher permeability compared to N₂ and CH₄.

1.3 Limitations of polymeric membranes

Many different polymers have been investigated as gas separation materials such as polycarbonate (PC) [24], cellulose acetate (CA) [25], polysulfone (PSF) [26] and polyimides (PI) [27] etc. CA, PSF and PI have been widely used for industrial scale applications [17]. Several companies are currently producing gas separation membranes on commercial scale (e.g. Membrane Technology Research, Air Products, UOP, Air Liquide, Paxair and GKSS Licensees etc.) [28]. Despite their advantages (low cost, good mechanical stability and easy processing) [4], polymeric membranes often limited by either low permeability or low selectivity. In polymeric membrane systems, a trade-off relationship exists between the permeability and selectivity of the membrane. This trade-off relationship was best presented graphically by Robeson in 1991, summarizing all pure gas separation data from literature for a specific gas pair at 1 bar pressure and 35 °C. This so-called Robeson plot is considered as a benchmark in gas separation membrane development [29] (Fig. 1.1). This trade-off established an upper bound when permeability and selectivity for most industrially relevant gas pairs are plotted on a log-log scale. The permeability and selectivity plot of 1991 was redrawn in 2008 [30] (Fig. 1.1). It shows that most of the glassy and rubbery membrane materials are below the previous and currently available trade-off lines. Nevertheless, over the last decades notable improvements in CO₂/CH₄ selective membranes have taken place especially in mixed gas separation performance and at more extreme conditions such as higher temperatures or pressures. The polymers of intrinsic microporosity (PIM-1 and PIM-7) showed good CO₂/CH₄ separation capabilities [30]. A series of rigid (thermally rearranged) polymer variants has recently been published which exhibit even improved separation characteristics (above the trade-off line of 2008) but involve complicated synthesis [31]. It is recognized that polymeric membranes have the potential to replace the conventional gas separation processes e.g. pressure swing adsorption (PSA), cryogenic distillation and absorption [6]. In order for polymeric membranes to be economically viable in industry, these materials need to surpass the gas transport properties of the state of the art polymeric materials [30].

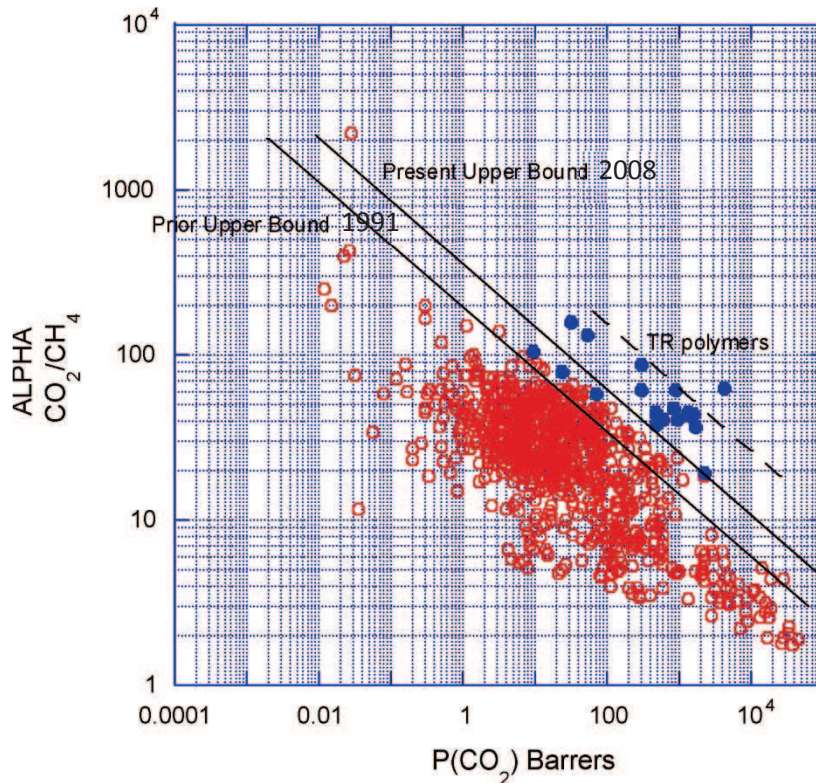


Fig. 1.1. Permeability and selectivity trade-off with the 1991 and 2008 Robeson upper bounds [30, 31].

Another issue, plasticization, is of particular concern for glassy polymer membranes for separation of gaseous mixtures (CO_2/CH_4 , CO_2/N_2 , propane/propene etc.). Plasticization has not been accounted for on the Robeson plot as it only shows the pure gas separation results at 1 bar pressure. Plasticization is defined as an increase in the segmental motion of polymer chains, due to the presence of one or more sorbates, such that the permeability of all components increases and the selectivity decreases [32]. The highly sorbing gas in the polymer matrix disrupts chain packing and enhances the segmental mobility of the polymer chains. Since the permeability of slower components (CH_4 , N_2) increases more than that of the faster component (CO_2), plasticization causes a decrease in membrane selectivity [32]. This loss in selectivity is mainly caused by the reduction in diffusivity selectivity due to excessive segmental motion. In other words, the membrane loses its ability to discriminate between the subtle size and shape differences. Fig. 1.2 is a schematic of CO_2 permeability versus pressure in a CO_2 gas separation.

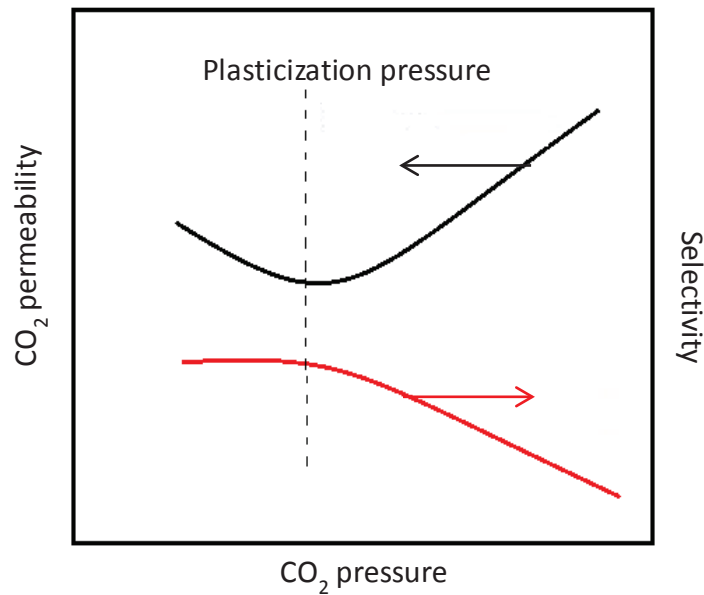


Fig. 1.2. Schematic of CO₂-induced plasticization behavior in polymer membranes.

As CO₂ pressure increases, the onset of plasticization occurs, the pressure at which the permeability versus CO₂ pressure curve shows a minimum is known as the plasticization pressure (dashed line). Below the plasticization pressure the permeability decreases due to saturation of the Langmuir sites. Above the plasticization pressure polymer chain mobility increases due to swelling by the dissolved CO₂, which results in upward inflection of CO₂ permeability with a corresponding loss of membrane selectivity. For a CO₂/CH₄ binary mixture for instance, increased feed pressures and CO₂ concentrations (10-45 mol%) lowered the CO₂/CH₄ selectivity for CA membranes by a factor of 1.5-1.2 between 10 and 50 bar [33]. In a similar study, the ideal selectivity of CO₂ over CH₄ was 3-5 times higher than the selectivity of the mixed gases for CA membranes at feed CO₂ concentrations higher than 50 % and pressure up to 54 bar [34]. This is attributed to swelling or/and plasticization effects of CO₂, since CO₂ is much more soluble in CA than CH₄. However, it was proven that CA membranes can still be used to remove both CO₂ and H₂S and reach the US pipeline specification for sour gases, if the feed gas contains less than 15 % CO₂ and 250 ppm H₂S, and no water vapor [35]. A detailed overview of plasticization phenomena in gas separation membranes is given by Ismail and Lorna [36].

There are several methods which have generally been utilized to suppress CO₂ plasticization. A short overview of these approaches is presented below. Chemical, thermal and radiation cross-linking are among the most comprehensive approaches

being used to improve the gas separation properties of membranes for applications in rigorous environments. Chemical cross-linking modification imparts anti-plasticization properties to the material, enhances chemical stability and reduces ageing [37]. Diamine cross-linking has proven to be one of the most simple and effective methods of cross-linking for polyimide membranes. p-Xylenediamine cross-linked 6FDA-(2,6-diaminotoluene) (DAT) PI-membranes resulted in reduced CO₂ plasticization and increased CO₂/CH₄ selectivity [38]. 1, 3-Propanediol (PDL) cross-linked PI-membranes showed a greatly suppressed CO₂ plasticization as well [39]. Another approach for crosslinking membranes is the formation of hyper-branched polyimides by reaction of triamines with dianhydrides [40]. Bos et al. [32] thermally cross-linked the polyimide films to stabilize against plasticization. At high temperature, polymer matrix cross-linked and resulted in a reduced segmental mobility of polymer chains, thereby suppresses plasticization. Kita et al. [41] studied the cross-linking of polyimides containing benzophenone using UV radiation. It was observed that duration of irradiation has a direct influence on the performance of membranes. The selectivity of gas pair showed improvement at the cost of reduced permeability, presumably due to densification of the membrane structure.

Polymer blending is another possibility to modify polymer properties. Kapantaidakis et al. prepare membranes with Matrimid®/PSF and observed a delay in plasticization pressure with increasing PSF fraction [42]. In another study, Bos and co-workers blended Matrimid with polysulfone and the co-polyimide P84 to improve membrane plasticization resistance [43]. The resulting membranes showed excellent resistance against plasticization at the cost of drop in permeability. Despite of excellent plasticization resistance of these above mentioned treated (chemically, thermally and UV cross-linked or blended) membranes their resulting transport properties lie significantly below the state of the art performance for polymers [30].

1.4 Mixed matrix membranes (MMMs)

As mentioned before, polymeric membranes are limited by a permeability and selectivity trade-off. On the other hand, inorganic membrane are expensive, brittle and difficult to upscale. Mixed matrix membranes (MMMs) with hybrid characteristics of polymer and inorganic materials, were developed as an alternative approach to overcome these limitation. Mixed matrix membranes or hybrid membranes are

considered as a class of composite membranes that comprise of inorganic materials embedded in a polymer matrix. Fig. 1.3 shows the schematic diagram of a MMM.

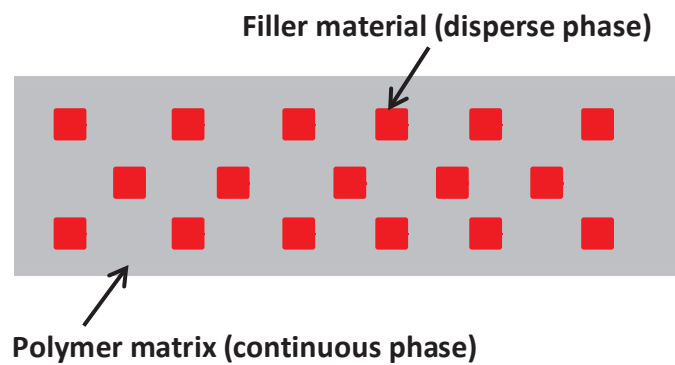


Fig. 1.3. Schematic representation of a mixed matrix membrane.

MMMs have the potential to surpass the Robeson's upper limit of the trade-off curve and approach the attractive properties of inorganic membranes [44]. Several molecular sieving materials such as zeolites [45], carbon molecular sieves (CMS) [46], metal peroxides (MOs) [47], carbon nanotubes (CNTs) [48] and metal organic frameworks (MOFs) [49] have been incorporated in different polymers. Generally, the inorganic dispersed phase has selectivity superior to the neat polymer. Hybrid membranes have transport properties in between the pure polymer and the dispersed phases. Ideally the incorporation of small fractions of inorganic fillers into the polymer matrix can result in a significant improvement in the overall performance.

Kulprathipanja et al. [25] were the first to report the superior behavior of MMMs compared to that of the pure polymer. The authors observed an increase in O_2/N_2 selectivity with the increase in silicalite content in the polymer cellulose acetate (CA). Over the years, MMMs have shown tremendous improvement in membrane performance in comparison to their pure polymer membrane counter parts [44]. However, successful industrial implementation for commercial separations has not yet been achieved because of several problems related to their processability [44]. The major factors that define the performance of MMMs are a suitable combination of polymers, particles and the physical properties of the inorganic phase (e.g., particle size, particle sedimentation and agglomeration, polymer/particle interface morphologies etc.) [44]. A short overview of these factors is presented here.

Suitable combination of polymer/inorganic filler: A suitable combination of polymer/inorganic filler is critical for MMM development. Polymers with low permeability and high selectivity are most suitable for MMM preparation [44]. Koros and Mahajan prepared MMMs containing 4A zeolite in polymers such as polyvinylacetate (PVAc), Ultem® polyetherimide (PEI) and Matrimid® polyimide (PI). The comparison of the performance of MMMs revealed that the higher intrinsic selectivity of Matrimid® and Ultem® gave superior properties to MMMs in comparison with MMMs based on lower selective PVAc [50, 51].

Particle size: Smaller particles offer several advantages over larger particles e.g. smaller particles provide more interfacial area and potentially more effectively disrupt the polymer chain packing and thereby enhance the membrane separation performance [44]. Also smaller particles are essential for thinner membranes.

Particle sedimentation and agglomeration: During the preparation of MMMs, due to the differences in physio-chemical properties and differences in density of fillers and polymers, precipitation of fillers may occur, resulting in the formation of a separate inhomogeneous layer of the filler phase and a separate layer of the polymer phase in the MMMs. The agglomeration of fillers results in pinholes that are lean in polymer phase, forming non-selective defects in MMMs [52].

Interface morphologies: The transport properties of MMMs are strongly dependent on the interface between the filler and the polymer matrix. Poor interaction between these two phases results in interfacial voids. The interfacial morphology between filler and the polymer phase can be categorized into three cases [52]: (I) an interfacial void or 'sieve-in-a-cage' morphology (II) a rigidified polymer layer (III) a reduced permeability region within the sieve.

Case I represent a situation where the filler is located freely in the cage formed by the polymer matrix. The interfacial voids are larger than the penetrating gas molecules. This morphology is highly undesirable since the voids are much more permeable than the polymer matrix and the selectivity of the membrane drops significantly. The main cause of such interfacial morphology is the residual stresses developed during solvent evaporation of the polymer film [52]. In Case II the reduction in free volume of the

polymer chains in the vicinity of the filler results in a low permeability and relative increased selectivity. During solvent evaporation, the polymer chains around the filler particles contract while the filler cannot. The difference in the mobility between the dispersed and continuous phase causes localized stresses. These localized stresses result in a rigidified polymer layer around the filler. Case III displays a situation in which the surface pores of the filler have been partially sealed by the rigidified polymer chains and the penetrants of interest enter or pass the filler slower than usual.

Several techniques have been used to overcome these issues and improve the interfacial contact, e.g. the preparation of highly concentrated (15-18 %) solutions in order to increase viscosity and reduce sedimentation [50], priming procedures [51], filler surface modification [53], high membrane formation temperature [50], use of coupling agents [54] and post-treatment of MMMs (e.g. annealing) [55] .

1.5 Metal organic frameworks and MMMs

Metal organic frameworks (MOFs) have attracted considerable research interest as crystalline porous materials. The tuneable pore size, as well as the chemical and physical properties of MOFs, attribute to the chemical functionalization of the organic ligands, make them a potential candidate to make high performance mixed-matrix membranes [56]. MOFs represent a class of porous materials that consist of an inorganic cluster connected by organic bridges, tuned into 1D, 2D, 3D dimensional arrangements. A schematic representation of the construction of a three-dimensional porous MOF is shown in Fig. 1.4.

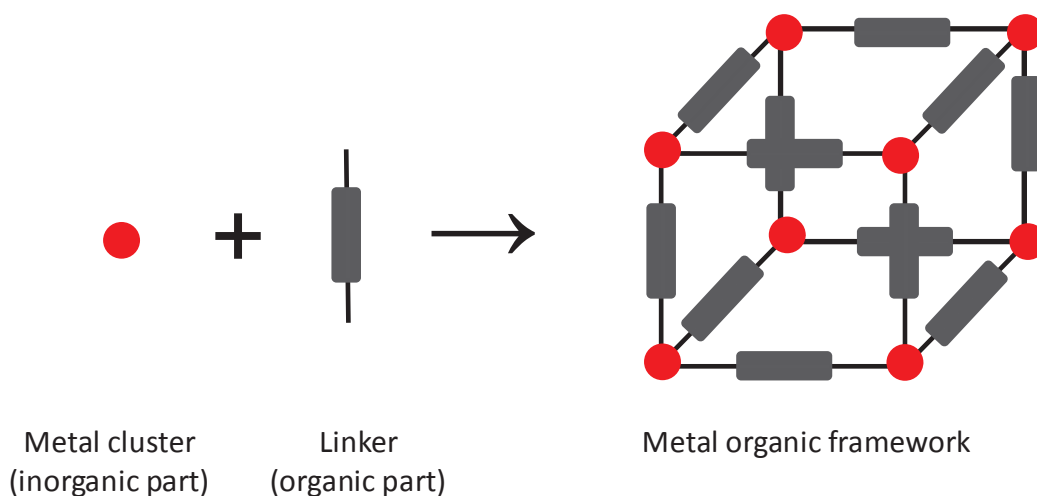


Fig. 1.4. Schematic representation showing construction of MOF (Metal cluster =red, organic linker =gray).

Virtually all designs and innumerable variations in both metal and organic linker in the MOF are possible using generic modular approaches to synthesize these materials [57]. Fig. 1.5 illustrates a few common MOFs with different structural architectures that could lead to various forms of frameworks and corresponding porosity [57]. A detailed overview on the synthesis, structures and properties of MOFs has been given by e.g. Rowsell [58].

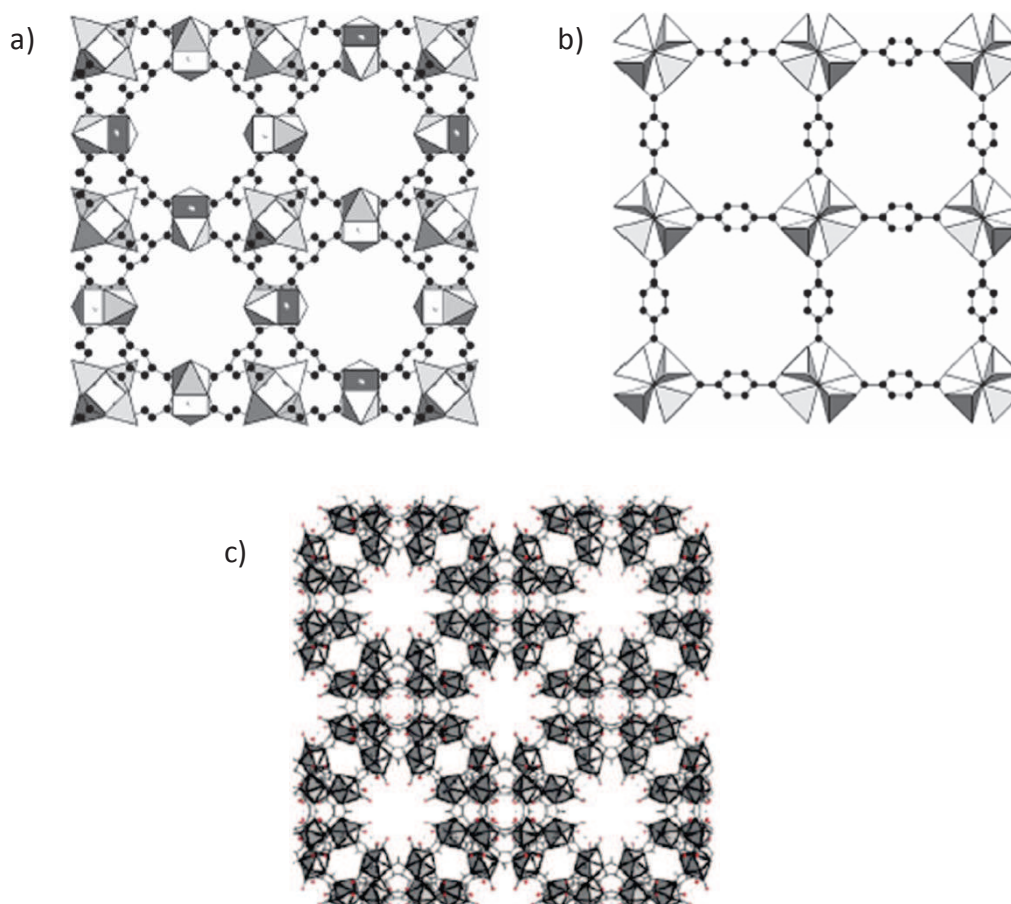


Fig. 1.5. Examples of common MOFs with different structural architectures that could lead to various forms of frameworks and porosities: (a) $\text{Cu}_3(\text{BTC})_2$, (b) MOF5, and (c) sodalite-ZMOF [57].

MOFs possess a highly crystalline nature, large pore sizes (up to 29 Å), large free volumes, high surface areas (500 - 4500 m^2/g), and designable pore topologies [59]. MOFs offer opportunities not available to more classical sorbents such as the aluminum silicates, zeolites and activated carbon, as their chemistry, pore sizes and functionality are more readily tuneable [60]. However, unlike zeolites that are thermally stable, MOFs are subjected to decomposition at higher temperatures (usually above 300 °C) [61].

In addition to many desired properties, MOFs also possess structural flexibility and dynamic behavior. These MOFs structures respond to external stimuli, such as pressure, light, guest molecules, and can change their pore dimensions reversibly [62]. MOFs have already shown progress in gas storage/separations [63] and catalysis [61] with many other potential applications like drug delivery [64] and magnetic [65] applications. A comprehensive overview on potential applications of MOFs has been given by Kuppler and Zhou [66]. There are various mechanisms that lead to gas separation by MOF materials. The two main ones are: size/shape exclusion and adsorbate-surface interactions.

Size/shape exclusion: Size/shape based selective adsorption and separation are the main applications for multiple MOFs [63]. Size and shape exclusion is also known as steric separation in which certain components of a gas mixture are prevented from entering the pores of the MOF while other components are allowed to enter the pores where they subsequently adsorbed.

Adsorbate-surface interactions: Apart from size exclusion, interaction between the penetrant gas molecules and the MOF framework is another separation mechanism that leads to preferential adsorption of one component over others in a gaseous mixture. In some MOFs, adsorption behavior and selectivity differences between different gases can be attributed to the differences in solubility of different gas molecules [63]. This is governed by the thermodynamic affinity or thermodynamic equilibrium effect. In these cases separation is significantly influenced by factors like quadruple moment, polarity, H-bonding, π - π interaction and van der Waals interaction as well as by the surface properties of the pores [63].

1.5.1 MOF based mixed matrix membranes

Recent developments showed some promising features of MOFs as gas storage media and adsorbent for gas separation [67-69]. Keskin and Sholl [70] used Maxwell model to predict mixture permeation for CO₂/CH₄ mixtures in MOF/Matrimid® MMM using molecular simulations and mixing theories. It was shown that the incorporation of either a highly permeable (but unselective) MOF like MOF-5 or highly selective MOF like Cu(hfipbb)(H₂hfipbb)_{0.5} can greatly influence the gas separation properties of MOF-MMMs. Different MOF based mixed-matrix membranes have been investigated in the

past with improved performance for gas separation. Addition of Cu-4,4'-bipyridine-hexafluorosilicate (Cu-BPY-HFS) to Matrimid®-PI enhanced the gas permeability but decreased the ideal CO₂/CH₄ gas selectivities, which suggests a strong affinity of Cu-BPY-HFS towards CH₄ [71]. Adams et al. added CuTPA (copper and terephthalic acid) into PVAc and this MMM exhibited increased selectivity for many gases, including CO₂ upon inclusion of MOF compared to pure PVAc membranes [72].

Recently, zeolitic imidazolate frameworks (ZIFs) have gathered a lot of attention because of their exceptional chemical stability and attractive molecular sieve effect [57]. ZIFs possess tetrahedral network and sodalite cage like structure that resemble the structure type of zeolite [73]. Ordonez and co-workers [74] reported the first ZIF-8 based polymer MMM using Matrimid®-PI as polymer phase. Addition of the ZIF phase substantially increased the membrane selectivity. MMMs with a ZIF loading of 50 wt.% showed an increase of 188 % in ideal selectivity. Mixed gas measurements of 10/90 CO₂/CH₄ also showed 110 % selectivity enhancement. Basu et al. prepared MMMs by combining the commercial MOFs Cu₃(BTC)₂, MIL-53 (Al) and ZIF-8 with Matrimid® and found that thermal, mechanical, as well as CO₂/CH₄ gas transport properties were improved [75]. Recently, Q. Song et al. [55] reported MMMs prepared using as-synthesized non-dried ZIF-8 nanoparticles particles in Matrimid® matrix. The as-synthesized ZIF-8 particles based MMMs showed better compatibility and higher gas separation performance.

Clearly, MOF-MMMs are promising next generation materials for gas separation. But, developments on the fabrication and application of MMMs containing inorganic (MOF) particles for gas separation are still quite low compared to those for pure polymeric membranes. This presents a chance for future research directions.

1.6 Dissertation overview

The previous sections established the importance of membranes for gas separation and the need for mixed matrix membranes with enhanced separation performance to broaden the scope of future membrane applications. But without proper polymer-filler (MOF) compatibility mixed matrix membranes will not be a viable alternative for industrial gas separations. Also CO₂ separation applications (e.g., biogas recovery, natural gas sweetening) involve high pressures. At these high feed pressures CO₂ acts as

plasticizer and causes swelling of the polymer (plasticization). The phenomenon of plasticization is well studied in literature for pure polymers but it is still difficult to find a fundamental explanation of plasticization for mixed matrix membranes and the ways to suppress it. This thesis presents the results that deal with above mentioned issues.

The polyimide Matrimid® is a commercially available gas separation polymer which exhibits good separation properties. However, the susceptibility of this polymer to CO₂ plasticization limits its use on commercial scale. In **Chapter 2**, the effect of MOF addition on the Matrimid® membrane performance is investigated. An attempt is made to analyze the plasticization behavior of Matrimid®-MOF MMMs containing mesoporous Fe(BTC). Both pure (CO₂ and CH₄) and mixed gas separation performances are investigated.

Chapter 3 describes the preparation of MMMs based on three distinctively different MOFs (MIL-53(Al) (breathing MOF), ZIF-8 (flexible MOF) and Cu₃BTC₂ (rigid MOF)) dispersed in Matrimid®. The ideal and mixed gas performance of the prepared MMMs is determined and the effect of MOF structure on the plasticization behavior of MMMs is also investigated.

Based on the previously obtained knowledge on plasticization of MOFs-MMMs and the behavior of MOFs in the polymer matrix, **Chapter 4** reports a strategy to prepare highly permeable plasticization resistant MMMs. The blending of PSF with Matrimid® is proposed and aims at imparting anti-plasticization properties to the blend membranes. Additionally, ZIF-8 is incorporated to enhance gas (CO₂) permeability. Gas transport properties of resulted membranes are investigated by means of pure and mixed gas separation experiments and sorption experiments, over a wide range of pressures. Based on the results, an insight about the mechanism of improved performance is presented in terms of ZIF-8 loading and pressure effects on the solubility, diffusion and the permeability coefficients.

One of the major problems in the preparation of successful MMMs is the insufficient adhesion between the polymer matrix and the fillers. This often results in the formation of voids at the filler/polymer interface, which degrades the performance of the membrane. In addition to formation of non-selective voids, higher MOF loadings cause agglomeration of filler and poor filler distribution. In order to eliminate these problems a new method of polymer-MOF MMM fabrication is introduced in **Chapter 5**. MMMs are prepared starting from a suspension of phase separated polymer particles and in-situ synthesized ZIF-8 nanoparticles. This improves the MOF polymer interaction and eliminates MOF agglomeration and improves compatibility and distribution, even at high loadings of MOF. The presence of non-selective voids between ZIF-8 and the polymer matrix is investigated by means of various analytical techniques and gas separation experiments.

Finally, the general conclusions and future work are presented in **Chapter 6**.

References

- [1] N.N. Li, A.G. Fane, W.S.W. Ho, T. Matsuura, *Advanced membrane technology and applications*, 2008.
- [2] V. Stannett, The transport of gases in synthetic polymeric membranes-an historic perspective, *J. Membr. Sci.*, 3 (1978) 97-115.
- [3] M. Smaïhi, T. Jermoumi, J. Marignan, R.D. Noble, Organic-inorganic gas separation membranes: Preparation and characterization, *J. Membr. Sci.*, 116 (1996) 211-220.
- [4] G. Dong, H. Li, V. Chen, Challenges and opportunities for mixed-matrix membranes for gas separation, *Journal of Materials Chemistry A*, 1 (2013) 4610-4630.
- [5] P.S. Goh, A.F. Ismail, S.M. Sanip, B.C. Ng, M. Aziz, Recent advances of inorganic fillers in mixed matrix membrane for gas separation, *Separation and Purification Technology*, 81 (2011) 243-264.
- [6] A. Brunetti, F. Scura, G. Barbieri, E. Drioli, Membrane technologies for CO₂ separation, *J. Membr. Sci.*, 359 (2010) 115-125.
- [7] R. Mahajan, D.Q. Vu, W.J. Koros, Mixed matrix membrane materials: An answer to the challenges faced by membrane based gas separations today?, *Journal of the Chinese Institute of Chemical Engineers*, 33 (2002) 77-86.

- [8] W.J. Koros, G.K. Fleming, S.M. Jordan, T.H. Kim, H.H. Hoehn, Polymeric membrane materials for solution-diffusion based permeation separations, *Progress in Polymer Science*, 13 (1988) 339-401.
- [9] L.M. Robeson, Polymer membranes for gas separation, *Current opinion in solid state & materials, Science*, 4 (1999) 549-552.
- [10] Energy information administration, US department of energy, *International energy outlook* (2013).
- [11] S.A. Rackley, *Carbon Capture and Storage*, Elsevier, (2010).
- [12] E.D. Bates, R.D. Mayton, I. Ntai, J.H. Davis, CO₂ capture by a task-specific ionic liquid, *Journal of the American Chemical Society*, 124 (2002) 926-927.
- [13] S. Ma'mun, V.Y. Dindore, H.F. Svendsen, Kinetics of the reaction of carbon dioxide with aqueous solutions of 2-((2-Aminoethyl)amino)ethanol, *Industrial & Engineering Chemistry Research*, 46 (2006) 385-394.
- [14] R.W. Baker, Future directions of membrane gas separation technology, *Industrial and Engineering Chemistry Research*, 41 (2002) 1393-1411.
- [15] K. Ghosal, B.D. Freeman, Gas separation using polymer membranes: An overview, *Polymers for Advanced Technologies*, 5 (1994) 673-697.
- [16] R.J. Gardner, R.A. Crane, J.F. Hannan, Hollow fiber permeator for separating gases, *Chemical Engineering Progress*, 73 (1977) 76-78.
- [17] Y. Zhang, J. Sunarso, S. Liu, R. Wang, Current status and development of membranes for CO₂/CH₄ separation: A review, *International Journal of Greenhouse Gas Control*, 12 (2013) 84-107.
- [18] R.W. Baker, *Membrane Technology and Applications*, 2012.
- [19] S. Kanehashi, K. Nagai, Analysis of dual-mode model parameters for gas sorption in glassy polymers, *J. Membr. Sci.*, 253 (2005) 117-138.
- [20] W.J. Koros, M.R. Coleman, D.R.B. Walker, Controlled permeability polymer membranes, *Annual Review of Materials Science*, 22 (1992) 47-89.
- [21] S. Basu, A. Cano-Odena, I.F.J. Vankelecom, Asymmetric Matrimid®/Cu₃(BTC)₂ mixed-matrix membranes for gas separations, *J. Membr. Sci.*, 362 (2010) 478-487.
- [22] Y. Yampolskii, B. Freeman, *Membrane Gas Separation*, 2010.
- [23] *CRC Handbook of Chemistry and Physics*. 85th ed., CRC Press: Boca Raton, FL, (2004-2005).
- [24] J.S. Chiou, D.R. Paul, Effects of CO₂ exposure on gas transport properties of glassy polymers, *J. Membr. Sci.*, 32 (1987) 195-205.
- [25] S. Kulprathipanja, R.W. Neuzil, N.N. Li, Separation of gases by means of mixed matrix membranes, US patent 5127925, (1992).
- [26] A.F. Ismail, I.R. Dunkin, S.L. Gallivan, S.J. Shilton, Production of super selective polysulfone hollow fiber membranes for gas separation, *Polymer*, 40 (1999) 6499-6506.

- [27] Y. Xiao, B.T. Low, S.S. Hosseini, T.S. Chung, D.R. Paul, The strategies of molecular architecture and modification of polyimide-based membranes for CO₂ removal from natural gas—A review, *Progress in Polymer Science*, 34 (2009) 561-580.
- [28] R.W. Baker, Future directions of membrane gas separation technology, *Industrial & Engineering Chemistry Research*, 41 (2002) 1393-1411.
- [29] L.M. Robeson, Correlation of separation factor versus permeability for polymeric membranes, *J. Membr. Sci.*, 62 (1991) 165-185.
- [30] L.M. Robeson, The upper bound revisited, *J. Membr. Sci.*, 320 (2008) 390-400.
- [31] H.B. Park, C.H. Jung, Y.M. Lee, A.J. Hill, S.J. Pas, S.T. Mudie, E. Van Wagner, B.D. Freeman, D.J. Cookson, Polymers with cavities tuned for fast selective transport of small molecules and ions, *Science*, 318 (2007) 254-258.
- [32] A. Bos, I.G.M. Pünt, M. Wessling, H. Strathmann, Plasticization-resistant glassy polyimide membranes for CO₂/CO₄ separations, *Separation and Purification Technology*, 14 (1998) 27-39.
- [33] A.Y. Houde, B. Krishnakumar, S.G. Charati, S.A. Stern, Permeability of dense (homogeneous) cellulose acetate membranes to methane, carbon dioxide, and their mixtures at elevated pressures, *Journal of Applied Polymer Science*, 62 (1996) 2181-2192.
- [34] M.D. Donohue, B.S. Minhas, S.Y. Lee, Permeation behavior of carbon dioxide-methane mixtures in cellulose acetate membranes, *J. Membr. Sci.*, 42 (1989) 197-214.
- [35] W.J. Schell, C.D. Houston, W.L. Hopper, *Gas Cond. Conf*, Norman, University of Oklahoma, (1983).
- [36] A.F. Ismail, W. Lorna, Penetrant-induced plasticization phenomenon in glassy polymers for gas separation membrane, *Separation and Purification Technology*, 27 (2002) 173-194.
- [37] C. Zhou, T.-S. Chung, R. Wang, Y. Liu, S.H. Goh, The accelerated CO₂ plasticization of ultra-thin polyimide films and the effect of surface chemical cross-linking on plasticization and physical aging, *J. Membr. Sci.*, 225 (2003) 125-134.
- [38] C. Cao, T.-S. Chung, Y. Liu, R. Wang, K.P. Pramoda, Chemical cross-linking modification of 6FDA-2,6-DAT hollow fiber membranes for natural gas separation, *J. Membr. Sci.*, 216 (2003) 257-268.
- [39] A.M.W. Hillock, W.J. Koros, Cross-Linkable Polyimide Membrane for Natural Gas Purification and Carbon Dioxide Plasticization Reduction, *Macromolecules*, 40 (2007) 583-587.
- [40] J. Fang, H. Kita, K.I. Okamoto, Gas permeation properties of hyperbranched polyimide membranes, *J. Membr. Sci.*, 182 (2001) 245-256.
- [41] H. Kita, T. Inada, K. Tanaka, K.-i. Okamoto, Effect of photocrosslinking on permeability and permselectivity of gases through benzophenone- containing polyimide, *J. Membr. Sci.*, 87 (1994) 139-147.
- [42] G.C. Kapantaidakis, S.P. Kaldis, X.S. Dabou, G.P. Sakellaropoulos, Gas permeation through PSF-PI miscible blend membranes, *J. Membr. Sci.*, 110 (1996) 239-247.

- [43] A. Bos, I. Punt, H. Strathmann, M. Wessling, Suppression of gas separation membrane plasticization by homogeneous polymer blending, *Aiche Journal*, 47 (2001) 1088-1093.
- [44] T.S. Chung, L.Y. Jiang, Y. Li, S. Kulprathipanja, Mixed matrix membranes (MMMs) comprising organic polymers with dispersed inorganic fillers for gas separation, *Progress in Polymer Science (Oxford)*, 32 (2007) 483-507.
- [45] G. Golemme, A. Bruno, R. Manes, D. Muoio, Preparation and properties of superglassy polymers - zeolite mixed matrix membranes, *Desalination*, 200 (2006) 440-442.
- [46] D. Vu, W.J. Koros, S.J. Miller, Effect of condensable impurity in CO₂/CH₄ gas feeds on performance of mixed matrix membranes using carbon molecular sieves, *J. Membr. Sci.*, 221 (2003) 233-239.
- [47] M. Sairam, M.B. Patil, R.S. Veerapur, S.A. Patil, T.M. Aminabhavi, Novel dense poly(vinyl alcohol)-TiO₂ mixed matrix membranes for pervaporation separation of water-isopropanol mixtures at 30 degrees C, *J. Membr. Sci.*, 281 (2006) 95-102.
- [48] S. Kim, T.W. Pechar, E. Marand, Poly(imide siloxane) and carbon nanotube mixed matrix membranes for gas separation, *Desalination*, 192 (2006) 330-339.
- [49] J.-R. Li, Y. Ma, M.C. McCarthy, J. Sculley, J. Yu, H.-K. Jeong, P.B. Balbuena, H.-C. Zhou, Carbon dioxide capture-related gas adsorption and separation in metal-organic frameworks, *Coordination Chemistry Reviews*, 255 (2011) 1791-1823.
- [50] R. Mahajan, W.J. Koros, Factors controlling successful formation of mixed-matrix gas separation materials, *Industrial and Engineering Chemistry Research*, 39 (2000) 2692-2696.
- [51] R. Mahajan, W.J. Koros, Mixed matrix membrane materials with glassy polymers. Part 1, *Polymer Engineering and Science*, 42 (2002) 1420-1431.
- [52] T.T. Moore, W.J. Koros, Non-ideal effects in organic-inorganic materials for gas separation membranes, *Journal of Molecular Structure*, 739 (2005) 87-98.
- [53] A.M.W. Hillock, S.J. Miller, W.J. Koros, Crosslinked mixed matrix membranes for the purification of natural gas: Effects of sieve surface modification, *J. Membr. Sci.*, 314 (2008) 193-199.
- [54] Y. Li, H.M. Guan, T.S. Chung, S. Kulprathipanja, Effects of novel silane modification of zeolite surface on polymer chain rigidification and partial pore blockage in polyethersulfone (PES)-zeolite A mixed matrix membranes, *J. Membr. Sci.*, 275 (2006) 17-28.
- [55] Q. Song, S.K. Nataraj, M.V. Roussanova, J.C. Tan, D.J. Hughes, W. Li, P. Bourgoin, M.A. Alam, A.K. Cheetham, S.A. Al-Muhtaseb, E. Sivaniah, Zeolitic imidazolate framework (ZIF-8) based polymer nanocomposite membranes for gas separation, *Energy and Environmental Science*, 5 (2012) 8359-8369.
- [56] A.R. Millward, O.M. Yaghi, Metal-organic frameworks with exceptionally high capacity for storage of carbon dioxide at room temperature, *Journal of the American Chemical Society*, 127 (2005) 17998-17999.

- [57] T. Devic, C. Serre, Porous Metal Organic Frameworks. From Synthesis to Applications, in: *Ordered Porous Solids*, 2009, pp. 77-99.
- [58] J.L.C. Rowsell, O.M. Yaghi, Metal-organic frameworks: a new class of porous materials, *Microporous and Mesoporous Materials*, 73 (2004) 3-14.
- [59] M. Eddaoudi, J. Kim, N. Rosi, D. Vodak, J. Wachter, M. O'Keeffe, O.M. Yaghi, Systematic design of pore size and functionality in isorecticular mofs and their application in Methane Storage, *Science*, 295 (2002) 469-472.
- [60] R. Krishna, J.M. van Baten, A comparison of the CO₂ capture characteristics of zeolites and metal-organic frameworks, *Separation and Purification Technology*, 87 (2012) 120-126.
- [61] J. Lee, O.K. Farha, J. Roberts, K.A. Scheidt, S.T. Nguyen, J.T. Hupp, Metal-organic framework materials as catalysts, *Chemical Society Reviews*, 38 (2009) 1450-1459.
- [62] S. Kitagawa, R. Kitaura, S.-i. Noro, Functional porous coordination polymers, *Angewandte Chemie International Edition*, 43 (2004) 2334-2375.
- [63] J.-R. Li, R.J. Kuppler, H.-C. Zhou, Selective gas adsorption and separation in metal-organic frameworks, *Chemical Society Reviews*, 38 (2009) 1477-1504.
- [64] N.J. Hinks, A.C. McKinlay, B. Xiao, P.S. Wheatley, R.E. Morris, Metal organic frameworks as no delivery materials for biological applications, *Microporous and Mesoporous Materials*, 129 (2010) 330-334.
- [65] M.C. Bernini, A.E. Platero-Prats, N. Snejkó, E. Gutierrez-Puebla, A. Labrador, R. Saez-Puche, J. Romero de Paz, M.A. Monge, Tuning the magnetic properties of transition metal MOFs by metal-oxygen condensation control: the relation between synthesis temperature, SBU nuclearity and carboxylate geometry, *CrystEngComm*, 14 (2012) 5493-5504.
- [66] R.J. Kuppler, D.J. Timmons, Q.-R. Fang, J.-R. Li, T.A. Makal, M.D. Young, D. Yuan, D. Zhao, W. Zhuang, H.-C. Zhou, Potential applications of metal-organic frameworks, *Coordination Chemistry Reviews*, 253 (2009) 3042-3066.
- [67] U. Mueller, M. Schubert, F. Teich, H. Puetter, K. Schierle-Arndt, J. Pastre, Metal-organic frameworks - prospective industrial applications, *Journal of Materials Chemistry*, 16 (2006) 626-636.
- [68] L. Pan, D.H. Olson, L.R. Ciemnomlonski, R. Heddy, J. Li, Separation of hydrocarbons with a microporous metal-organic framework, *Angewandte Chemie-International Edition*, 45 (2006) 616-619.
- [69] J.R. Long, O.M. Yaghi, The pervasive chemistry of metal-organic frameworks, *Chemical Society Reviews*, 38 (2009) 1213-1214.
- [70] S. Keskin, D.S. Sholl, Selecting metal organic frameworks as enabling materials in mixed matrix membranes for high efficiency natural gas purification, *Energy & Environmental Science*, 3 (2010) 343-351.
- [71] Y. Zhang, I.H. Musseman, J.P. Ferraris, K.J. Balkus, Jr., Gas permeability properties of Matrimid (R) membranes containing the metal-organic framework Cu-BPY-HFS, *J. Membr. Sci.*, 313 (2008) 170-181.

[72] R. Adams, C. Carson, J. Ward, R. Tannenbaum, W. Koros, Metal organic framework mixed matrix membranes for gas separations, *Microporous and Mesoporous Materials*, 131 (2010) 13-20.

[73] A.W. Thornton, D. Dubbeldam, M.S. Liu, B.P. Ladewig, A.J. Hill, M.R. Hill, Feasibility of zeolitic imidazolate framework membranes for clean energy applications, *Energy & Environmental Science*, 5 (2012) 7637-7646.

[74] M.J.C. Ordonez, K.J. Balkus, J.P. Ferraris, I.H. Musselman, Molecular sieving realized with ZIF-8/Matrimid[®] mixed-matrix membranes, *J. Membr. Sci.*, 361 (2010) 28-37.

[75] S. Basu, A. Cano-Odena, I.F.J. Vankelecom, MOF-containing mixed-matrix membranes for CO₂/CH₄ and CO₂/N₂ binary gas mixture separations, *Separation and Purification Technology*, 81 (2011) 31-40.

Chapter 2

High pressure gas separation performance of mixed-matrix polymer membranes containing mesoporous Fe(BTC)

This chapter has been published as:

S. Shahid, K. Nijmeijer, High pressure gas separation performance of mixed-matrix polymer membranes containing mesoporous Fe(BTC), *J. Membr. Sci.*, 459 (2014) 33-44.

ABSTRACT

Mixed-matrix membranes (MMMs), filled with inorganic particles, provide a mean to improve the gas separation performance of polymeric membranes. In this work, MMMs containing the mesoporous metal organic framework (MOF) Fe(BTC) in a Matrimid®-PI matrix were characterized for in terms of their carbon dioxide (CO₂) and methane (CH₄) separation performance at low and high pressures. Physical properties (density, thermal degradation, glass transition) of Fe(BTC) and prepared MMMs were analyzed. An optimized priming and suspension mixing protocol resulted in a homogeneous distribution of MOF particles in the Matrimid®-PI matrix, as observed by scanning electron microscopy (SEM). Experimental results showed decreased thermal degradation but increased membrane density and glass transition with increased Fe(BTC) loading, as well as improvement in CO₂ permeability and CO₂/CH₄ selectivity. At high pressures, the native Matrimid®-PI membrane showed typical plasticization behavior, but as the MOF loading increased gas transport properties seems to be controlled by MOF particles leading to reduced plasticization tendencies. The favorable performance of MOF containing membranes can be attributed to the strong increase in the sorption capacity and chain rigidity by the Fe(BTC) particles which suppressed plasticization. At a mixed gas feed pressure of 40 bar, MMMs with 30 wt.% MOF showed a CO₂/CH₄ selectivity increase of 62 % compared to the native Matrimid®-PI membrane, while the permeability was about 30 % higher than that of native polymer.

2.1 Introduction

There is an increasing necessity to develop environmentally friendly and energy efficient gas separation processes and as such, natural gas and biogas purification is of major importance. CO₂ is commonly found as undesired component in natural gas and biogas at significant concentrations [1, 2]. For fuel applications however, the removal of CO₂ is essential to (1) increase the calorific value, (2) reduce pipeline corrosion within the gas distribution network and (3) prevent atmospheric pollution [3-5]. CO₂ capture and gas separation through membranes has emerged as an important technology with several advantages over conventional separation processes such as cryogenic distillation and adsorption [6]. The conventional CO₂ capture processes have high energy consumption due to the involved phase changes of constituents, whereas the use of polymeric membranes provides a more energy efficient and cost effective process for CO₂ capture. Additionally, membranes have low capital costs and easy to fabricate [6]. However, performance of polymeric membranes is limited by a trade-off between membrane permeability and selectivity [7-9]. Over the last two decades, research has focused on increasing the polymeric membrane performance above this trade-off curve to make membranes more cost competitive with conventional processes. Additionally, especially in high pressure separations that involve CO₂ plasticization may play a significant role. The sorption of CO₂ in the polymer matrix leads to excessive swelling of the polymer film and associated increased macromolecular mobility.

Mixed-matrix membranes, comprising of inorganic particles e.g. zeolites [10-17], carbon molecular sieves (CMS) [18-21], metal peroxides (MOs) [22, 23], carbon nanotubes (CNTs) [24, 25] and MOFs [26], dispersed in a continuous polymeric matrix provide an interesting approach for improving the gas separation properties of polymeric membranes [27]. Recent developments showed some promising features of MOFs as gas storage media and adsorbent for gas separation [28-30]. MOFs represent a class of porous materials that consist of an inorganic cluster connected by organic bridges, tuned into 1D, 2D, 3D dimensional arrangements. MOFs offer opportunities not available to more classical sorbents such as the aluminum silicates, zeolites and activated carbon as their chemistry, pore sizes and functionality are more readily tuneable [31, 32]. A complete overview on synthesis, structures and properties of MOFs has been given by

Rowse [33]. The high surface area, controlled porosity, adjustable chemical functionality, high affinity for certain gases and compatibility with polymer chains, make them a potential candidate to make high performance mixed-matrix membranes [34-36].

Different MOF based mixed-matrix membranes have been investigated in the past with improved performance for gas separation. Addition of copper-4,4'-bipyridine-hexafluorosilicate (Cu-BPY-HFS) to Matrimid®-PI enhanced the gas permeability but decreased the ideal CO₂/CH₄ gas selectivities, which suggests a strong affinity of Cu-BPY-HFS towards CH₄ [37]. Adams et al. added CuTPA (copper and terephthalic acid) into polyvinyl acetate (PVAc) and this MMM exhibited increased selectivity for many gases, including CO₂ upon inclusion of MOF compared to pure PVAc membranes [38]. Musselman and co-workers [39] reported the first ZIF-8 based polymer MMM using Matrimid®-PI as polymer phase. Addition of the ZIF phase substantially increased the membrane selectivity. MMMs with a ZIF loading of 50 % showed an increase of 188 % in ideal selectivity. Mixed gas measurements of 10:90 CO₂/CH₄ also showed 110 % selectivity enhancement. Basu et al. prepared MMMs by combining the commercial MOFs Cu₃(BTC)₂, MIL-53 (Al) and ZIF-8 with Matrimid®-PI and found that thermal, mechanical, as well as gas transport properties were improved [40, 41]. Recently, Ploegmakers et al. studied the effect of Cu₃(BTC)₂ and its respective loading on ethylene and ethane separation [42, 43]. The authors observed an increase in selectivity with the loading of Cu₃(BTC)₂ while the permeability remains constant. The increase in selectivity with Cu₃(BTC)₂ loading was attributed to the higher diffusion coefficient of gases with sieve in a cage morphology. Considering the above, the majority of literature reported work on MOFs that are selected purely based on selectivity, in which separation is controlled by size exclusion effects. MOFs with mesoporous cavities have lately attracted a lot of attention for overcoming the potentially high sorption and mass transfer limitations in microporous MOFs [44]. Perez et al. incorporated MOF-5 in a Matrimid®-PI matrix for the separation of binary mixtures. At 30 wt.% of MOF-5 loading permeability of gases increased by 120 % while ideal selectivity remained constant [45]. Zornoza et al. incorporated amine functionalized flexible MIL-53 in polysulfone membranes. Functionalized MIL-53 particles showed excellent compatibility with the

matrix, even at higher MOF loadings. MMMs containing MIL-53 displayed a high selectivity for CO₂/CH₄ separation, at the same time enhancing the performance of the membranes at high pressures. The authors attributed this effect to the breathing of MIL-53 [46]. Mesoporous MOFs such as MOF-177, MIL-100 (Fe, Cr), MIL-101 (Fe, Cr), with open metal sites outperform activated carbon and zeolites in terms of adsorptive capacity and selectivity [32, 35]. Llewellyn et al. studied the adsorption behavior of MIL-100 (Cr) and MIL-101 (Cr) and found that both MOF structures show higher CO₂ capacities. In particular, MIL-101 (Cr) showed a record capacity of 40 mmol/g [47]. Despite the fact that MOF based membranes are growing regarding their performance and applications, the literature on gas transport through MMMs with mesoporous MOFs is still scarce. Recently, Harold et al. studied the incorporation of MIL-101 (Cr) in polysulfone (PSF) and results showed an unsurpassed O₂ permeability increase by a factor of four to six times for MIL-loadings of 24 wt.% [48]. Although this, MIL-101 (Cr) exhibits the highest surface area reported and high adsorption capacity, the costs of the transition metal (e.g. Cr) and its toxic nature are important concerns. Iron on the other hand is an environmentally benign and cheap component with redox properties and much more suitable for industrial use than copper, chromium or cobalt based MOFs regarding toxicity. As such Fe-containing MOFs may offer a promising alternative for achieving high performance mixed matrix membranes for gas separation [49]. Mesoporous Fe(BTC) has a high porosity, high molar CO₂ uptake (18 mmol/g at 50 bar [50]), coordinatively unsaturated sites [51] and high water stability [49], a property often lacking in many MOFs [52]. Considering these factors, the effect of mesoporous iron trimesic acid (FeBTC) in MMMs on the separation of CO₂/CH₄ is relevant. Fe(BTC) is composed of carboxylate moieties (1,3,5-benzene tricarboxylic acid) and iron trimesic octahedral clusters, sharing a common vertex, with removable terminal ligands (H₂O or OH). Consequently it provides potential unsaturated metal sites for strong interaction. The Fe(BTC) pore network is formed by two types of mesoporous cages (25 and 29 Å), accessible through microporous windows of ca. 5.5 and 8.6 Å [51]. The general characteristic data of Fe(BTC) considered in this study, are shown in Table 2.1. The high surface area, pore volume and adsorption capacity make Fe(BTC) a potential candidate for gas separation.

Table 2.1. Properties of MOF Fe(BTC) [50, 54].

| MOF | Pore topology | Pore diameter (nm) | Pore volume cm ³ /g | Bulk density (g/cm ³) | BET surface area (m ² /g) |
|---------|---------------|---------------------------|--------------------------------|-----------------------------------|--------------------------------------|
| Fe(BTC) | Cage/window | Cage:0.85 Window: 0.55 | >1.0 | 0.35 | 1400-1600 |

Fe(BTC) shows the same sodalite structure as Cu₃(BTC)₂ and can be synthesized in the same way using benzene trimesic acid (1,3,5- benzene tricarboxylic acid) and iron salt [53]. A significant amount of the Fe(III) sites is accessible and can be partially reduced to Fe(II) sites. These Fe(II) metal ions can be bridged by four carboxylic groups and yield the paddle-wheel clusters.

The present work provides for the first time the incorporation of the mesoporous Fe(BTC) as additive in polymeric MMMs based on Matrimid[®]-PI for high pressure gas separation applications to explore the mechanism of gas transport at elevated pressures through mesoporous MOFs. The study describes an improved method for preparing defect free MMMs with a homogeneous distribution of MOF particles in the polymeric matrix and investigates the effect of mesoporous MOF loading on high pressure gas separation performance of these membranes. Characterization is performed by a multitude of techniques such as XRD, SEM, density, TGA and DSC. In addition, both pure gas permeation and mixed gas separation experiments are performed over a wide range of pressures to investigate the effect of Fe(BTC) particles on performance and plasticization resistance of these MOF based MMMs at high pressures.

2.2 Experimental

2.2.1 Materials

Matrimid[®] 5218 PI was supplied by Huntsman, Germany. The MOF, iron benzene- 1,3,5-tricarboxylate (Fe(BTC)), was obtained from Sigma-Aldrich as Basolite F300. N-methyl-2-pyrrolidinone (NMP, 99 % extra pure) and 1,4 dioxane (99.5 %) were purchased from Acros Organics, Belgium. All solvents were analytical grade and used without further purification. CH₄, CO₂ and N₂ gases were supplied by Praxair, The Netherlands and used as received (purity 99.999 %).

2.2.2 Membrane preparation

2.2.2.1 Pure Matrimid®-PI membranes

The membrane samples were prepared by solution processing. Matrimid®-PI powder was dried at 100 °C under active vacuum overnight. The Matrimid®-PI solution was prepared by dissolving 18 wt.% Matrimid®-PI in a mixture of dioxane and NMP in a 20/80 ratio. First 10 wt.% of the total polymer was dissolved. The suspension was stirred for 2 h and then sonicated for 10 min followed by addition of 20 wt.% of the total polymer to the solution and stirred for another 2 h. This step was repeated until the requisite total amount of polymer was added. After that the solution was left overnight stirring. Then the solution was cast on a flat glass plate with a 0.47 mm casting knife and the membrane was left to dry under nitrogen for 4 days at room temperature. Subsequently, the membrane was dried in a WTC Binder oven at 100 °C under nitrogen flow for 2 days. Finally, the dried membrane was peeled off from the glass plate and vacuum dried at 150 °C for two days.

2.2.2.2 Mixed-matrix membranes

The MMM samples were prepared by suspension casting. As the FeBTC particles were bigger than 15-20 µm, these particles were first ground to smaller sizes using a ball mill and then sieved with a 5 µm sieve. Fe(BTC) powder was then dried at 100 °C overnight. After removal from the oven, vials were quickly capped to prevent hydration. The MOF loading of the MMMs was calculated as

$$\text{MOF loading (wt.\%)} = \left[\frac{\text{wt. MOF}}{\text{wt. MOF} + \text{wt. polymer}} \right] \times 100 \quad \text{Eq. 2.1}$$

10 wt.%, 20 wt.%, 30 wt.% dried Fe(BTC) powder was slurried into the solvent (20/80 dioxane/NMP) for 1 h and then sonicated for 1 h to disperse the fine powder. Subsequently, the suspensions were stirred for 1 h. Then, polymer powder was added to form a 10 wt.% solution. To adequately disperse the Fe(BTC) particles within the polymer matrix, the suspensions used for the membrane preparation were stirred and sonicated for five periods of 10 min each until a homogeneous suspension was obtained.

After five additional iterations of stirring and sonication, the mixture was stirred overnight.

After overnight stirring, 20 wt.% of polymer was added to the solution and the solution was stirred for 2 h. This step was repeated until the requisite total amount of polymer was added. Then, a final 30 min sonication period was applied before casting to remove any trapped air bubbles. Membranes were cast on a flat glass plate with a 0.47 mm casting knife and after that left to dry under nitrogen for 4 days at room temperature. Subsequently, membranes were dried in a WTC Binder oven at 100 °C for 2 days to remove residual solvent. Finally the membranes were removed from the glass plate and vacuum dried at 150 °C for 2 days. The membrane thickness of both the native membranes and the MMMs was determined using an IP65 Coolant Proof digital Micrometer from Mitutoyo and found to be between 50 and 75 μm .

2.2.3 Characterization techniques

2.2.3.1 SEM

Images of pure MOF powder and cross-sections of MMMs were taken using a JEOL-JSM-5600LV scanning electron microscope (SEM) to investigate the MOF homogeneity and compatibility with the polymer phase in the mixed-matrix membranes. SEM samples were prepared by freeze-fracturing the dried membranes in liquid nitrogen. The samples were dried in a vacuum oven at 30 °C overnight and coated with a 1.5-2 nm thick gold layer using a Balzers Union SCD040 sputter coater under argon flow to reduce sample charging under the electron beam.

2.2.3.2 XRD

The crystallinity of the samples under study was determined by powder X-ray diffraction (XRD) on a Bruker D2 PHASER using $\text{CuK}\alpha$ radiation with a wavelength (λ) = 1.54 Å at room temperature. All samples were gently grinded. As the particles turned out to be amorphous, preferential orientation of individual crystals did not play a role. Scans were made from 5-50° 2 θ with a step size of 0.02° in 40 min.

2.2.3.3 Thermal analysis

Thermal stability of the membranes was investigated by Thermal Gravimetric Analysis (TGA) using a Perkin Elmer TGA 4000. Samples were heated up to 900 °C at a heating rate of 20 °C/min. under a constant nitrogen flow of 20 ml/min. All measurements were repeated 3 times (3 different membranes). The glass transition temperature (T_g) of the membranes was measured on a Perkin Elmer DSC 8000. 3-5 mg of each sample was placed in an aluminum pan and heated up to 400 °C at a heating rate of 20 °C/min and held at that temperature for 1 min. Subsequently, the samples were cooled back to 50 °C at 20 °C/min. This cycle was repeated two times. No transition was recorded in the first heating scan. The T_g was determined from the second heating scan using the midpoint heat capacity transition method.

2.2.3.4 Density

The density of the samples was determined using a pycnometer (Micromeritics Accupyc 1330) at 25±0.8 °C. A weighted sample was placed in the sample cell and degassed by purging with a flow of dry gas (helium) by a series of pressurization cycles. Then, the measurement was performed by pressurizing the sample cell and subsequently expanding the gas into the reference chamber. From the difference between the two pressure readings the sample volume was calculated. The volume measured by pycnometer measures the volume of sample minus the volume of voids, open and closed pores. Using the weight, the volume density of the material was calculated. An average of 10 measurements per sample was used to calculate the average density. At least two samples of each material were tested to minimize the error.

2.2.3.5 Gas permeation

2.2.3.5.1 Pure gas

Gas permeation experiments were performed using a custom-built high pressure gas permeation set-up. Pure gas permeability measurements were performed using a constant volume, variable pressure method with vacuum at the permeate side, as described elsewhere [55]. For each experiment, a 4.7 cm diameter membrane was placed into the stainless steel cell and the permeate side was evacuated for 1 h. Subsequently, the desired feed pressure was applied at the top side of the membrane

while keeping the permeate side under vacuum. The gas permeability values were calculated from the steady state pressure increase with time in a well calibrated (constant) volume at the permeate side. Pressure dependence of the permeability for CO₂ and CH₄ was determined up to 40 bar total feed pressure. For all pure gas measurements all membranes were tested for CH₄ permeability for all pressures and then same membranes are used for CO₂ permeability measurements. All experiments were performed at a constant temperature of 35±0.5 °C. Furthermore in order to exclude time effects on permeability, all membranes had the same history (measurements started 3 weeks after preparation) and the permeability values were taken after 8 h of measurement.

2.2.3.5.2 Mixed gas

In mixed gas experiments always fresh membranes were prepared and measured also after a constant period of three weeks to eliminate the influence of membrane history [56, 57]. A mixture of CO₂ and CH₄ (50/50 mol%) was used to investigate the membrane performance under high pressure mixed gas conditions. In every gas separation experiment two samples from different membranes of the same composition were measured. The procedure used for the mixed gas separation experiments was as follows:

- 1) Degassing and evacuation of the membranes for 1 h.
- 2) Determination of the N₂ permeance properties at 5 bar.
- 3) Degassing for 1 h.
- 4) Determination of the separation properties for the CO₂/CH₄ gas mixture at 5 bar for at least 8 h.
- 5) Measurement of N₂ permeance decay overnight (about 14 h).
- 6) Thorough degassing and evacuation for 30 min.
- 7) Increasing the mixed gas feed pressure to the next desired value (e.g. 10 bar) and determination of the separation properties at this pressure.
- 8) Repetition of steps 5-7 up to the maximum pressure (i.e. 40 bar).

During permeation, the composition of feed and permeate were analyzed continuously by a Varian 3900 GC gas chromatograph using an Alltech alumina F-1 60/80 packed bed column at 150 °C. The gas selectivity (α) was calculated by the following relationship:

$$\alpha_{i/j} = \frac{y_i/y_j}{x_i/x_j} \quad \text{Eq. 2.2}$$

Where y_i and y_j are the mole fractions of the components in the permeate, while x_i and x_j are their corresponding mole fractions in the feed. The permeability and selectivity values reported are the average of 2-3 membranes. The gas permeation data presented are the average of at least two membranes of two separate batches. Standard deviations ranged from 4% to 10 %.

2.3 Results and discussion

2.3.1 MOF characterization

2.3.1.1 XRD

The x-ray diffraction pattern of Fe(BTC) is shown in Fig. 2.1. The XRD pattern shows no distinctive peaks, indicating that Fe(BTC) has a less ordered amorphous structure, as also reported in previous studies [43, 58, 59].

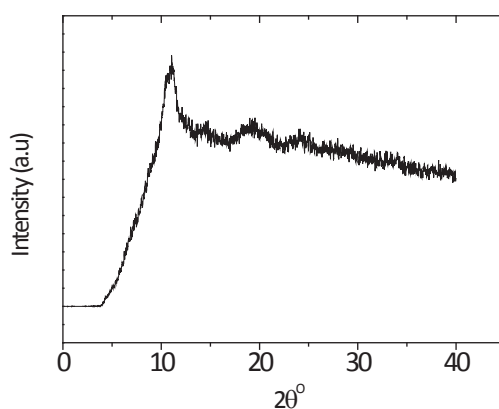


Fig. 2.1. XRD pattern of pure Fe(BTC).

2.3.1.2 TGA

Knowledge of the thermal stability of the MOF and MMMs is of importance for both high temperature gas separation applications and because heating of the polymer above

its Tg or thermal annealing is often applied to improve the properties of the membranes [60, 61].

The thermal stability of Fe(BTC) as analyzed by TGA is shown in Fig. 2.2a. The sample shows a large weight loss of 10 % between 50 and 130 °C. This can be attributed to the desorption of water. The largest weight loss is observed between 250 °C and 400 °C with a weight loss of 30 % that can be attributed to the calcination of the organic part [62, 63]. From this temperature onwards till the final temperature of 900 °C, the weight decreases continuously with increasing temperature with Fe₂O₃ as residue. In order to confirm the degradation temperature of Fe(BTC), isothermal weight loss experiments are performed as well (Fig. 2.2b). As can be seen in Fig. 2.2b, up to a temperature of 200 °C, the samples keep their structural integrity and do not form gaseous products. Beyond 250 °C, the samples show a decrease in weight with time and also change their color from red to black. The black color indicates the calcination of BTC unit in Fe(BTC). Similarly, Cu₃(BTC)₂ (a structural analogy of Fe(BTC)) shows a degradation temperature of around 300 °C [40] also confirming the collapse of the BTC unit [63]. These results suggest lower to moderate temperature applications for Fe(BTC) material.

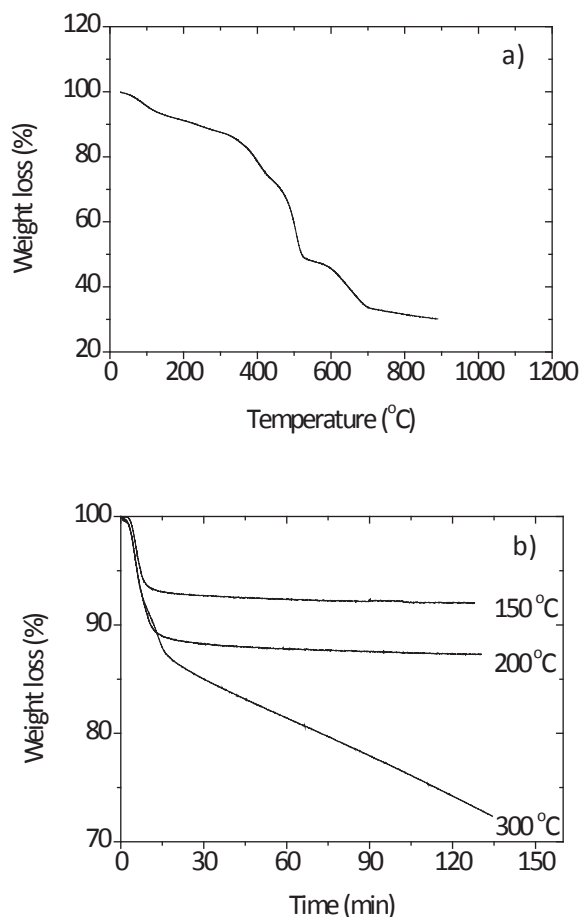


Fig. 2.2. (a) TGA of pure Fe(BTC) and (b) Isothermal TGA curves for pure Fe(BTC).

2.3.1.3 SEM

Fig. 2.3a shows the SEM image of unmilled Fe(BTC). No defined morphology is observed, also indicating the low order structure of this particular MOF. The particles seem to be agglomerated in the form of clumps. The particle diameter varies between 10 and 20 μm . Especially the larger particles can cause problems during membrane fabrication as settling of the particles may lead to non homogeneity in the MMMs and membrane defects, since larger particles are difficult to be encapsulated giving rise to non-selective voids. To avoid these problems, Fe(BTC) particles were ground and sieved to obtain sub 5 μm particles (Fig. 2.3b).

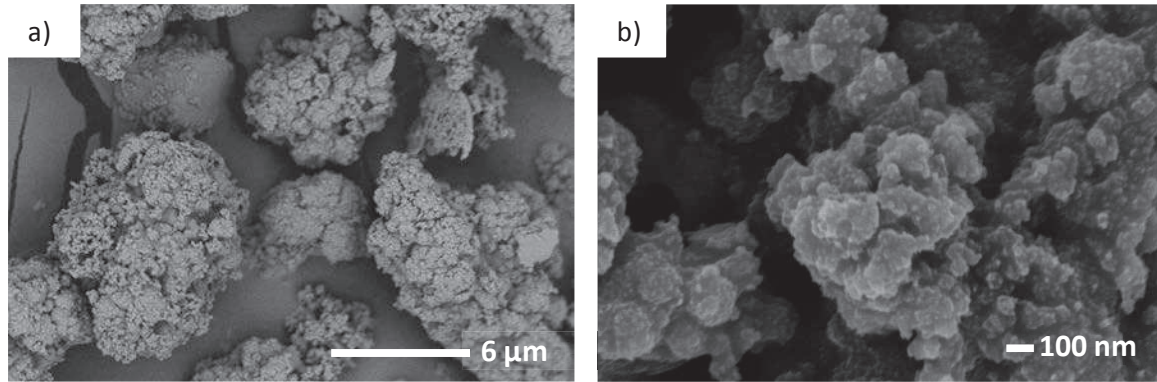


Fig. 2.3. SEM image of (a) as received pure Fe(BTC) (magnification: 5000x); (b) milled Fe(BTC) particles (magnification: 50000x).

2.3.2 Membrane characterization

2.3.2.1 TGA

The TGA curves of the Matrimid®-PI membrane and the MMMs are shown in Fig. 2.4.

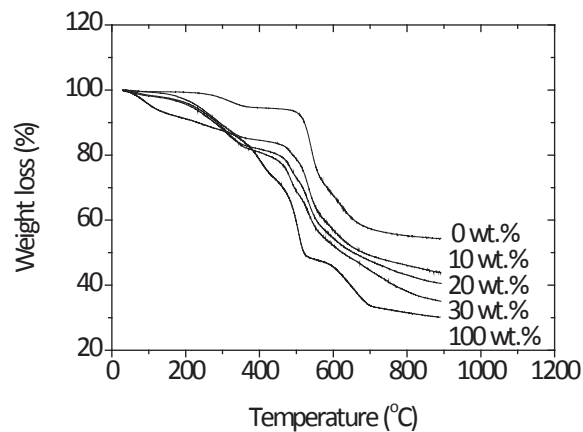


Fig. 2.4. TGA of Matrimid®-PI (0 wt.%), pure Fe(BTC) (100 wt.%) and MMMs at different MOF loadings.

The native Matrimid®-PI membrane has a weight loss of only 1.5 % when the temperature is raised to 150 °C. This is caused by evaporation of moisture. An additional 4 % weight loss is shown when the temperature is increased to 300 °C. This decrease can be attributed to the removal of residual trapped solvent. The temperature of 300 °C is related to the Tg of Matrimid®-PI considering that, at this temperature or above, the mobility of polymer chains are favorable to solvent desorption [64]. Near a temperature of 490 °C, the Matrimid®-PI membrane shows a drastic drop of 20 %, which marks the start of the thermal degradation process. Above this temperature there is a continuous loss of weight with temperature. At the final temperature of 900 °C, the Matrimid®-PI

membrane has lost 55 % of its original weight. The thermal decomposition (Td) of the pure MOF Fe(BTC) starts around 250 °C (Fig. 2.3). The MMMs with 10, 20 and 30 wt.% Fe(BTC) show a decomposition behavior intermediate to that of the pure Matrimid®-PI membrane and the pure MOF but with multiple weight loss stages. The MMMs show higher resistance against the temperature compared to pure Fe(BTC) because of the presence of the Matrimid®-PI polymer matrix. The MMMs with 10, 20, 30 wt.% Fe(BTC) show a drop of around 3 % up to a temperature of 120 °C. This is caused by dehydration of the sample. It is also visible that an extra weight loss stage appears between 250 °C and 400 °C when compared to the pure Matrimid®-PI membrane showing weight loss of 13 %, 16 % and 18 % for 10, 20 and 30 wt.% MMMs, respectively. This extra stage can be related to the removal of the solvent trapped inside the MOF and initiation of the decomposition of Fe(BTC) inside the matrix, since it also coincides with the decomposition temperature of Fe(BTC). As the temperature increases above 400 °C the MMMs show different decomposition temperatures depending on the loading of (FeBTC). The MMM with 10 wt.% Fe(BTC) shows a Td of 480 °C. The Td decreases with increasing Fe(BTC) content down to 450 °C for a loading of 30 wt.%. This decrease in thermal stability of MMMs can be attributed to the low thermal stability of Fe(BTC). Higher loadings of Fe(BTC) weaken the thermal stability of the MMMs as compared to the native polymer. Overall MMMs show higher thermal resistance compared to pure Fe(BTC) but lower resistance than native Matrimid®-PI.

2.3.2.2 DSC

DSC analysis was performed on pure Matrimid®-PI membranes and MMMs to determine the glass transition temperature. Table 2.2 reveals these glass transition temperatures. Pure Matrimid®-PI membrane shows a single Tg at 328 °C, consistent with literature values [24]. The Tg values of the MMMs are slightly higher than that of the native Matrimid®-PI membrane. The Tg of Fe(BTC) MMMs increases with Fe(BTC) content, from 328 °C at 0 wt.% loading to 335 °C at 30 wt.% loading. This increase in Tg can be attributed to reduced chain flexibility due to the presence of the dispersed particles. Such phenomenon has also been observed for Cu-BPY-HFS/Matrimid [37]. Chung et al. prepared Matrimid® membranes containing benzylamine-modified C₆₀ and a 14 °C increase in Tg was observed, which indicates a strong interfacial interaction between

Matrimid®-PI and benzylamine-modified C₆₀ particles [24]. Also polymer chains may penetrate into the pores of Fe(BTC), which leads to chain rigidification of the nearby polymer chains outside the pores [43, 65]. The increasing T_g indicates good compatibility between the phases with favorable interaction [66]. As the T_g of the MMMs is comparable to the decomposition temperature of the MOF, it is not possible to anneal these membranes above their T_g to minimize the history effects. In order to minimise the history effects nevertheless, all membranes were prepared such that all had the same history.

Table 2.2. Glass transition temperature of Fe(BTC) MMMs.

| MOF contents (wt.%) | Polymer content (wt.%) | T _g (°C) ¹ |
|---------------------|------------------------|----------------------------------|
| 0 | 100 | 328 |
| 10 | 90 | 330 |
| 20 | 80 | 333 |
| 30 | 70 | 335 |

¹Typical error in DSC results ranges from ± 0.5 -1 °C.

2.3.2.3 Density analysis

Results of the density measurements are shown in Table 2.3. Matrimid®-PI shows a density of 1.22 g/cm³, which is comparable to what has been reported in literature [67]. However the experimentally determined density of Fe(BTC) shows a higher value than the bulk density reported by the manufacturer [54]. This is caused by different measurement technique used here that does not include the void spaces in the MOF particles [68], but determines the density of the real MOF material only.

Table 2.3. Theoretical and experimental densities of MMMs.

| MOF (wt.%) | Polymer (wt.%) | ρ_{exp} (g/cm ³) ¹ | ρ_{theo} (g/cm ³) |
|---------------|-------------------|--|--|
| 0 | 100 | 1.22 | --- |
| 10 | 90 | 1.27 | 1.25 |
| 20 | 80 | 1.31 | 1.29 |
| 30 | 70 | 1.35 | 1.33 |
| 100 | 0 | 1.67 | --- |

¹ The density measurements show an error of $\pm 4\text{-}8\%$.

As shown in Table 2.3, an increase in MMM density with increasing MOF loading is observed as expected due to the higher density of the pure MOF compared to that of the native Matrimid®-PI. To investigate whether the fabricated MMMs contain voids, a comparison between the experimental densities and the theoretical densities is conducted. The theoretical densities (ρ_{theo}) are calculated using Eq. 2.3.

$$\rho_{\text{theo}} = \left[W_P \cdot \left(\frac{1}{\rho_P} \right) + W_M \cdot \left(\frac{1}{\rho_M} \right) \right]^{-1} \quad \text{Eq. 2.3}$$

Where, ρ_P and ρ_M are the theoretical densities (g/cm³) of the pure polymer membrane and the pure MOF, respectively, and W_P and W_M are the weight fractions (-) of the polymer and MOF, respectively. The calculated theoretical densities are shown in Table 2.3 as well. For all Fe(BTC) MMMs the experimental densities are slightly higher than the theoretical values, although this difference is very small (in the experimental error range). These higher experimental density values may be attributed to the formation of a dense structure around the MOF particles [65, 69]. It suggests good interaction between the MOF particles and the polymer matrix and minimal presence of defects [40].

2.3.2.4 SEM analysis

SEM images of the pure Matrimid®-PI membrane and Fe(BTC)-MMM are shown in the Fig. 2.5. Fig. 2.5a and b shows the cross-section of the native Matrimid®-PI membrane, and both images show a smooth surface without any cracks or plastic deformation, which is characteristic for dense pure polymer membranes. Fig. 2.5c-h shows the

corresponding SEM images of the MMMs containing different loadings of mesoporous Fe(BTC). In the cross-sections, many submicron particles can be observed. The overall morphology of the MMMs shows good embedment of the particles within the matrix, indicating a homogeneous distribution. Fig 6c-h show the crater like morphology typical for the MMMs and the eye of each crater is formed by a MOF particle. As the loading increases the size of the craters becomes smaller. The appearance of the elongated matrix around MOF particles is probably due to the interfacial stress concentrations as a result of particle-matrix debonding [65]. At higher loadings (30 wt.%), particles tend to start to agglomerate slightly, but also some particle free regions appear (highlighted by the white circles in Fig. 2.5h). A higher magnification image of the 30 wt.% MMM is shown in Fig. 2.6, where particles seem to be completely enfolded by the matrix. No micron size non-selective voids are observed, which suggests that the contact between polymer and Fe(BTC) particles is excellent. Fig. 2.6 shows a strong interaction between Fe(BTC) particles and the Matrimid®-PI matrix, most probably due to the optimized mixing protocol for membrane preparation and good affinity of the organic linkers in the MOF to the Matrimid®-PI chains. Also as Fe(BTC) has microporous windows of 5.5 Å and 8.5 Å, the polymer chains in the vicinity of MOF may slightly penetrate into the pores of the MOF, which may also lead to good adhesion [69]. Homogeneous distribution of Fe(BTC) and absence of non-selective voids are essential for high performance gas separation membranes.

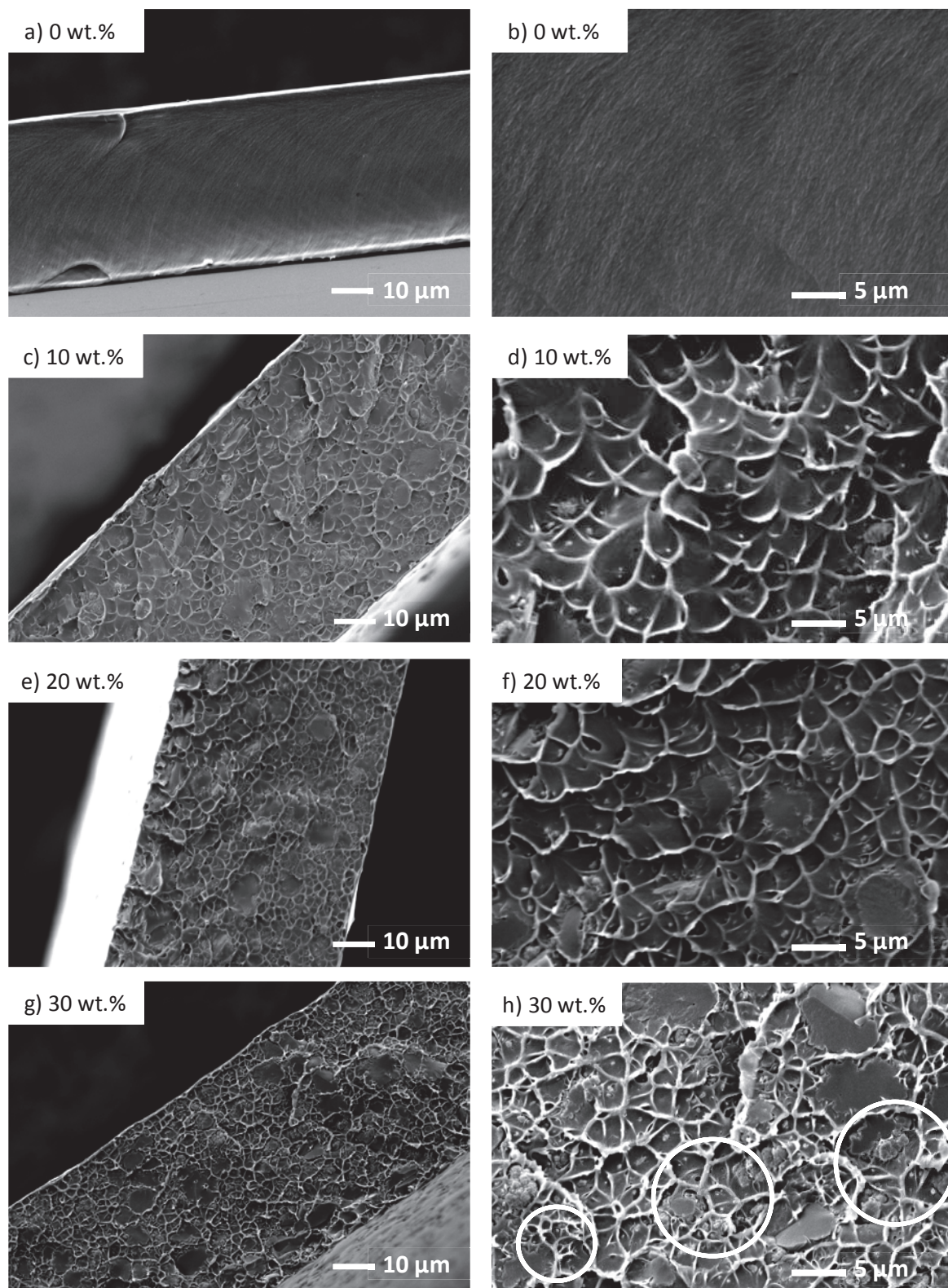


Fig. 2.5. SEM images of mixed-matrix membranes (a and b) cross section of native Matrimid®-PI membranes; (c and d) cross section 10 wt.% Fe(BTC); (e and f) cross section 20 wt.% Fe(BTC) (g and h) cross section 30 wt.% Fe(BTC) (magnification a ,c, e, g: 1000x; magnification b, d, f, h: 3000x)

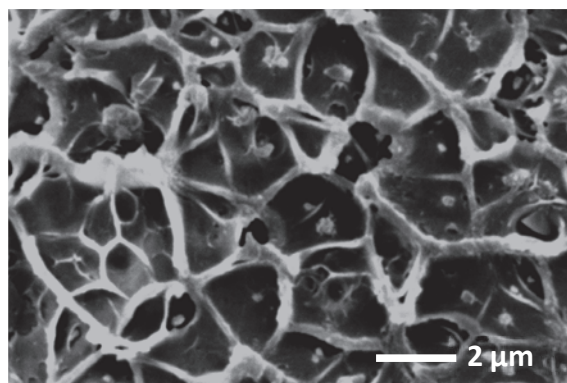


Fig. 2.6. SEM image of mixed-matrix membranes containing 30 wt.% Fe(BTC) particles (magnification: 9000x).

2.3.3 Gas separation measurements

2.3.3.1 Effect of Fe(BTC) loading

Fig. 2.7 shows the pure gas (a) absolute and (b) normalized CO_2 permeability at various concentrations of Fe(BTC) in Matrimid[®]-PI at 5 bar.

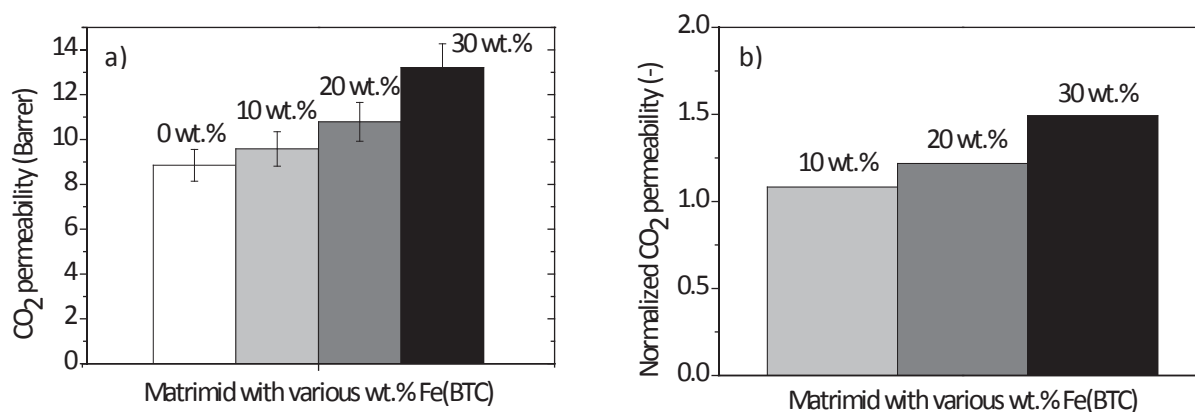


Fig. 2.7. Pure gas (a) absolute and (b) normalized CO_2 permeability (relative to pure Matrimid[®]-PI) of MMMs with various loadings of Fe(BTC) at 5 bar.

All MMMs show an increase in CO_2 permeability as the loading of Fe(BTC) increases, with the highest permeability increase for the 30 wt.% MMM (Fig. 2.7b). The CO_2 permeability of native Matrimid[®]-PI is around 8.5 Barrer and increases to 13.5 Barrer (60 % increase) with a Fe(BTC) loading of 30 wt.%. The enhanced CO_2 permeability may be attributed to the higher solubility of CO_2 in and diffusion through the MOF particles. The electrostatic interaction of CO_2 (strong quadrupole moment) with open metal sites of Fe(BTC), increases the sorption capacity of CO_2 , leading to higher gas sorption [36]. It

was previously reported that CO₂ molecules can form coordinated species on Lewis sites in other mesoporous MOFs (MIL-100 and MIL-101) [47]. These coordinated sites increase the uptake of CO₂ in mesoporous MOFs. Thus, increasing the solubility of CO₂ in the membranes.

Fig. 2.8 shows (a) the absolute and (b) normalized pure CH₄ permeability. The CH₄ permeability also slightly increases with increase in Fe(BTC) loading. However, the increase in CH₄ permeability is not as significant as it is for CO₂ (Fig. 2.7b, Fig. 2.8b), as there is no specific interaction present between CH₄ molecules (no quadrupole moment) and Fe(BTC) particles. The porous MOF particles provide an extra pore network for gas molecules, that facilitates the diffusion of gases (CO₂, CH₄) [45]. The increase in permeability with MOF loading can also be correlated to increased d-spacing of the membranes as observed by other researchers [40]. These results suggest that the increase in CO₂ permeability stems from an increase in both CO₂ solubility and diffusivity, while in the case of CH₄ the increase is due to an increase in diffusivity only.

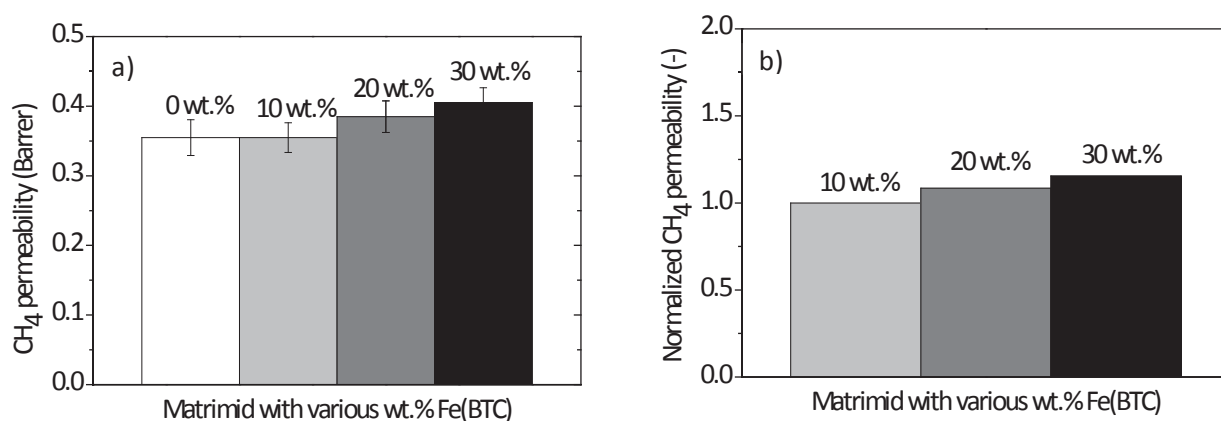


Fig. 2.8. Pure gas (a) absolute and (b) normalized CH₄ permeability of MMMs with various loadings of Fe(BTC) at 5 bar.

Ideal gas selectivity of MMMs shows a small improvement with Fe(BTC) loading as well (Fig. 2.9). All MMMs show enhanced selectivity compared to pristine Matrimid®-PI membranes indicating in general a higher intrinsic selectivity of the MOFs [36], although currently the intrinsic selectivity data of this particular MOF are still lacking in literature. As the relative increase in CO₂ permeability is higher than it is for CH₄ (Fig. 2.7b, Fig. 2.8b) it is clear that the higher ideal selectivity is a direct consequence of the higher

solubility of CO₂ gas because of the Fe(BTC) particles. When the Fe(BTC) loading increases from 0 wt.% to 30 wt.%, the selectivity increases from 24 to 30. Paired increase in permeability and selectivity suggests the absence of non-selective voids and good contact between Fe(BTC) particles and Matrimid®-PI. Similar results were observed by Chen et al. [70] for an amine functionalized MIL-53/PI system. These authors observed that for all MMMs, solubility selectivity is higher than diffusion selectivity. Moreover, the values increase with increasing MOF loading.

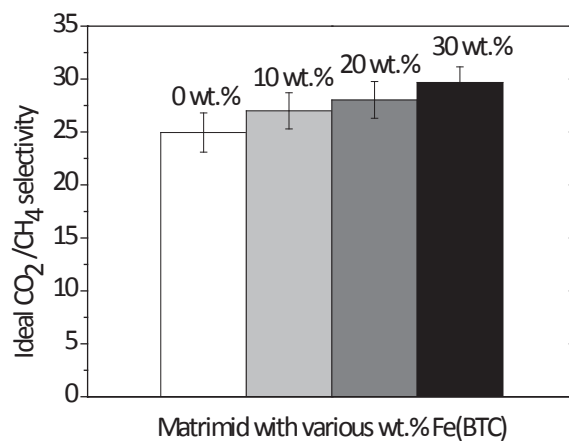


Fig. 2.9. Ideal CO₂/CH₄ selectivity of MMMs with various loadings of Fe(BTC) at 5 bar.

2.3.3.2 Effect of feed gas and feed pressure

It is known that high pressure CO₂ can plasticize glassy polymer membranes. Plasticization increases the permeability of especially the slower permeability component, thus decreasing the gas separation (selectivity) of gaseous mixtures [71]. To investigate this effect of the MOF MMMs, feed composition and feed pressures were varied and membrane permeability and selectivity were measured for Fe(BTC) MMMs. Fig. 2.10 shows the pure gas (a) absolute and (b) normalized CO₂ permeability as a function of the CO₂ pressure.

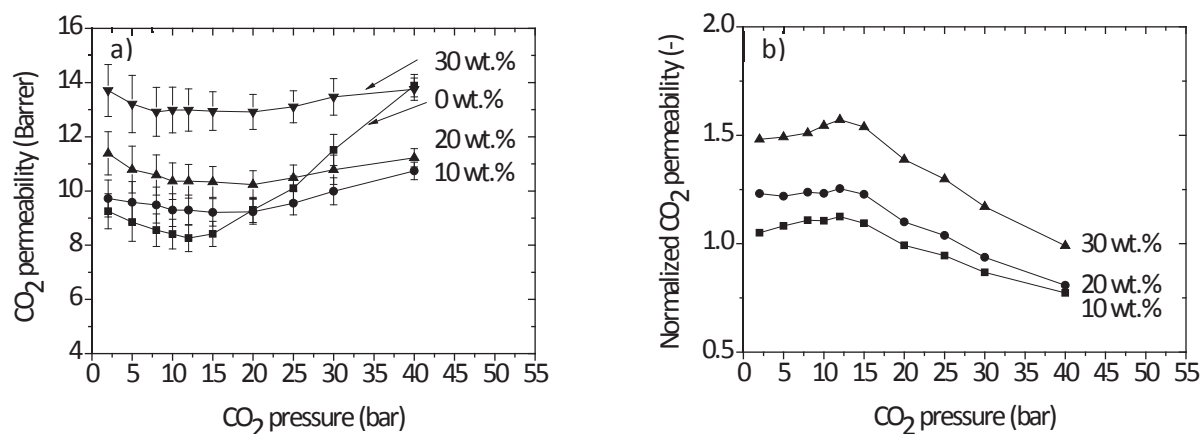


Fig. 2.10. Pure gas (a) absolute and (b) normalized CO₂ permeability of MMMs with different Fe(BTC) loading.

For the pure Matrimid®-PI membrane, below the plasticization pressure, as the pressure increases, the membranes permeability slightly decreases. This decrease in permeability at lower pressures stems from the decreasing solubility with increasing pressure, following the predicted behavior of dual-mode sorption model [72, 73]. As the CO₂ pressure increases further, more CO₂ is sorbed into the polymer matrix causing increased chain mobility and plasticization [74-76]. The enhanced chain mobility implies an increase in gas diffusion. This leads to an upward inflection in permeability with increase in pressure. For native Matrimid®-PI membranes Fig. 2.10a shows this behavior, with a plasticization pressure around 10 bar, which is consistent with literature [76].

All mixed-matrix membranes show a similar trend in permeability with pressure as that of the native Matrimid®-PI membrane. Below the plasticization pressure the permeability slightly decreases but the relative decrease in permeability is less compared to that of the native Matrimid®-PI membrane as shown by a continuous increase in normalized CO₂ permeability (Fig. 2.10b). At pressures higher than the plasticization pressure, permeability values only very slightly increase and even start to level off at higher loading of Fe(BTC). Normalized CO₂ permeabilities also decrease showing the relatively smaller increase in CO₂ permeability of the MMMs above the plasticization pressure compared to that of the pure polymer (Fig. 2.10b). This indicates the suppression of plasticization. Also the plasticization pressure seems to increase to higher values as the Fe(BTC) loading increases. It is hypothesized that MOF particles restrict the chain mobility in MMMs compared to the unfilled Matrimid®-PI membrane.

The increase in density and glass transition behavior also confirms this hypothesis. This restricted chain movement suppresses plasticization. Similar effects were achieved in literature by other techniques e.g. heat treatment of Matrimid®-PI films and blending with plasticization resistant polymers [77, 78].

Bos et al. reported that for pure glassy polymers above a critical plasticization concentration of CO₂, the increase in permeability is governed by the diffusion coefficient, which increases with pressure much more rapidly than the solubility coefficient, which decreases with pressure [76]. This increase in diffusion coefficient shoots up the CO₂ permeability in pure polymer membranes. For MMMs, as the increase in permeability above the plasticization pressure is limited compared to pure Matrimid®-PI, it is speculated that this small increase in permeability is due to the increase in solubility and diffusivity of MMMs due to the Fe(BTC) particles and not because of matrix plasticization. In a simulation study with Cu₃(BTC)₂ (structural analogy of Fe(BTC)) it was reported that CO₂ preferentially adsorbs around the metal site of the MOF, followed by adsorption in the small cage sites around the exposed metal sites and organic linkers. At high pressures the central cage gets filled [79]. As the central pore in Fe(BTC) is much larger than that of Cu₃(BTC)₂, it is believed to show even higher adsorption capacity and hence higher permeability. Considering this, the limited increase in permeability of the MMMs is a combined effect of strong adsorption, higher diffusion coefficient due to Fe(BTC) particles and suppression of CO₂ induced plasticization by the Fe(BTC) particles.

Fig. 2.11 shows the pure gas permeability of CH₄ of un-plasticized membranes. For pure CH₄ as feed all membranes show a continuous decrease in the CH₄ permeability with pressure as indicated by the dual mode sorption model. The decrease in permeability is due to a decrease in solubility coefficient with increasing pressure. For the MMMs containing Fe(BTC) the CH₄ permeability follows a similar trend as for pure Matrimid®-PI, except that the CH₄ permeability in the MOF containing membranes is higher than that of pure Matrimid®-PI membranes at all pressures. The decrease in permeability with increasing pressure is less pronounced with increasing MOF loading. So the decrease in matrix solubility with pressure is counterbalanced by the diffusivity increase of the membranes by the Fe(BTC) particles. This means that, since the pore size of

Fe(BTC) is larger than the kinetic diameter of CH₄, CH₄ can diffuse through the pores of the MOF more quickly than in the pure polymer.

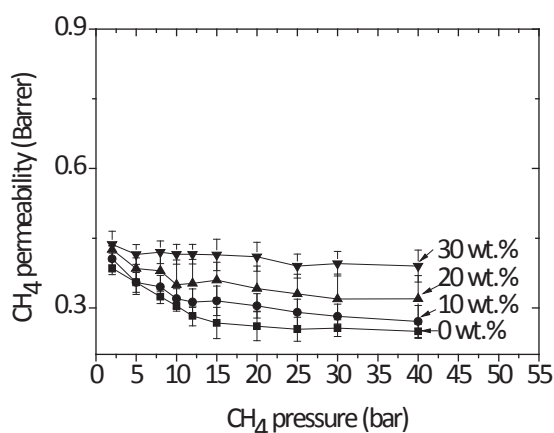


Fig. 2.11. Pure gas CH₄ permeability of MMMs with different Fe(BTC) loading.

In the case of mixed gases, CO₂ induced plasticization influences especially the permeation rate of the slower permeating component (i.e. CH₄). Due to the swelling of the polymer matrix and the associated local polymer mobility, the permeability of the slower component CH₄ increases to a larger extent than that of CO₂, leading to decreased (diffusion) selectivity. Therefore, pure gas measurements greatly over predict the real membrane performance due to the occurrence of plasticization effects. To investigate this effect mixed gas separation experiments with a gas mixture of CO₂/CH₄ (50/50 mol %) were performed over a range of pressures. The results for the mixed gas CO₂ permeability are depicted in Fig. 2.12.

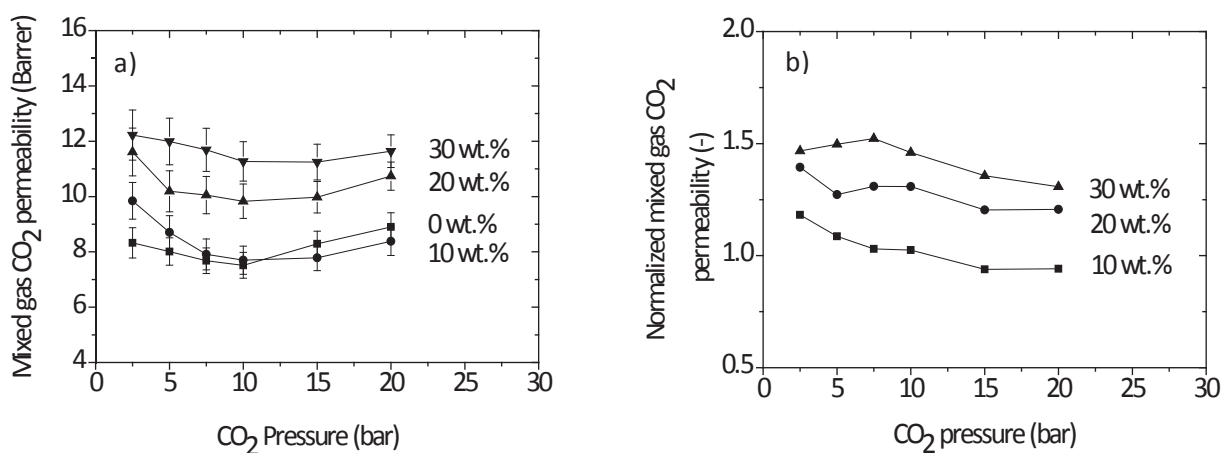


Fig. 2.1. Mixed gas (a) absolute and (b) normalized CO₂ permeability of MMMs with different Fe(BTC) loadings.

Pure Matrimid®-PI membranes show similar behavior as for pure gas measurements but slightly lower CO₂ permeability values than for pure gas measurements. The presence of CH₄ slightly reduces the CO₂ permeability as a result of competitive sorption [55]. This is in agreement with data reported in literature [80, 81]. For Fe(BTC) MMMs, as the Fe(BTC) loading increases the decrease in CO₂ permeability becomes smaller and almost vanishes at high pressures. This effect can be ascribed to the high CO₂ sorption capacity of mesoporous MOF (Fe(BTC)) [44, 80].

For mixed gas, the CH₄ permeability shows a different trend when compared to the pure gas measurements (Fig. 2.13). For pure Matrimid®-PI membranes, the CH₄ permeability shows the typical behavior of increased permeability of the less mobile component after the plasticization pressure is reached. For MMMs the permeability of CH₄ increases as the loading of the Fe(BTC) increases. The relative value of increment of permeability of CH₄ is less compared to that of pure gas measurements due the presence of a second gas (competitive sorption) (Fig. 2.13b). As the pressure increases below the plasticization pressure, the permeability of CH₄ slightly decreases similar to the pure gas measurements. But when the pressure increases above the plasticization pressure, the permeability of CH₄ shows a slight upward turn. This increase in CH₄ permeability becomes smaller as the loading of Fe(BTC) increases indicating an increased resistance against plasticization. The higher the MOF loading, the stronger this effect and the stronger the suppression of plasticization. This effect is more clear in Fig. 2.13b. At pressures below the plasticization pressure the normalized mixed gas CH₄ permeability stays more or less constant but as the plasticization pressure is reached the normalized mixed gas CH₄ permeability shows a sharp decrease in value as the absolute CH₄ permeability increase of pure Matrimid®-PI is higher than the absolute CH₄ permeability of MMMs.

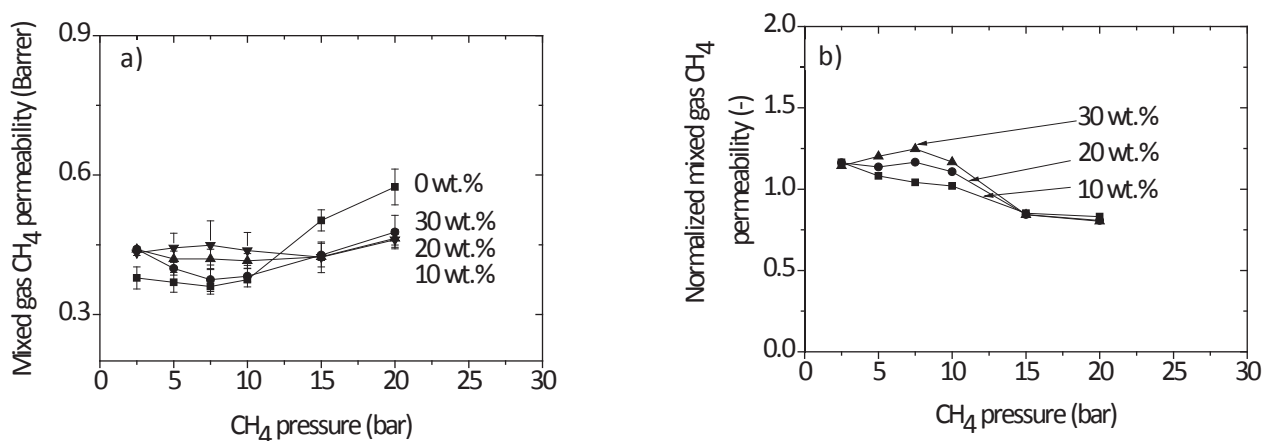


Fig. 2.23. Mixed gas (a) absolute and (b) normalized CH₄ permeability of MMMs with different Fe(BTC) loading.

Fig. 2.14a shows the pure gas CO₂/CH₄ selectivity of pristine Matrimid®-PI membranes and the MMMs while Fig. 2.14b shows the corresponding values for the gas mixtures. The pure gas selectivity of the native Matrimid®-PI membrane shows a slight increase below the plasticization pressure and increases swiftly as the pressure rises above the plasticization pressure showing a strong increase in CO₂ diffusion coefficient [76]. A high CO₂ concentration in the pure polymer membrane leads to excessive chain swelling, resulting in an accelerated increase in segmental mobility of the polymer chains leading to higher diffusion coefficients for CO₂ in this case. The pure gas selectivity of the MMMs is higher than that of the pure Matrimid®-PI membrane at all pressures below the plasticization pressure, but above the plasticization pressure the MOF-MMMs with higher loadings show the lowest ideal selectivity value. In MMMs, MOF particles limit the polymer chain mobility. As the MOF loading increases the chain mobility further decreases. Thus, 30 wt.% MMM shows highest resistance against CO₂ induced plasticization.

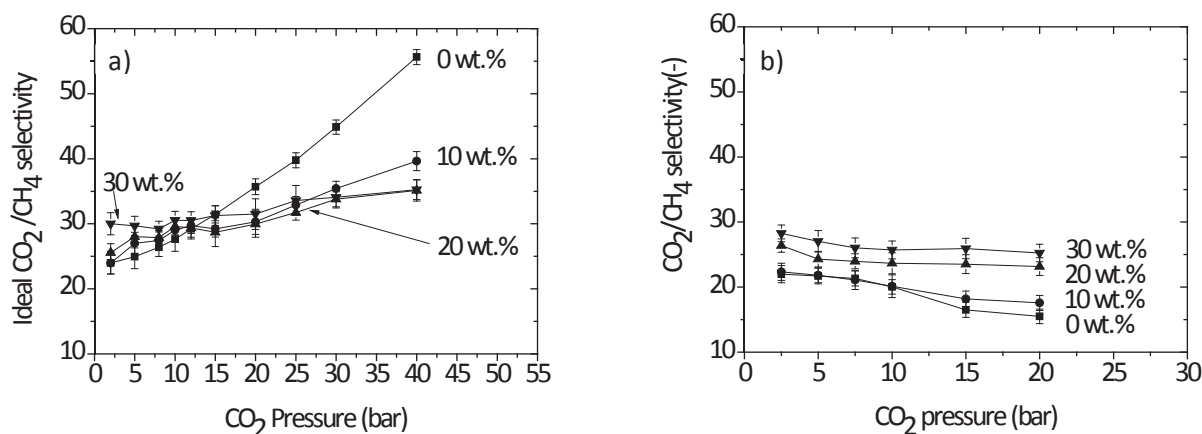


Fig. 2.34. (a) Pure gas CO₂/CH₄ selectivity and (b) mixed gas CO₂/CH₄ selectivity of MMMs with different Fe(BTC) loadings.

Fig. 2.14b shows the mixed gas separation factor obtained with a 50/50 mol % CO₂/CH₄ mixture as a function of the CO₂ pressure for different MOF loadings. The mixture selectivity is enormously different from ideal selectivity that can be attributed to the multicomponent effects in separating mixtures. For native Matrimid®-PI, the selectivity decreases with increasing feed pressure and plasticization is clearly evident by a significant decrease in CO₂/CH₄ selectivity (45%). The polymer matrix swells excessively due to the presence of CO₂, which in result increases the gas diffusion through the polymer of especially the slower permeating component CH₄ and thus decreases the selectivity.

The MMMs show an entirely different behavior. All MMMs show higher selectivity than pure Matrimid®-PI membranes at all pressures investigated and selectivity clearly increases with increasing Fe(BTC) loading. The increase in selectivity can be attributed to the high CO₂ adsorption of Fe(BTC) with pressure, a consequence of electrostatic interaction between CO₂ and Fe(BTC) framework. It is interesting to observe that as the Fe(BTC) loading increases, the membranes show more or less constant selectivity over the whole pressure range. The MOF loading increases the permeability of CO₂ more than that of CH₄, consequently the selectivity of the membrane also increases. On the other hand, plasticized matrix increases the permeability of CH₄, which reduces the selectivity of the membranes. The overall result on the membrane performance is a balance between these two competing phenomena. As diffusion selectivity is size dependent, it is in favor of CO₂ also the sorption selectivity strongly favors CO₂ over CH₄. When

comparing the permeability and selectivity data of pure and mixed gases in MMMs, it can be stated that the diffusion selectivity favors CO₂ over CH₄ and weakly contributed to mixture selectivity while mixture selectivity is dominated by the solubility selectivity enhancement of CO₂. This is also observed in other MOFs systems [79, 82, 83].

2.4 Conclusions

A series of flat sheet dense MMMs was prepared with mesoporous Fe(BTC) nanoparticles as filler and Matrimid®-PI as polymer matrix. An optimized priming and suspension mixing protocol resulted in a homogeneous distribution of MOF particles in the Matrimid-PI matrix, as observed by scanning electron microscope (SEM). Mesoporous Fe(BTC) MOF particles showed excellent compatibility with polymer. When Fe(BTC) was added to the Matrimid®-PI matrix both the permeability and selectivity were effectively enhanced. At low pressures of 5 bar MMMs showed an increase of 60 % and 29 % in permeability and ideal selectivity respectively, over pure Matrimid®-PI membranes. As the CO₂ pressure increases native Matrimid®-PI membranes showed typical plasticization behavior, while in MMMs, Fe(BTC) particles restrict the mobility of polymer chains thus suppressing CO₂ induced plasticization. As a consequence of this, the plasticization pressure also increases to higher values. At a pressure of 40 bar, MMMs showed a mixed gas (CO₂/CH₄ 50/50) selectivity increase of 62 % compared to the pure Matrimid®-PI membrane. As the Fe(BTC) loading increases, the membranes show more or less constant selectivity over the whole pressure range due to the suppression of CO₂ induced plasticization by the presence of MOF particles. The permeability and selectivity of Fe(BTC) MMMs are a combined effect of increased adsorption, diffusivity and reduced CO₂ induced plasticization.

Acknowledgements

The authors would like to thank the Erasmus Mundus Doctorate in Membrane Engineering (EUDIME) for funding this research.

References

[1] S. Basu, A.L. Khan, A. Cano-Odena, C. Liu, I.F.J. Vankelecom, Membrane-based technologies for biogas separations, *Chemical Society Reviews*, 39 (2010) 750-768.

- [2] Y. He, D.M. Bagley, K.T. Leung, S.N. Liss, B.-Q. Liao, Recent advances in membrane technologies for biorefining and bioenergy production, *Biotechnology Advances*, 30 (2012) 817-858.
- [3] E.D. Bates, R.D. Mayton, I. Ntai, J.H. Davis, CO₂ capture by a task-specific ionic liquid, *Journal of the American Chemical Society*, 124 (2002) 926-927.
- [4] S. Ma'mun, V.Y. Dindore, H.F. Svendsen, Kinetics of the reaction of carbon dioxide with aqueous solutions of 2-((2-Aminoethyl)amino)ethanol, *Industrial & Engineering Chemistry Research*, 46 (2006) 385-394.
- [5] S.A. Rackley, *Carbon capture and storage*, Elsevier, (2010).
- [6] A. Brunetti, F. Scura, G. Barbieri, E. Drioli, Membrane technologies for CO₂ separation, *J. Membr. Sci.*, 359 (2010) 115-125.
- [7] L.M. Robeson, Correlation of separation factor versus permeability for polymeric membranes, *J. Membr. Sci.*, 62 (1991) 165-185.
- [8] L.M. Robeson, Polymer membranes for gas separation, *Current Opinion in Solid State & Materials Science*, 4 (1999) 549-552.
- [9] L.M. Robeson, The upper bound revisited, *J. Membr. Sci.*, 320 (2008) 390-400.
- [10] Y. Li, T.S. Chung, Z. Huang, S. Kulprathipanja, Dual-layer polyethersulfone (PES)/BTDA-TDI/MDI co-polyimide (P84) hollow fiber membranes with a submicron PES-zeolite beta mixed matrix dense-selective layer for gas separation, *J. Membr. Sci.*, 277 (2006) 28-37.
- [11] T.W. Pechar, S. Kim, B. Vaughan, E. Marand, M. Tsapatsis, H.K. Jeong, C.J. Cornelius, Fabrication and characterization of polyimide-zeolite L mixed matrix membranes for gas separations, *J. Membr. Sci.*, 277 (2006) 195-202.
- [12] T.W. Pechar, S. Kim, B. Vaughan, E. Marand, V. Baranauskas, J. Riffle, H.K. Jeong, M. Tsapatsis, Preparation and characterization of a poly(imide siloxane) and zeolite L mixed matrix membrane, *J. Membr. Sci.*, 277 (2006) 210-218.
- [13] L.Y. Jiang, T.S. Chung, S. Kulprathipanja, An investigation to revitalize the separation performance of hollow fibers with a thin mixed matrix composite skin for gas separation, *J. Membr. Sci.*, 276 (2006) 113-125.
- [14] Y. Li, H.M. Guan, T.S. Chung, S. Kulprathipanja, Effects of novel silane modification of zeolite surface on polymer chain rigidification and partial pore blockage in polyethersulfone (PES)-zeolite A mixed matrix membranes, *J. Membr. Sci.*, 275 (2006) 17-28.
- [15] L.Y. Jiang, T.S. Chung, C. Cao, Z. Huang, S. Kulprathipanja, Fundamental understanding of nano-sized zeolite distribution in the formation of the mixed matrix single- and dual-layer asymmetric hollow fiber membranes, *J. Membr. Sci.*, 252 (2005) 89-100.
- [16] G. Golemme, A. Bruno, R. Manes, D. Muoio, Preparation and properties of superglassy polymers - zeolite mixed matrix membranes, *Desalination*, 200 (2006) 440-442.

- [17] H.M. Guan, T.S. Chung, Z. Huang, M.L. Chng, S. Kulprathipanja, Poly(vinyl alcohol) multilayer mixed matrix membranes for the dehydration of ethanol-water mixture, *J. Membr. Sci.*, 268 (2006) 113-122.
- [18] D. Vu, W.J. Koros, S.J. Miller, Effect of condensable impurity in CO₂/CH₄ gas feeds on performance of mixed matrix membranes using carbon molecular sieves, *J. Membr. Sci.*, 221 (2003) 233-239.
- [19] D.Q. Vu, W.J. Koros, S.J. Miller, Mixed matrix membranes using carbon molecular sieves - I. Preparation and experimental results, *J. Membr. Sci.*, 211 (2003) 311-334.
- [20] D.Q. Vu, W.J. Koros, S.J. Miller, Mixed matrix membranes using carbon molecular sieves - II. Modeling permeation behavior, *J. Membr. Sci.*, 211 (2003) 335-348.
- [21] M. Anson, J. Marchese, E. Garis, N. Ochoa, C. Pagliero, ABS copolymer-activated carbon mixed matrix membranes for CO₂/CH₄ separation, *J. Membr. Sci.*, 243 (2004) 19-28.
- [22] M. Sairam, M.B. Patil, R.S. Veerapur, S.A. Patil, T.M. Aminabhavi, Novel dense poly(vinyl alcohol)-TiO₂ mixed matrix membranes for pervaporation separation of water-isopropanol mixtures at 30 degrees C, *J. Membr. Sci.*, 281 (2006) 95-102.
- [23] D. Gomes, S.P. Nunes, K.V. Peinemann, Membranes for gas separation based on poly(1-trimethylsilyl-1-propyne)-silica nanocomposites, *J. Membr. Sci.*, 246 (2005) 13-25.
- [24] T.S. Chung, S.S. Chan, R. Wang, Z.H. Lu, C.B. He, Characterization of permeability and sorption in Matrimid/C-60 mixed matrix membranes, *J. Membr. Sci.*, 211 (2003) 91-99.
- [25] S. Kim, T.W. Pechar, E. Marand, Poly(imide siloxane) and carbon nanotube mixed matrix membranes for gas separation, *Desalination*, 192 (2006) 330-339.
- [26] J.-R. Li, Y. Ma, M.C. McCarthy, J. Sculley, J. Yu, H.-K. Jeong, P.B. Balbuena, H.-C. Zhou, Carbon dioxide capture-related gas adsorption and separation in metal-organic frameworks, *Coordination Chemistry Reviews*, 255 (2011) 1791-1823.
- [27] P.S. Goh, A.F. Ismail, S.M. Sanip, B.C. Ng, M. Aziz, Recent advances of inorganic fillers in mixed matrix membrane for gas separation, *Separation and Purification Technology*, 81 (2011) 243-264.
- [28] U. Mueller, M. Schubert, F. Teich, H. Puetter, K. Schierle-Arndt, J. Pastre, Metal-organic frameworks - prospective industrial applications, *Journal of Materials Chemistry*, 16 (2006) 626-636.
- [29] L. Pan, D.H. Olson, L.R. Ciemnomolonski, R. Heddy, J. Li, Separation of hydrocarbons with a microporous metal-organic framework, *Angewandte Chemie-International Edition*, 45 (2006) 616-619.
- [30] J.R. Long, O.M. Yaghi, The pervasive chemistry of metal-organic frameworks, *Chemical Society Reviews*, 38 (2009) 1213-1214.
- [31] J.-R. Li, R.J. Kuppler, H.-C. Zhou, Selective gas adsorption and separation in metal-organic frameworks, *Chemical Society Reviews*, 38 (2009) 1477-1504.

- [32] R. Krishna, J.M. van Baten, A comparison of the CO₂ capture characteristics of zeolites and metal-organic frameworks, *Separation and Purification Technology*, 87 (2012) 120-126.
- [33] J.L.C. Rowsell, O.M. Yaghi, Metal-organic frameworks: a new class of porous materials, *Microporous and Mesoporous Materials*, 73 (2004) 3-14.
- [34] S. Basu, M. Maes, A. Cano-Odena, L. Alaerts, D.E. De Vos, I.F.J. Vankelecom, Solvent resistant nanofiltration (SRNF) membranes based on metal-organic frameworks, *J. Membr. Sci.*, 344 (2009) 190-198.
- [35] A.R. Millward, O.M. Yaghi, Metal-organic frameworks with exceptionally high capacity for storage of carbon dioxide at room temperature, *Journal of the American Chemical Society*, 127 (2005) 17998-17999.
- [36] Q. Yang, C. Zhong, Molecular simulation of carbon dioxide/methane/hydrogen mixture adsorption in metal-organic frameworks, *Journal of Physical Chemistry B*, 110 (2006) 17776-17783.
- [37] Y. Zhang, I.H. Musselman, J.P. Ferraris, K.J. Balkus, Jr., Gas permeability properties of Matrimid® membranes containing the metal-organic framework Cu-BPY-HFS, *J. Membr. Sci.*, 313 (2008) 170-181.
- [38] R. Adams, C. Carson, J. Ward, R. Tannenbaum, W. Koros, Metal organic framework mixed matrix membranes for gas separations, *Microporous and Mesoporous Materials*, 131 (2010) 13-20.
- [39] M.J.C. Ordoñez, K.J. Balkus Jr, J.P. Ferraris, I.H. Musselman, Molecular sieving realized with ZIF-8/Matrimid® mixed-matrix membranes, *J. Membr. Sci.*, 361 (2010) 28-37.
- [40] S. Basu, A. Cano-Odena, I.F.J. Vankelecom, Asymmetric Matrimid®/Cu₃(BTC)₂ mixed-matrix membranes for gas separations, *J. Membr. Sci.*, 362 (2010) 478-487.
- [41] S. Basu, A. Cano-Odena, I.F.J. Vankelecom, MOF-containing mixed-matrix membranes for CO₂/CH₄ and CO₂/N₂ binary gas mixture separations, *Separation and Purification Technology*, 81 (2011) 31-40.
- [42] J. Ploegmakers, S. Japip, K. Nijmeijer, Mixed matrix membranes containing MOFs for ethylene/ethane separation-Part B: Effect of Cu₃BTC₂ on membrane transport properties, *J. Membr. Sci.*, 428 (2013) 331-340.
- [43] J. Ploegmakers, S. Japip, K. Nijmeijer, Mixed matrix membranes containing MOFs for ethylene/ethane separation Part A: Membrane preparation and characterization, *J. Membr. Sci.*, 428 (2013) 445-453.
- [44] D. Farrusseng, Metal organic frameworks: Applications from catalysis to gas storage, (2011) 112.
- [45] E.V. Perez, K.J. Balkus, Jr., J.P. Ferraris, I.H. Musselman, Mixed-matrix membranes containing MOF-5 for gas separations, *J. Membr. Sci.*, 328 (2009) 165-173.
- [46] B. Zornoza, A. Martinez-Joaristi, P. Serra-Crespo, C. Tellez, J. Coronas, J. Gascon, F. Kapteijn, Functionalized flexible MOFs as fillers in mixed matrix membranes for highly

selective separation of CO₂ from CH₄ at elevated pressures, *Chemical Communications*, 47 (2011) 9522-9524.

[47] P.L. Llewellyn, S. Bourrelly, C. Serre, A. Vimont, M. Daturi, L. Hamon, G. De Weireld, J.-S. Chang, D.-Y. Hong, Y.K. Hwang, S.H. Jung, G. Férey, High uptakes of CO₂ and CH₄ in mesoporous metal-organic frameworks MIL-100 and MIL-101, *Langmuir*, 24 (2008) 7245-7250.

[48] H.B.T. Jeazet, C. Staudt, C. Janiak, A method for increasing permeability in O₂/N₂ separation with mixed-matrix membranes made of water-stable MIL-101 and polysulfone, *Chemical Communications*, 48 (2012) 2140-2142.

[49] E. Soubeyrand-Lenoir, C. Vagner, J.W. Yoon, P. Bazin, F. Ragon, Y.K. Hwang, C. Serre, J.-S. Chang, P.L. Llewellyn, How Water Fosters a Remarkable 5-Fold Increase in Low-Pressure CO₂ Uptake within Mesoporous MIL-100(Fe), *Journal of the American Chemical Society*, 134 (2012) 10174-10181.

[50] J.W. Yoon, Y.-K. Seo, Y.K. Hwang, J.-S. Chang, H. Leclerc, S. Wuttke, P. Bazin, A. Vimont, M. Daturi, E. Bloch, P.L. Llewellyn, C. Serre, P. Horcajada, J.-M. Greneche, A.E. Rodrigues, G. Férey, Controlled Reducibility of a Metal-Organic Framework with Coordinatively Unsaturated Sites for Preferential Gas Sorption, *Angewandte Chemie-International Edition*, 49 (2010) 5949-5952.

[51] P. Horcajada, S. Surble, C. Serre, D.-Y. Hong, Y.-K. Seo, J.-S. Chang, J.-M. Greneche, I. Margiolaki, G. Férey, Synthesis and catalytic properties of MIL-100(Fe), an iron(III) carboxylate with large pores, *Chemical Communications*, (2007) 2820-2822.

[52] P. Kuesgens, M. Rose, I. Senkowska, H. Froede, A. Henschel, S. Siegle, S. Kaskel, Characterization of metal-organic frameworks by water adsorption, *Microporous and Mesoporous Materials*, 120 (2009) 325-330.

[53] H.-K. Youn, J. Kim, W.-S. Ahn, MWCNT synthesis over Fe-BTC as a catalyst/carbon source via CVD, *Materials Letters*, 65 (2011) 3055-3057.

[54] <http://www.sigmaaldrich.com/catalog/product/aldrich/690872lang=fr®ion=FR>.

[55] T. Visser, G.H. Koops, M. Wessling, On the subtle balance between competitive sorption and plasticization effects in asymmetric hollow fiber gas separation membranes, *J. Membr. Sci.*, 252 (2005) 265-277.

[56] P.H. Pfromm, W.J. Koros, Accelerated physical aging of thin glassy polymer-films - evidence from gas-transport measurements, *Polymer*, 36 (1995) 2379-2387.

[57] M. Wessling, I. Huisman, T. Vanderboomgaard, C.A. Smolders, Time-dependent permeation of carbon-dioxide through a polyimide membrane above the plasticization pressure, *Journal of Applied Polymer Science*, 58 (1995) 1959-1966.

[58] K.F. Babu, M.A. Kulandainathan, I. Katsounaros, L. Rassaei, A.D. Burrows, P.R. Raithby, F. Marken, Electrocatalytic activity of Basolite (TM) F300 metal-organic-framework structures, *Electrochemistry Communications*, 12 (2010) 632-635.

[59] A. Centrone, E.E. Santiso, T.A. Hatton, Separation of Chemical Reaction Intermediates by Metal-Organic Frameworks, *Small*, 7 (2011) 2356-2364.

- [60] T.T. Moore, W.J. Koros, Non-ideal effects in organic–inorganic materials for gas separation membranes, *Journal of Molecular Structure*, 739 (2005) 87-98.
- [61] P. Hacıoğlu, L. Toppare, L. Yılmaz, Effect of preparation parameters on performance of dense homogeneous polycarbonate gas separation membranes, *Journal of Applied Polymer Science*, 90 (2003) 776-785.
- [62] H. Leclerc, A. Vimont, J.-C. Lavalley, M. Daturi, A.D. Wiersum, P.L. Llewellyn, P. Horcajada, G. Férey, C. Serre, Infrared study of the influence of reducible iron(III) metal sites on the adsorption of CO, CO₂, propane, propene and propyne in the mesoporous metal-organic framework MIL-100, *Physical Chemistry Chemical Physics*, 13 (2011) 11748-11756.
- [63] R. Canioni, C. Roch-Marchal, F. Secheresse, P. Horcajada, C. Serre, M. Hardi-Dan, G. Férey, J.-M. Grenèche, F. Lefebvre, J.-S. Chang, Y.-K. Hwang, O. Lebedev, S. Turner, G. Van Tendeloo, Stable polyoxometalate insertion within the mesoporous metal organic framework MIL-100(Fe), *Journal of Materials Chemistry*, 21 (2011) 1226-1233.
- [64] C. Joly, D. Le Cerf, C. Chappey, D. Langevin, G. Muller, Residual solvent effect on the permeation properties of fluorinated polyimide films, *Separation and Purification Technology*, 16 (1999) 47-54.
- [65] Y. Zhang, K.J. Balkus Jr, I.H. Musselman, J.P. Ferraris, Mixed-matrix membranes composed of Matrimid® and mesoporous ZSM-5 nanoparticles, *J. Membr. Sci.*, 325 (2008) 28-39.
- [66] Z.-K. Zhu, Y. Yang, J. Yin, Z.-N. Qi, Preparation and properties of organosoluble polyimide/silica hybrid materials by sol-gel process, *Journal of Applied Polymer Science*, 73 (1999) 2977-2984.
- [67] <http://www.lindberg-lund.fi/files/Teknisk%20datablad/VAN-5218-TD.pdf>.
- [68] P.A. Webb, Volume and Density Determinations for Particle Technologists, http://www.anime.micrx.com/Repository/Files/Volume_and_Density_determinations_for_Particle_Technologists.pdf (2001).
- [69] H. Ren, J. Jin, J. Hu, H. Liu, Affinity between Metal-organic frameworks and polyimides in asymmetric mixed matrix membranes for gas separations, *Industrial & Engineering Chemistry Research*, 51 (2012) 10156-10164.
- [70] X.Y. Chen, H. Vinh-Thang, D. Rodrigue, S. Kaliaguine, Amine-Functionalized MIL-53 Metal-organic framework in polyimide mixed matrix membranes for CO₂/CH₄ separation, *Industrial & Engineering Chemistry Research*, 51 (2012) 6895-6906.
- [71] C. Staudt-Bickel, W.J. Koros, Improvement of CO₂/CH₄ separation characteristics of polyimides by chemical crosslinking, *J. Membr. Sci.*, 155 (1999) 145-154.
- [72] D.R. Paul, Gas sorption and transport in glassy-polymers, *Berichte Der Bunsen-Gesellschaft-Physical Chemistry Chemical Physics*, 83 (1979) 294-302.
- [73] V. Stannett, The transport of gases in synthetic polymeric membranes — an historic perspective, *J. Membr. Sci.*, 3 (1978) 97-115.
- [74] T. Visser, M. Wessling, When do sorption-induced relaxations in glassy polymers set in?, *Macromolecules*, 40 (2007) 4992-5000.

- [75] T. Visser, N. Masetto, M. Wessling, Materials dependence of mixed gas plasticization behavior in asymmetric membranes, *J. Membr. Sci.*, 306 (2007) 16-28.
- [76] A. Bos, I.G.M. Punt, M. Wessling, H. Strathmann, CO₂-induced plasticization phenomena in glassy polymers, *J. Membr. Sci.*, 155 (1999) 67-78.
- [77] A. Bos, I.G.M. Punt, M. Wessling, H. Strathmann, Suppression of CO₂-plasticization by semiinterpenetrating polymer network formation, *Journal of Polymer Science Part B-Polymer Physics*, 36 (1998) 1547-1556.
- [78] A. Bos, I. Punt, H. Strathmann, M. Wessling, Suppression of gas separation membrane plasticization by homogeneous polymer blending, *Aiche Journal*, 47 (2001) 1088-1093.
- [79] J. Jose Gutierrez-Sevillano, A. Caro-Perez, D. Dubbeldam, S. Calero, Molecular simulation investigation into the performance of Cu-BTC metal-organic frameworks for carbon dioxide-methane separations, *Physical Chemistry Chemical Physics*, 13 (2011) 20453-20460.
- [80] P.C. Raymond, W.J. Koros, D.R. Paul, Comparison of mixed and pure gas permeation characteristics for CO₂ and CH₄ in copolymers and blends containing methyl-methacrylate units, *J. Membr. Sci.*, 77 (1993) 49-57.
- [81] J. Ahn, W.J. Chung, I. Pinnau, M.D. Guiver, Polysulfone/silica nanoparticle mixed-matrix membranes for gas separation, *J. Membr. Sci.*, 314 (2008) 123-133.
- [82] S. Keskin, Atomistic simulations for adsorption, diffusion, and separation of gas mixtures in zeolite imidazolate frameworks, *Journal of Physical Chemistry C*, 115 (2011) 800-807.
- [83] R. Krishna, Adsorptive separation of CO₂/CH₄/CO gas mixtures at high pressures, *Microporous and Mesoporous Materials*, 156 (2012) 217-223.

Chapter 3

Performance and plasticization behavior of polymer-MOF membranes for gas separation at elevated pressures

This chapter has been published as:

S. Shahid, K. Nijmeijer, Performance and plasticization behavior of polymer-MOF membranes for gas separation at elevated pressures, *J. Membr. Sci.*, 470 (2014) 166-177.

ABSTRACT

Mixed matrix membranes (MMMs) based on three distinctively different MOFs (MIL-53(Al) (breathing MOF), ZIF-8 (flexible MOF) and Cu_3BTC_2 (rigid MOF)) dispersed in Matrimid[®]-PI have been investigated. MOF loading was varied between 0 wt% to 30 wt%. The fabricated MOF-MMMs were characterized for pure and binary gas mixture separations at low and high pressures and their performance in terms of CO_2 permeability and CO_2/CH_4 selectivity was evaluated. The use of a less volatile co-solvent, optimized priming protocol to prepare the MMMs and thermal annealing resulted in a good dispersion of MOF particles in the Matrimid[®]-PI matrix. Incorporation of MOFs resulted in increased density, T_g and improved degradation behavior of the membranes confirming a good compatibility between the polymer and the MOFs. Low pressure gas separation showed moderate enhancement in CO_2 permeability and CO_2/CH_4 selectivity of MOF-MMMs compared to native polymer membranes, but the improvement becomes pronounced at high pressures. At high pressures, the native Matrimid[®]-PI membrane showed typical plasticization behavior, while in MMMs, MOF particles limit the mobility of polymer chains thus suppressing CO_2 induced plasticization and maintain large separation factors over a wide pressure range investigated. The respective increase in performance of MMMs is very much dependent on MOF crystal structure and its interactions with CO_2 gas molecules. Among the three MOF-MMMs, membranes based on Cu_3BTC_2 showed highest selectivity while ZIF-8 based membranes showed highest permeability. In general it can be concluded that the high CO_2 permeability and CO_2/CH_4 selectivity of MMMs is the combined effect of an increased sorption and diffusion selectivity and reduced plasticization. Overall, this work reveals that MOF-MMMs delay CO_2 induced plasticization and show good separation performance even at high pressures, showing their potential to a wide range of newly emerging high pressure energy applications.

3.1 Introduction

CO₂ capture and gas separation through polymeric membranes has emerged as an important competitive technology. It offers several economic eco-friendly advantages over traditional separation processes such as cryogenic distillation and adsorption [1], which involve larger amounts of energy due to phase changes of constituents. However as frequently reported, development of polymeric membranes is limited by a trade-off between membrane permeability and selectivity [2, 3]. Additionally, especially in high pressure gas separations involving high concentrations of CO₂, plasticization is of major concern. The dissolution of CO₂ in the polymer matrix disrupts chain packing and enhances the intersegmental mobility and associated decrease in membrane performance [4].

As a mean to overcome material limitations, mixed-matrix membranes comprising of inorganic particles e.g. zeolites [5-9], carbon materials [10-13] and MOFs [14], dispersed in an easy processable polymer matrix provide an interesting approach for improving the gas separation properties of polymeric membranes [15]. MOFs have appeared as a new class of microporous hybrid materials that consist of an inorganic cluster connected by organic bridges, tuned into 1D, 2D, 3D dimensional arrangements. The self-assembling of complex structural units (organic and inorganic) in MOFs endows them with high surface area, controlled porosity, adjustable chemical functionality, high affinity for certain gases and compatibility with polymer chains, making them most outstanding candidates to make high performance mixed-matrix membranes [16, 17].

Incorporation of MOFs into a polymer matrix to fabricate MOF based MMMs has been intensively studied in recent years. Musselman and co-workers [18] reported the first ZIF-8 based polymer MMMs using Matrimid®-PI as polymer phase. Addition of the ZIF phase substantially increased the membrane selectivity. MMMs with a ZIF loading of 50 wt% showed an increase of 188 % in ideal selectivity. Also mixed gas measurements of 10:90 CO₂/CH₄ showed a 110 % selectivity enhancement. Basu et al. prepared MMMs by combining the commercial MOFs Cu₃BTC₂, MIL-53(Al) and ZIF-8 with Matrimid®-PI and found that thermal, mechanical, as well as gas transport properties were improved [19, 20].

Ploegmakers et al. studied the effect of Cu_3BTC_2 and its respective loading on ethylene and ethane separation [21]. The authors observed an increase in selectivity with the loading of Cu_3BTC_2 while the permeability remained constant. The increase in selectivity with Cu_3BTC_2 loading was attributed to the higher diffusion coefficient of gases with sieve in a cage morphology. Majority of literature reported work on MOF-MMMs dealing with low pressure gas separation applications and the reduced membrane performance at higher pressures due to CO_2 induced plasticization is barely addressed yet. Recently, some researchers reported MOF-MMMs in high pressure gas separation applications. Zornoza et al. incorporated amine functionalized flexible MIL-53(Al) in polysulfone membranes. Functionalized MIL-53(Al) particles showed excellent compatibility with the matrix, even at higher MOF loadings. MMMs containing MIL-53(Al) displayed a high selectivity for CO_2/CH_4 separation, at the same time enhancing the performance of the membranes at high pressures. The authors attributed this effect to the breathing of MIL-53(Al) [22]. Askari et al. incorporated ZIF-8 in cross-linkable polyimide for natural gas separation and olefin/paraffin separation. Addition of ZIF-8 nanoparticles to PI increased the CO_2/CH_4 ideal selectivity to a certain extent while the $\text{C}_3\text{H}_6/\text{C}_3\text{H}_8$ ideal selectivity improved by 134% with remarkable increase in C_3H_6 permeability [23].

In our previous study, we observed that the presence of MOF (Fe(BTC)) particles moderately improved the performance of membranes at low pressures while a significant improvement was observed especially at higher pressure compared to native Matrimid®-PI membranes. Also, the presence of Fe(BTC) particles improved the plasticization resistance of the MMMs by the rigidification of the matrix polymer [24]. This opens the route for MOF-MMMs to a wide range of newly emerging high pressure energy applications, where membranes have to operate under pressure and plasticization is an important concern. Recently published experimental and simulation studies based on the adsorption and separation of natural gas showed high potential of MOFs to be used at higher pressures [25-28]. Despite the fact that MOF based membranes are growing regarding their performance and applications, the literature on gas transport through MMMs at high pressure is still scarce and to our best knowledge there is very limited data available on the plasticization of MMMs containing MOFs. Research that systematically investigates and compares the behavior of different types

of MOFs in MMMs is needed to understand the gas transport through MOF-MMMs at high pressures and to control plasticization in MOF-MMMs.

Therefore, in this work, we selected three distinctively different MOFs (MIL-53(Al), ZIF-8 and Cu_3BTC_2) to explore and understand the mechanism of high pressure gas transport in MMMs based on these MOFs. A comprehensive study of the influence of MOF type on CO_2 induced plasticization in MOF-MMMs is presented. The separation of CO_2 and CH_4 gases in MOFs is based on (i) size-sieving based on MOF pore aperture and kinetic diameter of gas molecules and (ii) different electrostatic interactions and interaction strengths between guests and the MOF framework. The MOFs we selected are all well-studied but all show very different structures and properties (Table 3.1).

Table 3.1. Structural properties of MOFs [18, 20, 29-31].

| MOFs | Structural characteristics | Pore topology and dimensions | Pore volume (cm^3/g) | BET surface area (m^2/g) |
|-----------------------------|----------------------------|--|--|--|
| MIL-53 (Al) | Breathing structure | 1D diamond shaped channels with internal diameter of 0.85 nm | 0.293 | 1100-1300 |
| ZIF-8 | Flexible structure | Main pore cavity of 1.16 nm Windows 0.34 nm | 0.622 | 1300-1800 |
| $\text{Cu}_3(\text{BTC})_2$ | Rigid 3D cubic structure | Microcage of 1-1.2 nm Side pockets 0.6 nm Triangular Windows 0.34 nm | 0.34 | 1500-1700 |

MIL-53(Al) possesses unidirectional diamond shaped channels having an internal diameter of 0.85 nm. Moreover, MIL-53(Al) is a kind of 'breathing' MOF that can contract/expand its framework during CO_2 adsorption under pressure. High CO_2 pressures reopen the framework and increases the CO_2 uptake capacity of MIL-53(Al) [29]. ZIF-8 exhibits a sodalite topology formed by linking of zinc(II) cations and 2-methyleimidazole anions. ZIF-8 has a large pore cavity of 1.16 nm, that is accessible through pores with a small apertures of 0.34 nm [18]. Cu_3BTC_2 has a rigid 3D cubic structure with a main cage of 1-1.2 nm and intersectional pores with tetrahedral side pockets of 0.6 nm. The main cage and tetrahedral side pockets are connected by

triangular windows of 0.35 nm that provide the essential size sieving [30]. This work investigates the effect of MOF type and loading on CO₂/CH₄ high pressure gas separation performance and plasticization of these membranes and relates that to MOF structure and properties. Prepared membrane samples are characterized by different techniques such as XRD, SEM, density measurements, TGA and DSC to determine the physical and structural properties. Both pure gas permeation and mixed gas separation experiments are performed over a wide range of pressures (up to 40 bar) to investigate the effect of the MOF particles on the gas separation performance of the MMMs.

3.2 Experimental

3.2.1 Materials

Matrimid® 5218 polyimide (PI) was supplied by Huntsman, Germany. The MOFs, copper benzene-1, 3, 5-tricarboxylate (Cu₃BTC₂), aluminum terephthalate (MIL-53(Al)) and zeolite imidazole framework-8 (ZIF-8) were obtained from Sigma-Aldrich as Basolite® C300, A100 and Z1200. N-methyl-2-pyrrolidinone (NMP, 99 % extra pure) and 1, 4 dioxane (99.5 %) were purchased from Acros Organics, Belgium. All solvents were analytical grade and used without further purification. CH₄, CO₂ and N₂ gases were supplied by Praxair, The Netherlands and used as received (purity 99.999 %).

3.2.2 Membrane preparation

3.2.2.1 Pure Matrimid®-PI membranes

The membrane samples were prepared by solution processing. Matrimid®-PI powder was dried at 100 °C under vacuum overnight. The solution was prepared by dissolving 18 wt% Matrimid®-PI in a mixture of dioxane and NMP in a 40/60 weight ratio. First 10 wt% of the total polymer was dissolved. The suspension was stirred for 2 h and then sonicated for 10 min followed by addition of 20 wt% of the total polymer to the solution and stirred for another 2 h. This step was repeated until the requisite total amount of polymer was added. After that, the solution was left stirring overnight. Then the solution was cast on a flat glass plate with a 0.47 mm casting knife and the membrane was left to dry under nitrogen at room temperature for 4 days. Subsequently, the membrane was peeled off from the glass plate and annealed to 200 °C at a rate of 20 °C/h and then kept

it at this temperature for 2 days under vacuum and then slowly cooled down to room temperature.

3.2.2.2 Mixed-matrix membranes

The MMM samples were prepared by suspension casting. Prior to use, Matrimid®-PI and the MOF powders were dried at 100 °C under vacuum overnight. After removal from the oven, vials were quickly capped to prevent hydration. 10 wt%, 20 wt% and, 30 wt% dried MOF powder was slurried into the solvent dioxane/NMP (40/60 weight ratio) for 1 h and then sonicated for 1 h to disperse the fine powder. Subsequently, the suspensions were stirred for 1 h. Then, 10 wt% of total polymer powder was added into the MOF suspensions. To adequately disperse the MOF particles within the polymer matrix, the suspensions used for the membrane preparation were stirred and sonicated for five periods of 10 min each until a homogeneous suspension was obtained. After these five additional iterations of stirring and sonication, the mixture was stirred overnight.

After overnight stirring, an additional 20 wt% of total polymer was added to the solution and the solution was stirred for 2 h. This step was repeated until the requisite total amount of polymer was added. Then, a final 10 min sonication period was applied before casting. Membranes were cast on a flat glass plate with a 0.47 mm casting knife and after that left to dry under nitrogen at room temperature for 4 days. Subsequently, the membrane was peeled off from the glass plate and annealed to 200 °C at a rate of 20 °C/h and then kept it at this temperature for 2 days under vacuum and then slowly cooled down to room temperature. For both Matrimid®-PI and MOF-MMMs the presence of residual solvent can have detrimental effects on the performance of the membranes. The above mentioned annealing protocol removes the residual solvent and also helps to open the pores of the MOFs to make them accessible to gas molecules and remove the residual stress buildup during solvent evaporation.

The membrane thickness of both the native membranes and the MMMs was determined using an IP65 Coolant Proof digital Micrometer from Mitutoyo and were all found to be between 50 and 60 µm.

3.2.3 Characterization techniques

Images of pure MOF powder and cross-sections of MMMs were taken using a JEOL-JSM-5600LV scanning electron microscope (SEM) to investigate the homogeneity of MOF distribution and the compatibility of the MOFs with the polymer phase in the mixed-matrix membranes. SEM samples were prepared by freeze-fracturing the dried membranes in liquid nitrogen. The samples were dried in a vacuum oven at 30 °C overnight and coated with a 1.5-2 nm thick gold layer using a Balzers Union SCD040 sputter coater under argon flow to reduce sample charging under the electron beam.

The crystallinity of the samples under study was determined by powder X-ray diffraction (XRD) on a Bruker D2 PHASER using CuK α radiation with a wavelength (λ) = 1.54 Å at room temperature. All samples were gently grinded. Scans were made from 5-50° 2 θ with a step size of 0.02° in 40 minutes.

Investigation of thermal stability of the MOFs and membranes was performed by Thermal Gravimetric Analysis (TGA) on a Perkin Elmer TGA 4000. Samples were heated up to 900 °C at a heating rate of 20 °C/min under a constant nitrogen flow of 20 ml/min. All measurements were repeated 3 times (3 different membranes). The standard deviation was ± 0.5 °C.

The glass transition temperature (T_g) of the membranes was measured on a Perkin Elmer DSC 8000 with a heating rate of 20 °C/min, as in our previous study [24]. No transitions were recorded in the first heating run. The T_g was determined from the second heating run using the midpoint heat capacity transition method. The standard deviation was ± 1 °C.

The density measurements were performed on a pycnometer (Micromeritics Accupyc 1330) at 25 \pm 0.8 °C, as explained elsewhere [24]. An average of 10 measurements per sample was used to calculate the average density. At least two samples of each material were characterized to minimize the error.

3.2.4 Gas permeation

3.2.4.1 Pure gas

For pure gas permeation measurements the same procedure as in our previous study was followed [24]. The membranes were placed into a stainless steel cell and the permeate side was evacuated for 1 h. Subsequently, the desired feed pressure was applied at the top side of the membranes while keeping the permeate side under vacuum. The gas permeability values were calculated from the steady state pressure increase with time in a well calibrated (constant) volume at the permeate side. Pressure dependence of the permeability for CO₂ and CH₄ was determined up to 40 bar total feed pressure. For all pure gas measurements all membranes were tested first for their CH₄ permeability for all pressures and then the same membranes were used for CO₂ permeability measurements. All experiments were performed at a constant temperature of 35±0.5 °C.

3.2.4.2 Mixed gas

For the mixed gas measurements a mixture of CO₂ and CH₄ (50/50 mol%) was used to investigate the membrane performance under high pressure mixed gas conditions. Always fresh membranes were prepared and measured after a fixed period of three weeks to eliminate the influence of membrane history [32, 33]. A similar protocol as in our previous work was used for the mixed gas separation experiments [24].

The permeate side of the membranes was evacuated for 1 h. The membranes were pressurized with the CO₂/CH₄ gas mixture to 5 bar and the separation properties were measured for at least 8 h. After each mixed gas pressure measurement, N₂ gas permeation at 5 bar was measured to determine the plasticization pressure. Subsequently, the mixed gas feed pressure was increased to the next desired value (e.g. 10 bar) and the separation properties at this pressure were measured. Similarly the pressure was increased up to 40 bar and gas separation properties were measured. In the case of a mixed gas feed, the composition of both the feed and the permeate were analyzed by a Varian 3900 GC gas chromatograph using an Alltech alumina F-1 60/80 packed bed column at 150 °C. The gas selectivity (α) was calculated by the following relationship:

$$\alpha_{i/j} = \frac{y_i/y_j}{x_i/x_j} \quad \text{Eq. 3.1}$$

Where y_i and y_j are the mole fractions of the components in the permeate, while x_i and x_j are their corresponding mole fractions in the feed. The permeability and selectivity values reported are the average of 2-3 membranes. Standard deviations ranged from 4 % to 10 %.

3.3 Results and discussion

3.3.1 TGA

3.3.1.1 MOF characterization

The thermal stability of Cu₃BTC₂, MIL-53(Al) and ZIF-8 as analyzed by TGA, is presented in supporting information (Fig. S3.1). Cu₃BTC₂ shows an initial weight loss of 10 % below 200 °C indicating a loss of hydrated water and solvent from the pores [34]. A corresponding weight loss of 5 % is observed for MIL-53(Al) up to 200 °C. ZIF-8 showed no significant drop in weight till 200 °C indicating hydrophobic pores of ZIF-8 [35]. Cu₃BTC₂, ZIF-8 and MIL-53(Al) show a degradation temperature of 310 °C, 450 °C and 505 °C, respectively, which is in agreement with the literature data [20]. From this temperature upwards till the final temperature of 900 °C, the weight decreases with increasing temperature. This weight decrease is caused by the degradation of MOF into gaseous products.

3.3.1.2 MMMs

The thermal stability of Matrimid®-PI and the MMMs, is shown in the Supporting information as well (Fig. S3.2). The thermal degradation of Matrimid®-PI starts around 490 °C and increases with increasing MOF content up to 496 °C, 498 °C and 500 °C for MMMs with up to 30 wt% Cu₃BTC₂, MIL-53(Al) and ZIF-8, respectively. The increase in thermal stability of the MMMs can be attributed to the high thermal stability of the MOFs and the existence of favorable interactions between the MOFs and the PI matrix.

3.3.2 Glass transition

Table 3.2 reveals the glass transition temperatures of all membranes as investigated by DSC. The pure Matrimid®-PI membrane shows a single T_g at 328 °C, consistent with

literature [12]. The Tg values of the MMMs are slightly higher than that of the native Matrimid®-PI membrane.

The Tg of MMMs increases with increasing MOF content, from 328 °C at 0 wt% loading to 340 °C, 337 °C and 339 °C at 30 wt% loading of MIL-53(Al), ZIF-8 and Cu₃BTC₂ respectively. This increase in Tg can be attributed to the reduced chain flexibility due to the presence of the dispersed particles. Introduction of the MOF in the polymer matrix caused the formation of physical crosslinks between the polymer chains and the MOF particles, which results in the formation of a more rigid intermediate phase between the polymer and the MOF particles. Such phenomenon has also been observed for Cu-BPY-HFS/Matrimid [12, 36]. Also, the solution preparation protocol may cause the polymer chains to slightly penetrate into the pores of the MOFs, which leads to chain rigidification of the nearby polymer chains in the vicinity of the MOF particles [37, 38]. The increased Tg indicates good compatibility between the phases with favorable interactions.

Table 3.2. Glass transition temperature and density of MMMs.

| MOF type added | MOF loading (wt%) | T _g (°C) ^a | Density (g/cm ³) ^b |
|----------------------------------|-------------------|----------------------------------|---|
| Matrimid®-PI | 0 | 328 | 1.22 |
| MIL-53(Al) | 10 | 330 | 1.26 |
| MIL-53(Al) | 20 | 335 | 1.29 |
| MIL-53(Al) | 30 | 340 | 1.33 |
| MIL-53(Al) | 100 | -- | 1.64 |
| ZIF-8 | 10 | 330 | 1.25 |
| ZIF-8 | 20 | 334 | 1.27 |
| ZIF-8 | 30 | 337 | 1.29 |
| ZIF-8 | 100 | -- | 1.45 |
| Cu ₃ BTC ₂ | 10 | 330 | 1.28 |
| Cu ₃ BTC ₂ | 20 | 335 | 1.32 |
| Cu ₃ BTC ₂ | 30 | 339 | 1.35 |
| Cu ₃ BTC ₂ | 100 | -- | 1.66 |

^aTypical error in DSC results ranges from $\pm 1-1.5$ °C

^b Particle density. The density measurements show an error of $\pm 4-8\%$.

3.3.3 Density analysis

Results of the particle density measurements are also shown in Table 3.2. Matrimid®-PI shows a density of 1.22 g/cm³, which is comparable to what has been reported in literature [39]. MOF mixed matrix membranes show higher densities than the native Matrimid®-PI membranes. These higher experimental density values of the MMMs can be attributed to the higher density of the MOF particles. Additionally, it can be related to the good embedding of MOF particles in the polymer matrix and the formation of a denser structure around the MOF particles [37, 40]. Also the density values suggest good interaction between the MOFs particles and the polymer matrix and minimal presence of defects [19].

3.3.4 SEM analysis

The as received MOF particles are agglomerated because of the high temperature drying (Supporting information Fig. S3.3)[41]. These agglomerated particles could pose a

problem for membrane fabrication as larger particles tend to sediment and also need thicker films to be completely encapsulated. To avoid these problems, particles of MIL-53(Al), ZIF-8 and Cu_3BTC_2 were smoothly grinded. Fig. 3.1 shows the SEM images of pure grinded MIL-53(Al), ZIF-8 and Cu_3BTC_2 particles, respectively. A distinctive crystalline structure is visible for all the MOFs comparable to that observed for non-grinded particles. No change of the crystalline structure (as confirmed by XRD) was observed upon milling of the particles. The average crystal size for MIL-53 is around 200 nm while it is 300 nm and 10 μm for ZIF-8 and Cu_3BTC_2 , respectively.

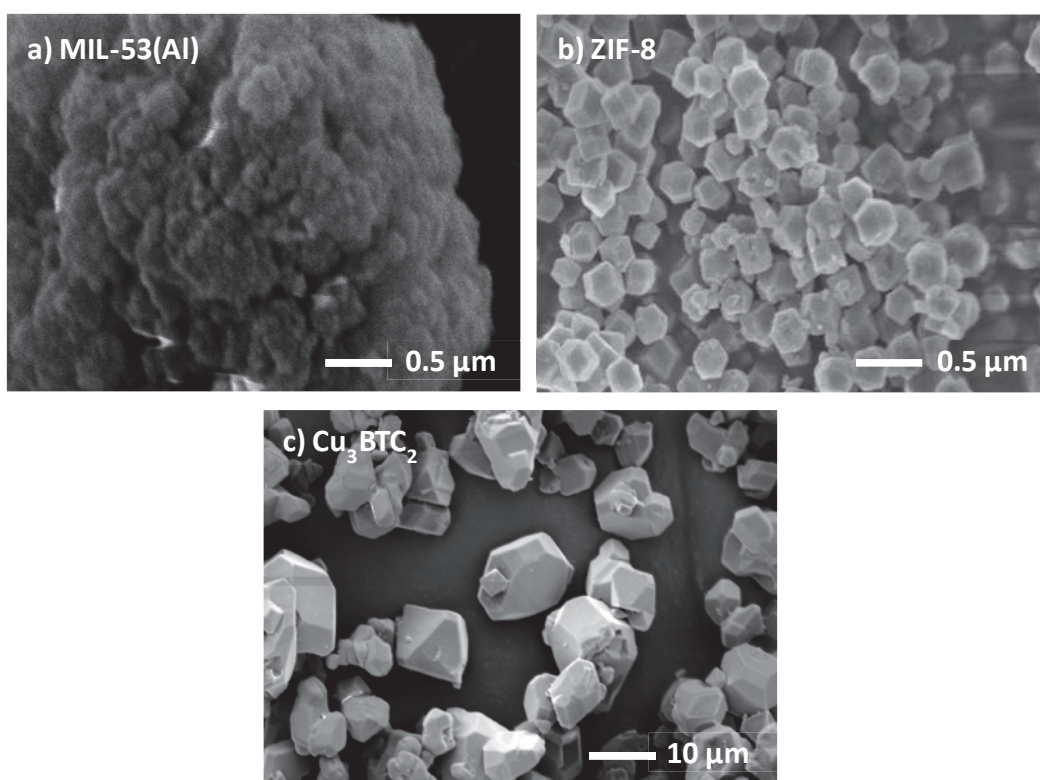


Fig. 3.1. SEM images of milled pure (a) MIL-53(Al) (magnification: 35000x), (b) ZIF-8 (magnification: 20000x) and (c) Cu_3BTC_2 (magnification: 1500x).

SEM images of the cross-sectional morphology of MOF-MMMs are shown in Fig. 3.2. The cross-sections show, many submicron particles, well distributed and embedded in the Matrimid[®]-PI matrix. In comparison, the cross-section of the native Matrimid[®]-PI membrane shows a smooth surface without any cracks or plastic deformation (Supporting information Fig. S3.4). MIL-53 and ZIF-8 MMMs show the crater like morphology typical for the MOF- MMMs and the eye of each crater is formed by a MOF particle [24]. As the loading increases the size of the craters decreases. The concentric

cavities in the MMMs (Fig. 3.2a and b) indicate a strong interaction between the polymer and the MOF particles [37, 42]. The appearance of the elongated matrix around the MOF particles is probably due to the interfacial stress concentrations as a result of particle-matrix delamination [37]. Non-selective voids are not observed, which suggests that the contact between polymer and MOFs particles is good.

Fig. 3.2c and d displays the SEM images of the cross section morphology of MMMs with different loading of Cu_3BTC_2 . The figures show a good distribution of Cu_3BTC_2 particles all over the cross section. The Cu_3BTC_2 MMMs show a different morphology than the MIL-53(Al) and ZIF-8 MMMs, as also observed by some other researchers. This can be attributed to the larger crystal size of Cu_3BTC_2 [20, 21]. The large Cu_3BTC_2 particles are completely wrapped by the polymer matrix and fracturing under liquid N_2 causes the polymer layer to break by brittle fracture without plastic deformation giving a more smooth cross-section than the crater-like morphology obtained for nanosized particles (Fig. 3.2a and b). As the Cu_3BTC_2 loading increases the cross-section becomes more rough. No interfacial voids are present under these conditions. This indicates a strong interaction between Cu_3BTC_2 particles and the Matrimid[®]-PI matrix, most probably due to the optimized mixing protocol and annealing conditions for membrane preparation and good affinity of the organic linkers in the MOF to the Matrimid[®]-PI chains. Also the polymer chains in the vicinity of Cu_3BTC_2 may slightly penetrate into the pores of Cu_3BTC_2 , which may also lead to good adhesion [40]. Homogeneous distribution of Cu_3BTC_2 and absence of non-selective voids are essential for high performance gas separation membranes.

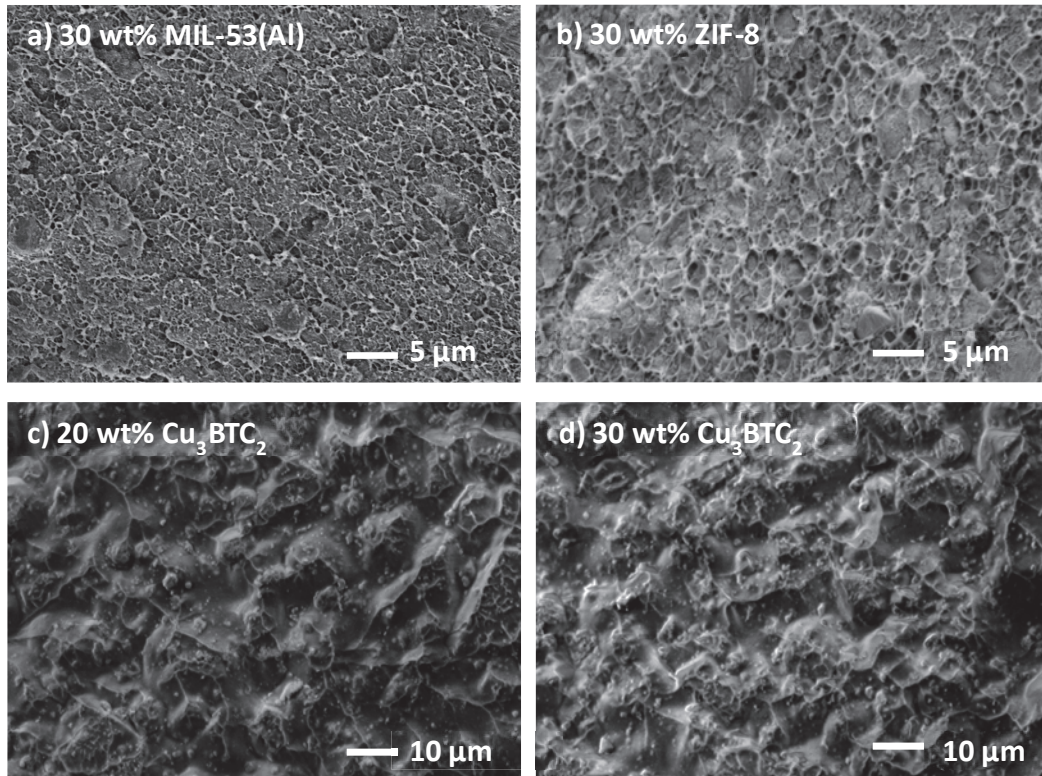


Fig. 3.2. SEM images of cross section of mixed matrix membranes with different MOFs (magnification: a and b = 3000x; c and d = 1500x).

3.3.5 Gas separation

3.3.5.1 Effect of MOF type and loading

The pure gas CO₂ and CH₄ permeabilities for the membranes containing various concentrations of different MOFs in Matrimid®-PI at 5 bar are shown in Fig. 3.3a and b. MMMs show an increase in CO₂ permeability as the MOF loading increases, with the highest permeability increase for the 30 wt% MMM (Fig. 3.3a). The MMMs show a 132 %, 144 % and 89 % increased CO₂ permeability for 30 wt% of MIL-53(Al), ZIF-8 and Cu₃BTC₂ respectively, compared to native Matrimid®-PI membranes. The enhanced CO₂ permeability can be partly attributed to the higher diffusivity of CO₂ through the MOF particles. The porous MOF particles provide an extra pore network for gas molecules, that facilitates the diffusion of CO₂ [42]. Also the strong quadrupole moment of CO₂ has higher affinity for MOFs thus increasing the sorption capacity of CO₂, leading to higher gas sorption [17]. The increase in permeability with MOF loading can also be correlated to increased d-spacing of the membranes as observed by other researchers [19].

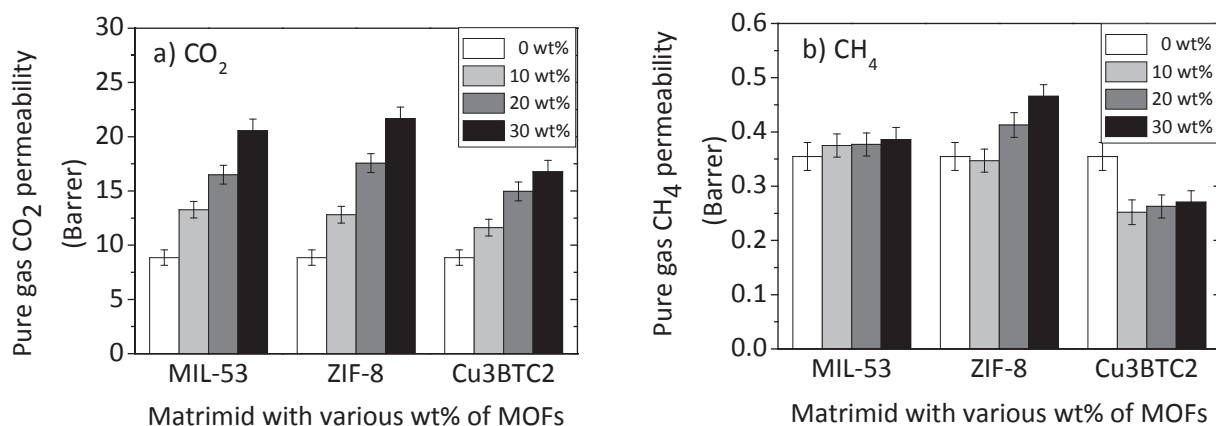


Fig. 3.3. Pure gas (a) CO₂ permeability and (b) CH₄ permeability of MMMs with 0, 10, 20 and 30 wt% of MOF at 5 bar and 35 °C.

Fig. 3.3b shows the pure CH₄ permeability. The changes in CH₄ permeability with increasing MOF loading are less clear. For ZIF-8 there is an increase in CH₄ permeability with loading. As CH₄ does not interact (no quadrupole moment) with the MOF, this can be attributed to an increased diffusivity. For MIL-53(Al) the addition of MOF does not seem to have any effect on the CH₄ permeability and effects seem to be cancel out. The Cu₃BTC₂ containing MMMs show different behavior than the other MMMs, i.e. a reduced permeability compared to the native polymer. This is mostly because of the dominant molecular sieving character of Cu₃BTC₂. Also the slight penetration of polymer chains narrows the pore opening thus reducing more the diffusivity of larger gas molecules (CH₄) than that of smaller ones (CO₂) [40].

The role of the MOFs can be differentiated based on their structural arrangements and the extent of interaction with CO₂ molecules to the MOF framework. The breathing nature of MIL-53(Al) allows the MOF framework to contract and expand, thus reducing or increasing the pore dimensions. Additionally, MIL-53(Al) has strong interactions with CO₂ because of its hydroxyl groups in the framework. CO₂ has a significant quadrupole moment (-1.4×10^{-35} C m) that induces specific interactions with MIL-53(Al) (molecular orientation, hydrogen bonding etc.), while CH₄ does not have that. The interaction between CO₂ and hydroxyl groups located at the metal-oxygen-metal link of MIL-53(Al) may be responsible for the breathing character upon CO₂ adsorption in MIL-53(Al) [43]. In contrast, CH₄, lacking a strong interaction with the MIL-53(Al) framework, is adsorbed to a lesser extent. The permeability increases for CO₂ but stay nearly constant for CH₄,

highlighting the role of the permanent quadrupole moment of CO₂ in sorption capacity [44].

ZIF-8 is comprised of larger cavities (1.1 nm) interconnected by narrow windows of 0.34 nm and ideally should only allow the transport of smaller gas molecules like CO₂. However, the swinging of the imidazolate linker allows some flexibility (via gate-opening) and causes the adsorption and transport of larger molecules like CH₄ as well and hence increases the permeability of CH₄ to some extent, as observed in Fig. 3.3b [45]. Zhang et al. reported that in ZIF-8, CO₂ has a lower energy barrier for diffusion than CH₄ and hence much higher diffusivity [46]. The higher diffusivity of CO₂ and high affinity (CO₂ sorption capacity) explains the more significant increase in CO₂ permeability compared to CH₄.

Cu₃BTC₂ has smaller triangular windows (0.35 nm) connecting the main channels and these tetrahedral side pockets perform the sieving. The partially charged (quadrupole moment) CO₂ has a stronger interaction with unsaturated Cu sites than CH₄, therefore higher adsorption and hence permeability. Also partial pore blockage influences the gas diffusivity, making it more difficult for the larger gas molecules to pass through the main channel and the tetrahedral side pockets. This is seen as a decrease in CH₄ permeability upon the addition of Cu₃BTC₂.

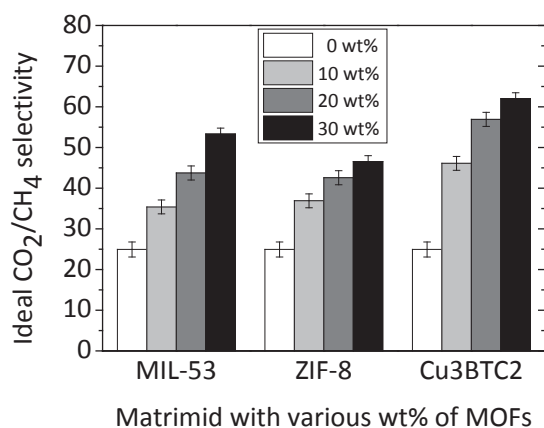


Fig. 3.4. Ideal CO₂/CH₄ selectivity of MMMs with various loadings of MOFs at 5 bar and 35 °C.

The ideal pure gas selectivity of the MMMs shows a clear improvement with MOF loading (Fig. 3.4). All MMMs show enhanced selectivity compared to pristine Matrimid®-PI membranes indicating in general a higher intrinsic selectivity of the MOFs [17]. The

relative increase in CO₂ permeability is higher than for CH₄ (Fig. 3.3a and b) resulting in a higher selectivity [17, 47]. Paired increase in permeability and selectivity suggests the absence of non-selective voids and good contact between MOF particles and polymer matrix. The low pressure ideal selectivity of Cu₃BTC₂ based MMMs is the highest suggesting Cu₃BTC₂ is a good candidate to separate CO₂ and CH₄.

Similar results of increased performance were also observed in literature for Cu-BPY-HFS [36] and MOF-5 [42] filled Matrimid. Ren et al. [40] studied the incorporation of different MOFs in polyimide and observed an increase in permeability of CO₂ with no significant change in CH₄ permeability. The authors attributed this effect to the increased interaction between the MOF particles and CO₂ molecules and slight rigidification of the polymer chains around the MOF particles.

3.3.5.2 Effect of feed pressure and plasticization behavior

Most of the data reported for MOF-MMMs is for low pressure gas separation applications. There is a significant lack of literature for high pressure gas separation and plasticization of MOF-MMMs. Therefore, we also studied the effect of feed pressure on the permeability and selectivity of MMMs containing different MOFs. The pressure range investigated includes the onset of plasticization previously reported for the polymer matrix. The CO₂ permeation behavior as a function of the feed pressure for the MMMs containing MIL-53(Al), ZIF-8 and Cu₃BTC₂ is shown in Fig. 3.5a, b and c. The native Matrimid[®]-PI membranes show a minimum at 10-12 bar (plasticization pressure) in the permeability versus pressure curve, which is consistent with literature [4]. The permeability first decreases with increasing pressure and after reaching the plasticization pressure further increases with increasing CO₂ pressure. The decrease in permeability at lower pressures stems from the decreasing solubility of the polymer (gradual saturation of microvoids) with increasing pressure, following the predicted behavior of the dual-mode sorption model [48, 49]. As the CO₂ pressure increases further, more CO₂ is sorbed into the polymer matrix causing increased segmental mobility and plasticization [4, 50, 51]. The plasticization effectively increases the chain spacing and mobility in the polymer so that the diffusion and permeation coefficient

increase with pressure. This leads to an upward inflection in permeability with increase in pressure.

For all MOF-MMMs the pure gas CO₂ permeability is higher than that of the native Matrimid®-PI membranes over the whole pressure range. For the ZIF-8 and Cu₃BTC₂ MMMs the permeability first shows a slight decrease in value and then further increases with increase in pressure, but the relative decrease in permeability is less compared to that of the native Matrimid®-PI membrane. As mentioned before, the decrease in permeability is a consequence of the decrease in solubility of the gas in the polymer with increasing pressure. For the MOF-MMMs this decrease is compensated by an increase in sorption capacity of the MOF particles with increase in pressure. In a study with Cu₃(BTC)₂, it was reported that at low pressures CO₂ preferentially adsorbs around the metal site of the MOF, followed by adsorption in the small cage sites around the exposed metal sites and organic linkers. At higher pressures the central cage get filled [30]. In all cases the adsorption of CO₂ was higher than the adsorption of CH₄ due to the higher affinity between CO₂ and the adsorption sites. For ZIF-8 MMMs, the major contribution to the increase in CO₂ permeability stems from the high diffusion and solubility coefficient of CO₂ in the MOF [52]. The preferential adsorption sites for CO₂ molecules lie in the vicinity of the imidazole rings and windows connecting the pores, giving rise to high adsorption capacity of the framework [53].

MIL-53(Al) containing MMMs show a completely different behavior due to the breathing character of MIL-53(Al). At low pressures, permeability of CO₂ decreases slightly. This can be explained by the solubility decrease of the polymer matrix and contraction of the MIL-53(Al) framework. The interaction between partially charged CO₂ molecules and O-atom of the corner hydroxyl groups induces a contraction of the framework reducing the pore size [27]. At high pressures (around 10 bar), the MIL-53(Al) MMMs show a sudden jump in permeability. At this pressure, the breathing character i.e., the transition from narrow pore (np) structure to a large pore (lp) structure of the MOF, is obvious, leading to increased permeability. The adsorption of CO₂ at higher pressures reopens (expands) the framework resulting in larger CO₂ adsorption capacity [22].

At pressures higher than the plasticization pressure, the permeability values of all MOF-MMMs slightly increase but the increase is clearly less than that observed for the native polymer. This indicates the suppression of plasticization upon the addition of MOF. Also the plasticization pressure seems to increase to higher values as the MOF loading increases. In our last study with Fe(BTC) based MMMs, we hypothesized that MOF particles hinder the chain mobility in MMMs compared to the native Matrimid®-PI membrane. The above mentioned results for MOF-MMMs and the increase in density and glass transition behavior confirm this hypothesis. Similar effects were achieved in literature using other approaches e.g. heat treatment of Matrimid®-PI films and blending with plasticization resistant polymers [54, 55].

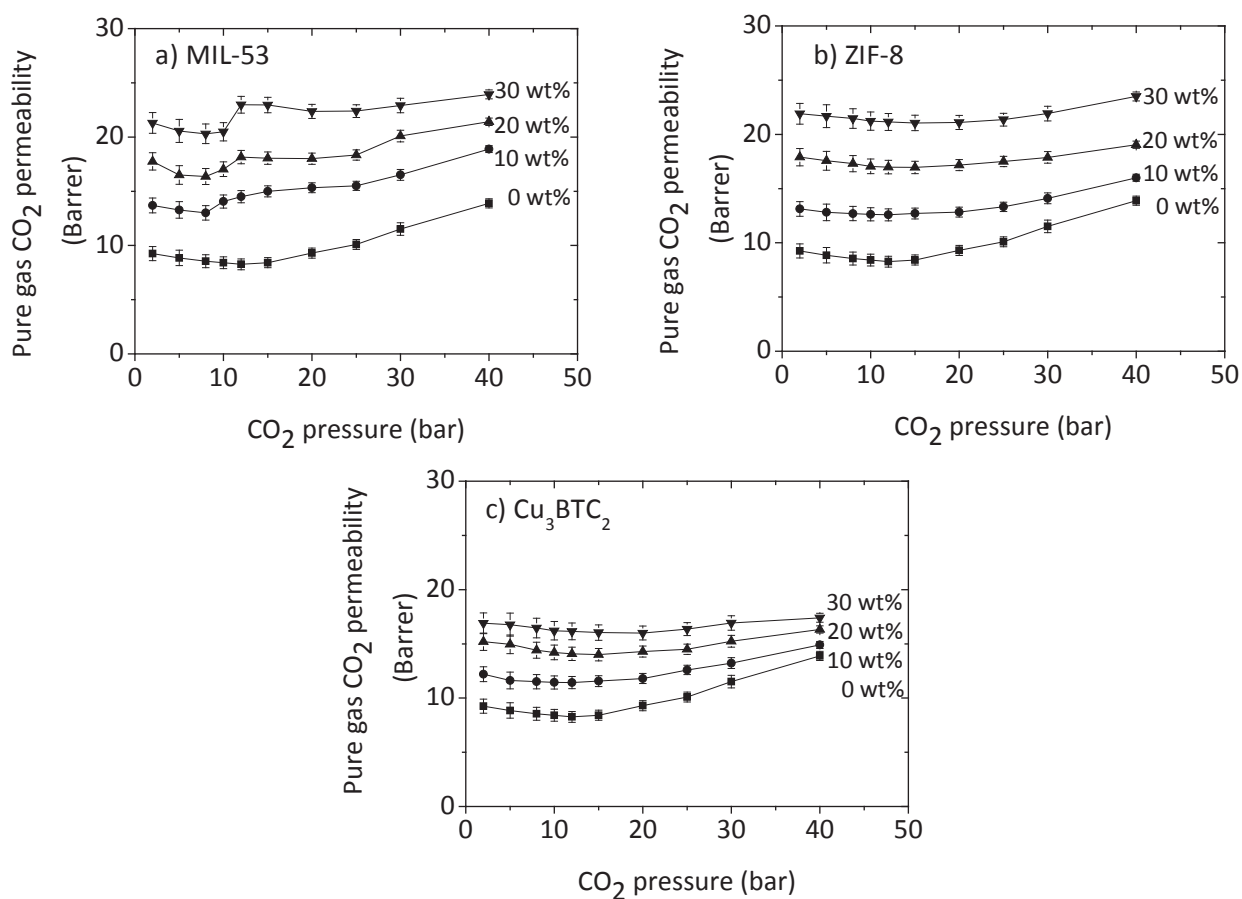


Fig. 3.5. Pure gas CO₂ permeability versus pressure curves for MMMs containing different loadings of (a) MIL-53(Al), (b) ZIF-8 and (c) Cu₃BTC₂.

Fig. 3.6 shows the ideal CO₂/CH₄ selectivity of native Matrimid®-PI membranes and the MMMs. The ideal selectivity of the native Matrimid®-PI membrane shows a slight increase below the plasticization pressure and increases swiftly as the pressure rises

above the plasticization pressure showing a strong increase in CO₂ diffusion coefficient. A high CO₂ concentration in the pure polymer membrane leads to excessive polymer swelling, resulting in an accelerated increase in segmental mobility of the polymer chains leading to higher diffusion coefficients for CO₂ in this case. The ideal selectivity of the MOF-MMMs is higher than that of the pure Matrimid®-PI membranes at all pressures. This can be attributed to the high sorption capacity and diffusion of gases. For all MOF-MMMs, ideal selectivity shows a slight increase in value till a pressure of around 25 bar. Above this pressure the ideal selectivity starts to increase more swiftly, indicating a large increase in CO₂ permeability. This behavior can be attributed to the combined effects of plasticization of the polymer matrix and increase of CO₂ adsorption with pressure by the MOF particles. It is difficult to discriminate the effect of each factor. However, the MOF-MMMs with higher loadings show the lowest relative increase in ideal selectivity attributed to suppression of plasticization by MOF particles. MOF particles limit the polymer chain mobility and as the MOF loading increases the chain mobility further decreases. 30 wt% MMM shows highest resistance against CO₂ induced plasticization.

MIL-53(Al) MMMs show a similar trend in ideal selectivity as for CO₂ permeability. Strong interaction between CO₂ and the MOF framework results in high CO₂ adsorption and 'breathing' of the framework. In contrast, CH₄, lacking a strong specific interaction with the framework, is adsorbed to a lesser extent and breathing is not observed [44]. For ZIF-8 MMMs the ideal selectivity increase is less compared to that of the other two MOF-MMMs. This behavior can be attributed to the structural flexibility of the ZIF-8 framework leading to higher diffusivity of CH₄. It was reported that structural flexibility of the ZIF-8 has an indiscernible effect on the adsorption of CO₂ and CH₄, while diffusion of CH₄ in ZIF-8 is significantly affected. At higher pressures the structural flexibility effects become more important and the relative increase in diffusion of CH₄ is higher compared to that of CO₂, although, its absolute value remains lower [56]. The high diffusion of CH₄ leads to high CH₄ permeability, hence relatively lower ideal selectivity than for the other two MOF-MMMs. For Cu₃BTC₂ MMMs the ideal selectivity shows the highest value compared to the other two MOF-MMMs. The extent of CO₂ adsorption is larger than that of methane in Cu₃BTC₂ over the whole pressure range. Also the diffusion

of CO₂ is faster than that of CH₄, leading to high ideal selectivity [57]. Considering these results, the overall behavior of the CO₂ and CH₄ permeability and ideal CO₂/CH₄ selectivity is the net result of an increase in CO₂ diffusivity and solubility and CH₄ diffusivity combined with suppression of plasticization upon the addition of MOF to the polymer matrix.

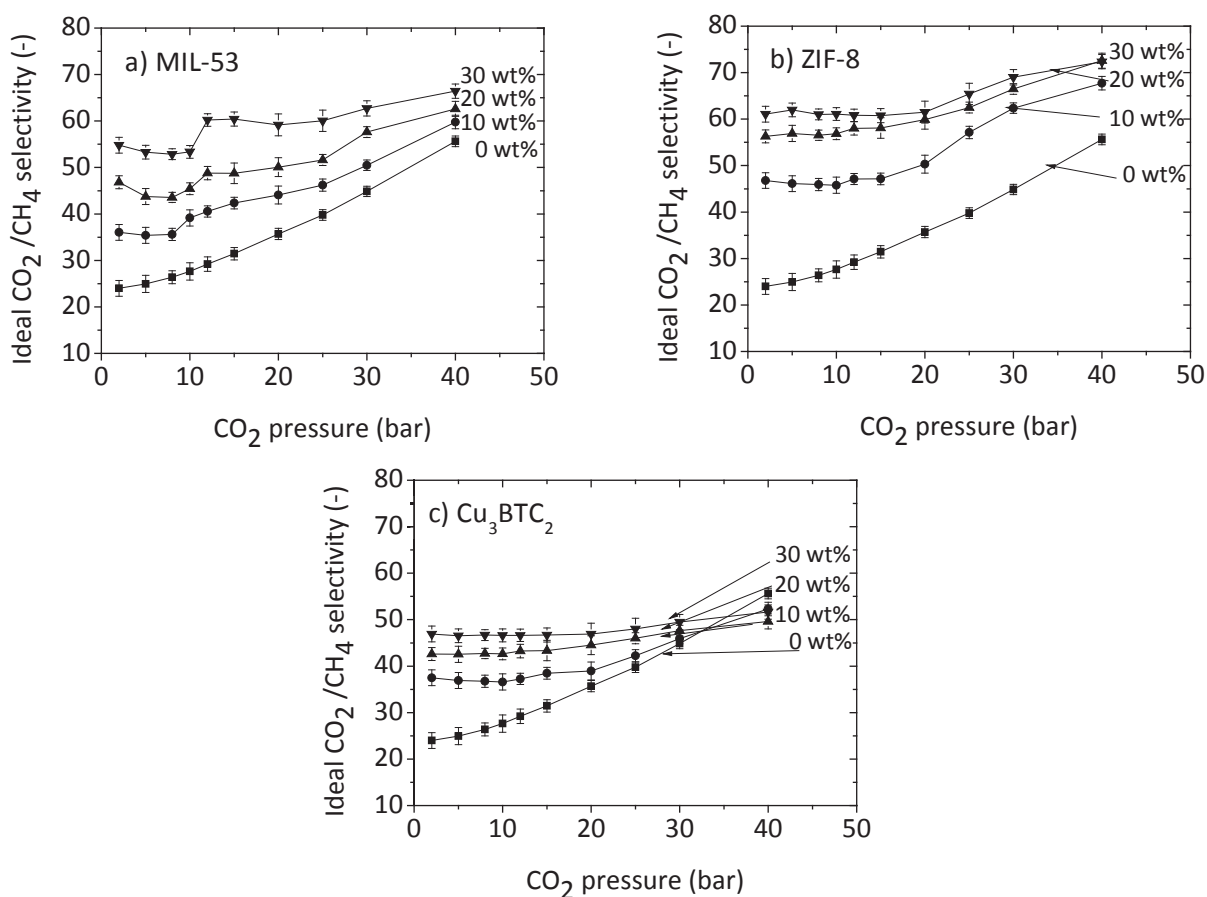


Fig. 3.6. Ideal CO₂/CH₄ selectivity of MMMs with various loadings of MOFs (a) MIL-53(Al) (b) ZIF-8 (c) Cu₃BTC₂.

3.3.5.3 Mixed gas separation performance

Mixed gas CO₂ permeabilities of MMMs containing MIL-53(Al), ZIF-8 and Cu₃BTC₂ are shown in Fig 7a, b and c respectively, as a function of the MOF loading. Pure Matrimid®-PI membranes show similar behavior as for pure gas measurements, both permeability and selectivity decrease slightly on increasing pressure, in line with previously reported literature [58, 59]. Slightly lower CO₂ permeability values were observed for Matrimid®-PI in mixed gas conditions than for pure gas measurements. The presence of CH₄ only slightly reduces the CO₂ permeability as a result of competitive sorption [60].

For MOF-MMMs, a similar trend is observed as for native Matrimid®-PI, but the permeability is increased. This effect can be attributed to the increasing CO₂ sorption capacity of the MOFs. Regardless of the MOF type and its nature, the same qualitative trends were observed on varying the feed pressure as for pure gas measurements. Compared to pure gas measurements, lower CO₂ permeabilities are obtained and plasticization is decelerated and dilation of the polymer network is less (N₂ permeability decay measurements confirm this (see Fig. S3.5 in the Supporting information)). The onset of plasticization starts at higher pressures compared to pure CO₂ gas measurements. The reduced plasticization in mixed gas conditions can additionally be attributed to competitive sorption. Kapantadaikis et al. [25] and Visser et al. [60] observed a suppression of CO₂ plasticization for the separation of CO₂/CH₄ for polyimide membranes, and explained this as a competitive sorption effects that offset or counterbalances the plasticization effect.

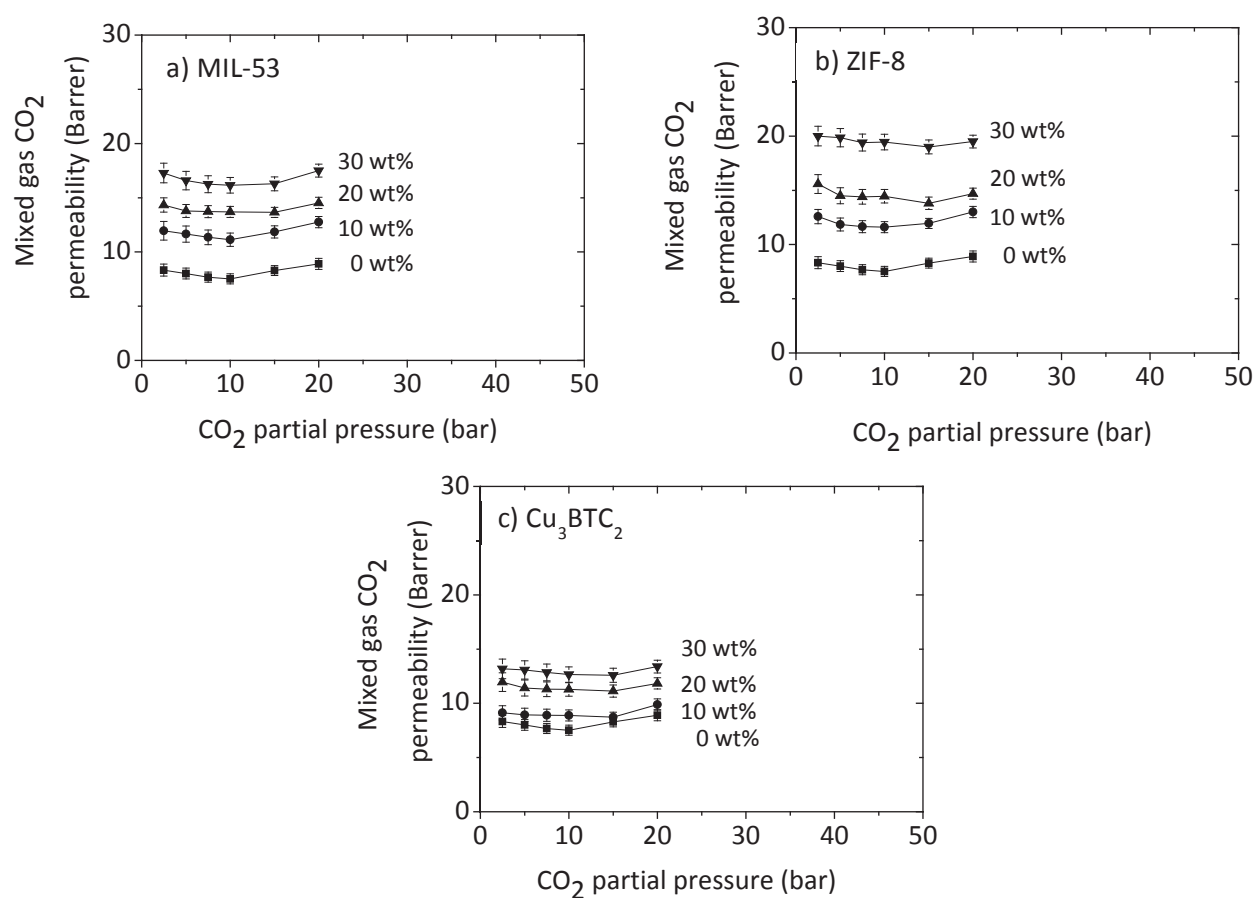


Fig. 3.7. Mixed gas CO₂ permeability of MMMs with different MOF loadings of (a) MIL-53(Al), (b) ZIF-8 and (c) Cu₃BTC₂.

Fig. 3.8a, b and c shows the mixed gas separation factor of the different MOF-MMMs obtained with a 50/50 mol% CO₂/CH₄ mixture as a function of the CO₂ pressure for different MOF loading. The mixture selectivity is enormously different from the ideal selectivity that can be attributed to the multicomponent effects in separating mixtures. When CO₂ and CH₄ permeabilities are measured in a 50/50 mol% mixture of CO₂ and CH₄, the selectivity of Matrimid®-PI actually goes down with increasing CO₂ pressure as a consequence of plasticization and the associated decrease in diffusivity selectivity of Matrimid®-PI. The high sorbing CO₂ increases the chain mobility of the polymer thus reducing its size sieving ability. The incorporation of MOFs brought about a noticeable improvement in the selectivity of the MMMs and all MOF-MMMs show higher selectivity than pure Matrimid®-PI membranes at all pressures investigated. Selectivity clearly increases with increasing MOF loading.

For MIL-53(Al) MMMs, similar to pure gas measurements, the permeability of CO₂ increases with pressure (Fig. 3.7a) in a mixture with CH₄. Moreover, for CH₄, the permeability also increases, which is not the case for pure CH₄ gas measurements. This increase in CH₄ permeability at higher pressures leads to a drop in mixed gas selectivity. The increase in CH₄ permeability can be attributed to the breathing of the framework and plasticization of the polymer matrix because of the presence of CO₂ in the mixture. The specific interaction of CO₂ (in a mixture with CH₄) with the framework opens the pores giving access to new space for both CO₂ and CH₄ to adsorb [61].

ZIF-8 MMMs show more or less a constant selectivity value over the whole pressure range, while Matrimid shows a continuous decrease in selectivity. This indicates that the presence of ZIF-8 in the polymer matrix suppresses the plasticization effect. This suppression in plasticization at least can be partially attributed to the hindering effect on the diffusion of CH₄ by CO₂ in the ZIF-8 framework. It was reported that the diffusion of CO₂ in ZIF-8 is not influenced by CH₄. However, the diffusion of CH₄ is hindered by the strongly adsorbing CO₂ in the framework [62]. The improvement in selectivity of MMMs containing ZIF-8 is thus caused by suppression of plasticization by ZIF-8 and by hindrance of CH₄ transport.

The selectivity of Cu₃BTC₂ MMMs also shows a stabilized behavior with increase in pressure. At all pressures the MMMs show higher selectivity than native Matrimid®-PI membranes. The constant selectivity in favor of CO₂ with increasing pressure is due to two effects: high adsorption of CO₂ due to the electrostatic interactions between the quadrupole moment of CO₂ and unsaturated sites of the Cu₃BTC₂ framework and the confinement effect (efficient packing of CO₂ molecules inside the MOF particles) in the octahedral cage of Cu₃BTC₂. Hence, adsorption selectivity favor CO₂ over CH₄. In addition, at higher pressures CO₂ adsorbs strongly in the structure, reducing the diffusion rate of CH₄ and leading to an increase in diffusion selectivity [30]. On the other hand, the slightly rigidified polymer matrix continues to swell at higher feed pressures due to plasticization, increasing the diffusivity of CH₄ relatively more than that of CO₂, which reduces the diffusivity selectivity of the matrix polymer of the membrane. The Cu₃BTC₂ particles however, increase the sorption and diffusion selectivity. Consequently, the overall selectivity is a balance between these competing phenomena. Similar results were observed in literature. Rodenas et al. observed that pure polymer membranes show a decrease in performance at increasing trans-membrane pressure difference while the functionalized MIL-53(Al) filled MMMs maintained their performance even at high transmembrane pressure difference [63].

When comparing the performance of MMMs for pure and mix gas measurements, it can be stated that the gas transport behavior is very much dependent on the structure of the MOF and its specific interactions with the gas molecules and the polymer matrix. The MOF loading increases the permeability of CO₂ more than that of CH₄, consequently the selectivity of the membrane will increase. On the other hand, voids and plasticized matrix increases the permeability of CH₄, which reduces the selectivity of the membranes. The overall result on the membrane performance is a balance between these counter balancing phenomena. At low pressures, diffusion and the sorption selectivity favor CO₂ over CH₄ but at higher pressures mixture selectivity is especially dominated by the MOFs solubility selectivity enhancement for CO₂. Similar results were observed in simulation studies with MOF and MOF-MMMs [30, 57, 64].

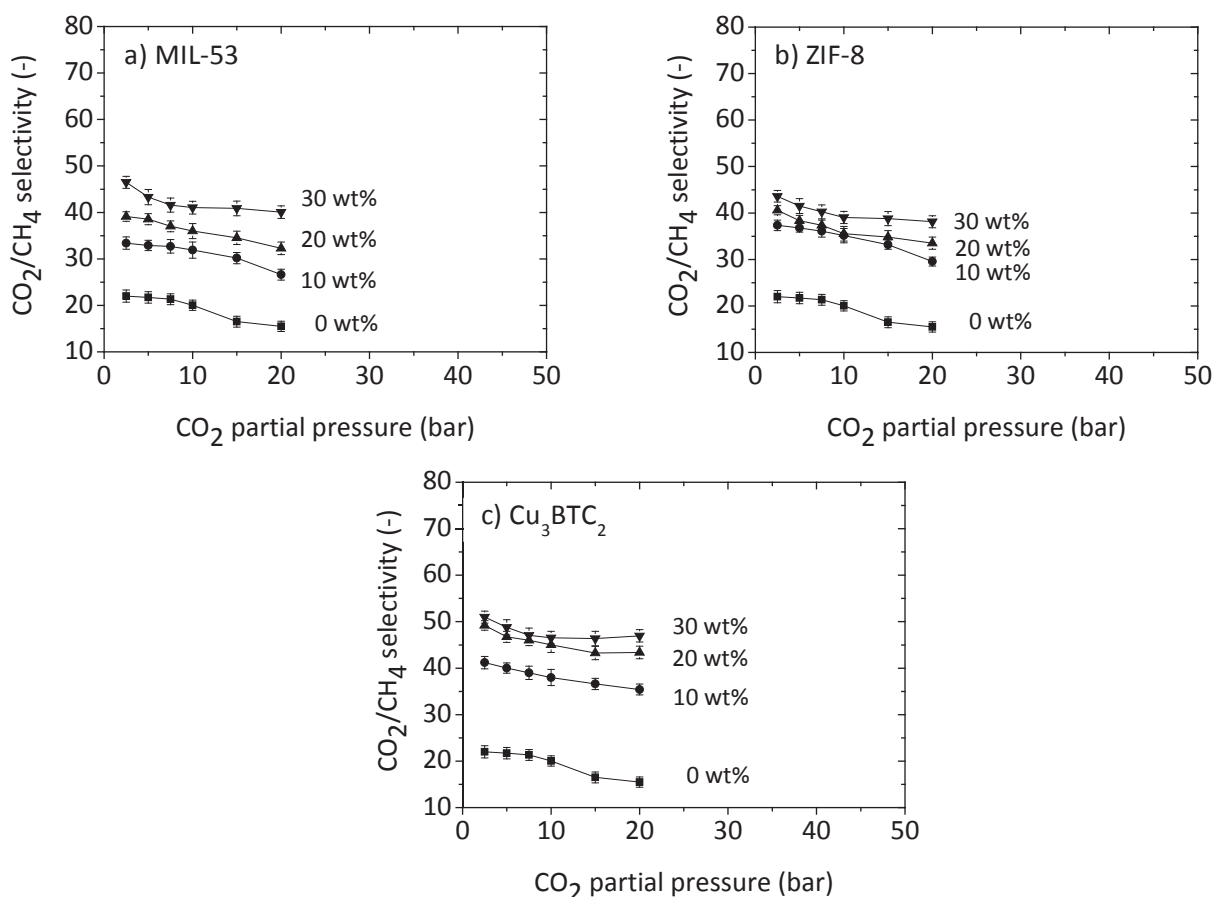


Fig. 3.8. Mixed gas selectivity of MMMs with different MOF loadings of (a) MIL-53(Al), (b) ZIF-8 and (c) Cu₃BTC₂.

3.4 Conclusion

The influence of three different MOFs in MMMs for pure and binary gas mixture separations at high pressures was studied by preparing flat sheet Matrimid®-PI membrane filled with MIL-53(Al), ZIF-8 and Cu₃BTC₂. The use of a less volatile co-solvent and optimized priming protocol to prepare the MMMs and annealing temperature resulted in a good compatibility and distribution of MOFs in the Matrimid®-PI matrix. Incorporation of MOFs in PI-membranes resulted in increased density, and glass transition properties and improved degradation behavior of the membranes, confirming a good compatibility of the polymer and MOFs. SEM images showed good contact between the MOF particles and polymer matrix.

At low pressures, MIL-53(Al) and Cu₃BTC₂ showed higher CO₂/CH₄ selectivity than ZIF-8, attributed to the strong CO₂ interaction with MIL-53(Al) and Cu₃BTC₂. The availability of

unsaturated sites in Cu_3BTC_2 and the breathing nature of MIL-53(Al), favor CO_2 sorption and hence increase the CO_2 permeability and CO_2/CH_4 selectivity.

Although moderate improvements are shown by MOF-MMMs over native Matrimid®-PI membranes at low pressures, the benefits of MOF incorporation become more significant at higher pressures. At high CO_2 pressures, pure Matrimid®-PI membranes show typical plasticization behavior, showing a decrease in selectivity. In MMMs, MOF particles hinder an increase in mobility of the polymer chains while enhancing CO_2 sorption in the MOF thus suppressing CO_2 induced plasticization and maintain large separation factor over the whole pressure range investigated.

As a consequence of the restricted chain mobility, the plasticization pressure increases to higher values. Among the three MOF-MMMs, membranes based on Cu_3BTC_2 showed highest selectivity while ZIF-8 based membranes showed highest permeability. As the MOF loading increases, the membranes maintain nearly constant selectivity over the whole pressure range due to the suppression of CO_2 induced plasticization by the presence of MOF particles. The respective increase in performance of MMMs is very much dependent on MOF crystal structure and its interactions with CO_2 gas molecules. In general it can be stated that the higher CO_2 permeability and CO_2/CH_4 selectivity of MOF-MMMs at higher pressures are a combined effect of increased sorption selectivity, diffusion selectivity and reduced CO_2 induced plasticization.

Acknowledgement

The authors would like to thank Erasmus Mundus Doctorate in Membrane Engineering (EUDIME) for funding this project.

Reference

- [1] A. Brunetti, F. Scura, G. Barbieri, E. Drioli, Membrane technologies for CO_2 separation, *J. Membr. Sci.*, 359 (2010) 115-125.
- [2] L.M. Robeson, Correlation of separation factor versus permeability for polymeric membranes, *J. Membr. Sci.*, 62 (1991) 165-185.
- [3] L.M. Robeson, The upper bound revisited, *J. Membr. Sci.*, 320 (2008) 390-400.
- [4] A. Bos, I.G.M. Punt, M. Wessling, H. Strathmann, CO_2 -induced plasticization phenomena in glassy polymers, *J. Membr. Sci.*, 155 (1999) 67-78.

- [5] Y. Li, T.S. Chung, Z. Huang, S. Kulprathipanja, Dual-layer polyethersulfone (PES)/BTDA-TDI/MDI co-polyimide (P84) hollow fiber membranes with a submicron PES-zeolite beta mixed matrix dense-selective layer for gas separation, *J. Membr. Sci.*, 277 (2006) 28-37.
- [6] T.W. Pechar, S. Kim, B. Vaughan, E. Marand, M. Tsapatsis, H.K. Jeong, C.J. Cornelius, Fabrication and characterization of polyimide-zeolite L mixed matrix membranes for gas separations, *J. Membr. Sci.*, 277 (2006) 195-202.
- [7] L.Y. Jiang, T.S. Chung, S. Kulprathipanja, An investigation to revitalize the separation performance of hollow fibers with a thin mixed matrix composite skin for gas separation, *J. Membr. Sci.*, 276 (2006) 113-125.
- [8] L.Y. Jiang, T.S. Chung, C. Cao, Z. Huang, S. Kulprathipanja, Fundamental understanding of nano-sized zeolite distribution in the formation of the mixed matrix single- and dual-layer asymmetric hollow fiber membranes, *J. Membr. Sci.*, 252 (2005) 89-100.
- [9] H.M. Guan, T.S. Chung, Z. Huang, M.L. Chng, S. Kulprathipanja, Poly(vinyl alcohol) multilayer mixed matrix membranes for the dehydration of ethanol-water mixture, *J. Membr. Sci.*, 268 (2006) 113-122.
- [10] D.Q. Vu, W.J. Koros, S.J. Miller, Mixed matrix membranes using carbon molecular sieves - II. Modeling permeation behavior, *J. Membr. Sci.*, 211 (2003) 335-348.
- [11] M. Anson, J. Marchese, E. Garis, N. Ochoa, C. Pagliero, ABS copolymer-activated carbon mixed matrix membranes for CO₂/CH₄ separation, *J. Membr. Sci.*, 243 (2004) 19-28.
- [12] T.S. Chung, S.S. Chan, R. Wang, Z.H. Lu, C.B. He, Characterization of permeability and sorption in Matrimid/C-60 mixed matrix membranes, *J. Membr. Sci.*, 211 (2003) 91-99.
- [13] S. Kim, T.W. Pechar, E. Marand, Poly(imide siloxane) and carbon nanotube mixed matrix membranes for gas separation, *Desalination*, 192 (2006) 330-339.
- [14] J.-R. Li, Y. Ma, M.C. McCarthy, J. Sculley, J. Yu, H.-K. Jeong, P.B. Balbuena, H.-C. Zhou, Carbon dioxide capture-related gas adsorption and separation in metal-organic frameworks, *Coordination Chemistry Reviews*, 255 (2011) 1791-1823.
- [15] P.S. Goh, A.F. Ismail, S.M. Sanip, B.C. Ng, M. Aziz, Recent advances of inorganic fillers in mixed matrix membrane for gas separation, *Separation and Purification Technology*, 81 (2011) 243-264.
- [16] A.R. Millward, O.M. Yaghi, Metal-organic frameworks with exceptionally high capacity for storage of carbon dioxide at room temperature, *Journal of the American Chemical Society*, 127 (2005) 17998-17999.
- [17] Q. Yang, C. Zhong, Molecular simulation of carbon dioxide/methane/hydrogen mixture adsorption in metal-organic frameworks, *Journal of Physical Chemistry B*, 110 (2006) 17776-17783.
- [18] M.J.C. Ordóñez, K.J. Balkus, J.P. Ferraris, I.H. Musselman, Molecular sieving realized with ZIF-8/Matrimid® mixed-matrix membranes, *J. Membr. Sci.*, 361 (2010) 28-37.

- [19] S. Basu, A. Cano-Odena, I.F.J. Vankelecom, Asymmetric Matrimid®/Cu₃(BTC)₂ mixed-matrix membranes for gas separations, *J. Membr. Sci.*, 362 (2010) 478-487.
- [20] S. Basu, A. Cano-Odena, I.F.J. Vankelecom, MOF-containing mixed-matrix membranes for CO₂/CH₄ and CO₂/N₂ binary gas mixture separations, *Separation and Purification Technology*, 81 (2011) 31-40.
- [21] J. Ploegmakers, S. Japip, K. Nijmeijer, Mixed matrix membranes containing MOFs for ethylene/ethane separation-Part B: Effect of Cu₃BTC₂ on membrane transport properties, *J. Membr. Sci.*, 428 (2013) 331-340.
- [22] B. Zornoza, A. Martinez-Joaristi, P. Serra-Crespo, C. Tellez, J. Coronas, J. Gascon, F. Kapteijn, Functionalized flexible MOFs as fillers in mixed matrix membranes for highly selective separation of CO₂ from CH₄ at elevated pressures, *Chemical Communications*, 47 (2011) 9522-9524.
- [23] M. Askari, Y. Xiao, P. Li, T.-S. Chung, Natural gas purification and olefin/paraffin separation using cross-linkable 6FDA-Durene/DABA co-polyimides grafted with α , β , and γ -cyclodextrin, *J. Membr. Sci.*, 390–391 (2012) 141-151.
- [24] S. Shahid, K. Nijmeijer, High pressure gas separation performance of mixed-matrix polymer membranes containing mesoporous Fe(BTC), *J. Membr. Sci.*, 459 (2014) 33-44.
- [25] A. Martín-Calvo, E. García-Pérez, J. Manuel Castillo, S. Calero, Molecular simulations for adsorption and separation of natural gas in IRMOF-1 and Cu-BTC metal-organic frameworks, *Physical Chemistry Chemical Physics*, 10 (2008) 7085-7091.
- [26] D. Liu, Y. Wu, Q. Xia, Z. Li, H. Xi, Experimental and molecular simulation studies of CO₂ adsorption on zeolitic imidazolate frameworks: ZIF-8 and amine-modified ZIF-8, *Adsorption*, 19 (2013) 25-37.
- [27] N. Heymans, S. Vaesen, G. De Weireld, A complete procedure for acidic gas separation by adsorption on MIL-53 (Al), *Microporous and Mesoporous Materials*, 154 (2012) 93-99.
- [28] J.A. Thompson, J.T. Vaughn, N.A. Brunelli, W.J. Koros, C.W. Jones, S. Nair, Mixed-linker zeolitic imidazolate framework mixed-matrix membranes for aggressive CO₂ separation from natural gas, *Microporous and Mesoporous Materials*, (2013).
- [29] A.U. Ortiz, M.-A. Springuel-Huet, F.-X. Coudert, A.H. Fuchs, A. Boutin, Predicting Mixture Co-adsorption in Soft Porous Crystals: Experimental and Theoretical Study of CO₂/CH₄ in MIL-53(Al), *Langmuir*, 28 (2011) 494-498.
- [30] J. Jose Gutierrez-Sevillano, A. Caro-Perez, D. Dubbeldam, S. Calero, Molecular simulation investigation into the performance of Cu-BTC metal-organic frameworks for carbon dioxide-methane separations, *Physical Chemistry Chemical Physics*, 13 (2011) 20453-20460.
- [31] <http://www.sigmaaldrich.com/catalog/search?interface=All&term=basolite&N=0&mode=match%20partialmax&focus=product&lang=en®ion=NL>.
- [32] P.H. Pfromm, W.J. Koros, Accelerated physical aging of thin glassy polymer-films - evidence from gas-transport measurements, *Polymer*, 36 (1995) 2379-2387.

- [33] M. Wessling, I. Huisman, T. Vanderboomgaard, C.A. Smolders, Time-dependent permeation of carbon-dioxide through a polyimide membrane above the plasticization pressure, *Journal of Applied Polymer Science*, 58 (1995) 1959-1966.
- [34] S.S.-Y. Chui, S.M.-F. Lo, J.P.H. Charmant, A.G. Orpen, I.D. Williams, A chemically functionalizable nanoporous material $[\text{Cu}_3(\text{TMA})_2(\text{H}_2\text{O})_3]_n$, *Science*, 283 (1999) 1148-1150.
- [35] K. Zhang, R.P. Lively, C. Zhang, R.R. Chance, W.J. Koros, D.S. Sholl, S. Nair, Exploring the Framework hydrophobicity and flexibility of ZIF-8: From biofuel recovery to hydrocarbon separations, *The Journal of Physical Chemistry Letters*, 4 (2013) 3618-3622.
- [36] Y. Zhang, I.H. Musselman, J.P. Ferraris, K.J. Balkus, Jr., Gas permeability properties of Matrimid® membranes containing the metal-organic framework Cu-BPY-HFS, *J. Membr. Sci.*, 313 (2008) 170-181.
- [37] Y. Zhang, K.J. Balkus Jr, I.H. Musselman, J.P. Ferraris, Mixed-matrix membranes composed of Matrimid® and mesoporous ZSM-5 nanoparticles, *J. Membr. Sci.*, 325 (2008) 28-39.
- [38] J. Ploegmakers, S. Japip, K. Nijmeijer, Mixed matrix membranes containing MOFs for ethylene/ethane separation Part A: Membrane preparation and characterization, *J. Membr. Sci.*, 428 (2013) 445-453.
- [39] <http://www.lindberg-lund.fi/files/Teknische%20datablad/VAN-5218-TD.pdf>.
- [40] H. Ren, J. Jin, J. Hu, H. Liu, Affinity between Metal-organic frameworks and polyimides in asymmetric mixed matrix membranes for gas separations, *Industrial & Engineering Chemistry Research*, 51 (2012) 10156-10164.
- [41] J. Cravillon, S. Münzer, S.-J. Lohmeier, A. Feldhoff, K. Huber, M. Wiebcke, Rapid room-temperature synthesis and characterization of nanocrystals of a prototypical zeolitic imidazolate framework, *Chemistry of Materials*, 21 (2009) 1410-1412.
- [42] E.V. Perez, K.J. Balkus, Jr., J.P. Ferraris, I.H. Musselman, Mixed-matrix membranes containing MOF-5 for gas separations, *J. Membr. Sci.*, 328 (2009) 165-173.
- [43] P. Rallapalli, K.P. Prasanth, D. Patil, R.S. Somani, R.V. Jasra, H.C. Bajaj, Sorption studies of CO_2 , CH_4 , N_2 , CO , O_2 and Ar on nanoporous aluminum terephthalate [MIL-53(Al)], *Journal of Porous Materials*, 18 (2011) 205-210.
- [44] S. Bourrelly, P.L. Llewellyn, C. Serre, F. Millange, T. Loiseau, G. Férey, Different Adsorption Behaviors of Methane and Carbon Dioxide in the Isotypic Nanoporous Metal Terephthalates MIL-53 and MIL-47, *Journal of the American Chemical Society*, 127 (2005) 13519-13521.
- [45] D. Fairen-Jimenez, R. Galvelis, A. Torrisi, A.D. Gellan, M.T. Wharmby, P.A. Wright, C. Mellot-Draznieks, T. Düren, Flexibility and swing effect on the adsorption of energy-related gases on ZIF-8: Combined experimental and simulation study, *Dalton Transactions*, 41 (2012) 10752-10762.
- [46] L. Zhang, G. Wu, J. Jiang, Adsorption and diffusion of CO_2 and CH_4 in zeolitic imidazolate framework-8: effect of structural flexibility, *The Journal of Physical Chemistry C*, 118 (2014) 8788-8794.

- [47] Q. Yang, C. Xue, C. Zhong, J.-F. Chen, Molecular simulation of separation of CO₂ from flue gases in CU-BTC metal-organic framework, *Aiche Journal*, 53 (2007) 2832-2840.
- [48] D.R. Paul, Gas sorption and transport in glassy-polymers, *Berichte Der Bunsen-Gesellschaft-Physical Chemistry Chemical Physics*, 83 (1979) 294-302.
- [49] V. Stannett, The transport of gases in synthetic polymeric membranes — an historic perspective, *J. Membr. Sci.*, 3 (1978) 97-115.
- [50] T. Visser, M. Wessling, When do sorption-induced relaxations in glassy polymers set in?, *Macromolecules*, 40 (2007) 4992-5000.
- [51] T. Visser, N. Masetto, M. Wessling, Materials dependence of mixed gas plasticization behavior in asymmetric membranes, *J. Membr. Sci.*, 306 (2007) 16-28.
- [52] Q. Song, S.K. Nataraj, M.V. Roussanova, J.C. Tan, D.J. Hughes, W. Li, P. Bourgoin, M.A. Alam, A.K. Cheetham, S.A. Al-Muhtaseb, E. Sivaniah, Zeolitic imidazolate framework (ZIF-8) based polymer nanocomposite membranes for gas separation, *Energy and Environmental Science*, 5 (2012) 8359-8369.
- [53] J. Pérez-Pellitero, H. Amrouche, F.R. Siperstein, G. Pirngruber, C. Nieto-Draghi, G. Chaplais, A. Simon-Masseron, D. Bazer-Bachi, D. Peralta, N. Bats, Adsorption of CO₂, CH₄, and N₂ on Zeolitic Imidazolate Frameworks: Experiments and Simulations, *Chemistry – A European Journal*, 16 (2010) 1560-1571.
- [54] A. Bos, I.G.M. Punt, M. Wessling, H. Strathmann, Suppression of CO₂-plasticization by semiinterpenetrating polymer network formation, *Journal of Polymer Science Part B-Polymer Physics*, 36 (1998) 1547-1556.
- [55] A. Bos, I. Punt, H. Strathmann, M. Wessling, Suppression of gas separation membrane plasticization by homogeneous polymer blending, *Aiche Journal*, 47 (2001) 1088-1093.
- [56] L. Zhang, G. Wu, J. Jiang, Adsorption and diffusion of CO₂ and CH₄ in zeolitic imidazolate framework-8: Effect of structural flexibility, *Journal of Physical Chemistry C*, 118 (2014) 8788-8794.
- [57] S. Keskin, Atomistic Simulations for Adsorption, Diffusion, and Separation of Gas Mixtures in Zeolite Imidazolate Frameworks, *Journal of Physical Chemistry C*, 115 (2011) 800-807.
- [58] P.C. Raymond, W.J. Koros, D.R. Paul, Comparison of mixed and pure gas permeation characteristics for CO₂ and CH₄ in copolymers and blends containing methyl-methacrylate units, *J. Membr. Sci.*, 77 (1993) 49-57.
- [59] J. Ahn, W.J. Chung, I. Pinnau, M.D. Guiver, Polysulfone/silica nanoparticle mixed-matrix membranes for gas separation, *J. Membr. Sci.*, 314 (2008) 123-133.
- [60] T. Visser, G.H. Koops, M. Wessling, On the subtle balance between competitive sorption and plasticization effects in asymmetric hollow fiber gas separation membranes, *J. Membr. Sci.*, 252 (2005) 265-277.
- [61] V. Finsy, L. Ma, L. Alaerts, D.E. De Vos, G.V. Baron, J.F.M. Denayer, Separation of CO₂/CH₄ mixtures with the MIL-53(Al) metal-organic framework, *Microporous and Mesoporous Materials*, 120 (2009) 221-227.

[62] C. Chmelik, J. van Baten, R. Krishna, Hindering effects in diffusion of CO₂/CH₄ mixtures in ZIF-8 crystals, *J. Membr. Sci.*, 397–398 (2012) 87-91.

[63] T. Rodenas, M. van Dalen, P. Serra-Crespo, F. Kapteijn, J. Gascon, Mixed matrix membranes based on NH₂-functionalized MIL-type MOFs: Influence of structural and operational parameters on the CO₂/CH₄ separation performance, *Microporous and Mesoporous Materials*.

[64] R. Krishna, Adsorptive separation of CO₂/CH₄/CO gas mixtures at high pressures, *Microporous and Mesoporous Materials*, 156 (2012) 217-223.

Appendix 1. Supporting information Chapter 3:

***Performance and plasticization behavior of polymer-
MOF membranes for gas separation at elevated
pressures***

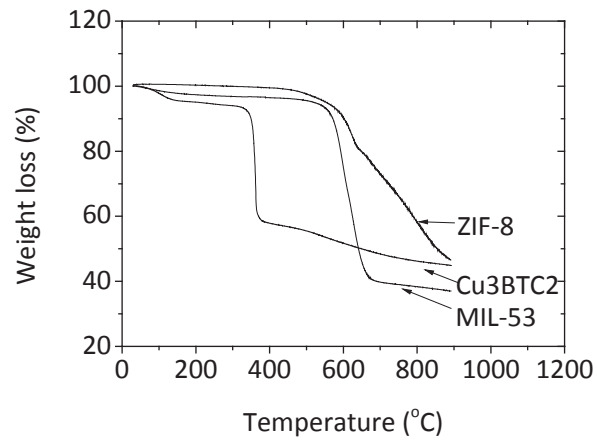


Fig. S3.1. TGA of pure MIL-53(Al), ZIF-8 and Cu₃BTC₂.

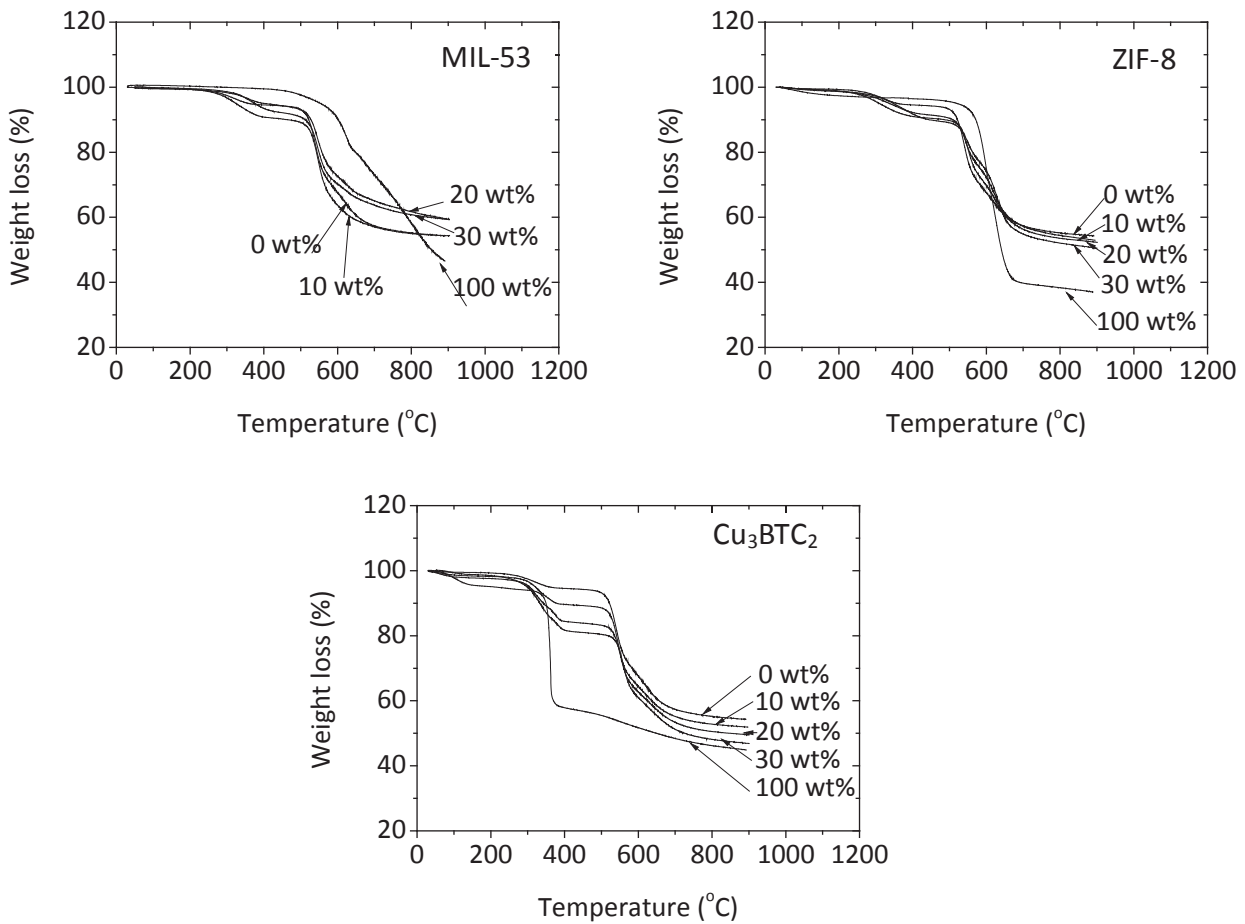


Fig. S3.2. TGA of pure Matrimid[®]-PI and MIL-53(Al), ZIF-8 and Cu₃BTC₂ filled MMMs, at 10-30 wt% loading.

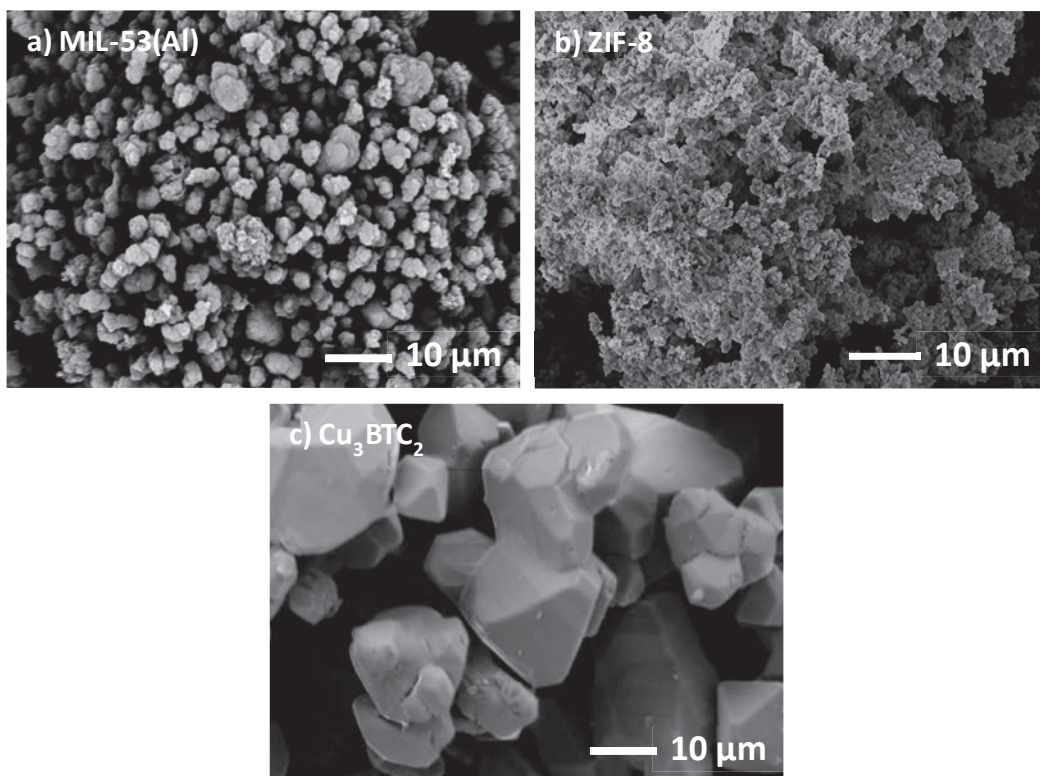


Fig. S3.3. SEM image of as received pure (a) MIL-53(Al), (b) ZIF-8 and (c) Cu₃BTC₂ (magnification a, b and c: 1500x).

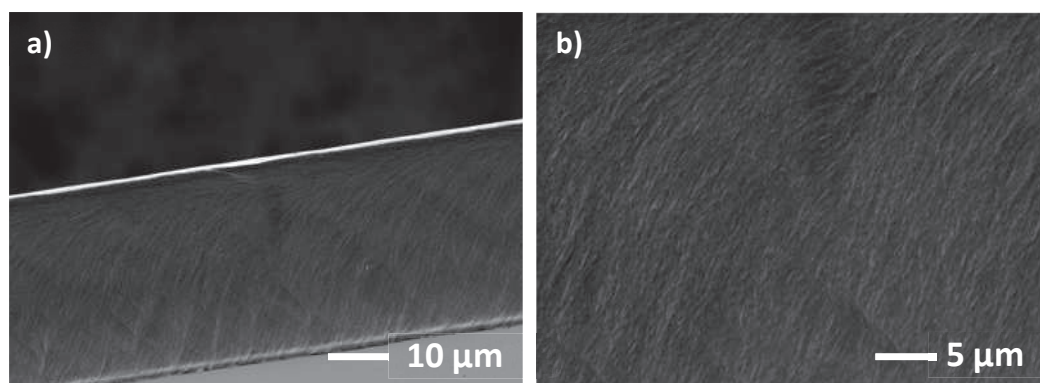


Fig. S3.4. SEM images of pure Matrimid-PI membranes (a) magnification 1500 x; (b) magnification 3000 x.

N₂ permeability decay in time

In order to assess the effect of CO₂ induced plasticization, N₂ permeability decay measurements in time were performed after each mixed gas separation measurements.

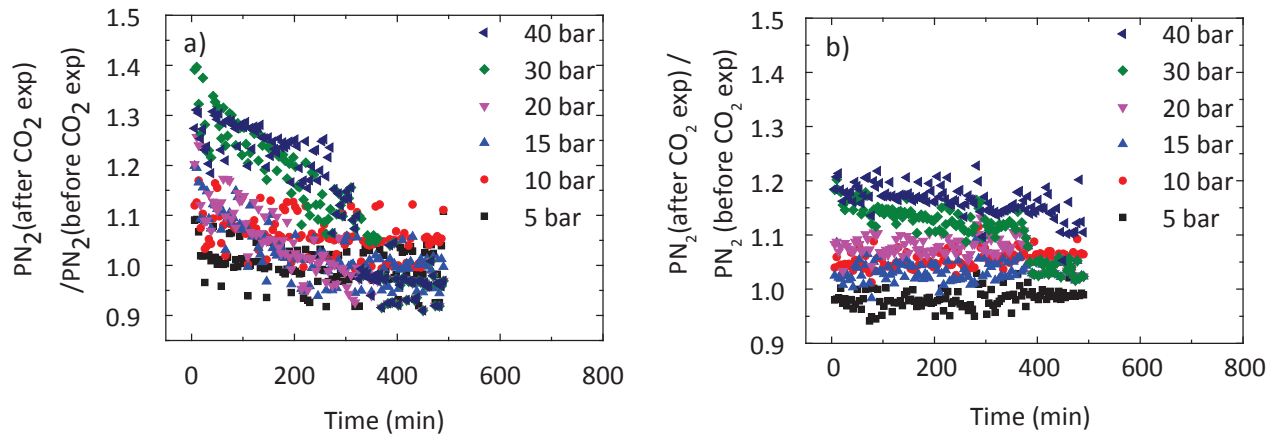


Fig. S3.5. Normalized N₂ permeability decay in time after exposure to CO₂/CH₄ gas mixture of (a) Matrimid[®]-PI membranes and (b) 30% MIL-53(Al) MMMs for different feed pressures.

Fig. S3.5 shows the normalized N₂ permeability decay in time after mixed gas separation measurements for (a) Matrimid[®]-PI and (b) 30 wt% MIL-53(Al) loaded Matrimid[®]-PI membranes. The N₂ permeabilities of each run are normalized by the initial N₂ permeability as measured before exposure to the CO₂ gas mixture.

For native Matrimid[®]-PI, the normalized permeability in time after exposure to a mixed gas feed pressures of 5 and 10 bar is relatively low (~1) and decreases only slightly in time. As the mix feed pressure increases above the plasticization pressure of Matrimid[®]-PI, the normalized N₂ permeability starts at much higher values than the initial value and decreases slowly in time. The decrease in N₂ normalized permeability in time shows the recovery (relaxation) of the dilated network after CO₂ exposure. However, on the experimental time-scale, the membrane does not relax to its original structure completely. Instead, a higher permeability remains, indicating larger extent of polymer network dilation at higher pressures.

In order to compare this behavior with MMMs, 30 wt% MIL-53(Al) MMM is selected. Fig. S3.5b shows that for filled membranes the normalized N₂ permeability also increases in value compared to the initial value of N₂ permeability but it stays constant in time till a mixed gas pressure of 20 bar. At higher pressures the N₂ permeability starts at slightly

higher values than the initial value but this increase is much less compared to that observed for the native Matrimid®-PI membranes. After this initial increase in value the permeability decreases in time, but also this decrease is much less compared to that of pure polymer membrane. The above results confirm that the MMMs show less dilation of the polymer network and plasticization than native polymer membrane, indicating increased rigidity of the filled MMMs.

Chapter 4

**Matrimid[®]/polysulfone blend mixed matrix
membranes containing ZIF-8 nanoparticles
for high pressure natural gas separation**

This chapter has been submitted to Journal of Membrane Science as:

S. Shahid, K. Nijmeijer, Matrimid[®]/polysulfone blend mixed matrix membranes containing ZIF-8 nanoparticles for high pressure natural gas separation

ABSTRACT

Plasticization is of important concern in high-pressure natural gas separation. In this work, different mixed matrix membranes (MMMs) with Matrimid® (PI)/polysulfone (PSF) blend as matrix polymer containing different concentrations of ZIF-8 were prepared. These materials are chosen because 1) Matrimid® is frequently used for high pressure gas separation membranes and PSF is known for its good plasticization resistance; 2) ZIF-8 has an easy tunable structure, chemical functionality and pore sizes. The effect of ZIF-8 loading on the gas transport and plasticization behavior of the membranes is investigated. Experimental results show that the permeability of both CO₂ and CH₄ increases with ZIF-8 loading due to moderate increase in sorption capacity and faster diffusion through the ZIF-8 particles. The ideal selectivity slightly increases, which can mainly be attributed to the increase in diffusion selectivity and only to a smaller extent to an increase in corresponding solubility selectivity. For pure gases, native PI/PSF blends show a plasticization pressure of ~18 bar, which increases to ~25 bar up to 30 wt.% ZIF-8 loading. In mixed gas experiments, pure PI/PSF membranes and MMMs do not show plasticization over the pressure range investigated, as confirmed by a constant mixed gas CH₄ permeability and nearly constant selectivity with pressure (up to 20 bar CO₂ partial pressure). The results show that the combination of simple polymer blending and the mixed matrix membrane approach offers a method to tailor gas separation and antiplasticizing properties.

4.1 Introduction

Membrane technology for gas separation is gaining momentum because of its low energy demands, low maintenance cost, easy up-scaling and relatively simple equipment [1]. Polymers are widely used for membrane fabrication because of their easy processing, moldability and low cost. It is recognized that polymeric membranes have the potential to replace conventional gas separation processes e.g. pressure swing adsorption, cryogenic distillation and absorption [1], if membranes can surpass the so-called “upper bound” limit of the permeability-selectivity trade-off curve [2, 3].

Metal organic frameworks (MOFs) are a promising class of nanoporous materials that are produced from metal ions or clusters linked by organic ligands. The self-assembly of these ion clusters and ligands leads to 1D, 2D and 3D structural arrangements [4, 5]. Among many other types of MOFs, zeolitic imidazolate frameworks (ZIFs), in particular ZIF-8, have gained a lot of attention. Its facile synthesis, tuneable structure and pore sizes, and chemical functionality coupled with high internal surface area and chemical and water stability compared to other MOFs, makes it a potential candidate for adsorption and gas separation applications [6-9]. ZIF-8 is formed by self-assembly of zinc (II) cations and 2-methyleimidazole anions, giving a sodalite topology with a pore size of 11.6 Å and crystallographically-determined pore aperture of 3.4 Å [10]. Several published experimental and simulation studies based on the adsorption and purification of natural gas showed high potential of ZIF-8 as adsorbent material for CO₂ [10-12]. ZIF materials have the potential to separate differently sized molecules (molecular sieving character) coupled with very high CO₂ solubilities [12]. Many ZIF structures have been used in mixed matrix membranes (MMMs) for gas separation applications [13]. Ordonez and co-workers [14] reported the first ZIF-8/Matrimid® MMMs with different loadings. Addition of the ZIF phase substantially enhanced the membrane permeability. Higher loadings of ZIF-8 caused aggregation of nanoparticles as evident from the published SEM images. The defects at the ZIF-8-polymer interface lead to high permeabilities of gases but selectivity decreased. Zhang et al. reported a significant improvement in C₃H₆/C₃H₈ separation performance of ZIF-8/6FDA-DAM membranes [15]. Bae et al. reported the preparation of ZIF-90/polyimide membranes with improved CO₂ permeability and

selectivity. However higher filler loading made it difficult to prepare defect free membranes [4]. Song et al. synthesized MMMs using colloidal ZIF-8 in the polymer Matrimid by solution mixing. This led to flexible transparent membranes with improved gas separation performance. The increase in free volume due to the presence of the ZIF-8 particles together with the enhanced diffusion of gases through the cage of ZIF-8 resulted in a high permeability of the membrane while the selectivity stayed more or less constant [16].

In spite of excellent performance shown by ZIF-8 mixed matrix membranes, plasticization is still a big issue for high-pressure gas separation. In our previous research on MOF-MMMs, we showed that the presence of MOF increases the separation performance of the filled membranes at high CO₂ partial pressures [17, 18]. The permeability of the filled membranes showed a significant increase compared to native Matrimid® attributed to high sorption and diffusion through MOF particles, while selectivity showed a nearly constant behavior with pressure. Despite the better membrane performance of the MMMs, plasticization was still observable at higher CO₂ partial pressures.

Polymer blending is an effective tool to modify polymer properties and stabilize membrane performance under high-pressure CO₂ environments. The importance of polymer blending lies in the advantages of its simplicity, reproducibility, easy processability and low development cost. Commercially available gas separation membranes are usually based on polyimides (PI), which are thermally stable high performance polymers with excellent mechanical properties and a good correlation between permeability and selectivity. However PI is susceptible to plasticization in CO₂ environments already at low CO₂ pressures (~8 bar) [19]. Considering polyimides, Matrimid® in particular, numerous examples can be found in literature where membranes are prepared by blending Matrimid® with PSF [20, 21], PBI [22, 23], P84 [24] and PES [25], to further increase its stability. Among these reported polymers, PSF is most extensively studied as it exhibits good thermo-mechanical stability, good gas permeability and selectivity and high plasticization resistance (above 30 bar) [21]. All these properties make PSF suitable for membrane advancement [26]. Blending of these two polymers offers a way to reduce the tendency to plasticize in high pressure (CO₂)

feed conditions [24]. Kapantaidakis et al. prepared membranes with Matrimid®/PSF and observed a delay in plasticization pressure with increasing PSF fraction, while the CO₂ permeability and selectivity of the blend (with different PSF fractions) decreased below that of the pure polymers [20]. Bos et al. [24] used the same approach and concluded similar results of improved plasticization behavior. In the same study they investigated another polymer blend comprising of Matrimid®/P84. This blend showed excellent resistance against plasticization while simultaneously improving the gas separation properties, but at the cost of lower permeability. Basu et al. [27] studied asymmetric membranes prepared from Matrimid®/PSF blends, with different ratios of the two polymers, at elevated temperature and varying CO₂ feed composition. They reported that membranes prepared from a 3:1 (PI/PSF) blend ratio showed a consistent increase in CO₂/CH₄ selectivity at elevated temperatures, high CO₂ feed compositions and pressure, while pure Matrimid® membranes showed deterioration in separation performance.

All literature referred to above on PI/PSF membranes showed good membrane stability, but suffered from low gas permeability problems. In this work, we aimed to synergistically combine the strengths of ZIF-8 and PI/PSF blend MMMs for CO₂/CH₄ separation at high pressures. The focus of this work is to develop MMMs with high plasticization resistance by blending an optimized fraction of PI/PSF/(3:1), as reported by Basu and others [20, 27], combined with ZIF-8 particles with improved gas separation performance. The porous structure, high surface area and molecular sieving character of ZIF-8 is expected to increase the separation properties of the blend polymer membranes, while PSF will add increased plasticization resistance to the system. The effect of ZIF-8 loading on the morphology of the membranes and its influence on the pure and mixed gas separation properties is also reported. The membranes are characterized and both pure gas permeation and mixed gas separation experiments are performed over a wide range of pressures to investigate the effect of the ZIF-8 particles on performance and plasticization resistance. In addition, based on pure gas sorption data, we also tried to elucidate the mechanism of improved performance in terms of solubility, diffusion and permeability coefficients that is lacking in the previously reported literature.

4.1.1 Theory

4.1.1.1 Gas sorption

Several models have been established to describe the sorption of gas molecules in glassy polymeric membranes. The dual mode sorption model is most commonly used [28]. It assumes two different sorption mechanisms to take place simultaneously: Henry's law can be used to describe sorption of gas molecules in a polymer matrix in an ideal, hypothetical equilibrium state, and Langmuir sorption describes sorption in the non-equilibrium excess free volume microcavities. Gas molecules are either sorbed by Henry type sorption (sorption directly proportional to pressure) or by Langmuir type sorption ('hole-filling of microcavities'). The combined pressure dependent concentration C , in the polymer thus equals:

$$C = k_D \cdot p + \frac{C'_H \cdot b \cdot p}{1 + (b \cdot p)} \quad \text{Eq. 4.1}$$

Where k_D represents the Henry law constant ($\text{cm}^3(\text{STP})/\text{cm}^3 \cdot \text{cmHg}$), p is the pressure (cmHg), C'_H is the Langmuir capacity constant ($\text{cm}^3(\text{STP})/\text{cm}^3$), which varies with the polymer type and structure and b is the Langmuir affinity constant ($1/\text{cmHg}$) associated to the affinity of a gas molecule for the Langmuir adsorption site. Subsequently, the solubility coefficient ($\text{cm}^3(\text{STP})/\text{cm}^3 \cdot \text{cmHg}$) is the ratio of the total penetrant concentration to pressure, given by eq. 4.2.

$$S = \frac{C}{p} = k_D + \frac{C'_H \cdot b}{1 + (b \cdot p)} \quad \text{Eq. 4.2}$$

4.1.1.2 Gas separation

The solution-diffusion mechanism is widely employed to explain gas transport through dense polymeric membranes [29]:

$$P = S \cdot D \quad \text{Eq. 4.3}$$

According to this model, the gas permeability coefficient P in Barrer ($1 \text{ Barrer} = 10^{-10} \text{ cm}^3(\text{STP}) \cdot \text{cm}/\text{cm}^2 \cdot \text{s} \cdot \text{cmHg}$) is the product of the solubility coefficient S ($\text{cm}^3(\text{STP})/\text{cm}^3 \cdot \text{cmHg}$) and the diffusivity coefficient D (cm^2/s). The ideal gas pair (A/B) selectivity comprises the solubility selectivity (S_A/S_B) and the diffusivity selectivity (D_A/D_B) of component A and B, respectively.

$$\alpha_{AB} = \frac{P_A}{P_B} = \frac{S_A}{S_B} \cdot \frac{D_A}{D_B} \quad \text{Eq. 4.4}$$

The solubility coefficient of polymeric membranes increases with increasing polymer-penetrant interactions, condensability of the penetrant gases and decreasing temperature [30]. On the other hand, the diffusivity coefficient increases with decreasing size of the penetrants, increasing fractional free volume and increasing polymer chain flexibility [31].

4.2 Experimental

4.2.1 Materials

Matrimid® 5218 PI was supplied by Huntsman, Germany. Polysulfone Udel® P-3500 was purchased from Solvay, Belgium. The MOF, ZIF-8, was obtained from Sigma-Aldrich as Basolite Z1200. N-methyl-2-pyrrolidinone (NMP, 99 % extra pure) and 1, 4 dioxane (99.5 %) were purchased from Acros Organics, Belgium. All solvents were analytical grade and used without further purification. CH₄, CO₂ and N₂ were supplied by Praxair, The Netherlands and used as received (purity 99.999 %).

4.2.2 Membrane preparation

4.2.2.1 Pure Matrimid®/PSF membranes

To fabricate the membranes, the polymers, PSF and Matrimid®-PI, were dried at 100 °C under active vacuum overnight. The casting solution was prepared by dissolving 18 wt.% PI/PSF (3:1) in a mixture of dioxane and NMP in a 1:1 w/w ratio, as explained in previous studies [17, 18]. This ratio of 3:1 PI/PSF was chosen based on the work of Basu et al. [27]. The suspension was stirred for 2 h and then sonicated for 1 h followed by an overnight stirring step to obtain a clear solution. Before casting the solution was bath sonicated for 15 min to degas. Subsequently, the solution was cast on a flat glass plate and left to dry under nitrogen for 3 days at room temperature. Then the membrane was dried in a WTC Binder oven at 100 °C under nitrogen flow for 2 days. Finally, the dried membrane was peeled off from the glass plate and vacuum dried at 150 °C for 2 days.

4.2.2.2 Mixed-matrix membranes

The MMM samples were prepared by suspension casting using 18 wt.% PI/PSF (3:1) in a mixture of dioxane and NMP in a 1:1 w/w ratio and different ZIF-8 loadings (10-30 wt.%). Casting and drying of the MMMs are carried out using the same procedure explained above for the pure polymer membranes. The membrane thickness of both the native membranes and the MMMs was determined using an IP65 Coolant Proof digital Micrometer from Mitutoyo and found to be between 60 and 70 μm .

4.2.3 Characterization techniques

4.2.3.1 SEM

The morphology of pure PI/PSF and MMMs was observed using low vacuum scanning electron microscopy (JEOL-JSM-5600LV). The samples were prepared by freeze-fracturing the dried membranes in liquid nitrogen. The samples were coated with a 1.5-2 nm thick gold layer using a Balzers Union SCD040 sputter coater under argon flow to reduce sample charging under the electron beam.

4.2.3.2 Thermal analysis

Thermal stability of the membranes was investigated by Thermal Gravimetric Analysis (TGA) using a Perkin Elmer TGA 4000. Samples were heated in N_2 from 50 $^\circ\text{C}$ to 900 $^\circ\text{C}$ at a ramp of 20 $^\circ\text{C}/\text{min}$. TGA analysis was performed to determine the thermal stability and amount of residual solvent remaining in the samples. All measurements were repeated 3 times (3 different membranes).

DSC measurements were carried out with a Perkin Elmer 8000 differential scanning calorimeter. The samples were heated to a temperature of 400 $^\circ\text{C}$ at a temperature ramp of 20 $^\circ\text{C}/\text{min}$. Then, the samples were quenched back to 50 $^\circ\text{C}$ at 20 $^\circ\text{C}/\text{min}$. This cycle was repeated two times. The T_g was determined from the second heating scan using the midpoint heat capacity transition method. In this way, the recording method was standardized, with elimination of any thermal history.

4.2.3.3 Sorption measurements

Pure CO_2 and CH_4 gas sorption experiments were conducted for fabricated membranes and pure ZIF-8, using a Rubotherm Prazisions Mess Technik GmbH magnetic suspension

balance. CH₄ sorption over the full pressure range (0-40 bar) was first determined, subsequently followed by CO₂ sorption over the full pressure range as well. The temperature was kept constant at 35.0 ± 0.5 °C. Approximately 50 mg of the weighed sample was placed in the sample holder. The system was evacuated for 24 h prior to testing. After the measurement showed a constant weight, the pressure was increased by introducing either pure CO₂ or pure CH₄ into the system and sample started to sorb the gas until equilibrium was achieved. From the calculated mass gain m_t (g) (eq. 4.5), the amount of gas dissolved (cm³ (STP)/cm³ of polymer) in the sample was calculated using the molar volume at standard temperature and pressure (STP, 1 bar and 273.15 K) after accounting the buoyancy correction.

$$m_t = (w_t + V_t \rho_g) - w_0 \quad \text{Eq. 4.5}$$

Where V_t (cm³) is the sample volume, w_0 (g) is the initial weight of the sample, w_t (g) is the measured weight and ρ_g (g/cm³) is the density gas of the surrounding gas. The gas density was estimated using the Peng Robinson equation of state. The sorption isotherms were curve fitted by using eq. 4.1 for pure ZIF-8 and MMMs.

4.2.3.4 Gas permeation

4.2.3.4.1 Pure gas

Pure gas permeability measurements were performed using a constant volume variable pressure permeation cell with vacuum at the permeate side, as described elsewhere [17]. A desired feed pressure was applied at the top side of the membrane while keeping the permeate side under vacuum. The gas permeability values were calculated from the change in pressure in a calibrated volume. Pressure dependence of the permeability for CO₂ and CH₄ was determined up to 40 bar total feed pressure. For pure gas measurements, the CH₄ permeability at all pressures was measured first, followed by the CO₂ permeability measurements. All experiments were performed at a constant temperature of 35±0.5 °C. Furthermore in order to exclude time effects on permeability, all membranes had the same history (measurements started 2 weeks after preparation and the permeability values were taken after 8 hours of measurement). All membranes were vacuumed overnight prior to test.

4.2.3.4.2 Mixed gas

A mixture of CO₂ and CH₄ (50/50 mol %) was used to investigate the membrane performance under high pressure mixed gas conditions, using the same procedure as in our previous studies [17, 18]. In all cases fresh membranes were prepared and measured, also after a constant period of three weeks to eliminate the influence of membrane history [32, 33]. Alternatingly single gas nitrogen and CO₂/CH₄ mixed gas separation measurements were performed on the same membrane sample. N₂ feed pressure was kept constant (5 bar) to investigate plasticization effects. The CO₂/CH₄ mixed gas feed pressure was increased to the next desired value and the separation properties were measured at this pressure. The samples were measured continuously at a total feed pressure of 5 up to 40 bars at 35 °C using a retentate flow of 3 cm³/min. The gas permeating through the membrane was collected and directly injected into a Varian 3900 GC gas chromatograph using an Alltech alumina F-1 60/80 packed bed column at 150 °C to analyze its composition. The gas permeation data presented are the average of at least two membranes of two separate batches. Standard deviations ranged from 4-10%.

4.3 Results and discussion

4.3.1 Thermal analysis

4.3.1.1 TGA

The thermal stability of ZIF-8 and the MMMs as analyzed by TGA, is presented in Fig. 4.1. ZIF-8 shows no significant drop in weight till 400 °C indicating that no water is adsorbed due to the hydrophobic pores of ZIF-8 [34]. ZIF-8 shows a degradation temperature of 450 °C, which is in agreement with literature data [35].

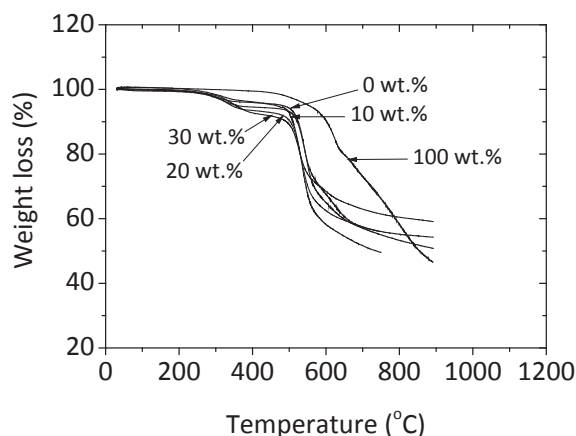


Fig. 4.1. TGA of PI/PSF (0 wt.%), pure ZIF-8 (100 wt.%) and MMMs at different ZIF-8 loadings.

The unfilled PI/PSF membrane has a weight loss of only 1.5 % (stage 1) when the temperature is raised to 150 °C. This is caused by evaporation of moisture. An additional 5 % weight loss (stage 2) is shown at a temperature range of 200-300 °C. This decrease can be attributed to the removal of residual trapped solvent from the PI/PSF membrane. The temperatures of 200 °C and 300 °C correspond to the T_g of PSF and Matrimid[®], respectively. Above the T_g of the polymer, the increased mobility of the polymer chains (rubbery state) favors solvent desorption [36]. Significant weight loss in the range of 480-550 °C corresponds to the decomposition of the polymers. PI/PSF blend membranes show a degradation temperature of 485 °C. The MMMs show similar weight loss in the temperature range 150 to 300 °C but show a higher degradation temperature than that of the unfilled PI/PSF membranes. The degradation temperature increases with ZIF-8 loading up to 500 °C for MMMs containing 30 wt.% ZIF-8. This increase in degradation temperature can be attributed to the high thermal stability of ZIF-8 particles. Above this temperature there is a continuous loss of weight with temperature attributed to the decomposition of the chemical structure of the polymer and ZIF-8.

4.3.1.2 Glass transition temperature

The miscibility of polymer blends and the effect of different ZIF-8 loadings on the glass transition temperature was studied using differential scanning calorimeter. Table 4.1 reveals these glass transition temperatures. The pure PI/PSF membrane shows two glass transition temperatures, indicating a phase separated blend morphology. The DSC results showed two T_g's (Table 4.1) very close to those of the pure components. During

the first run, the samples were heated well above their T_g, which causes the polymers to phase separate. Earlier studies on the T_g of PI/PSF blends showed similar results [21, 24, 26].

Table 4.1. Glass transition temperatures of the PI/PSF-ZIF-8 MMMs.

| ZIF-8 contents wt.%) | PI/PSF (3:1) contents (wt.%) | T _g (°C) ¹ | |
|----------------------|------------------------------|----------------------------------|-----|
| | | PSF | PI |
| 0 | 100 | 191 | 328 |
| 10 | 90 | 195 | 332 |
| 20 | 80 | 196 | 334 |
| 30 | 70 | 199 | 337 |

¹Typical error in DSC results $\pm 1-1.5$ °C.

Despite that, based on previously reported literature [21], we conclude that the PI/PSF blends are homogeneous, and as the membranes are not heat treated before gas separation, they are considered homogeneous during separation as well. Also the PI/PSF MMMs show two glass transition temperatures but the T_g values of the MMMs are slightly higher than those of the pure PI/PSF membrane. The T_g of the ZIF-8 MMMs increases with ZIF-8 loading as shown. This increase in T_g can be attributed to a reduced chain flexibility due to the presence of the dispersed ZIF-8 particles combined with the penetration of the polymer chains into the MOF structure, which causes slight rigidification in the vicinity of the ZIF-8 particles [37].

4.3.2 SEM analysis

SEM images of the cross-sectional morphology of pure PI/PSF membranes and the MMMs are shown in Fig. 4.2a-d. Fig. 4.2a shows the cross-section of the pure PI/PSF membrane. It displays a homogeneous structure. The ZIF-8 particles show good adhesion to the polymer matrix and are wrapped by a polymer film. Interfacial voids between the polymer matrix and the ZIF-8 particles are not observed, indicating good compatibility between the phases. Fig. 4.2d shows slight agglomeration of ZIF-8 particles in some regions of the cross-section of the 30 wt.% ZIF-8 MMMs.

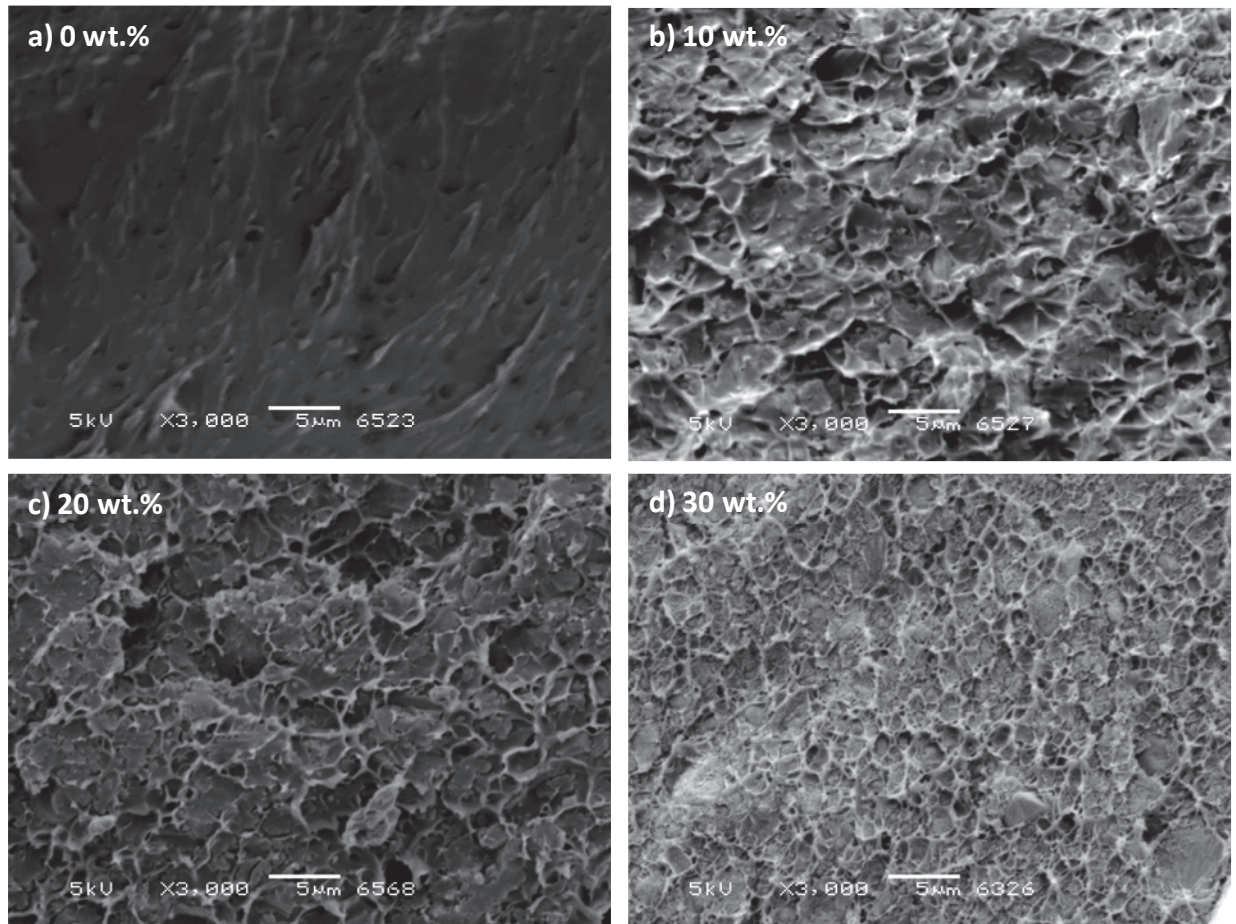


Fig. 4.2. SEM images of the cross-section of pure PI/PSF and mixed-matrix membranes containing different loadings of ZIF-8 (magnification a-d: 3000x).

4.3.3 Gas sorption

The sorption isotherms of CO_2 and CH_4 in an unfilled PI/PSF membrane are shown in Fig. 4.3. Dual mode sorption can be observed for both CO_2 and CH_4 . At low pressures, the microvoid space in the polymer matrix is rapidly filled (Langmuir sorption), but this levels off at higher pressure and Henry sorption starts to dominate [38]. When both sorption isotherms of CO_2 and CH_4 are fitted with the dual mode sorption model (eq. 4.1), Henry's law constants (K_D), the Langmuir capacity (C'_H) and the Langmuir affinity constant (b) can be obtained. These parameters are shown in Table 4.2.

The two gases show different sorption behavior and CO_2 sorbs relatively more than CH_4 . The critical temperature (T_c) of CO_2 is much higher than that of CH_4 ($T_{c-\text{CO}_2}$: 304K, $T_{c-\text{CH}_4}$: 190K) [39] so condensability and thus the sorption of CO_2 molecules in the polymer matrix is much higher at similar pressures [40]. Furthermore, CH_4 does not possess

favorable quadrupolar interactions, which also contribute to the higher sorption of CO₂ [41].

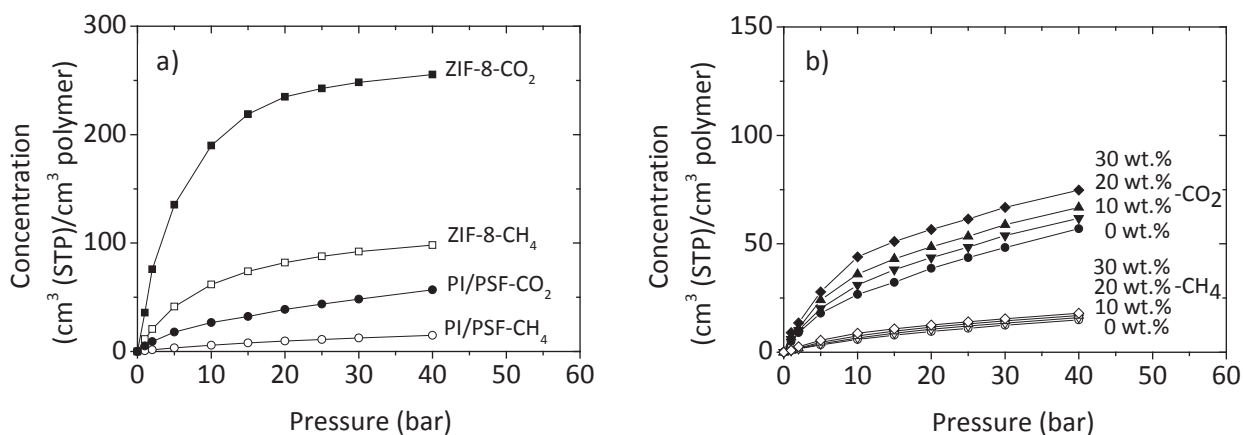


Fig. 4.3. Pure gas sorption isotherms of CO₂ (closed) and CH₄ (open) for (a) pure ZIF-8 (■, □) and pure PI/PSF (●, ○) and (b) pure PI/PSF (●, ○), 10 wt.% (▼, ▽), 20 wt.% (▲, △) and 30 wt.% (◆, ◇) ZIF-8 MMMs as function of the applied gas pressure.

Table 4.2. Dual mode sorption parameters for CO₂ and CH₄ in PI/PSF blend membranes with various wt.% of ZIF-8.

| Feed gas | ZIF-8 (wt.%) | Dual mode sorption model | | |
|-----------------|-----------------|---|--------------|---|
| | | C'_H (cm ³ (STP)/cm ³) | b (1/cmHg) | k_D (cm ³ (STP)/cm ³ ·cmHg) |
| CO ₂ | 0 | 29 | 0.17 | 0.78 |
| | 10 | 41 | 0.18 | 0.63 |
| | 20 | 50 | 0.21 | 0.55 |
| | 30 | 62 | 0.24 | 0.45 |
| | 100 | 280 | 0.26 | 0.00 |
| CH ₄ | 0 | 11 | 0.06 | 0.17 |
| | 10 | 14 | 0.06 | 0.14 |
| | 20 | 17 | 0.07 | 0.12 |
| | 30 | 20 | 0.07 | 0.09 |
| | 100 | 122 | 0.10 | 0 |

In comparison to the PI/PSF membranes, pure ZIF-8 shows much higher sorption of CO₂ and CH₄ attributed to the high surface area (1300-1800 m²/g [42]) of the nanoparticles.

The effect of ZIF-8 on the CO₂ and CH₄ sorption in MMMs with 10, 20 and 30 wt.% ZIF-8 is shown in Fig. 4.3b. The increase in ZIF-8 loading in the polymer matrix enhances the sorption of both gases. This can be attributed to the extra space available in the nanocages of ZIF-8 and the increase in excess free volume of the polymer due to the presence of the particles [16]. CO₂ is more preferentially sorbed over CH₄, because of the stronger interaction of CO₂ with ZIF-8. The results tabulated in Table 4.2 for the MMMs suggest that the addition of ZIF-8 in the PI/PSF membrane affects both the Langmuir and the Henry's sorption. The high values of Henry's law constants (Table 4.2) for pure PI/PSF membranes (compared to MMMs) dictate that the major contribution to the overall sorption in the pure PI/PSF membrane is through Henry's law sorption [43]. The value of Henry's law constant decreases with increasing ZIF-8 loading indicating that the sorption mechanism shifts from Henry's law sorption to Langmuir sorption or a hole filling mechanism for ZIF-8 MMMs. This can be explained by the increasing fraction of ZIF-8, which reduces the polymer fraction in the MMMs and hence Henry sorption, as ZIF-8 particles only sorb gases through a hole filling mechanism.

The presence of ZIF-8 particles in PI/PSF membranes leads to higher Langmuir sorption capacity and Langmuir affinity constant for both CO₂ and CH₄. The higher values of C'_H and b for the MMMs reflect the contribution of ZIF-8 in increasing the sorption capacity of pure PI/PSF. C'_H is also a measure for the amount of excess free volume in the polymer [44]. Addition of ZIF-8 particles to the polymer matrix increases the excess free volume of the polymer [16], which contributes as well to the higher gas sorption. In addition the increase in b indicates that the ZIF-8 MMMs show a stronger interaction with the gases compared to the pure PI/PSF membrane. The of CO₂ and CH₄ in the ZIF-8 framework has been investigated extensively both by experiments and simulations. It was reported [45] that at low pressure, both CO₂ and CH₄ are preferentially sorbed in the vicinity of the organic imidazolate linkers. At high pressures, CH₄ resides near the aperture, but CO₂ sorbs in the central cage. As the pressure increases, the nanocages of ZIF-8 get saturated, leaving only Henry sorption in the polymer matrix. ZIF-8 is known to be a flexible MOF but the structural flexibility of ZIF-8 was found to have negligible effect on the sorption of CO₂ and CH₄. Recently, Hu et al. [46] studied the effect of CO₂ sorption on the flexibility of the ZIF-8 framework using FTIR spectroscopy. They

demonstrated that CO₂ can be inserted into the ZIF-8 framework until high pressures of around 0.8 GPa without any structural transition, indicating no influence of structural flexibility during sorption.

Notably the maximum sorption capacity, C'_H , in the 30 wt.% PI/PSF MMMs decreases by a factor 4 and 6 for CO₂ and CH₄, respectively, compared to the sorption in pure ZIF-8. This difference in sorption capacity between MMMs and pure ZIF-8 can be related to the limited sorption capacity of the polymer matrix surrounding the ZIF-8 particles. This finding provides indirect evidence that the ZIF-8 nanoparticles have excellent adhesion to the polymer matrix with minimal defects at the interfaces (which would give high sorption capacities).

4.3.4 Pure gas separation

4.3.4.1 Effect of ZIF-8 loading and feed pressure

4.3.4.1.1 Permeability

Fig. 4.4 shows the pure gas CO₂ permeability of MMMs as a function of pressure for different ZIF-8 loadings.

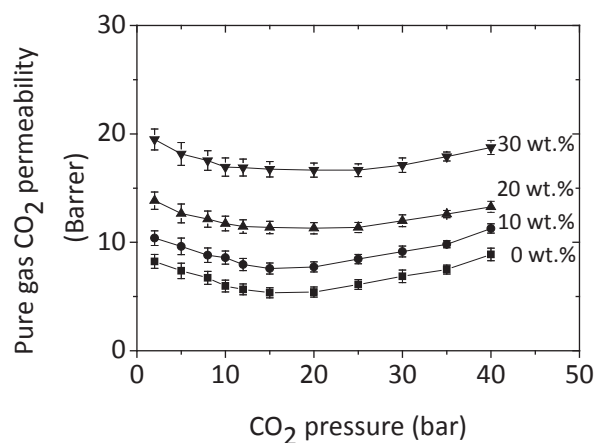


Fig. 4.4. Pure gas CO₂ permeabilities as a function of pressure for different ZIF-8 loadings at 35 °C.

As predicted, MMMs show higher CO₂ permeability compared to pure PI/PSF membranes, at a constant pressure over the whole pressure range. At low loadings of 10 wt.% ZIF-8, the gas separation performance of the MMMs shows a slight improvement over pure PI/PSF membrane, and when the ZIF-8 loading increases, the enhancement of

the CO₂ permeability becomes much more significant. This increase in permeability can be attributed to the porous network formed and increase in excess free volume of MMMs by the ZIF-8 particles.

For pure gas measurements, at low pressures, the PI/PSF membrane shows a slight decrease in permeability with pressure that can be attributed to the saturation of Langmuir sites reducing the solubility of CO₂ gas with pressure, following the predicted behavior of the dual mode sorption model [44, 47]. As the pressure increases, the concentration of CO₂ in the PI/PSF matrix increases (Fig. 4.3). Above a certain pressure the highly sorbing CO₂ gas causes the polymer chains to swell and plasticize [19, 48, 49]. The swelling of the polymer enhances the chain mobility resulting in enhanced gas diffusion of CO₂. The pressure at which the CO₂ permeability reaches its minimum and the curve shows an inflection point, is the plasticization pressure. Pure PI/PSF membranes show a CO₂ plasticization pressure of ~18 bar which is in agreement with the documented plasticization pressures of pure Matrimid® (~10 bar) and pure PSF (~34 bar) [19].

All MMMs show a similar trend in permeability with pressure as that of the pure PI/PSF membrane, although the MMMs show much higher permeabilities. First permeability shows a slight decrease with pressure attributed to the saturation of Langmuir sites (or solubility decrease). After the plasticization pressure, permeability starts to increase. For the ZIF-8 MMMs this initial decrease in solubility of CO₂ in polymer matrix is compensated by the slight increase in sorption capacity and faster diffusion of CO₂ in the framework of ZIF-8 [16]. In addition to CO₂ permeability enhancement, the presence of ZIF-8 particles also delays the plasticization pressure of the polymer matrix because of the restricted movement of the polymer chains caused by the ZIF-8 particles [18]. The 30 wt.% ZIF-8 MMM shows a plasticization pressure of ~25bar compared to a value of ~18 bar only for the pure PI/PSF membrane.

Fig. 4.5 shows the pure gas CH₄ permeability of non-plasticized membranes. For the MMMs containing ZIF-8 the CH₄ permeability follows a similar trend as that of the pure PI/PSF membrane. At all pressures the CH₄ permeabilities in the MOF containing membranes are higher than that of the pure PI/PSF membranes. The CH₄ permeability

shows a slight initial decrease with pressure but when the pressure increases the CH₄ permeability becomes independent of the pressure. CH₄ permeability does not show an inflection point, as is the case for the CO₂ permeability (plasticization). The solubility of CH₄ is relatively low and it does not reach sufficiently high concentrations to induce plasticization. Consequently, its permeability is almost independent of the feed pressure.

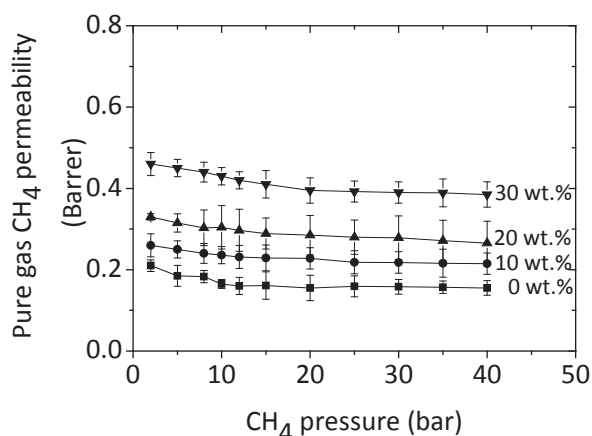


Fig. 4.5. Pure gas CH₄ permeabilities as a function of pressure for different loadings of ZIF-8

All MMMs show higher CH₄ permeabilities compared to pure PI/PSF membranes over the whole pressure range and the difference becomes more significant as the loading of ZIF-8 increases. This increase in permeability is a consequence of the moderate increase in sorption and larger increase in diffusivity of CH₄ molecules as will be discussed in more detail in the next section.

4.3.4.1.2 Diffusivity

The pure gas diffusivity for CO₂ and CH₄ as a function of the feed pressure for different ZIF-8 loadings is shown in Fig. 4.6a and b. The diffusivities have been calculated from the measured pure gas permeabilities and solubilities according to equation 3. The solubility coefficients are derived from the measured sorption isotherms according to equation 2. The diffusivity values show clear trends although the actual values may be somewhat less accurate as solubility is determined from a measurement where the sample is fully surrounded by the gas, while during permeation measurements, the permeate side of the membrane experiences vacuum. For PI/PSF membranes the CO₂ diffusivity slightly increases up to a pressure of 20 bar but plasticization does not yet set in. As the

pressure increases above 20 bar the diffusivity shows a relatively stronger increase in value with pressure indicating the start of plasticization as also observed by the increase in CO₂ permeability with pressure in Fig. 4.4. For the MMMs, over the full pressure range, the diffusivity shows a higher value than that of the pure PI/PSF membranes, attributed to the faster diffusion of CO₂ molecules through the ZIF-8 particles. As the pressure increases, especially at higher ZIF-8 loadings, CO₂ diffusivity increases almost linearly with pressure, this in contrast to the pure membranes. The reason for this almost linear increase over the full pressure range is twofold: ZIF-8 suppresses plasticization to a certain extent as also shown in Fig. 4.4 and at higher pressures (concentrations) diffusivity of CO₂ through the ZIF-8 particles slightly decreases because of stronger steric hindrance (because of inefficient packing) [45].

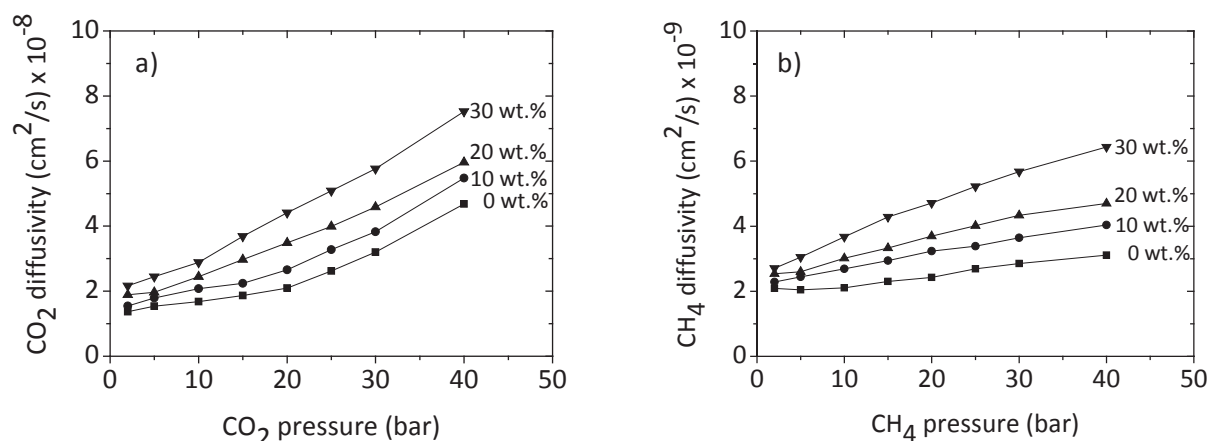


Fig. 4.6. Diffusivity of (a) CO₂ and (b) CH₄ of the MMMs containing different ZIF-8 loadings.

The diffusivity of CH₄ (Fig. 4.6b) shows a similar trend of increasing diffusivity with pressure and this increase is stronger with higher ZIF-8 loading. However, the relative increase is lower than in the case of CO₂ and also, the increase is more close to linear. The increase in diffusion coefficient is a direct consequence of the higher diffusion of CH₄ through the ZIF-8 particles. Similar trends were observed based on molecular dynamics simulations by Pantatosaki et al. [50]. The reason for higher diffusion coefficient of CH₄ with pressure can be explained based on sorption sites for CH₄ and associated free energies of sorption. At low pressures, both CO₂ and CH₄ are preferentially sorbed in the vicinity of the organic imidazolate linkers of the MOF. At higher pressures, CH₄ resides near the aperture, but CO₂ sorbs in the central cage. At

high pressures and hence high sorption densities, the free energy drops for both CO₂ and CH₄. This drop is higher for CH₄ than for CO₂, as CH₄ tends to be more densely located at the aperture which facilitates inter-cage hopping [51]. Consequently, the barrier for diffusion of CH₄ drops to a larger extent and its diffusivity increases more relative to its diffusivity in the native polymer. Also the structural flexibility of ZIF-8 due to swinging of the imidazolate linker causes a faster diffusion of larger molecules like CH₄ in MMMs compared to pure polymer [11] and hence increases the diffusivity of CH₄ with pressure as observed in Fig. 4.9b.

Fig. 4.7 compares the pure gas solubility selectivity (α_s) and diffusion selectivity (α_D) of pure PI/PSF membrane and a 30 wt.% ZIF-8 MMM. As shown, for both the pure PI/PSF membrane and the 30 wt.% ZIF-8 MMM, the diffusivity selectivity is more dominant to the overall selectivity, while the solubility selectivity only moderately contributes. The dominant effect of diffusivity selectivity was also observed by Ploegmakers et al. for the separation of propylene and propane using Cu₃BTC₂ MMMs [52]. The solubility selectivities of the native PI/PSF membrane and the 30 wt.% ZIF-8 MMM are comparable (it is slightly higher for the MMM), and the same is valid for the diffusivity selectivity up to ~18 bar. Above a feed pressure of ~18 bar, the diffusivity selectivity of the pure PI/PSF membrane shows a steeper increase compared to the 30 wt.% ZIF-8 MMM. This can be attributed to the occurrence of plasticization in the PI/PSF membranes. This result confirms that the polymer blending and the mixed matrix approach delay plasticization to occur.

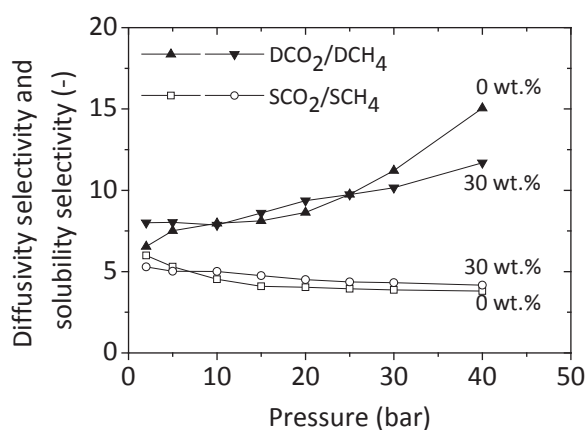


Fig. 4.7. Diffusivity selectivity (α_D) and solubility selectivity (α_s) of pure PI/PSF and 30 wt.% ZIF-8 MMM as a function of pressure.

Fig. 4.8 finally shows the ideal selectivity of the PI/PSF and PI/PSF-ZIF-8 MMMs as a function of pressure. The ideal selectivity of the PI/PSF membranes and the 10 wt.% MMMs clearly shows the occurrence of plasticization, visible as an increase in pure gas selectivity from ~18 bar on, while the MMMs with higher ZIF-8 loadings show a delay and suppression of plasticization up to a pressure of ~25 bar.

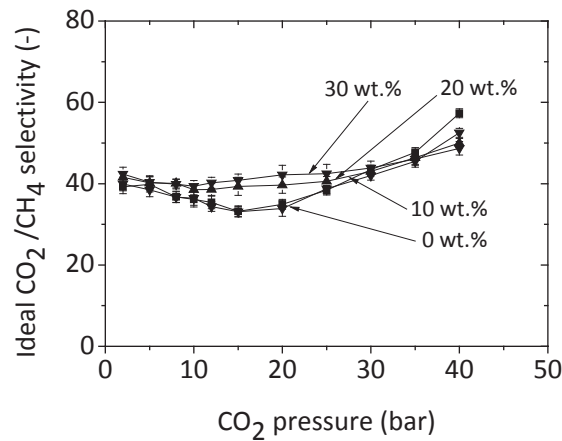


Fig. 4.8. Ideal CO₂/CH₄ selectivity of MMMs with different loading of ZIF-8 as a function of pressure.

4.3.5 Mixed gas separation

Fig. 4.9 shows the mixed gas CO₂ permeability of pure PI/PSF and the 30 wt.% ZIF-8 MMMs as function of the CO₂ partial pressure. For comparison the results of mixed gas separation of pure PI and PI membranes with 30 wt.% ZIF-8 loading from our previous study [18] are also shown.

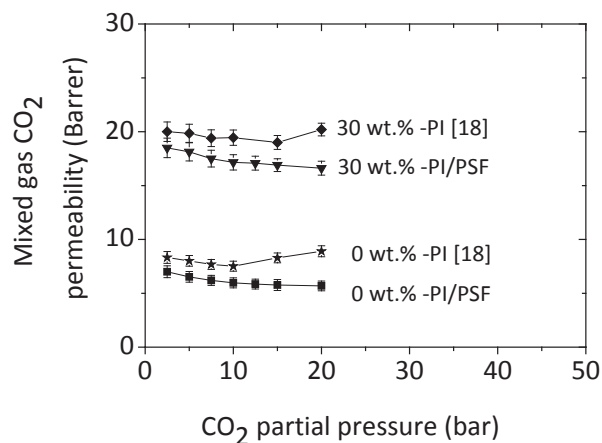


Fig. 4.9. Mixed gas CO₂ permeabilities of PI [18] and PI/PSF MMMs as a function of pressure for different ZIF-8 loadings at 35 °C.

The mixed gas permeabilities of the PI/PSF membranes are slightly lower than the pure gas permeabilities and permeability shows a small decrease with increasing pressure. The pure PI membrane shows a plasticization pressure of ~10 bar, which is consistent with literature [19, 48, 49]. The PI/PSF membrane in contrast, does not show any plasticization phenomena over the whole pressure range investigated (up to 20 bar CO₂ partial pressure), while the pure gas measurements (Fig. 4.4) do show plasticization in the PI/PSF membrane and the ZIF-8 MMMs. This can be attributed to the occurrence of competitive sorption that limits the sorption of CO₂ and counterbalances the effect of plasticization [53, 54].

Similar to PI/PSF membranes, also all PI/PSF MMMs did not show plasticization phenomena over the whole mixed gas pressure range, while in the case of the PI-30 wt.% ZIF-8 MMM plasticization is visible around a CO₂ partial pressure of 15 bar. The presence of ZIF-8 nanoparticles thus increases the plasticization pressure in PI to a certain extent (from 10 bar to 15 bar), but subsequent blending of PSF with PI further suppresses plasticization, while at the same time increasing the CO₂ permeability.

Fig. 4.10 shows the CH₄ permeability as a function of the CO₂ partial pressure for the pure polymers and the MMMs with different ZIF-8 loadings. For the pure PI membrane, the CH₄ permeability shows a strong increase in permeability typical for the less mobile component after the plasticization pressure (~10 bar CO₂ partial pressure) is reached. Pure PI/PSF membranes show nearly constant CH₄ permeabilities with increasing CO₂ partial pressure, indicating the suppression of plasticization. For pure PI/PSF membranes, the mixed gas CH₄ permeabilities show relatively lower values than those obtained for the pure gas CH₄ permeabilities, which is attributed to competitive sorption [55].

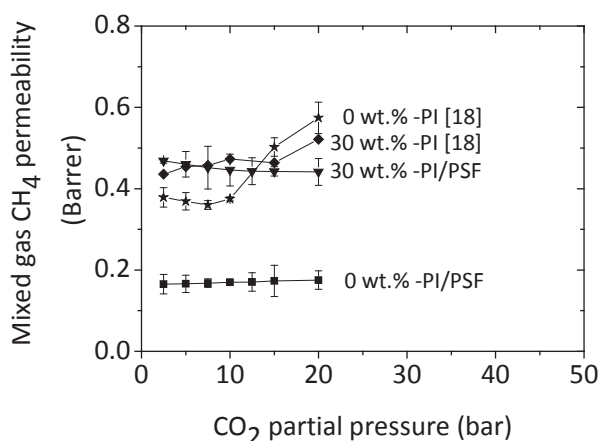


Fig. 4.10. Mixed gas CH₄ permeabilities of PI [18] and PI/PSF blend MMMs as a function of pressure for different ZIF-8 loadings at 35 °C.

For 30 wt.% loadings of ZIF-8 in PI/PSF, the CH₄ permeability remains almost constant with increasing CO₂ partial pressure. This is in contrast to the PI-30 wt.% ZIF-8 membrane without PSF, which shows distinctive plasticization at pressures above ~15 bar. This almost constant CH₄ permeability for the PI/PSF-ZIF-8 MMM suggests the suppression of plasticization. The permeability of CH₄ is lower than the pure gas CH₄ measurements. The reason can be two-fold: it can be due to competitive sorption and ZIF-8 nanoparticles may hinder CH₄ transport with increasing pressure thus reducing the CH₄ permeability. It was reported that the preponderance of CO₂ at the window pore regions hinders the inter-cage hopping of CH₄ molecules present in the mixture with CO₂ [56]. Zhang et al. [51] also reported that for the separation a of mixture of CO₂/CH₄, the diffusion of CH₄ is distinctively reduced by the presence of CO₂ molecules in the mixture. The authors attributed this effect to the blocking of the diffusional pathway by CO₂.

The mixed gas CO₂/CH₄ selectivity (Fig. 4.11) show a decrease in selectivity with increasing CO₂ partial pressure for the pure PI and PI/PSF membranes. For the pure PI membranes this decrease in selectivity is much more stronger (45 %) than for the PI/PSF membranes. This drop in selectivity can be attributed to two counteracting effects; the decreasing solubility of the polymer matrix and occurrence of plasticization phenomena, with increasing CO₂ partial pressure. It is not possible to distinguish between these two effects here.

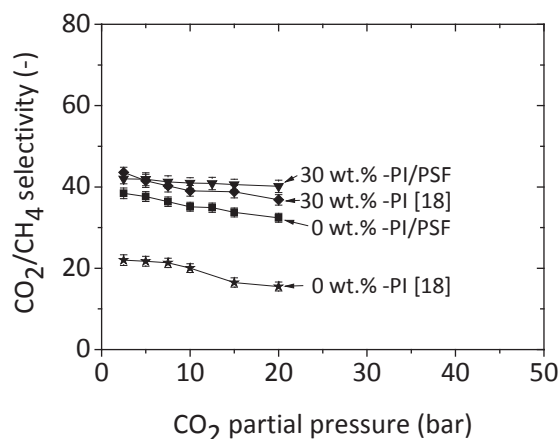


Fig. 4.11. Mixed gas CO₂/CH₄ selectivity of PI [18] and PI/PSF blend MMMs as a function of pressure for different ZIF-8 loadings at 35 °C.

At low pressures, the PI/PSF MMMs with high ZIF-8 loadings (30 wt.%) show comparable results as that of the pure PI/PSF membranes. At high CO₂ partial pressure PI/PSF MMMs show relatively higher and nearly constant selectivity with pressure, while the PI-30 wt.% ZIF-8 shows a drop in selectivity above 15 bar CO₂ partial pressure. In summary, comparison of the results for PI/PSF MMMs with PI MMM [18] and similar literature data on PI/PSF membranes from Basu [27, 57] and others [20, 25, 58] reveals that PSF blending with PI and high loadings of ZIF-8 successfully suppress CO₂ induced plasticization, while keeping the advantages of high CO₂ permeabilities. The permeability of the pure PI/PSF membranes is comparable to that of Basu [27, 57]. However, the PI/PSF-ZIF-8 MMMs outperform all these membranes in terms of permeability and selectivity.

4.4 Conclusion

Different mixed matrix membranes with an optimized PI/PSF blend ratio (3:1) filled with different concentrations of ZIF-8 were prepared in order to investigate the effect of ZIF-8 loading and polymer blending on gas separation performance and plasticization behavior. PI and PSF are miscible and provide good compatibility with the ZIF-8 particles, even at high loadings. TGA results show higher thermal stability of the MMMs compared to the pure PI/PSF blend. Experimental results show that the permeability of both CO₂ and CH₄ increases with ZIF-8 loading due to moderate increase in sorption capacity but faster diffusion through the ZIF-8 particles. In pure gas measurements, the MMMs show plasticization at higher plasticization pressures (~25 bar) compared to the pure PI/PSF

membranes (~18 bar). The delay in plasticization pressure can be attributed to the increased restriction in polymer chain mobility in the MMMs due to the presence of the ZIF-8 particles. In mixed gas measurements, PI/PSF membranes and ZIF-8 MMMs both show suppression of plasticization as confirmed by a constant mixed gas CH₄ permeability and nearly constant selectivity with pressure (up to 20 bar CO₂ partial pressure). The work reveals that polymer blending of PI and PSF combined with a ZIF-8 mixed matrix approach is a versatile tool to suppress CO₂ induced plasticization while at the same time combining this with higher CO₂ permeabilities and nearly constant CO₂/CH₄ selectivities.

Acknowledgments

The authors would like to thank the Erasmus Mundus Doctorate in Membrane Engineering (EUDIME) for funding this research and Dr. Jeroen Ploegmakers for his help in measuring the gas sorption data.

References

- [1] A. Brunetti, F. Scura, G. Barbieri, E. Drioli, Membrane technologies for CO₂ separation, *J. Membr. Sci.*, 359 (2010) 115-125.
- [2] L.M. Robeson, The upper bound revisited, *J. Membr. Sci.*, 320 (2008) 390-400.
- [3] L.M. Robeson, Correlation of separation factor versus permeability for polymeric membranes, *J. Membr. Sci.*, 62 (1991) 165-185.
- [4] Y.-S. Bae, R.Q. Snurr, Development and evaluation of porous materials for carbon dioxide separation and capture, *Angewandte Chemie-International Edition*, 50 (2011) 11586-11596.
- [5] O.M. Yaghi, M. O'Keeffe, N.W. Ockwig, H.K. Chae, M. Eddaoudi, J. Kim, Reticular synthesis and the design of new materials, *Nature*, 423 (2003) 705-714.
- [6] K.S. Park, Z. Ni, A.P. Côté, J.Y. Choi, R. Huang, F.J. Uribe-Romo, H.K. Chae, M. O'Keeffe, O.M. Yaghi, Exceptional chemical and thermal stability of zeolitic imidazolate frameworks, *Proceedings of the National Academy of Sciences of the United States of America*, 103 (2006) 10186-10191.
- [7] A.R. Millward, O.M. Yaghi, Metal-organic frameworks with exceptionally high capacity for storage of carbon dioxide at room temperature, *Journal of the American Chemical Society*, 127 (2005) 17998-17999.
- [8] S.R. Venna, J.B. Jasinski, M.A. Carreon, Structural evolution of zeolitic imidazolate framework-8, *Journal of the American Chemical Society*, 132 (2010) 18030-18033.

- [9] D. Ge, H.K. Lee, Water stability of zeolite imidazolate framework 8 and application to porous membrane-protected micro-solid-phase extraction of polycyclic aromatic hydrocarbons from environmental water samples, *Journal of Chromatography A*, 1218 (2011) 8490-8495.
- [10] H. Bux, F. Liang, Y. Li, J. Cravillon, M. Wiebcke, J. Caro, Zeolitic Imidazolate framework membrane with molecular sieving properties by microwave-assisted solvothermal synthesis, *Journal of the American Chemical Society*, 131 (2009) 16000-16001.
- [11] D. Fairen-Jimenez, R. Galvelis, A. Torrisi, A.D. Gellan, M.T. Wharmby, P.A. Wright, C. Mellot-Draznieks, T. Düren, Flexibility and swing effect on the adsorption of energy-related gases on ZIF-8: Combined experimental and simulation study, *Dalton Transactions*, 41 (2012) 10752-10762.
- [12] M.C. McCarthy, V. Varela-Guerrero, G.V. Barnett, H.K. Jeong, Synthesis of zeolitic imidazolate framework films and membranes with controlled microstructures, *Langmuir*, 26 (2010) 14636-14641.
- [13] A.W. Thornton, D. Dubbeldam, M.S. Liu, B.P. Ladewig, A.J. Hill, M.R. Hill, Feasibility of zeolitic imidazolate framework membranes for clean energy applications, *Energy & Environmental Science*, 5 (2012) 7637-7646.
- [14] M.J.C. Ordonez, K.J. Balkus, J.P. Ferraris, I.H. Musselman, Molecular sieving realized with ZIF-8/Matrimid® mixed-matrix membranes, *J. Membr. Sci.*, 361 (2010) 28-37.
- [15] C. Zhang, Y. Dai, J.R. Johnson, O. Karvan, W.J. Koros, High performance ZIF-8/6FDA-DAM mixed matrix membrane for propylene/propane separations, *J. Membr. Sci.*, 389 (2012) 34-42.
- [16] Q. Song, S.K. Nataraj, M.V. Roussanova, J.C. Tan, D.J. Hughes, W. Li, P. Bourgoïn, M.A. Alam, A.K. Cheetham, S.A. Al-Muhtaseb, E. Sivaniah, Zeolitic imidazolate framework (ZIF-8) based polymer nanocomposite membranes for gas separation, *Energy and Environmental Science*, 5 (2012) 8359-8369.
- [17] S. Shahid, K. Nijmeijer, High pressure gas separation performance of mixed-matrix polymer membranes containing mesoporous Fe(BTC), *J. Membr. Sci.*, 459 (2014) 33-44.
- [18] S. Shahid, K. Nijmeijer, Performance and plasticization behavior of polymer-MOF membranes for gas separation at elevated pressures, *J. Membr. Sci.*, 470 (2014) 166-177.
- [19] A. Bos, I.G.M. Punt, M. Wessling, H. Strathmann, CO₂-induced plasticization phenomena in glassy polymers, *J. Membr. Sci.*, 155 (1999) 67-78.
- [20] G.C. Kapantaidakis, S.P. Kaldis, X.S. Dabou, G.P. Sakellaropoulos, Gas permeation through PSF-PI miscible blend membranes, *J. Membr. Sci.*, 110 (1996) 239-247.
- [21] G.C. Kapantaidakis, S.P. Kaldis, G.P. Sakellaropoulos, E. Chira, B. Loppinet, G. Floudas, Interrelation between phase state and gas permeation in polysulfone/polyimide blend membranes, *Journal of Polymer Science Part B: Polymer Physics*, 37 (1999) 2788-2798.

- [22] S.S. Hosseini, M.M. Teoh, T.S. Chung, Hydrogen separation and purification in membranes of miscible polymer blends with interpenetration networks, *Polymer*, 49 (2008) 1594-1603.
- [23] T.-S. Chung, W.F. Guo, Y. Liu, Enhanced Matrimid membranes for pervaporation by homogenous blends with polybenzimidazole (PBI), *J. Membr. Sci.*, 271 (2006) 221-231.
- [24] A. Bos, I. Punt, H. Strathmann, M. Wessling, Suppression of gas separation membrane plasticization by homogeneous polymer blending, *Aiche Journal*, 47 (2001) 1088-1093.
- [25] G.C. Kapantaidakis, G.H. Koops, M. Wessling, S.P. Kaldis, G.P. Sakellaropoulos, CO₂ Plasticization of polyethersulfone/polyimide gas-separation membranes, *Aiche Journal*, 49 (2003) 1702-1711.
- [26] S. Rafiq, Z. Man, S. Maitra, A. Maulud, F. Ahmad, N. Muhammad, Preparation of asymmetric polysulfone/polyimide blended membranes for CO₂ separation, *Korean J. Chem. Eng.*, 28 (2011) 2050-2056.
- [27] S. Basu, A. Cano-Odena, I.F.J. Vankelecom, Asymmetric membrane based on Matrimid® and polysulphone blends for enhanced permeance and stability in binary gas (CO₂/CH₄) mixture separations, *Separation and Purification Technology*, 75 (2010) 15-21.
- [28] S. Matteucci, Y. Yampolskii, B.D. Freeman, I. Pinnau, Transport of gases and vapors in glassy and rubbery polymers, in *Materials science of membranes for gas and vapor separation*, John Wiley & Sons, Ltd, 2006, pp. 1-47.
- [29] J.G. Wijmans, R.W. Baker, The solution-diffusion model: a review, *J. Membr. Sci.*, 107 (1995) 1-21.
- [30] B.D. Bhide, A. Voskericyan, S.A. Stern, Hybrid processes for the removal of acid gases from natural gas, *J. Membr. Sci.*, 140 (1998) 27-49.
- [31] M.L. Cecopieri-Gómez, J. Palacios-Alquisira, J.M. Domínguez, On the limits of gas separation in CO₂/CH₄, N₂/CH₄ and CO₂/N₂ binary mixtures using polyimide membranes, *J. Membr. Sci.*, 293 (2007) 53-65.
- [32] P.H. Pfromm, W.J. Koros, Accelerated physical aging of thin glassy polymer-films - evidence from gas-transport measurements, *Polymer*, 36 (1995) 2379-2387.
- [33] M. Wessling, I. Huisman, T. Vanderboomgaard, C.A. Smolders, Time-dependent permeation of carbon-dioxide through a polyimide membrane above the plasticization pressure, *Journal of Applied Polymer Science*, 58 (1995) 1959-1966.
- [34] K. Zhang, R.P. Lively, C. Zhang, R.R. Chance, W.J. Koros, D.S. Sholl, S. Nair, Exploring the framework hydrophobicity and flexibility of zif-8: from biofuel recovery to hydrocarbon separations, *The Journal of Physical Chemistry Letters*, 4 (2013) 3618-3622.
- [35] S. Basu, A. Cano-Odena, I.F.J. Vankelecom, MOF-containing mixed-matrix membranes for CO₂/CH₄ and CO₂/N₂ binary gas mixture separations, *Separation and Purification Technology*, 81 (2011) 31-40.

- [36] C. Joly, D. Le Cerf, C. Chappey, D. Langevin, G. Muller, Residual solvent effect on the permeation properties of fluorinated polyimide films, *Separation and Purification Technology*, 16 (1999) 47-54.
- [37] H. Ren, J. Jin, J. Hu, H. Liu, Affinity between metal-organic frameworks and polyimides in asymmetric mixed matrix membranes for gas separations, *Industrial & Engineering Chemistry Research*, 51 (2012) 10156-10164.
- [38] C.A. Scholes, W.X. Tao, G.W. Stevens, S.E. Kentish, Sorption of methane, nitrogen, carbon dioxide, and water in Matrimid 5218, *Journal of Applied Polymer Science*, 117 (2010) 2284-2289.
- [39] R.W. Baker, *Membrane Technology and Applications*, 2012.
- [40] N.N. Li, A.G. Fane, W.S.W. Ho, T. Matsuura, *Advanced Membrane Technology and Applications*, 2008.
- [41] S. Alavi, Selective Guest Docking in Metal-Organic Framework Materials, *ChemPhysChem*, 11 (2010) 55-57.
- [42]
<http://www.sigmaaldrich.com/catalog/product/aldrich/691348?lang=en®ion=NL>.
- [43] D. Raucher, D. Sefcik Michael, Sorption and transport in glassy polymers, in: *industrial gas separations*, AMERICAN CHEMICAL SOCIETY, 1983, pp. 111-124.
- [44] D.R. Paul, Gas sorption and transport in glassy-polymers, *Berichte Der Bunsen-Gesellschaft-Physical Chemistry Chemical Physics*, 83 (1979) 294-302.
- [45] C. Sitprasert, F.Y. Wang, V. Rudolph, Z.H. Zhu, Ideal and mixture permeation selectivity of flexible prototypical zeolitic imidazolate framework-8 Membranes, *Chemical Engineering Science*, 108 (2014) 23-32.
- [46] Y. Hu, Z. Liu, J. Xu, Y. Huang, Y. Song, Evidence of Pressure enhanced CO₂ Storage in zif-8 probed by FTIR spectroscopy, *Journal of the American Chemical Society*, 135 (2013) 9287-9290.
- [47] V. Stannett, The transport of gases in synthetic polymeric membranes-an historic perspective, *J. Membr. Sci.*, 3 (1978) 97-115.
- [48] T. Visser, M. Wessling, When do sorption-induced relaxations in glassy polymers set in?, *Macromolecules*, 40 (2007) 4992-5000.
- [49] T. Visser, N. Masetto, M. Wessling, Materials dependence of mixed gas plasticization behavior in asymmetric membranes, *J. Membr. Sci.*, 306 (2007) 16-28.
- [50] E. Pantatosaki, G. Megariotis, A.-K. Pusch, C. Chmelik, F. Stallmach, G.K. Papadopoulos, On the impact of sorbent mobility on the sorbed phase equilibria and dynamics: a study of methane and carbon dioxide within the zeolite imidazolate framework-8, *The Journal of Physical Chemistry C*, 116 (2011) 201-207.
- [51] L. Zhang, G. Wu, J. Jiang, Adsorption and diffusion of CO₂ and CH₄ in zeolitic imidazolate framework-8: effect of structural flexibility, *The Journal of Physical Chemistry C*, 118 (2014) 8788-8794.

- [52] J. Ploegmakers, S. Japip, K. Nijmeijer, Mixed matrix membranes containing MOFs for ethylene/ethane separation-Part B: Effect of Cu_3BTC_2 on membrane transport properties, *J. Membr. Sci.*, 428 (2013) 331-340.
- [53] T. Visser, G.H. Koops, M. Wessling, On the subtle balance between competitive sorption and plasticization effects in asymmetric hollow fiber gas separation membranes, *J. Membr. Sci.*, 252 (2005) 265-277.
- [54] D. Vu, W.J. Koros, S.J. Miller, Effect of condensable impurity in CO_2/CH_4 gas feeds on performance of mixed matrix membranes using carbon molecular sieves, *J. Membr. Sci.*, 221 (2003) 233-239.
- [55] P.C. Raymond, W.J. Koros, D.R. Paul, Comparison of mixed and pure gas permeation characteristics for CO_2 and CH_4 in copolymers and blends containing methyl-methacrylate units, *J. Membr. Sci.*, 77 (1993) 49-57.
- [56] C. Chmelik, J. van Baten, R. Krishna, Hindering effects in diffusion of CO_2/CH_4 mixtures in ZIF-8 crystals, *J. Membr. Sci.*, 397–398 (2012) 87-91.
- [57] S. Basu, A. Cano-Odena, I.F.J. Vankelecom, Asymmetric Matrimid®/ $\text{Cu}_3(\text{BTC})_2$ mixed-matrix membranes for gas separations, *J. Membr. Sci.*, 362 (2010) 478-487.
- [58] F. Dorosti, M.R. Omidkhah, M.Z. Pedram, F. Moghadam, Fabrication and characterization of polysulfone/polyimide-zeolite mixed matrix membrane for gas separation, *Chemical Engineering Journal*, 171 (2011) 1469-1476.

Chapter 5

MOF-mixed matrix membranes: precise dispersion of MOF particles with better compatibility *via* a particle fusion approach for enhanced gas separation properties

ABSTRACT

Mixed matrix membranes (MMMs) incorporating conventional fillers frequently suffer from insufficient adhesion between the polymer matrix and the fillers. This often results in the formation of non-selective voids at the filler/polymer interface, which decreases the performance of the membrane. A novel approach is presented here to develop metal organic framework (MOF) based MMMs by using the self-assembly of MOF-polymer particles followed by their controlled fusion. MOF-polymer interaction is optimized through this strategy and it overcomes MOF-polymer incompatibility, MOF agglomeration and MOF distribution problems, happening especially at high loadings of MOFs. Matrimid® polymer particles were first prepared by precipitating a Matrimid® polymer solution in water. The surface of these particles was then modified by the introduction of imidazole groups, being chemically compatible with ZIF-8. ZIF-8 nanoparticles were then grown in-situ to this modified polymer particle suspension by addition of the precursor for ZIF-8 synthesis. The resulted suspension was cast to dryness and annealed in solvent-vapor environment to induce particle fusion, leading to a dense MMM structure. Scanning electron microscopy (SEM) images showed an excellent dispersion of the ZIF-8 nanoparticles forming a percolating pathway without any agglomeration, even at 40 wt.% loading of the ZIF-8. Excellent dispersion of ZIF-8 and an excellent ZIF-8-polymer interfacial adhesion resulted in a significant improvement in both CO₂ permeability and CO₂/CH₄ selectivity. The CO₂ permeability of the MMMs showed an increase of more than 200 % and the CO₂/CH₄ selectivity increased by 65 % compared to pure Matrimid®. More detailed analysis of the gas transport performance of the MMMs showed that the CO₂ permeability and the CO₂/CH₄ selectivity are mainly governed by the increase in diffusivity of CO₂. The presented approach is a very versatile MMM preparation route, not only for this specific ZIF and polymer but for a wide range of material combinations.

5.1 Introduction

Membrane technology offers energy efficient and environmentally friendly separation processes and has become important for many sustainable process applications e.g. energy generation, energy storage, water purification and gas separation [1]. During the last two decades, polymeric membranes have experienced major expansion in gas separation applications and substantial research efforts have been devoted to develop new polymeric membranes to improve the membrane separation performance [2-4]. Despite all these efforts, polymeric membranes are limited by a permeability-selectivity trade-off behavior indicated via an empirical upper bound, as presented in the famous Robeson plot [5, 6]. On the other hand, inorganic membrane materials offer excellent separation performances combined with high chemical and thermal stability in contrast to polymeric membranes [1]. However, the biggest hurdle in large scale production of inorganic membranes lies in their high cost and lack of processability [7]. Mixed matrix membranes (MMMs) offer the opportunity to combine the benefits of low cost and easy processing of polymeric materials with the excellent transport performance of inorganic fillers. Successful implementation of this approach can produce robust membranes with enhanced permeability and selectivity exceeding the Robeson upper bound limit [8]. However, MMMs often do not possess their predicted separation performance behavior, as these frequently suffer from insufficient adhesion between the polymer matrix and the fillers [9]. The polymer-filler interface morphology is a critical factor to determine the overall gas transport properties as poor interaction between the polymer and filler could lead to non-selective void formation, which results in high fluxes but low selectivities [10-13].

Among the common strategies to improve the polymer-filler adhesion, the use of mesoporous materials [14, 15] and silane coupling agents [13, 16, 17] has been extensively studied. However, use of coupling agents to modify the filler surface could risk blocking of the pores of filler.

Recently, metal organic frameworks (MOFs) have been identified as attractive fillers. Due to the high flexibility of the MOF design, these allow to specifically tune their properties towards high selectivity and permeability for specific separations. At the same time, the current MOF chemistry allows to some extent to improve the embedding

of the MOF in the polymer matrix [18]. Nevertheless, still non-selective voids at the MOF-polymer matrix interface are frequently formed [18, 19].

Perez et al. [20] incorporated MOF-5 in a Matrimid® matrix for the separation of binary mixtures. At 30 wt.% loading, permeability of gases increased by 120 %. Nevertheless, this increase was the result of MOF aggregation and poor interconnectivity at the interface between MOF and polymer matrix, as observed by scanning electron microscopy (SEM).

In other studies, Cu-4,4'-bipyridine-hexafluorosilicate (Cu-BPY-HFS) and $\text{Cu}_3(\text{BTC})_2$ were embedded in a Matrimid® polymer matrix [21, 22]. In both these studies, enhanced gas permeability was observed while the selectivity remained approximately equal to that of the pure polymer. Ordonez et al. [23] studied a Matrimid®-ZIF-8 MMMs. The permeability of these membranes was enhanced with increasing loading of ZIF-8 up to 40 wt.%. The published SEM images showed aggregated ZIF-8 particles in the polymer matrix with visible interfacial voids.

Ploegmakers et al. [24] observed that the $\text{Cu}_3(\text{BTC})_2$ crystals were deposited at the bottom of the membrane during the membrane preparation, leading to an inhomogeneous membrane. The resulting MMMs showed an increased selectivity with $\text{Cu}_3(\text{BTC})_2$ loading while the permeability remained constant.

Recently, Song et al. [25] reported MMMs prepared using as-synthesized non-dried ZIF-8 nanoparticles in Matrimid®. The as-synthesized ZIF-8 particles showed a relatively better compatibility with the polymer matrix compared to previously reported ZIF-8 MMMs [23, 26, 27]. But still at high loadings (> 20 wt.%), the MMMs showed enhanced CO_2 permeability combined with decreased selectivity, even below that of the native polymer, attributed to non-selective voids.

Several attempts have been reported to improve the interaction between polymer and fillers, including proper selection of compatible polymers and filler particles [9, 28], priming of filler particles [29], use of more concentrated (viscous) suspensions [30], controlling evaporation rates of solvents [31], use of silane coupling agents [16, 32], annealing treatments [25] and coating the outer surface of MMMs with thin appropriate layers. But the fabrication of the MMMs poses several challenges as mentioned above in

order to obtain the desired morphology, gas separation properties and mechanical/chemical stability.

To enhance the performance of polymer-MOF MMMs tremendously, we here report a novel strategy to prepare high-performing MOF-polymer MMMs by using particle fusion of the phase separated polymer particles and the in-situ synthesized MOF particles.

First PI polymer particles are prepared by precipitating a Matrimid® solution into a non-solvent. Subsequently the surface of these particles is chemically modified by introduction of a MOF compatible (imidazole) functionality. The MOF particles are then grown into this modified polymer particle suspension by addition of the MOF precursors. The resulting suspension is cast onto a flat substrate and dried in a solvent-vapor environment to transform the particulate morphology into a dense MMM structure.

Surface modification of polymer, in-situ growth of MOF particles in a polymer particle environment and subsequent fusion of the polymer particles in a controlled solvent vapor environment offers a new, exceptionally versatile and easy method to prepare polymer-MOF MMMs without encountering the usual problem of poor adhesion between MOF and polymer as observed in MMMs prepared by standard blending and membrane casting. Growing of the MOF particles in the spaces between the polymer particles will provide a more continuous MOF phase throughout the membrane cross-section without agglomeration, even at higher loadings. The proposed method of particle fusion improves the polymer-MOF interactions far more than the solvent casting method and eliminates the major obstacles stemming from polymer-MOF incompatibility, MOF agglomeration and MOF misdistribution, pore blockage and chain rigidification.

In this work, ZIF-8 and Matrimid® polyimide (PI) are selected as model MOF and polymer matrix. The reason for choosing this particular MOF is threefold; (i) it is readily available and well understood in terms of structure and behavior, (ii) it has excellent thermal, chemical and moisture resistance and (iii) it has been widely used in CO₂/CH₄ gas separation studies. Several experimental and simulation studies based on the adsorption and separation of natural gas showed high potential of ZIF-8 as adsorbent material [33-

35]. Matrimid® is a widely used PI in industry because of its high glass transition temperature and good processability. Nevertheless, the proposed particle fusion method is very versatile and can be applied to many other combinations of polymer and MOF.

In this approach, polyimide polymer particles are first prepared by emulsifying the Matrimid® polyimide polymer solution into a non-solvent. The surface of these particles is chemically modified by introducing imidazole functionality. The ZIF-8 particles are then grown into this modified polymer particles suspension by addition of the precursors for ZIF-8 synthesis. The resulted suspension is casted onto a flat substrate and dried in a controlled solvent-vapor environment to transform the particulate morphology into dense MMMs.

The characteristics of the MMMs prepared through this novel particle fusion approach are investigated by a multitude of characterization techniques e.g. XRD, FTIR, NMR, TGA and DSC etc. Additionally the effect of ZIF-8 in terms of gas separation performance of the MMMs is studied and the results confirm the exceptionally good performance of the obtained membranes. As such, the MMMs prepared by the developed particle fusion approach clearly outperform MMMs prepared by traditional polymer-MOF blending and subsequent membrane casting.

5.2 Experimental

5.2.1 Materials

Matrimid® 5218 PI was supplied by Huntsman, Germany. The number average molecular weight was 50000 g mol^{-1} with a polydispersity of 1.62, as analyzed by gel permeation chromatography (GPC) calibrated by polystyrene standards. Zinc nitrate hexahydrate $[\text{Zn}(\text{NO}_3)_2 \cdot 6\text{H}_2\text{O}]$ and 2-methylimidazole $[\text{C}_4\text{H}_6\text{N}_2]$ were obtained from Sigma-Aldrich. Mili-Q water (with a resistivity of $18.0 \text{ M}\Omega \cdot \text{cm}$) was used for the aqueous synthesis of ZIF-8. DMF (99 % extra pure) was used as a solvent for the polymer and was purchased from Acros Organics, Belgium. All solvents were of analytical grade and used without further purification. CO_2 , CH_4 and a mixture of (50/50 mol% CO_2/CH_4) were supplied by Praxair, The Netherlands, and used as received (purity 99.999 %).

5.2.2 Membrane preparation

5.2.2.1 Synthesis of ZIF-8 nanocrystals

The ZIF-8 nanocrystals were synthesized in either aqueous conditions at room temperature [36] or under microwave irradiation conditions [33]. For both methods starting reactants were $\text{Zn}(\text{NO}_3)_2 \cdot 6\text{H}_2\text{O}$ and 2-methylimidazole. 0.13 g of $\text{Zn}(\text{NO}_3)_2 \cdot 6\text{H}_2\text{O}$ was dissolved in 3 g Mili-Q water. Secondly, 2.5 g 2-methylimidazole was dissolved in another 6.8 g Mili-Q water. The zinc nitrate solution was then dropwise added to the 2-methylimidazole solution under stirring at room temperature. The synthesis solution turned milky almost instantly after the two solutions mixed. After stirring for 12 h, the product was collected by centrifuging and then washed with deionized water (DI) for several times. For the microwave assisted synthesis of ZIF-8, the same recipe was used as for the synthesis at room temperature. The reactants were mixed in a Teflon-lined autoclave. Synthesis was carried out at 140 °C for 2 h in a Milestone ATC-FO 300 microwave oven, equipped with a MultiSYNTH Touch Screen Controller-Terminal 640. The mixture was heated to 140 °C for 2 h using a microwave power of 300 W. The resulting powder was recovered by centrifugation and washed with DI water for several times. The yield of both syntheses was ~80 % based on the amount of zinc. As model samples, two batches of ZIF-8 nanocrystals were as well dried under vacuum at 100 °C for 24 h and stored dry for further analysis.

5.2.2.2 Synthesis and modification of the polymer particles

A 3, 5, 8 and 10 wt.% Matrimid® solution in DMF was prepared. The solutions were stirred at room temperature overnight to make sure that the Matrimid® was completely dissolved. The final solutions were left for 2-3 h to allow complete release of air bubbles. The polymer solutions were subsequently injected in the form of droplets into a water tank using a fine stainless steel syringe tip with a size of 18 G (inner diameter of 0.7 mm) at a flow rate of 1 ml/min. For the rapid breaking of the polymer droplets, a Branson digital sonifier probe (101-135-066R) was used with a 100 % probe amplitude. Solid polymer spheres were formed immediately in water via solvent/water exchange. The resulting polymer spheres were dialyzed to remove solvent using a cellulose dialysis tubing from Sigma-Aldrich with a MWCO value of 12000 Da.

The surface of the polymer particles was subsequently modified by giving them an imidazole functionality using 1-(3-aminopropyl)-imidazole as a linker. An amount of 1-(3-aminopropyl)-imidazole equivalent to 10 wt.% of the polymer quantity was added to the suspension of the polymer particles under stirring at room temperature for 3-4 h. The chemical structure of the resulting material was confirmed by ^1H NMR and FTIR. The percentage of modification was evaluated by ^1H NMR, as explained in the supporting information.

5.2.2.3 Preparation of pure membranes and MMMs from a mixture of phase separated polymer particles and ZIF-8

To prepare the MMMs, the surface modified polymer particles (prepared from 8 wt.% Matrimid[®] solution, as described above) were used. The ZIF-8 particles were grown into this modified polymer particle suspension by addition of the precursors ($\text{Zn}(\text{NO}_3)_2 \cdot 6\text{H}_2\text{O}$ and 2-methylimidazole) for ZIF-8 synthesis using the same procedure as used for pure ZIF-8 nanocrystals synthesis. The resulting suspension was uniformly cast on a glass plate using a casting knife [300 μm slit] and the film was kept in a controlled DMF vapor environment for 5 days to dissolve the polymer particles around the ZIF-8 particles and to obtain dense MMMs. Finally, the resulting dense MMMs were vacuum dried at 150 $^\circ\text{C}$ for 24 hours. The same procedure was used to prepare pure polymer membranes without ZIF-8 particles.

5.2.3 Characterization techniques

Scanning electron microscopy (SEM) was performed using a low vacuum SEM (Hitachi S-4500) operated at a spatial resolution of 1.5 nm. The samples for SEM characterization were prepared by freeze-fracturing the dried membranes in liquid nitrogen. The samples were coated with a 1.5-2 nm thin platinum layer using a Balzers Union SCD040 sputter coater under argon flow to reduce sample charging under the electron beam.

The crystallinity of the samples under study was determined by powder X-ray diffraction (XRD) on a Bruker D2 PHASER operated at 40 mA and 40 kV using $\text{CuK}\alpha$ radiation with a wavelength (λ)=1.54 \AA at room temperature. Scans were made from 5 $^\circ$ to 50 $^\circ$ 2 θ with a step size of 0.02 $^\circ$ and a scan speed of 0.2 s per step. The membrane sample was attached onto a sample holder with a single crystal silicon substrate.

Thermal stability of the membranes was investigated by Thermal Gravimetric Analysis (TGA) using a Perkin Elmer TGA 4000. Samples were heated in N₂ from 50 °C to 900 °C at a ramp of 20 °C/min. The values reported in this study are an average of 3 membranes.

The glass transition temperature (T_g) of the membranes was determined on a Perkin Elmer 8000 differential scanning calorimeter. The samples were heated to a temperature of 400 °C at a temperature ramp of 10 °C/min. Then, the samples were quenched back to 50 °C at 10 °C/min. This cycle was repeated two times. The T_g was determined from the second heating scan using the midpoint heat capacity transition method.

¹H NMR (Nuclear Magnetic Resonance) spectra were recorded on a 300-MHz Bruker ACF300 spectrometer using deuterated chloroform as solvent (chloroform-d, Sigma-Aldrich, 99.9%).

The mechanical strength testing of the membranes with different ZIF-8 loadings was performed on a dynamic mechanical analyzer (DMAQ800) at a frequency of 2 Hz. Film samples with approximate dimensions of 17 × 5 × 0.1 mm³ were mounted in jaws. An average of 3 membranes was reported.

Fourier transform infrared spectroscopy (FTIR) was performed on a FTIR 710 de Nicolet over a wavelength range of 400–4000 cm⁻¹, with a spectral resolution of 4 cm⁻¹ and 32 scans. Thin slices of pure and mixed matrix membranes were measured directly.

Nitrogen adsorption analysis at 77K was conducted using a Tristar 3000 instrument. The membrane sample (0.1 g) was cut into small pieces. All samples were degassed at 150 °C overnight under a helium blanket and then placed in the adsorption station for analysis. The apparent surface area was calculated using the Brunauer-Emmett-Teller (BET) equation [37].

Gas sorption measurements of the fabricated membranes and pure ZIF-8 were performed on a Rubotherm Präzisions Mess Technik GmbH magnetic suspension balance. Approximately 50 mg of the sample was placed in the sample holder and evacuated till constant weight was achieved (to remove all air and water vapor from the sample). In order to determine the exact weight of the sample, a measurement at 0 bar pressure was conducted. After the measurement showed a constant value, the pressure

was increased by introducing either pure CO₂ or pure CH₄ into the system. The measurement was conducted at pressures of 0, 1, 2, 5 and 10 bars. The temperature was kept constant in the range of 35.0 ± 0.5 °C. The measured weight w_t (g) was corrected for buoyancy according to Archimede's principle. On the basis of the exact sample volume V_t (cm³) and the initial weight w_0 (g) of the sample and the gas density ρ_g (g/cm³), the mass gain m_t (g) could be calculated as

$$m_t = (w_t + V_t \rho_g) - w_0 \quad \text{Eq. 5.1}$$

The gas density was estimated using the Peng Robinson equation of state. The gas concentration in the polymer (cm³ (STP) gas per cm³ of polymer) was calculated using the molar volume at standard temperature and pressure (STP, 1 bar and 273.15 K), the polymer volume, and the molecular weight of the specific gas. The sorption isotherms were curve fitted by using a dual mode sorption model. Subsequently the solubility of the gas in the polymer (cm³(STP)/cm³·cmHg), was calculated as

$$S_i = \frac{C_i}{p_i} \quad \text{Eq. 5.2}$$

where C_i is the gas concentration in the polymer (cm³(STP)/cm³), p_i is the partial pressure of component i (cmHg) .

5.2.4 Gas permeation

Gas permeability measurements were performed using a constant volume-variable pressure permeation cell with vacuum at the permeate side, as described elsewhere [38]. The desired feed pressure was applied at the top side of the membrane while keeping the permeate side under vacuum. The gas permeability values were calculated from the increase in pressure in a calibrated volume. A mixture of CO₂ and CH₄ (50/50 mol %) was used to investigate the membrane performance. All membranes were vacuumed overnight prior to testing. In all cases, two to three samples from different membranes of the same composition were measured. The samples were measured continuously at a temperature of 35 °C and a retentate flow of 5 cm³/min. Furthermore, in order to exclude time effects, permeability values were taken after 8 hours of measurement. The gas that permeated through the membrane was collected and

directly injected into a Varian 3900 GC gas chromatograph using an Alltech alumina F-1 60/80 packed bed column at 150 °C to analyze the composition of the permeate.

5.3 Results and discussion

The synthesized ZIF-8 nanoparticles were characterized by various characterization techniques. The morphological features of the nanocrystals are of great importance for the preparation of MMMs, as these influence the distribution of the filler particles in the polymer matrix and the interactions at the interface between filler and polymer. As revealed by SEM (Fig. 5.1), the synthesized ZIF-8 consisted of homogeneous dodecahedron crystals. The average crystal dimensions were ca. 120 nm after aqueous synthesis and slightly smaller crystals were obtained by microwave heating (95 nm). The use of the (fast) microwave heating method has been reported to reduce the synthesis time and to result in smaller and more uniformly sized MOF crystals compared to the aqueous room temperature synthesis method [33].

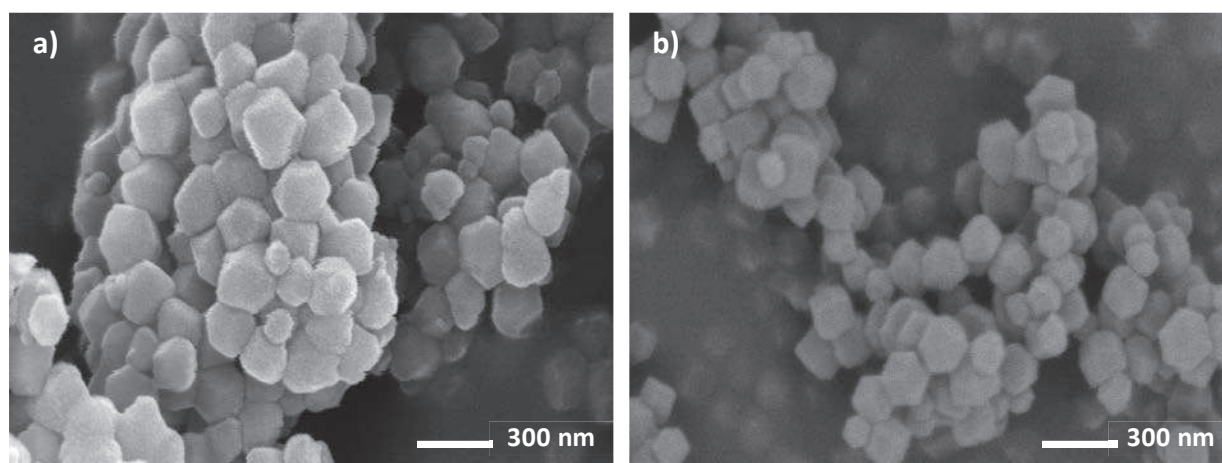


Fig. 5.1. SEM images of ZIF-8 nanoparticles prepared by (a) aqueous room temperature method and (b) microwave assisted method. (Magnification: a and b: 100000x).

Fig. S5.1 (supporting information) shows the XRD patterns for the synthesized ZIF-8 materials. Virtually identical diffractograms were observed for all ZIF-8 samples, irrespective the synthesis method. This pattern is in agreement with the literature [25], indicating that pure ZIF-8 indeed was obtained.

In line with the XRD results, N₂ adsorption did not indicate any significant differences in the porous structure of ZIF-8 for the two synthesis methods (Fig. S5.2). BET surface areas

of respectively 1300 m²/g and 1450 m²/g were obtained for the aqueous room temperature and microwave assisted synthesized ZIF-8 nanocrystals.

In summary, physico-chemical characterization of the synthesized ZIF-8 nanocrystals evidenced that the heating method applied during the synthesis does not have a significant influence on the properties of the final product in the case of ZIF-8. Based on these results and its ease of synthesis, the aqueous synthesis of ZIF-8 at room temperature was selected to be used in the assembly of the MMMs. All later discussion on MMMs contained water-based synthesized ZIF-8 nanocrystals at room temperature.

5.3.1 Synthesis of polymer particles: effect of polymer solution concentration

Fig. 5.2 shows the SEM images of the polymer particles prepared from different concentrations of polymer solutions. The size of the polymer particles increases when the polymer concentration increases. A 3 wt.% polymer solution generated polymer particles of ca. 20-30 nm, while an 8 wt.% polymer solution resulted in ca. 40-50 nm particles. At polymer concentrations higher than 10 wt.%, clumps of polymer beads (1-2 μm) were observed instead of individual nanoparticles.. The dependence of the particle size on the polymer concentration, stirring speed and precipitation temperature is well known [39]. An increase in the polymer content will increase the solution viscosity and the fragmentation stage of the emulsification process will be altered. As membranes prepared from solutions with polymer concentrations below 8 wt.% experienced higher shrinkage leading to cracks in the final membrane, the 8 wt.% polymer solution was selected for membranes preparation.

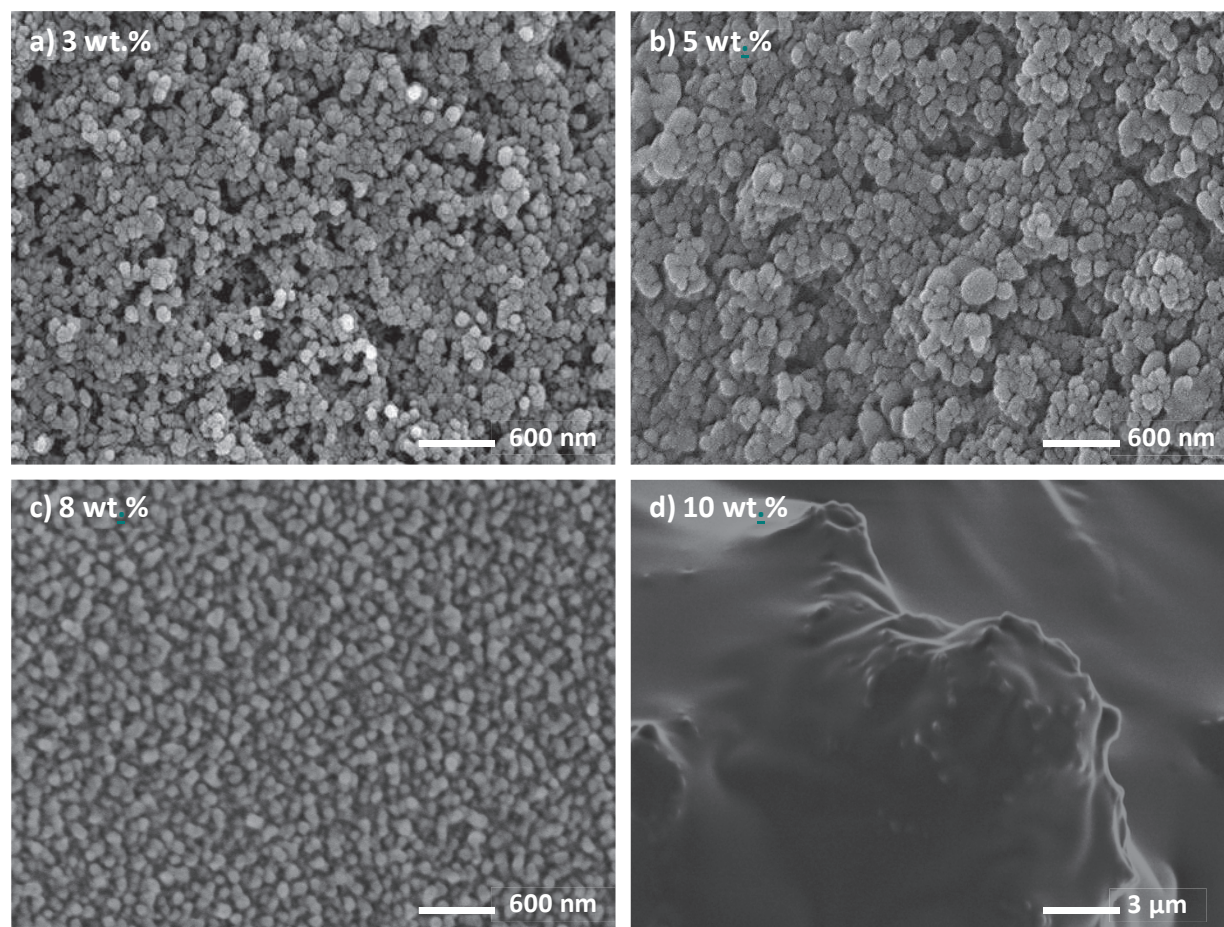


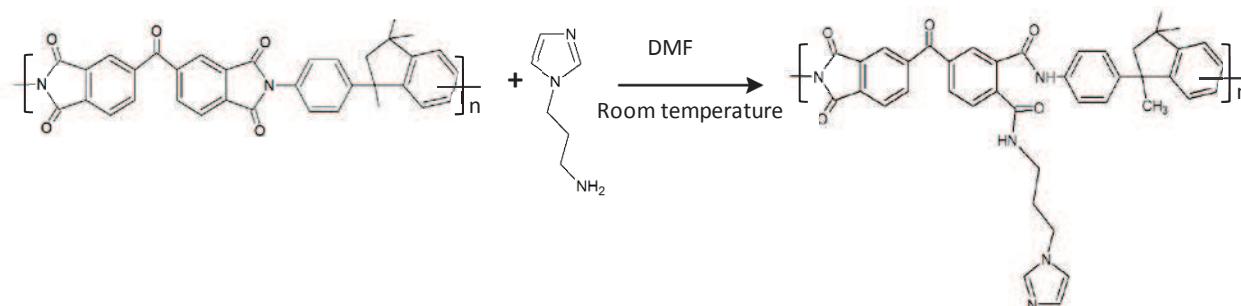
Fig. 5.2. SEM images of polymer particles prepared from polymer solutions containing different polymer concentrations (Magnification: a-c: 50000x and d: 10000x).

5.3.2 Polymer modification via grafting of 1-(3-aminopropyl)-imidazole

The grafting of 1-(3-aminopropyl)-imidazole on Matrimid® beads was done via an imide ring opening reaction induced by 1-(3-aminopropyl)-imidazole. As shown in scheme 1, the amine group of 1-(3-aminopropyl)-imidazole reacts with the imide functions in Matrimid® to form ortho-diamide functions. The chemical structures of the resulting ‘polyimide-amide’ materials (referred to as modified Matrimid® from now on) were confirmed by ^1H NMR (supporting information Fig. S5.3 and Fig. S5.4) and FTIR (Fig. S5.5). The percentage of modification was evaluated by ^1H NMR. Details of the calculation of the modification degree are given in the supporting information.

As known from literature, the modification of the particle surface chemistry can facilitate the assembly of the particles (Fig. S5.6) [40]. In a synergistic effect, the amine modification of Matrimid® will also result in improved CO_2 gas permeabilities [41], while

the pendent imidazole units will lead to a better compatibility between the polymer phase and the ZIF-8 nanoparticles.



Scheme 1. Grafting of 1-(3-aminopropyl)-imidazole on Matrimid®.

5.3.3 Characterization of MMMs

To prepare MMMs, as an example some ZIF-8 nanocrystals were grown in the spaces between the polymer particles. Fig. S5.7 shows SEM images of mixtures of polymer particles at different ZIF-8 loadings. In all cases the ZIF-8 nanoparticles are homogeneously dispersed among the polymer particles and no agglomeration of ZIF-8 nanoparticles is observed, even at high loadings (30 wt.% and 40 wt.%). In order to obtain a dense MMM structure, suspensions of polymer particles with different ZIF-8 loadings were cast and dried and subsequently exposed to a saturated atmosphere of DMF vapor at room temperature for 5 days. Fig. 5.3 shows the surface and cross-sectional SEM images of the transformation of the particulate morphology into a dense MMMs morphology over a total period of 5 days.

Controlled drying in DMF environment

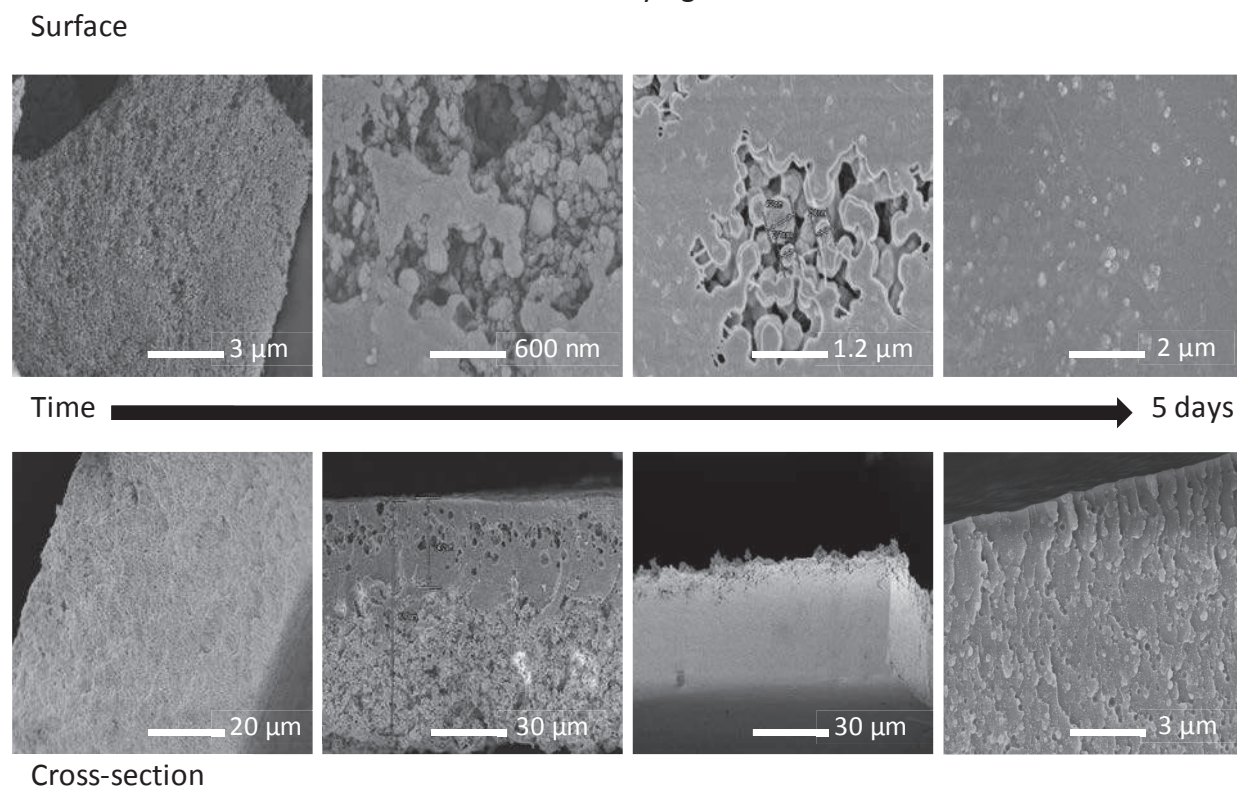


Fig. 5.3. Surface and cross-sectional transformation from particulate morphology to dense MMM morphology over a period of 5 days.

While water evaporation leads to the formation of a solid film through the assembly of particles, the exposure to DMF vapor leads to a controlled fusion of the polymer particles into a dense layer, progressing from the top to the bottom of the membrane with progressing annealing time (Fig. 5.3). In the cross-section, it is visible that this densification starts from the top, as the solvent starts to sorb at the top surface, and slowly moves towards the lower parts of the cross-section. During transformation from a particle morphology to a dense MMM structure, the color also changes from slightly opaque yellowish to a translucent amber.

SEM images of the cross-section of a 30 wt.% MMM are shown in Fig. 5.4. For comparison, a 30 wt.% MMM prepared using dried ZIF-8 nanoparticles (conventional solution casting approach) is also shown. The membrane prepared using the conventional method shows aggregation of ZIF-8 particles and poor adhesion at the ZIF-8 polymer interface. Also the ZIF-8 particles show poor dispersion in some regions of the cross-section. On the contrary, MMMs prepared by particle fusion show ZIF-8

MOF-mixed matrix membranes: precise dispersion of MOF particles with better compatibility via a particle fusion approach for enhanced gas separation properties

nanocrystals completely wrapped by the polymer matrix. Fracturing under liquid N₂ causes the polymer layer to break by brittle fracture without plastic deformation, giving a more smooth cross-section than the crater-like morphology obtained for conventional solution casted membranes [42]. Using the particle fusion approach, excellent dispersion of ZIF-8 nanoparticles in the polymer matrix (up to ZIF-8 loadings of 40 wt.%), were obtained. Large aggregates of ZIF-8 particles are not observed. Each ZIF-8 particle is separated by a very thin layer of the matrix polymer theoretically creating an ideal percolating pathway for gas permeation. At higher loadings (40 wt.%), the MMMs do show good dispersion and good contact between the ZIF-8 nanoparticles and the polymer, but the membranes are very brittle in terms of mechanical properties. The particle fusion technique significantly improved the particle dispersion and interface morphology as compared to previous work on such MMM systems [23, 25, 27, 43, 44].

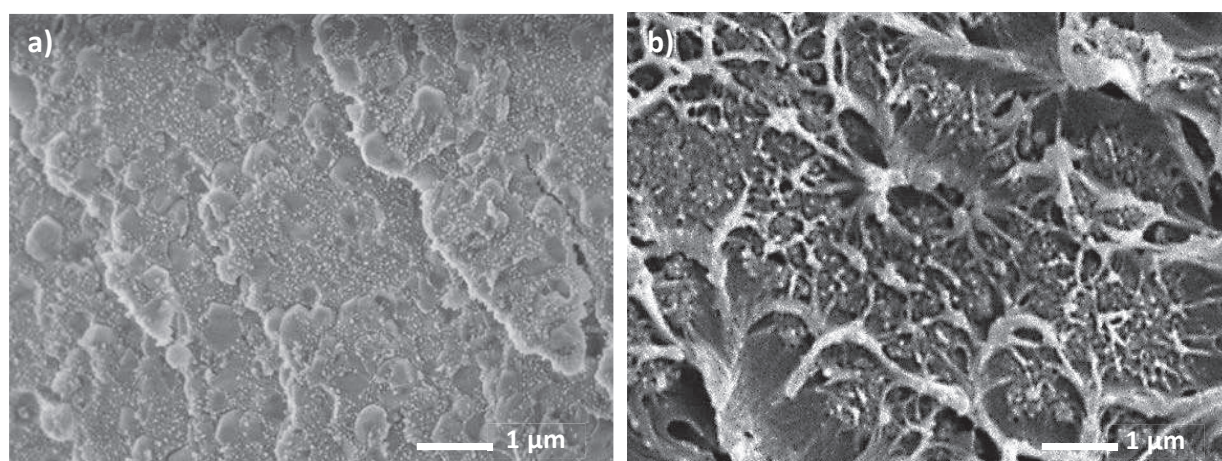


Fig. 5.4. MMM containing 30 wt.% ZIF-8 prepared by (a) particle fusion and (b) conventional solution casting. (Magnification: a: 25000x and b: 20000x).

XRD patterns of the pure polymer and the mixed matrix membranes are presented in Fig. S5.8. The pure Matrimid® polymer membrane is completely amorphous and shows a broad spectrum, typical of amorphous materials. For all the Matrimid®-ZIF-8 MMMs, the crystalline structure of the ZIF-8 nanoparticles is clearly the same as that of pure ZIF-8.

The thermal stability of the synthesized ZIF-8, as evaluated by TGA is presented in Fig. S5.9. Fig. S5.9 shows no significant weight loss till 200 °C due to the hydrophobic pores of ZIF-8 that prevents adsorption of e.g. water vapor [45]. At temperature above 450 °C degradation of ZIF-8 occurs, which is in agreement with literature [46]. By comparison, the thermal degradation of modified Matrimid® starts around 485 °C and increases with

increasing MOF content up to 500 °C for MMMs with up to 30 wt.% ZIF-8. The increase in thermal stability of the MMMs can be attributed to the high thermal stability of the ZIF-8 nanoparticles and the existence of favorable interactions between the ZIF-8 and the modified Matrimid® polymer matrix.

Table 5.1 shows the glass transition temperature of the different membranes measured by DSC. The glass transition temperature of pure Matrimid® (unmodified) is 328 °C, which is consistent with literature [47]. The surface modified pure Matrimid® shows a Tg around 278 °C. This drop in Tg can be attributed to plasticization caused by the surface modifier (the molecular weight measurement did not show a reduction in molecular weight as confirmed by GPC (not shown here)). The 1-(3-aminopropyl)-imidazole linker increases the inter-chain distance, giving the polymer chains more inter-segmental mobility.

For MMM, with increasing ZIF-8 loading, the Tg increases from 278 °C to 300 °C. At low ZIF-8 loadings, the increase in Tg is low. But at loadings of 40 wt.%, a significant increase of 22 °C in the Tg is observed (Table 5.1), indicating a restricted chain movement. As mentioned before, each ZIF-8 nanoparticle is surrounded by a thin layer of the polymer, significantly restricting the polymer chain movement. Additionally, the strong polymer-particle interactions, thanks to the particle surface modification, increase the Tg. Such phenomenon has also been observed for Cu-BPY-HFS/Matrimid® [22]. Chung et al. prepared Matrimid® membranes containing benzylamine-modified C₆₀ and a 14 °C increase in Tg was reported, which indicates a strong interfacial interaction between Matrimid® and the benzylamine-modified C₆₀ particles [47].

Table 5.1. Glass transition temperature and mechanical properties of MMMs with different ZIF-8 loadings.

| Polymer content (wt.%) | MOF loading (wt.%) | T _g (°C) ¹ | Young's modulus (GPa) | Tensile strength (MPa) | Elongation at break (%) |
|------------------------|--------------------|----------------------------------|-----------------------|------------------------|-------------------------|
| 100 (non-modified) | 0 | 328 | 2.5 | 107 | 119 |
| 100 (modified) | 0 | 278 | 2.35 | 111 | 125 |
| 90 | 10 | 282 | 2.91 | 98 | 104 |
| 80 | 20 | 289 | 3.42 | 93 | 95 |
| 70 | 30 | 295 | 3.63 | 85 | 85 |
| 60 | 40 | 300 | 3.51 | 80 | 70 |

¹Typical error in DSC results ranges from $\pm 1-1.5$ °C.

The influence of the ZIF-8 content on the Young's modulus is shown in Table 5.1. The Young's modulus of the MMMs exhibits a linear increase with increasing ZIF-8 loading up to 30 wt.%, followed by a decrease at 40 wt.% ZIF-8 loading. The increase in Young's modulus suggests that the interfacial adhesion between the ZIF-8 nanoparticles and the polymer chains is good [48] up to 30 wt.% loading of ZIF-8. This is higher than that of other reported ZIF-8-MMMs systems [23, 46]. This enhanced compatibility between ZIF-8 and the polymer chains can be attributed to the imidazolate functionality of the polymer and ZIF-8. However, at a loading of 40 wt.%, the MMM becomes more brittle, resulting in a decreased Young's modulus. This effect might be due to the slight aggregation of the ZIF-8 nanoparticles at higher loadings, resulting in less contact between the ZIF-8 nanoparticles and the polymer matrix. Both the tensile strength and the elongation at break decrease with increasing ZIF-8 loading due to the reduced flexibility due to the presence of ZIF-8 nanoparticles [49] and the formation of a more rigid MMM with increasing ZIF-8 loading [22]. Such phenomenon has also been observed for other MOF/Matrimid® systems [46].

5.3.4 Gas separation

5.3.4.1 Gas sorption

Both CO₂ and CH₄ show a dual mode sorption isotherm in the different membranes as shown in Fig. S5.11 and Fig. S5.12. Fitting of the data with the dual mode sorption model provides the parameters summarized in Table 5.2.

Table 5.2. Dual mode sorption parameters for CO₂ and CH₄ in the different membranes.

| Feed gas | ZIF-8 (wt.%) | Dual mode sorption model | | |
|-----------------|-----------------|--|------------|---|
| | | C'_H cm ³ (STP)/cm ³ | b (1/cmHg) | k_D (cm ³ (STP)/cm ³ ·cmHg) |
| CO ₂ | 0 | 29.59 | 0.16 | 0.78 |
| | 0-M* | 31.11 | 0.17 | 0.78 |
| | 10 | 39.28 | 0.17 | 0.69 |
| | 20 | 47.21 | 0.20 | 0.59 |
| | 30 | 57.16 | 0.24 | 0.52 |
| | 40 | 69.26 | 0.24 | 0.35 |
| | 100 | 280.20 | 0.26 | 0 |
| CH ₄ | 0 | 10.25 | 0.059 | 0.17 |
| | 0-M* | 11.15 | 0.056 | 0.17 |
| | 10 | 13.10 | 0.057 | 0.14 |
| | 20 | 15.40 | 0.062 | 0.13 |
| | 30 | 16.24 | 0.075 | 0.09 |
| | 40 | 18.95 | 0.079 | 0.09 |
| | 100 | 122.0 | 0.102 | 0 |

* 0-M modified Matrimid®

CO₂ shows a higher sorption compared to CH₄, attributed to the higher critical temperature (T_c) and consequently condensability of CO₂ compared to CH₄ (T_c -CO₂: 304K, T_c -CH₄: 190K) [1]. Also the favorable quadrupolar interactions of CO₂ contribute to this. In comparison to the pure polymer membranes, pure ZIF-8 shows a much higher adsorption attributed to the high surface area of the nanoparticles. Compared to pure Matrimid® membranes, the value of k_D decreases as the ZIF-8 loading increases, indicating that overall sorption is dominated by Langmuir sorption (in the nanocages of ZIF-8) at higher filler loadings. The presence of ZIF-8 particles in the MMMs provides extra sorption sites for both gases (more for CO₂ than for CH₄) that lead to higher C'_H and b values for both CO₂ and CH₄ with increasing ZIF-8 loading. It was reported [50], that at low pressures, both CO₂ and CH₄ are preferentially sorbed in the vicinity of the organic imidazolate linkers. At high pressures, CH₄ resides near the aperture, but CO₂ sorbs in

the central cage. As the pressure increases, the nanocages of ZIF-8 get saturated, leaving only Henry sorption in the polymer matrix.

5.3.4.2 Effect of ZIF-8 loading on gas separation performance

Fig. 5.5 shows the gas transport data of pure Matrimid® membranes and MMMs with various loadings of ZIF-8. The pure modified Matrimid® membranes show a higher CO₂ permeability than the non-modified Matrimid® membranes. This can be attributed to the interaction between CO₂ and the imidazolate linker of the modified polymer chains. The permeability of CH₄ remained stable. Upon addition of ZIF-8 to the MMMs, the CO₂ permeability clearly increases, while the effect on the CH₄ permeability is only very strong at a ZIF-8 loading as high as 40 wt.%. Consequently, the CO₂/CH₄ selectivity significantly increases with increasing ZIF-8 loading up to 30 wt.%. Modification of Matrimid® clearly improves the compatibility between ZIF-8 and the polymer matrix and consequently increases the CO₂/CH₄ selectivity of the membrane. Looking at the relative increase in permeability, this increase is definitely more dominant for CO₂ than for CH₄ (Fig. S5.10). The porous MOF particles provide a percolating porous network [20] that facilitate the transport of gases. Additionally, CO₂ molecules have a strong quadrupolar moment that interacts well with ZIF-8 [51]. Hence, CO₂ permeability increases considerably with increasing ZIF-8 loadings in the MMMs. This result also suggests that the 30 wt.% MMM is defect-free and that the contact between the ZIF-8 nanoparticles and the polymer is excellent. At higher loadings (40 wt.%), the permeability increased more than 4 times compared to that of the pure polymer, while the selectivity decreased, however still maintaining a higher value (15 %) than that of pure modified Matrimid®. This decrease could be the consequence of the presence of some minor defects (non-selective voids) at this high loading.

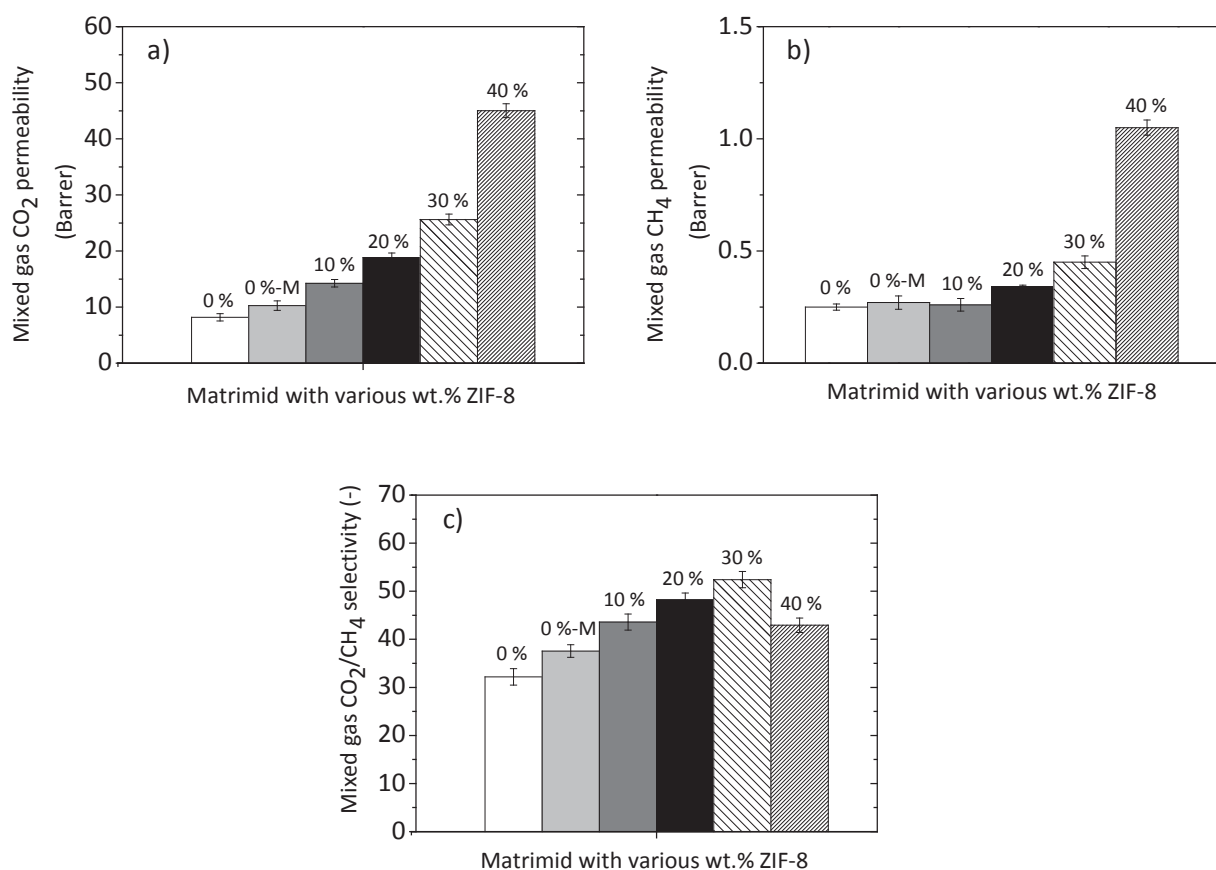


Fig. 5.5. Mixed gas (a) CO₂ permeability, (b) CH₄ permeability and (c) CO₂/CH₄ selectivity of prepared membranes for different ZIF-8 loadings at 5 bar and 35 °C.

The gas sorption and separation data were further analyzed and using the solution diffusion model ($P=D \cdot S$) the corresponding diffusivities were calculated using the pure gas sorption and permeation data. As sorption data were obtained from a system with gas surrounding the complete sample, while permeation data were obtained from a system with gas at the feed, but vacuum at the permeate side of the membrane, the diffusion data should be considered as a rough estimate.

Fig. 5.6 presents the measured normalized solubility and diffusion coefficients of CO₂ and CH₄, as a function of the ZIF-8 loading. The data were normalized based on the data of pure modified Matrimid®. The normalized CO₂ diffusivity increased more than the normalized diffusivity of CH₄ up to 30 wt.%, but the normalized solubility of CO₂ was comparable to that of CH₄. The CH₄ diffusion coefficient showed a rapid increase in value as the ZIF-8 loading increased above 30 wt.%, attributed to non-selective voids. However at all ZIF-8 loadings, the increase in normalized diffusivity was always more significant

compared to the increase in normalized solubility. In ZIF-8, CO₂ has a lower energy barrier for diffusion than CH₄ and hence higher diffusivity [52]. The results show that the major contribution to the increase in CO₂ permeability comes from the diffusion coefficient. This behavior can be explained when considering the structural details of ZIF-8. ZIF-8 is comprised of larger cavities (1.1 nm) interconnected by narrow windows of 0.34 nm. Ideally it should only allow the transport of smaller gas molecules like CO₂ [46]. However, the swinging of the imidazolate linker provides some flexibility and causes the adsorption and transport of larger molecules, like CH₄, as well and hence increases the permeability of CH₄ to some extent, as observed in Fig. 5.5.

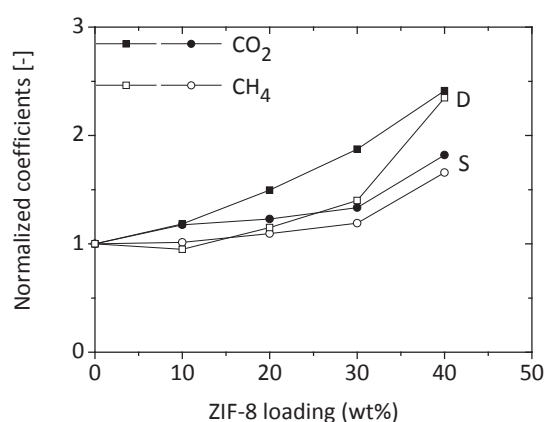


Fig. 5.6. Normalized solubility and diffusion coefficients for CO₂ (closed symbols) and CH₄ (open symbols) as a function of ZIF-8 loading. Results are normalized based on the data of pure modified Matrimid®.

5.3.5 Overall membrane performance

A comparative study of the performance of the presented membranes with literature data for polyimide-based filled and unfilled membranes with respect to permeability and CO₂/CH₄ selectivity is shown in Fig. 5.7. Also other MOF-MMMs (with 30 wt.% MOF loading) are added for comparison. Table 5.3 presents the details and operating conditions of the data presented in Fig. 5.7.

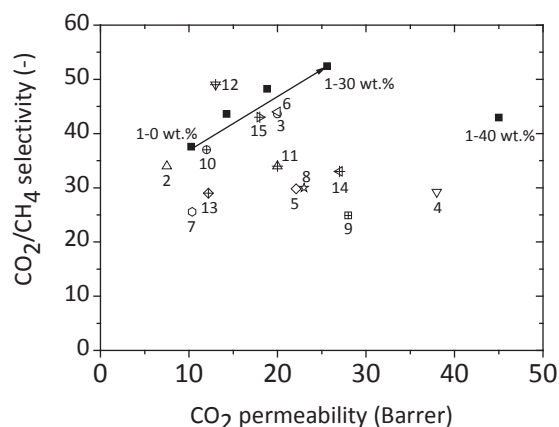


Fig. 5.7. Comparison study of MOF-MMMs from literature and MMMs prepared via particle fusion (this work-closed symbols) for CO₂/CH₄ gas separation. See Table 5.3 for details of different membranes and specific experimental details.

Due to the lack of mixed gas data available for most other MOF based MMMs systems, pure gas data for MOF based membranes from literature were also included for comparison. The performance of the membranes developed by particle fusion was clearly better than that of the previously reported data for PI membranes with identical (ZIF-8) or different MOFs (Fig. 5.7). A systematic trend of increasing permeability and selectivity was clearly visible with increase in ZIF-8 loading. Most other literature on MOF based membranes showed clearly lower selectivities than pure PI, indicating a poor interfacial contact between MOF and matrix. Particle fusion MOF based membranes showed a 200 % increase in permeability combined with a 65 % increase in selectivity compared to pure Matrimid® membranes. This indicated that it is possible to achieve much higher gas separation performance by establishing good adhesion at the interface between MOF and polymer using the particle fusion technique.

Table 5.3. Experimental details of the data presented in Fig. 5.7.

| Code | Membrane | Gas type | Casting solvent | T (°C) | P (bar) | Reference |
|------|-------------------------------------|----------|---------------------------------|--------|---------|-----------|
| 1 | PI- ZIF-8 | Mix gas | DMF | 35 | 5 | This work |
| 2 | PI | pure gas | CHCl ₃ | 35 | 2 | [22] |
| 3 | PI-ZIF-8 | Mix gas | Dioxane, NMP | 35 | 5 | [42] |
| 4 | PI-IRMOF | pure gas | CHCl ₃ | 50 | 7 | [53] |
| 5 | PI-Cu ₃ BTC ₂ | pure gas | CHCl ₃ | 50 | 7 | [53] |
| 6 | PI-MOF-5 | pure gas | CHCl ₃ | 35 | 4 | [20] |
| 7 | PI-CuMOF | pure gas | CHCl ₃ | 35 | 2 | [22] |
| 8 | PI-ZIF-8 | pure gas | CHCl ₃ | 35 | 3 | [23] |
| 9 | PI-ZIF-8 | pure gas | CHCl ₃ | 25 | 4 | [25] |
| 10 | PI-ZIF-8-ambz | pure gas | CHCl ₃ | 35 | 3.5 | [54] |
| 11 | PI-ZIF-8 | pure gas | CHCl ₃ | 35 | 3.5 | [54] |
| 12 | PI-Cu ₃ BTC ₂ | Mix gas | Dioxane, NMP | 35 | 5 | [42] |
| 13 | PI-Fe(BTC) | Mix gas | Dioxane, NMP | 35 | 5 | [38] |
| 14 | PI-ZIF-8 | Mix gas | CH ₂ Cl ₂ | 35 | 5 | [46] |
| 15 | PI-MIL-53(Al) | Mix gas | Dioxane, NMP | 35 | 5 | [42] |

*PI= Matrimid® 5218

5.4 Conclusion

A facile and versatile novel route for the preparation of MMMs composed of phase separated polymer particles and in-situ synthesized ZIF-8 nanoparticles with excellent adhesion between the filler and the polymer matrix, is presented. Chemical modification of the polymer has led to an excellent ZIF-8-polymer interfacial compatibility. The particulate morphology of a mixture of polymer and filler particles was transformed to a dense membrane structure by DMF vapor annealing. It was possible to successfully prepare MMMs with MOF loadings as high as 30 wt.% without any non-selective defects. Upon increasing the ZIF-8 loading, MMMs showed significantly better performance in the separation of CO₂/CH₄ mixtures as compared to the native polymer. The CO₂ permeability increased up to 200 % combined with a 65 % increase in CO₂/CH₄ selectivity, compared to the native Matrimid®. In-depth analysis of gas transport performance of the membranes showed that the higher diffusion and moderate

sorption of CO₂ gas enhances the CO₂ permeability. Gas sorption studies further confirmed that the selective gas transport (CO₂/CH₄ selectivity) is mainly governed by the increase in diffusivity selectivity, which is in all cases higher than the solubility selectivity.

The overall results of our experiments show that this novel method to prepare MMMs with embedded MOF particles provides new opportunities to develop highly compatible, well dispersed and highly loaded mixed matrix membranes, with enhanced permeability to the limit of the Robeson upper bound by proper selection of polymer matrix and high performing fillers. The approach is very versatile and can be expanded to numerous combinations of polymers and MOFs. Future work in this area will focus on the use of more selective MOFs other than ZIF-8 to exert more control on the membrane selectivities.

Acknowledgements

The authors would like to thank the Erasmus Mundus Doctorate in Membrane Engineering (EUDIME) for funding this research.

References

- [1] N.N. Li, A.G. Fane, W.S.W. Ho, T. Matsuura, *Advanced membrane technology and applications*, 2008.
- [2] W.J. Koros, G.K. Fleming, *Membrane-based gas separation*, *J. Membr. Sci.*, 83 (1993) 1-80.
- [3] R.W. Baker, *Future directions of membrane gas separation technology*, *Industrial & Engineering Chemistry Research*, 41 (2002) 1393-1411.
- [4] P. Bernardo, E. Drioli, G. Golemme, *Membrane gas separation: a review/state of the art*, *Industrial & Engineering Chemistry Research*, 48 (2009) 4638-4663.
- [5] L.M. Robeson, *Correlation of separation factor versus permeability for polymeric membranes*, *J. Membr. Sci.*, 62 (1991) 165-185.
- [6] L.M. Robeson, *The upper bound revisited*, *J. Membr. Sci.*, 320 (2008) 390-400.
- [7] Y. Zhang, J. Sunarso, S. Liu, R. Wang, *Current status and development of membranes for CO₂/CH₄ separation: A review*, *International Journal of Greenhouse Gas Control*, 12 (2013) 84-107.
- [8] T.S. Chung, L.Y. Jiang, Y. Li, S. Kulprathipanja, *Mixed matrix membranes (MMMs) comprising organic polymers with dispersed inorganic fillers for gas separation*, *Progress in Polymer Science (Oxford)*, 32 (2007) 483-507.

- [9] G. Dong, H. Li, V. Chen, Challenges and opportunities for mixed-matrix membranes for gas separation, *Journal of Materials Chemistry A*, 1 (2013) 4610-4630.
- [10] J.T. Chen, C.C. Shih, Y.J. Fu, S.H. Huang, C.C. Hu, K.R. Lee, J.Y. Lai, Zeolite-filled porous mixed matrix membranes for air separation, *Industrial and Engineering Chemistry Research*, 53 (2014) 2781-2789.
- [11] F. Dorosti, M.R. Omidkhah, M.Z. Pedram, F. Moghadam, Fabrication and characterization of polysulfone/polyimide-zeolite mixed matrix membrane for gas separation, *Chemical Engineering Journal*, 171 (2011) 1469-1476.
- [12] A. Car, C. Stropnik, K.-V. Peinemann, Hybrid membrane materials with different metal-organic frameworks (MOFs) for gas separation, *Desalination*, 200 (2006) 424-426.
- [13] S. Husain, W.J. Koros, Mixed matrix hollow fiber membranes made with modified HSSZ-13 zeolite in polyetherimide polymer matrix for gas separation, *J. Membr. Sci.*, 288 (2007) 195-207.
- [14] B.D. Reid, F.A. Ruiz-Trevino, I.H. Musselman, K.J. Balkus, J.P. Ferraris, Gas Permeability properties of polysulfone membranes containing the mesoporous molecular sieve MCM-41, *Chemistry of Materials*, 13 (2001) 2366-2373.
- [15] B. Zornoza, C. Téllez, J. Coronas, Mixed matrix membranes comprising glassy polymers and dispersed mesoporous silica spheres for gas separation, *J. Membr. Sci.*, 368 (2011) 100-109.
- [16] Y. Li, H.M. Guan, T.S. Chung, S. Kulprathipanja, Effects of novel silane modification of zeolite surface on polymer chain rigidification and partial pore blockage in polyethersulfone (PES)-zeolite A mixed matrix membranes, *J. Membr. Sci.*, 275 (2006) 17-28.
- [17] I.F.J. Vankelecom, S. Van Den Broeck, E. Merckx, H. Geerts, P. Grobet, J.B. Uytterhoeven, Silylation to improve incorporation of zeolites in polyimide films, *Journal of Physical Chemistry*, 100 (1996) 3753-3758.
- [18] H.B.T. Jeazet, C. Staudt, C. Janiak, Metal-organic frameworks in mixed-matrix membranes for gas separation, *Dalton Transactions*, 41 (2012) 14003-14027.
- [19] T.T. Moore, W.J. Koros, Non-ideal effects in organic-inorganic materials for gas separation membranes, *Journal of Molecular Structure*, 739 (2005) 87-98.
- [20] E.V. Perez, K.J. Balkus, Jr., J.P. Ferraris, I.H. Musselman, Mixed-matrix membranes containing MOF-5 for gas separations, *J. Membr. Sci.*, 328 (2009) 165-173.
- [21] S. Basu, A. Cano-Odena, I.F.J. Vankelecom, Asymmetric Matrimid®/ Cu₃(BTC)₂ mixed-matrix membranes for gas separations, *J. Membr. Sci.*, 362 (2010) 478-487.
- [22] Y. Zhang, I.H. Musseman, J.P. Ferraris, K.J. Balkus, Jr., Gas permeability properties of Matrimid® membranes containing the metal-organic framework Cu-BPY-HFS, *J. Membr. Sci.*, 313 (2008) 170-181.
- [23] M.J.C. Ordonez, K.J. Balkus, J.P. Ferraris, I.H. Musselman, Molecular sieving realized with ZIF-8/Matrimid® mixed-matrix membranes, *J. Membr. Sci.*, 361 (2010) 28-37.

- [24] J. Ploegmakers, S. Japip, K. Nijmeijer, Mixed matrix membranes containing MOFs for ethylene/ethane separation-Part B: Effect of Cu_3BTC_2 on membrane transport properties, *J. Membr. Sci.*, 428 (2013) 331-340.
- [25] Q. Song, S.K. Nataraj, M.V. Roussenova, J.C. Tan, D.J. Hughes, W. Li, P. Bourgoïn, M.A. Alam, A.K. Cheetham, S.A. Al-Muhtaseb, E. Sivaniah, Zeolitic imidazolate framework (ZIF-8) based polymer nanocomposite membranes for gas separation, *Energy and Environmental Science*, 5 (2012) 8359-8369.
- [26] C. Zhang, Y. Dai, J.R. Johnson, O. Karvan, W.J. Koros, High performance ZIF-8/6FDA-DAM mixed matrix membrane for propylene/propane separations, *J. Membr. Sci.*, 389 (2012) 34-42.
- [27] Y. Dai, J.R. Johnson, O. Karvan, D.S. Sholl, W.J. Koros, Ultem((R))/ZIF-8 mixed matrix hollow fiber membranes for CO_2/N_2 separations, *J. Membr. Sci.*, 401 (2012) 76-82.
- [28] R.W. Baker, Future directions of membrane gas separation technology, *Industrial and Engineering Chemistry Research*, 41 (2002) 1393-1411.
- [29] R. Mahajan, W.J. Koros, Mixed matrix membrane materials with glassy polymers. Part 1, *Polymer Engineering and Science*, 42 (2002) 1420-1431.
- [30] R. Mahajan, W.J. Koros, Factors controlling successful formation of mixed-matrix gas separation materials, *Industrial and Engineering Chemistry Research*, 39 (2000) 2692-2696.
- [31] T. Rodenas, M. van Dalen, E. García-Pérez, P. Serra-Crespo, B. Zornoza, F. Kapteijn, J. Gascon, Visualizing MOF Mixed matrix membranes at the nanoscale: towards structure-performance relationships in CO_2/CH_4 separation over $\text{NH}_2\text{-MIL-53(Al)}@\text{PI}$, *Advanced Functional Materials*, 24 (2014) 249-256.
- [32] S. Basu, M. Maes, A. Cano-Odena, L. Alaerts, D.E. De Vos, I.F.J. Vankelecom, Solvent resistant nanofiltration (SRNF) membranes based on metal-organic frameworks, *J. Membr. Sci.*, 344 (2009) 190-198.
- [33] H. Bux, F. Liang, Y. Li, J. Cravillon, M. Wiebcke, J. Caro, Zeolitic Imidazolate Framework Membrane with Molecular Sieving Properties by Microwave-Assisted Solvothermal Synthesis, *Journal of the American Chemical Society*, 131 (2009) 16000-16001.
- [34] D. Fairen-Jimenez, R. Galvelis, A. Torrisi, A.D. Gellan, M.T. Wharmby, P.A. Wright, C. Mellot-Draznieks, T. Düren, Flexibility and swing effect on the adsorption of energy-related gases on ZIF-8: Combined experimental and simulation study, *Dalton Transactions*, 41 (2012) 10752-10762.
- [35] M.C. McCarthy, V. Varela-Guerrero, G.V. Barnett, H.K. Jeong, Synthesis of zeolitic imidazolate framework films and membranes with controlled microstructures, *Langmuir*, 26 (2010) 14636-14641.
- [36] Y. Pan, Y. Liu, G. Zeng, L. Zhao, Z. Lai, Rapid synthesis of zeolitic imidazolate framework-8 (ZIF-8) nanocrystals in an aqueous system, in: *Chemical Communications*, 2011, pp. 2071-2073.

- [37] S. Brunauer, P.H. Emmett, E. Teller, Adsorption of Gases in Multimolecular Layers, *Journal of the American Chemical Society*, 60 (1938) 309-319.
- [38] S. Shahid, K. Nijmeijer, High pressure gas separation performance of mixed-matrix polymer membranes containing mesoporous Fe(BTC), *J. Membr. Sci.*, 459 (2014) 33-44.
- [39] Z. Chai, X. Zheng, X. Sun, Preparation of polymer microspheres from solutions, *Journal of Polymer Science Part B: Polymer Physics*, 41 (2003) 159-165.
- [40] M.A. Ray, H. Kim, L. Jia, Dynamic Self-assembly of polymer colloids to form linear patterns, *Langmuir*, 21 (2005) 4786-4789.
- [41] R.A. Hayes, Amine-modified polyimide membranes, European patent EP 0401005 A1, (1990).
- [42] S. Shahid, K. Nijmeijer, Performance and plasticization behavior of polymer-MOF membranes for gas separation at elevated pressures, *J. Membr. Sci.*, 470 (2014) 166-177.
- [43] V. Nafisi, M.B. Hägg, Gas separation properties of ZIF-8/6FDA-durene diamine mixed matrix membrane, *Separation and Purification Technology*, 128 (2014) 31-38.
- [44] A.F. Bushell, M.P. Atfield, C.R. Mason, P.M. Budd, Y. Yampolskii, L. Starannikova, A. Rebrov, F. Bazzarelli, P. Bernardo, J. Carolus Jansen, M. Lanč, K. Friess, V. Shantarovich, V. Gustov, V. Isaeva, Gas permeation parameters of mixed matrix membranes based on the polymer of intrinsic microporosity PIM-1 and the zeolitic imidazolate framework ZIF-8, *J. Membr. Sci.*, 427 (2013) 48-62.
- [45] K. Zhang, R.P. Lively, C. Zhang, R.R. Chance, W.J. Koros, D.S. Sholl, S. Nair, Exploring the framework hydrophobicity and flexibility of zif-8: from biofuel recovery to hydrocarbon separations, *The Journal of Physical Chemistry Letters*, 4 (2013) 3618-3622.
- [46] S. Basu, A. Cano-Odena, I.F.J. Vankelecom, MOF-containing mixed-matrix membranes for CO₂/CH₄ and CO₂/N₂ binary gas mixture separations, *Separation and Purification Technology*, 81 (2011) 31-40.
- [47] T.S. Chung, S.S. Chan, R. Wang, Z.H. Lu, C.B. He, Characterization of permeability and sorption in Matrimid®/C60 mixed matrix membranes, *J. Membr. Sci.*, 211 (2003) 91-99.
- [48] D.Q. Vu, W.J. Koros, S.J. Miller, Mixed matrix membranes using carbon molecular sieves - I. Preparation and experimental results, *J. Membr. Sci.*, 211 (2003) 311-334.
- [49] Y. Zhang, K.J. Balkus Jr, I.H. Musselman, J.P. Ferraris, Mixed-matrix membranes composed of Matrimid® and mesoporous ZSM-5 nanoparticles, *J. Membr. Sci.*, 325 (2008) 28-39.
- [50] C. Sitprasert, F.Y. Wang, V. Rudolph, Z.H. Zhu, Ideal and mixture permeation selectivity of flexible prototypical zeolitic imidazolate framework-8 Membranes, *Chemical Engineering Science*, 108 (2014) 23-32.
- [51] Q. Yang, C. Zhong, Molecular simulation of carbon dioxide/methane/hydrogen mixture adsorption in metal-organic frameworks, *Journal of Physical Chemistry B*, 110 (2006) 17776-17783.

[52] L. Zhang, G. Wu, J. Jiang, Adsorption and diffusion of CO₂ and CH₄ in zeolitic imidazolate framework-8: effect of structural flexibility, *The Journal of Physical Chemistry C*, 118 (2014) 8788-8794.

[53] C. Liu, M. Beth, T. W. Stephen, I.B. Annabelle, S. Mark, Metal organic framework-polymer mixed-matrix membranes, (2009), US Pat. 7637983.

[54] J.A. Thompson, J.T. Vaughn, N.A. Brunelli, W.J. Koros, C.W. Jones, S. Nair, Mixed-linker zeolitic imidazolate framework mixed-matrix membranes for aggressive CO₂ separation from natural gas, *Microporous and Mesoporous Materials*, (2013).

MOF-mixed matrix membranes: precise dispersion of MOF particles with better compatibility via a particle fusion approach for enhanced gas separation properties

Appendix 2. Supporting information Chapter 5.

MOF-mixed matrix membranes: precise dispersion of MOF particles with better compatibility via a particle fusion approach for enhanced gas separation properties

1 ZIF-8 particle characterization

ZIF-8 samples are prepared using two different synthesis methods: 1) aqueous synthesis at room temperature and 2) microwave assisted aqueous synthesis. Fig. S5.1 shows the XRD patterns for the synthesized ZIF-8 materials. Virtually identical diffractograms are observed for ZIF-8, irrespective of the synthesis method

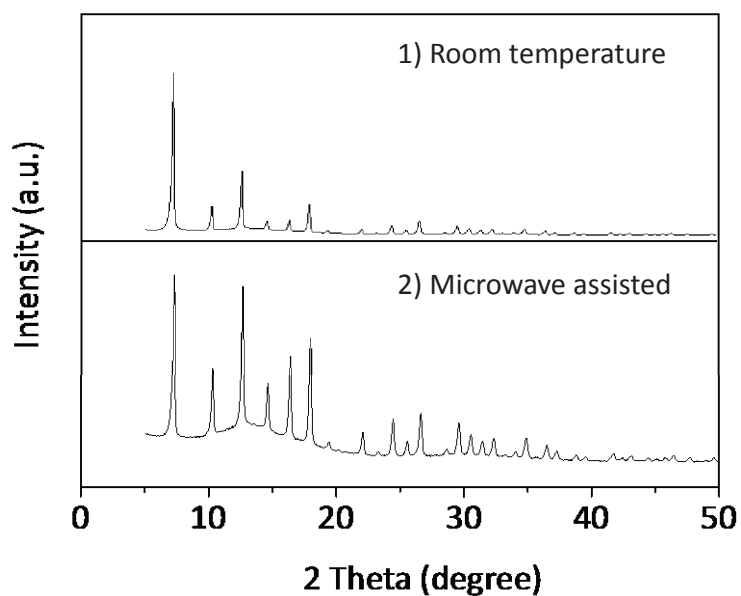


Fig. S5.1. XRD patterns of ZIF-8 nanocrystals prepared by 1) room temperature synthesis and 2) microwave assisted aqueous synthesis.

Fig. S5.2 shows the N₂ adsorption isotherms for the ZIF-8 nanoparticles synthesized via the room temperature and the microwave assisted aqueous method.

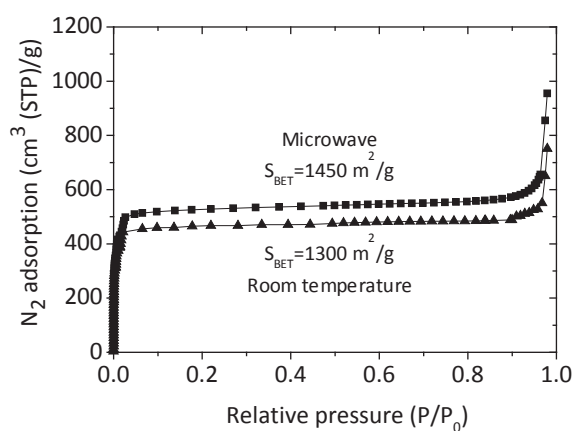


Fig. S5.2. N₂ adsorption isotherms of ZIF-8 nanoparticles prepared using two different synthesis methods.

2 Modification of polymer via grafting of 1-(3-aminopropyl)-imidazole

To modify the polymer matrix, Matrimid® 5218 (3.019 g, Mn= 50000 gmol⁻¹) was dissolved in DMF (18 ml) at 50°C for 2h in a round bottom flask. This solution was cooled to reach room temperature. 1-(3-aminopropyl)-imidazole (0.66 g) was added dropwise, and the resulting solution was stirred at room temperature for 3-4 h. The solution was then diluted by adding 22 ml of DMF and precipitated in ethanol (97% purity) and was filtrated through a Büchner flask. A yellow powder was obtained and dried under vacuum for 2h. The ¹H NMR spectrum of the modified Matrimid® (Fig. S5.4) showed the appearance of peaks at 8.8 ppm and 10.5 ppm, which are the characteristic peaks of the secondary imide (A and B in Fig. S5.4 respectively). The appearance of these two peaks clearly indicates the successful formation of the product, as these peaks are absent in the spectrum of native Matrimid® (Fig. S5.3). Furthermore, the FTIR spectrum (Fig. S5.5) of the modified Matrimid® shows the clear characteristic peaks of the secondary amine around 2392 and 1663 cm⁻¹. A further proof of the successful transformation of Matrimid® was obtained from solubility tests. Native Matrimid® is soluble in chloroform while modified Matrimid® is only soluble in polar solvents such as DMF and DMSO.

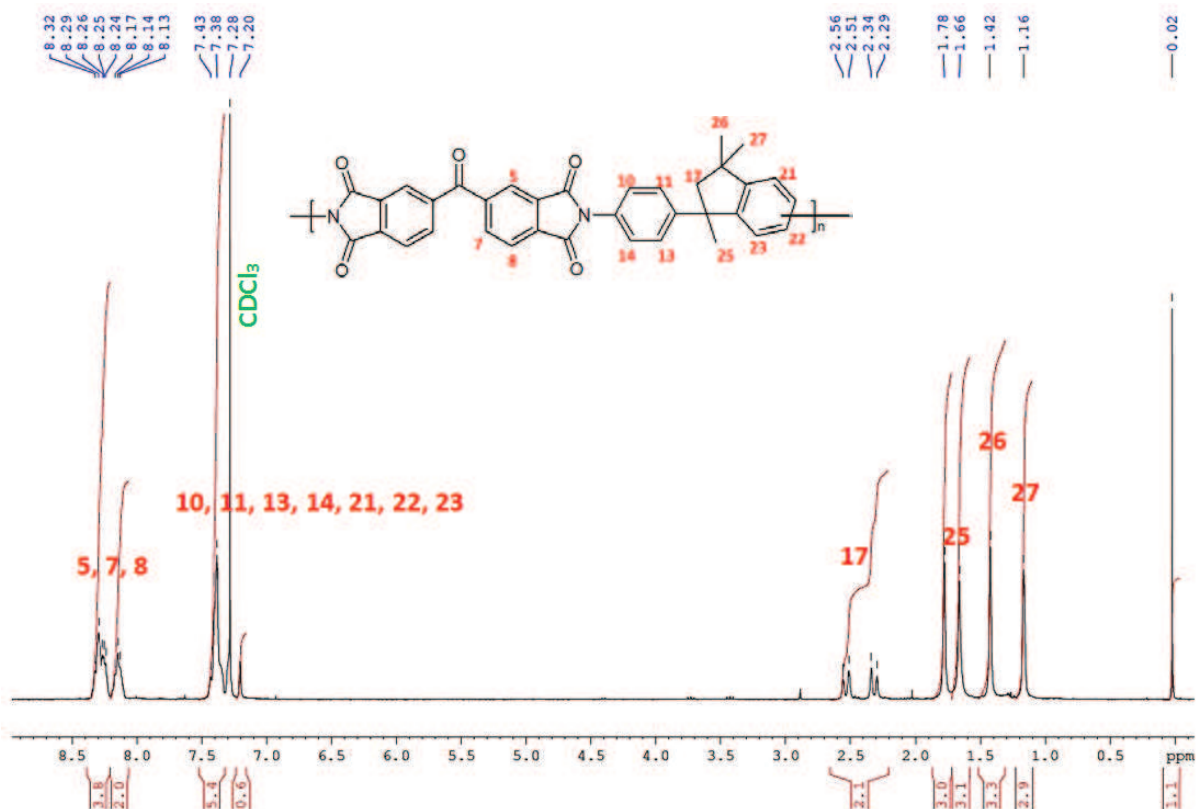


Fig. S5.3. ¹H NMR of pure Matrimid®5218 in CDCl₃.

NMR ¹H (CDCl₃) δ/ppm= 1.16 (s, 3H, 27)- 1.42 (s, 3 H, 26)- 1.66 (s, 3H, 25)- from 2.29 to 2.56 (dd, 2H, 17)- from 7.28 to 7.43 (m, 7H, 10,11,13,14,21,22,23)- from 8.13 to 8.32 (m, 6H, 5,7,8).

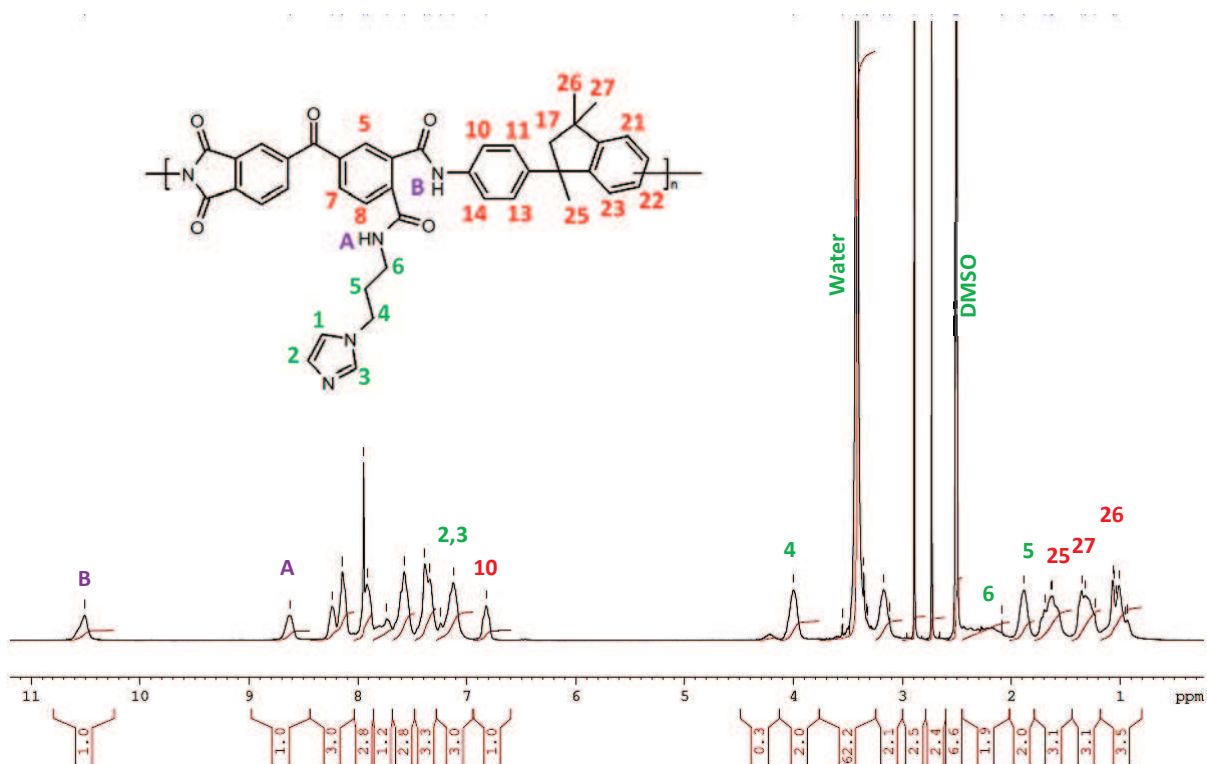


Fig. S5.4. ^1H NMR of 100% modified Matrimid[®]5218 in DMSO- d_6 .

NMR ^1H (DMSO- d_6) δ/ppm = 1.6 (s, 3H, 26)- 1.35 (s, 3 H, 27)- 1.69 (s, 3H, 25)- 1.87 (m, 2H, 5)- from 2.5 to 2.30 (m, 2H, 6)- 4 (t, 2H, 4)- 6.8 (s, 1H, 10)- 7.1 (m, 2H, 2,3)- 7.3 (m, 1H, 1)- 8.6 (s, 1H, A)- 10.5 (s, 1H, B).

The percentage of grafting was determined by comparing the integration of the signal of the methyl group (**27** at 1.35 ppm in Fig. S5.3) in the polymer backbone with that of the methylene group (**4** at 4 ppm in Fig. S5.4) in the grafted 1-(3-aminopropyl)-imidazole groups. This suggests that 100 % of the imide groups of Matrimid[®] is modified, since 6 protons of the Matrimid[®] backbone (peak 27 in Fig. S5.3) coincides with only 2 protons of the grafted species (peak 4 in Fig. S5.4).

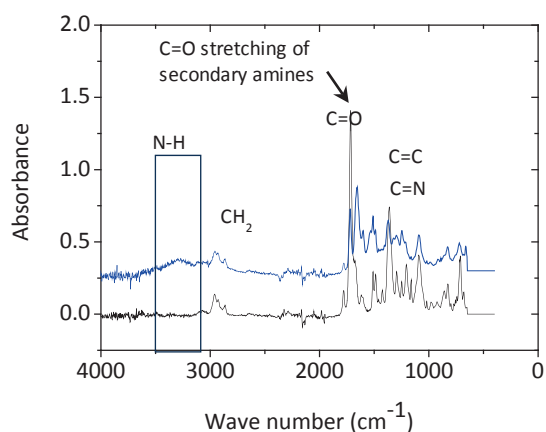


Fig. S5.5. FTIR of native Matrimid® (black) and 100% modified Matrimid® (blue).

The appearance of the broad NH band at 3200-3500 cm^{-1} as well as the C=O band (secondary amine) at 1660 cm^{-1} in the FTIR spectrum (Fig. S5.5) indicate the successful grafting of 1-(3-aminopropyl)-imidazole. The signal at 3400 cm^{-1} is typical for the N-H moiety of the secondary amide and the signal at 1660 cm^{-1} shows the appearance of the C=O stretching vibration in the secondary amines. This is due to the opening of the imide ring and the addition of 1-(3-aminopropyl)-imidazole. Furthermore, there is an increase in the signal strength of the C=C and C=N bond signals (1500-1650 cm^{-1}) for modified Matrimid® compared to non-modified Matrimid® due to the introduction of the imidazole group.

Fig. S5.6 shows the SEM images of polymer particles with and without modification with 1-(3-aminopropyl)-imidazole. The modification of polymer particles facilitates the self-assembly of these particles and helps them organize.

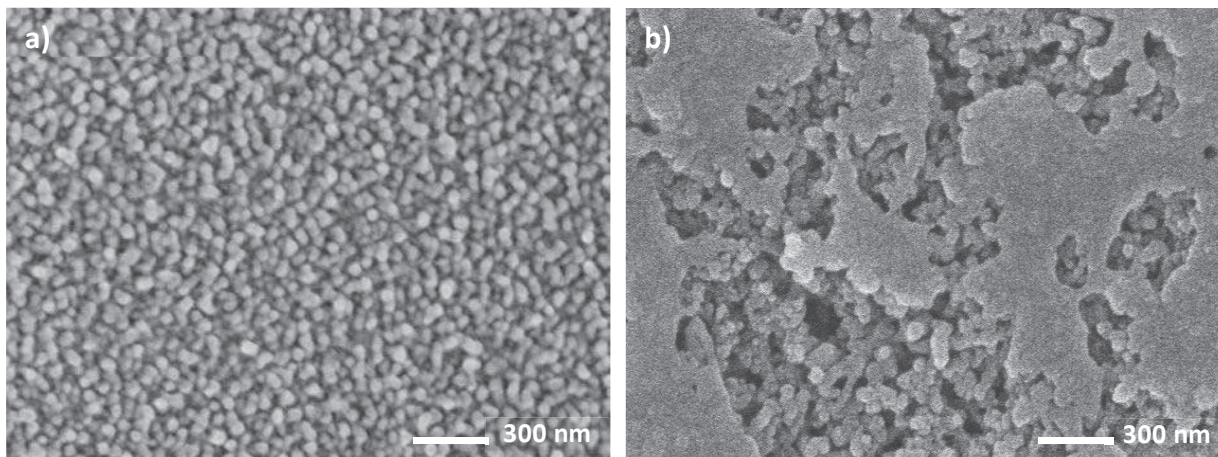


Fig. S5.6. SEM images of the polymer particles (a) without and (b) with modification with 1-(3-aminopropyl)-imidazole. (Magnification: a and b: 50000x).

Fig. S5.7 shows the SEM images of the MMMs prepared with phase separated polymer particles and inter-grown ZIF-8 before solvent vapor treatment. ZIF-8 particles are present throughout the cross-section and agglomeration is not observed, even at high loadings of ZIF-8.

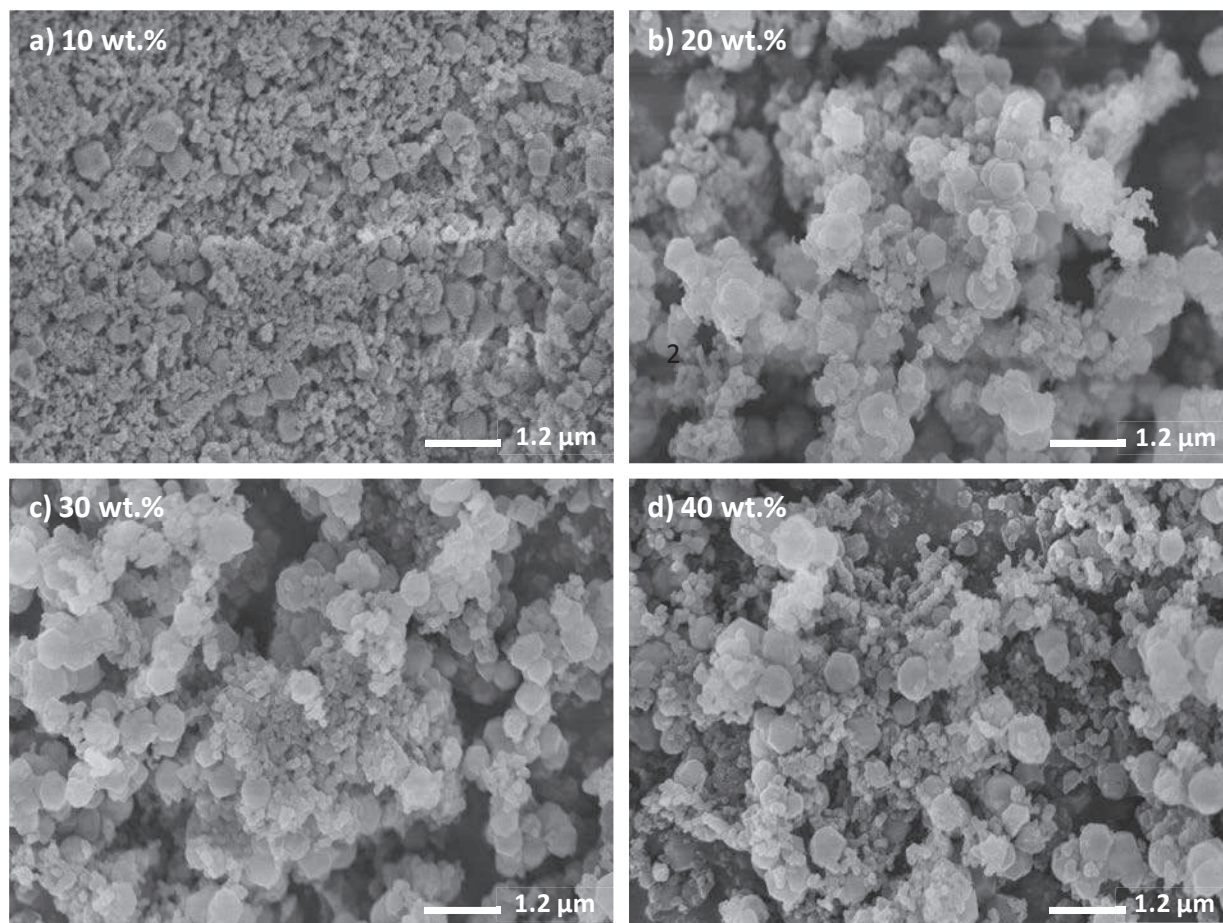


Fig. S5.7. SEM images of the prepared MMMs containing polymer particles and ZIF-8 nanoparticles at different ZIF-8 loadings. (Magnification: a-d: 25000x).

Fig. S5.8 shows the XRD pattern of the prepared MMMs with different ZIF-8 loadings. The pure polymer shows no crystalline peak because of its amorphous nature. For the MMMs the XRD peaks coincide with the XRD peaks of pure ZIF-8. This indicates the presence of ZIF-8 in the MMMs.

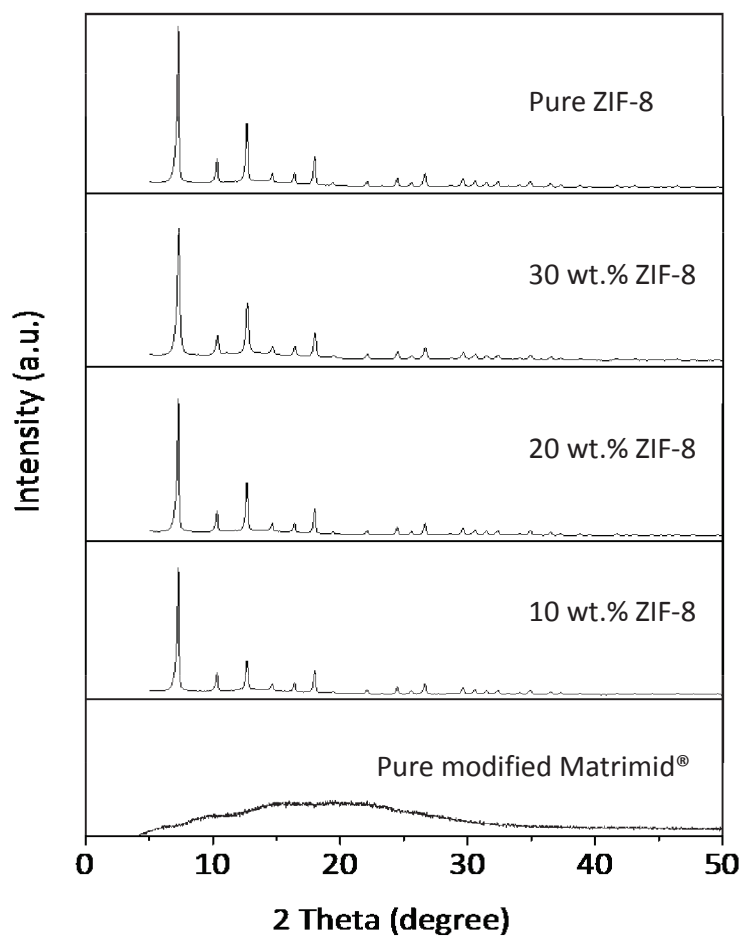


Fig. S5.8. XRD patterns of pure modified Matrimid®, pure ZIF-8 and the MMMs at different ZIF-8 loadings.

Fig. S5.9 shows the TGA results of the pure Matrimid and MMMs with different loadings of ZIF-8. Pure modified Matrimid[®] and pure ZIF-8 show a degradation around 485 and 450 °C, respectively. The degradation temperature of the MMMs show an increase with the ZIF-8 loading.

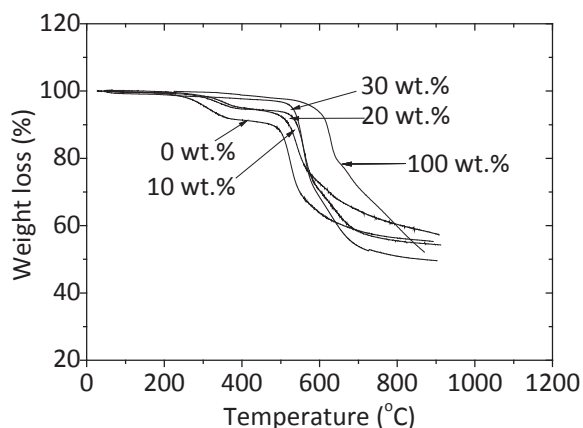


Fig S5.9. TGA of pure Matrimid[®], pure ZIF-8 and MMMs at different ZIF-8 loadings.

Fig. S5.10 shows the normalized mixed gas CO₂ and CH₄ permeabilities of the MMMs with different ZIF-8 loadings. The permeability of CO₂ shows a relatively larger increase in value compared to that of CH₄. The results are normalized based on the data for pure Matrimid[®].

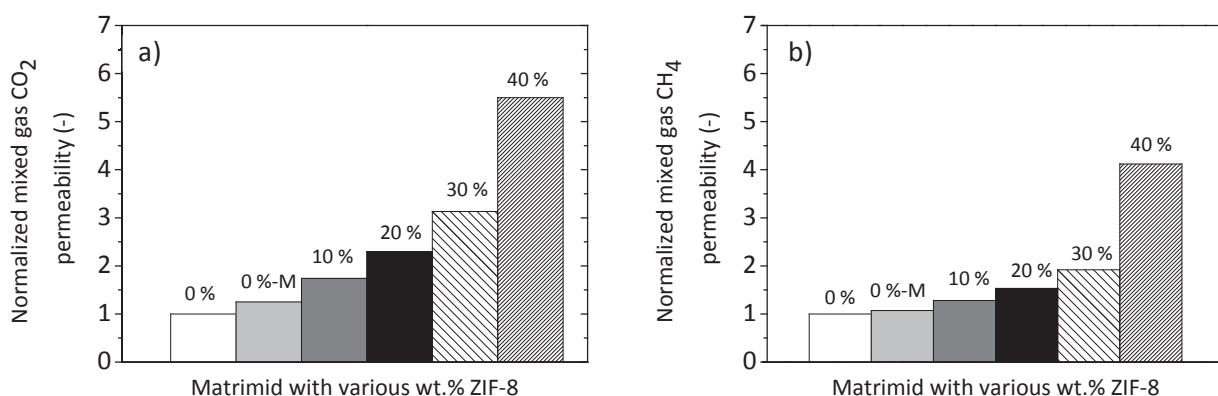


Fig. S5.10. Normalized (a) CO₂ and (b) CH₄ permeability of MMMs with various loadings of ZIF-8 at 5 bar. Results normalized based on the data for pure Matrimid[®].

Fig. S5.11 and S5.12 show the pure gas sorption isotherms of CO₂ and CH₄ for pure ZIF-8, pure polymers and MMMs as function of the applied gas pressure at 35 °C. CO₂ shows higher sorption compared to CH₄ attributed to the higher critical temperature (T_c) and consequently stronger condensability of CO₂ compared to CH₄. Also the favorable quadrupolar interactions contribute to this.

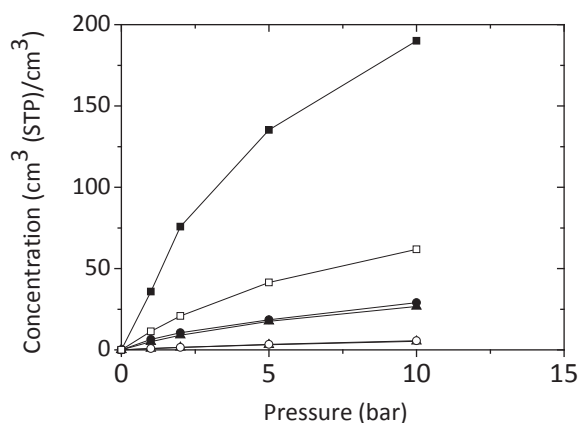


Fig. S5.11. Pure gas sorption isotherms of CO₂ (closed) and CH₄ (open) for (a) pure ZIF-8 (■, □), pure Matrimid® (●, ○), and modified Matrimid® (▲, △) as function of the applied gas pressure at 35 °C.

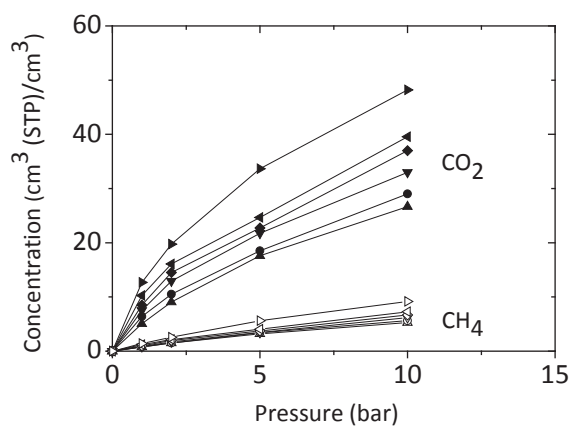


Fig. S5.12. Sorption isotherms of CO₂ (closed) and CH₄ (open) in pure Matrimid® (▲, △) and modified Matrimid® (●, ○), 10 wt.% (▼, ▽), 20 wt.% (◆, ◇), 30 wt.% (◄, ◃) and 40 wt.% (►, ▷) ZIF-8 MMMs as function of the applied gas pressure at 35 °C.

Chapter 6

Reflections and Outlook

6.1 Reflections

Mixed matrix membranes (MMM) are a promising approach to improve the performance of polymeric membranes by combining high performance polymer materials with inorganic particles with excellent gas transport properties. MOFs are porous crystalline materials that possess high surface areas (500-4500 m²/g), large pore volumes and designable pore topologies [1]. MOF-mixed matrix membranes have the potential to compete with conventional gas separation processes if these surpass the permeability-selectivity trade-off. This thesis dealt with metal organic framework (MOFs) based mixed matrix membranes for gas separation. Different MOF materials were incorporated in mixed matrix membranes and the performance of the resulting membranes was evaluated in terms of gas separation enhancement. In addition to this, the problems associated with the permeability-selectivity trade-off (Robeson upper bound) [2] and CO₂ induced plasticization in MOF-mixed matrix membranes were investigated. In this last chapter a short reflection on the results obtained in this thesis will be given, followed by suggestions for the future.

Fe(BTC)/Matrimid® mixed matrix membranes

Matrimid® is a commercially available polymer for gas separation membranes. It exhibits good separation properties. However, Matrimid® membranes suffer from low stability and plasticize in high pressure CO₂ streams. The plasticization behavior of Matrimid® is well studied in literature [3]. However, there are only few studies on the plasticization behavior of mixed matrix membranes. In **Chapter 2**, MMMs were prepared with mesoporous Fe(BTC) nanoparticles as filler and Matrimid® as a polymer matrix. An attempt is made to analyze the plasticization behavior of Matrimid®-MOF MMMs containing mesoporous Fe(BTC). Both pure (CO₂ and CH₄) and mixed gas separation performances were investigated.

A mixture of solvent (dioxane/NMP 20/80) and priming protocol was developed as an appropriate technique to obtain a good dispersion of Fe(BTC) in the Matrimid® matrix, as observed by a scanning electron microscopy (SEM). Mesoporous Fe(BTC) MOF particles showed good compatibility with the polymer. Incorporation of Fe(BTC) in Matrimid® membranes resulted in increased permeability and selectivity. At low pressures of 5 bar MMMs showed an increase of 60 % and 29 % in CO₂ permeability and

ideal selectivity, respectively, over pure Matrimid® membranes. As Fe(BTC) is a mesoporous MOF with relatively large pores, it was expected to increase the CO₂ permeability. However the experimental results showed only a minor increase in both CO₂ permeability and selectivity. This can be attributed to the slight rigidification of the polymer phase around the MOF particles. As the CO₂ pressure increases native Matrimid® membranes showed typical plasticization behavior, while in MMMs, Fe(BTC) particles restrict the mobility of the polymer chains thus suppressing CO₂ induced plasticization. As a consequence of this, the plasticization pressure also increases to higher values. At a feed pressure of 40 bar, MMMs showed a mixed gas (CO₂/CH₄ 50/50) selectivity increase of 62 % compared to pure Matrimid® membranes. As the Fe(BTC) loading increases, the membranes showed more or less constant selectivity over the whole pressure range due to the suppression of CO₂ induced plasticization by the presence of MOF particles. The permeability and selectivity of Fe(BTC) MMMs are a combined effect of slight rigidification, increased adsorption, and diffusivity and reduced CO₂ induced plasticization. This study shows that the presence of MOF particles not only helps in delaying plasticization but also increases the gas transport performance of the MMMs.

Performance and plasticization of MOF-MMMs

Chapter 3 describes the preparation of MMMs based on three distinctively different MOFs (MIL-53(Al) (breathing MOF), ZIF-8 (flexible MOF) and Cu₃(BTC)₂ (rigid MOF)) dispersed in Matrimid®. The ideal and mixed gas performance of the prepared MMMs is determined and the effect of MOF structure on the plasticization behavior of MMMs were investigated. Similar to our previous study, the use of a less volatile co-solvent and optimized priming protocol to prepare the MMMs and annealing temperature resulted in a good compatibility and distribution of the MOFs in Matrimid®. Incorporation of MOFs in Matrimid® membranes resulted in increased density, glass transition temperature and improved degradation behavior of the membranes. This confirmed a good interfacial contact between the polymer and the MOFs. At low pressures, MIL-53(Al) and Cu₃(BTC)₂ showed higher CO₂/CH₄ selectivity than ZIF-8, attributed to the strong CO₂ interaction with MIL-53(Al) and Cu₃(BTC)₂. The quadrupolar CO₂ is selectively attracted towards the unsaturated sites in Cu₃(BTC)₂ while breathing effects and

interactions with the hydroxyl groups of the MIL-53(Al) resulted in high gas separation performance. Although moderate improvements were shown by MOF-MMMs over native Matrimid® membranes at low pressures, the benefits of MOF incorporation became more significant at higher pressures. At high CO₂ pressures, pure Matrimid® membranes showed plasticization. In MMMs, MOF particles hindered an increase in mobility of the polymer chains while enhancing CO₂ sorption in the MOF thus suppressing CO₂ induced plasticization. High separation factors over the whole pressure range investigated were obtained. As a consequence of the restricted chain mobility, the plasticization pressure increased to higher values. Among the three MOF-MMMs, membranes based on Cu₃(BTC)₂ showed highest selectivity while ZIF-8 based membranes showed highest permeability. The respective increase in performance of the MMMs is very much dependent on the MOF crystal structure and the CO₂-MOF interactions. All MOF-MMMs showed a comparable delay in plasticization pressure irrespective of the MOF structure.

ZIF-8 based PI/PSF MMMs

Earlier research showed that Matrimid® blended with polysulfone (PSF) greatly improved the CO₂ plasticization resistance of Matrimid® but suffered from low CO₂ permeability. Considering their enhanced stability, these blends were used as a matrix for MMMs with ZIF-8 (**Chapter 4**). An optimized PI/PSF blend ratio (3:1) was used and performance and stability of PI/PSF mixed matrix membranes filled with different concentrations of ZIF-8 were investigated. PI and PSF were miscible and provided good compatibility with the ZIF-8 particles, even at high loadings. TGA results showed higher thermal stability of the MMMs compared to the pure PI/PSF blend. As predicted, experimental results showed that the permeability of both CO₂ and CH₄ increased with ZIF-8 loading due to moderate increase in sorption capacity of and faster diffusion through the ZIF-8 particles. In pure gas measurements, the PI/PSF blend (3:1) showed a plasticization pressure of ~18 bar, which is comparable to previous literature [4, 5]. The ZIF-8 MMMs showed a higher plasticization pressures (~25 bar) attributed to the increased restriction in polymer chain mobility in the MMMs due to the presence of the ZIF-8 particles. In mixed gas separation measurements, PI/PSF membranes and ZIF-8 MMMs both showed suppression of plasticization as confirmed by a constant mixed gas

CH₄ permeability and nearly constant selectivity with pressure (up to 20 bar CO₂ partial pressure), but the effect was clearly stronger with higher ZIF-8 loading. This work revealed that the enhanced stability of Matrimid® by blending it with PSF and the higher CO₂ permeabilities due to the incorporation of the ZIF-8 particles increased the commercial viability of Matrimid® and broadened their applicability, especially at high pressure CO₂ gas separations.

Novel method for preparing MMMs

As mentioned before MMMs show potential for economically viable separation processes. But MMMs often do not show their predicted separation performance behavior, as they frequently suffer from insufficient adhesion between the polymer matrix and the fillers [6]. This often results in the formation of non-selective voids at the filler-polymer interface, leading to high fluxes but low selectivities. In **Chapter 5**, a novel route for the preparation of mixed matrix membranes via a particle fusion approach was introduced. This approach improved the MOF polymer interaction and eliminated MOF incompatibility, agglomeration and MOF distribution problems, even at high loadings of MOF. Matrimid® polymer particles were first prepared by emulsifying the Matrimid® polymer solution into water. These polymer particles were modified using 1-(3-aminopropyl)-imidazole linker and subsequently ZIF-8 nanocrystal were synthesized in the suspension of modified polymer particles. Surface modification of polymer led to excellent ZIF-8-polymer interfacial compatibility. The particulate morphology of the mixture of particles was then transformed into a dense membrane structure by keeping the film in a controlled DMF vapor environment. By using this approach it was possible to successfully prepare MMMs with MOF loadings as high as 30 wt.% without any non-selective defects. Upon increasing the loading of ZIF-8 nanoparticles, MMMs showed significantly better performance in the separation of CO₂/CH₄ mixtures as compared to the native Matrimid® membranes and previous MMMs based on Matrimid and ZIF-8. The CO₂ permeability increased up to 200 % with a 65 % increase in CO₂/CH₄ selectivity. Gas sorption studies further confirmed that the selective gas transport (CO₂/CH₄ selectivity) is mainly governed by the increase in diffusivity selectivity, which is in all cases higher than the solubility selectivity. The presented approach provides a simple

and very versatile tool to synthesize defect free MMMs, not only for ZIF-8 and Matrimid® but also for a wide range of other material combinations.

Evaluation of MOF-MMMs overall performance

An overall comparison of the gas separation performance of MOF-MMMs prepared over the course of this PhD and the Robeson upper bound (2008) as a benchmark, is presented in Fig. 6.1. The comparison only includes our data obtained for MOF-MMMs with 30 wt.% MOF loading at a pressure of 5 bar and 35°C. Table 6.1 presents the details and operating conditions of the data presented in Fig. 6.1. As shown in Fig. 6.1, significant improvement was achieved for different MOF-MMMs compared to pure Matrimid® membranes. Irrespective of the preparation method, incorporation of different MOFs in a Matrimid® matrix resulted in enhanced CO₂ permeability and selectivity. Fe(BTC) based MMMs showed a relatively lower increase in permeability and selectivity compared to other MOF-MMMs attributed to polymer chain rigidification around the Fe(BTC) particles. Among ZIF-8, MIL-53(Al) and Cu₃(BTC)₂, membranes based on ZIF-8 and MIL-53(Al) showed enhanced CO₂ permeability with moderate increase in selectivity, while Cu₃(BTC)₂-MMM showed higher selectivity. Comparing the membrane preparation method, membranes prepared by the particle fusion approach showed better gas separation performance than the membranes prepared via solution casting. This can be attributed to a better MOF dispersion and improved compatibility at the MOF-Polymer interface. This overall evaluation of our results show that MMMs with MOF particles can provide new opportunities for enhanced permeability and selectivity. Especially proper selection of MOF, polymer and fabrication method shows potential to reach membrane performances beyond the Robeson upper bound.

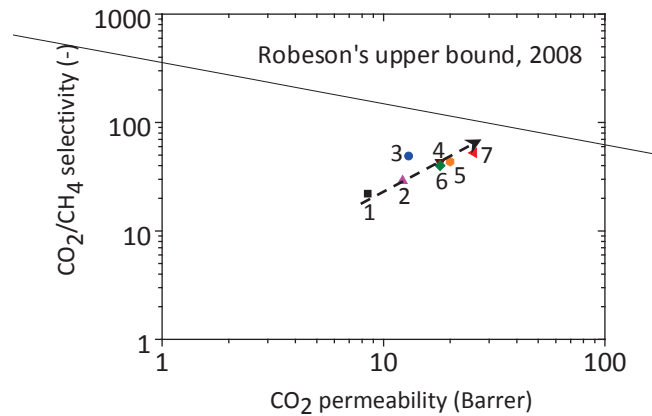


Fig.6.1. Summary of gas separation results of MOF-MMMs (30 wt.% loading) prepared during this PhD and measured at 5 bar and 35°C under mixed gas conditions. See Table 6.1 for details of different membranes and specific experimental details.

Table 6.1. Experimental details of the data presented in Fig. 6.1. All membranes measured at 5 bar and 35 °C under mixed gas conditions.

| Code | Membrane | Preparation method |
|------|---------------------------------------|--------------------|
| 1 | PI | Solution casting |
| 2 | PI-Fe(BTC) | Solution casting |
| 3 | PI-Cu ₃ (BTC) ₂ | Solution casting |
| 4 | PI-MIL-53(Al) | Solution casting |
| 5 | PI-ZIF-8 | Solution casting |
| 6 | PI/PSF-ZIF-8 | Solution casting |
| 7 | PI-ZIF-8 | Particle fusion |

*PI Matrimid® 5218

This PhD thesis presented high-performance mixed matrix membranes (MMMs) based on metal organic frameworks (MOFs) for low and high pressure gas separation applications. A significant improvement was achieved in terms of MOF-matrix adhesion and gas separation performance stability but still some challenges remain to further increase the separation properties of MMMs and stabilize the performance under practical industrial conditions. The subsequent section gives some recommendations to resolve these issues.

6.2 Future perspective

Methods to increase the performance of MMMs

As mentioned before, the successful implementation of MOF-mixed matrix membranes in industrial separations requires to overcome several challenges related to morphology, gas separation properties and mechanical/chemical stability. These challenges include a homogeneous dispersion of particles in the polymer matrix, a defect-free polymer/inorganic particle interface and the proper selection of polymer and inorganic (MOF) materials.

From the membrane preparation point of view, the currently used method (solution casting followed by solvent evaporation) could be further improved by proper selection of solvent, fabrication protocol and post treatment (e.g. annealing). Stress release and matrix rigidification during solvent evaporation result in non-selective voids at the polymer-MOF interface. If the residual stresses due to solvent evaporation are high, annealing near/above the glass transition temperature (T_g) of the polymer has proven effective. But heating the membrane to high temperatures (around T_g of the polymer) can be complicated as some MOF materials start to decompose at higher temperatures. A possible solution to this would be low temperature annealing in the presence of a solvent.

To limit residual stresses and matrix rigidification, proper selection of solvent is very important. A systematic study for the choice of best solvents in the preparation of the MMMs is still missing. But it has been observed that fast evaporating solvent are preferred because they limit the penetration of polymer chains in the pores of the MOF structure. However, fast evaporating solvent also lead to high residual stresses after evaporation. As a solution we used a mixture of a fast evaporating solvent (dioxane) and a slow evaporating solvent (NMP). The role of solvent in the preparation of MMMs should be explored in more detail. In addition to proper selection of fabrication parameters, the solution casting method can be improved if we can initiate direct monomer polymerization starting directly from the external surface of the MOF nanoparticles e.g. by functionalizing MOF to allow polymerization. As such we ensure a strong interfacial connection between the MOF particles and the polymer.

From membrane design perspective, there is still a lot of room for improvement regarding the MOF synthesis side of MOF-MMMs. Functionalization of MOFs e.g. grafting of amines onto the surfaces of MOF materials to enhance adsorption of the acidic CO₂ is one of the strategies to enhance the gas separation properties and adhesion between the matrix and the MOF. To date, several types of MOFs containing amino groups have been described in the scientific literature [7]. Synthesizing MOFs with organic linkers and functionalizing them with polymer compatible moieties can improve the interfacial adhesion between MOF and polymer. Another possibility is to use mixed-linker MOFs. Possibly the systematic synthesis of mixed-linker amine-MOFs with different linker ratios help to find optimized functional MOFs. For mixed-linker ZIF MMMs, both the linker functionality and the composition were shown to have significant effects on the permeability of CO₂ and CH₄. It was also reported that gate-opening behavior was not observed and there were noticeable changes in the pore size distribution of the materials [8]. Chemical bonding between the MOF and polymer phase can also be another way to improve the adhesion and hence the gas separation performance.

Asymmetric MOF mixed matrix membranes and the particle fusion technique

All membranes described in this thesis were prepared in dense membrane form to allow investigation of the inherent transport properties of the membrane materials. However, for industrial applications, membranes should be processed into an asymmetric structure, where a porous support layer is covered by a thin dense skin layer responsible for the actual separation. This ensures a high flux by minimizing mass transport resistance. However, the formation of asymmetric membranes may induce additional stresses generated at the MOF-polymer interface due to constraints at the support separating layer interface. In future work, the MOF-polymer adhesion and the gas transport properties of such asymmetric membranes should be investigated.

Another important factor in making successful MMMs is the size/shape of the MOF particles. Although a smaller particle size is also more beneficial for making dense MMMs, it is crucial for asymmetric membranes because of thickness limitations. Also, smaller particles have higher surface area/volume ratios, which normally results in enhanced mass transfer between the phases. Particle distribution within the thin skin

layer is another important issue. Particles can agglomerate, especially at high loadings. This can result in non-selective voids between the particles that minimize the separating effectiveness. For the case of asymmetric MMMs, the particle fusion technique as introduced in this thesis, has great potential. Thin asymmetric MOF-MMMs can be prepared by casting the suspension of polymer-MOF particles followed by controlled densification by controlling the time in the vapor environment. Also different membrane morphologies can be fabricated using coated and composite membranes. In future work, more detailed analysis of dense and asymmetric MMMs using particle fusion technique should be made.

The shape of the MOF particles is also important for good dispersion and contact between the MOF and the polymer. It is possible to synthesize MOF fillers with different crystal sizes and shapes with the aid of modulators. For example highly selective MOFs with larger aspect (L/D) ratio or in the form of flakes can lead to much higher selectivities of permeating species as this will cause much longer diffusion paths for the less mobile species.

Screening of MOFs

Currently, MOF based MMMs fabrication is pursued from MOFs that show interesting adsorption behavior for single gases. Adsorption studies related to mixed gases are still scarce [9], but are of great significance and required for the proper selection of MOFs for a given mixture to be separated.

Also kinetics (diffusion of species) plays a major role in the case of membranes but literature available on the diffusion of gases through a specific MOF is still rare. A large variety of MOFs have already been reported in literature but experimental characterization of a large number of different MOFs is a very expensive and time-consuming procedure. Therefore, significant progress could be made if computational methods could be applied to help screening MOF materials suitable for the separation of specific mixtures. In this regard molecular simulation models based on the interaction between CO₂ and MOF, adsorption isotherms and transport diffusivities of pure and mixed gases in various MOFs can be a new direction to explore.

Plasticization behavior in multicomponent mixture

The results presented in this work mainly focused on the separation of pure and binary gas mixtures. The next step in membrane development is to evaluate the performance of MOF based MMMs under industrially operating conditions, as industrial feed streams usually consist of more than two component e.g. water, H₂S, NO_x and SO_x. The presence of water in the MOFs may be beneficial or adverse to CO₂ capture performance. For example the presence of moisture increases the gas separation performance of MIL-53(Al) [10], while it has adverse effects on Cu₃(BTC)₂ [11]. Hence, future studies should focus on studying the effects of water vapor on the CO₂ separation performance. This would give a better idea of the role of water (vapour) in the interaction of and possible blocking of the open metal sites and active adsorption sites. Furthermore, the presence of other components like H₂S etc. will certainly alter the separation behavior of MOF-MMMs and could lead to a reduction in CO₂ performance in MOFs. Also there is no or very limited literature available on the plasticization behavior of polymers in the presence these trace contaminants. So, there is a need to study and understand the impact of contaminants on MOF structure and CO₂ separation properties of MMMs.

Plasticization studies of asymmetric MMMs

This work has enhanced the fundamental understanding of CO₂ plasticization of dense MOF-MMMs in the context of pure and mixed gas feeds. However, studies [12-14] have shown that thin glassy polymer films undergo physical aging more rapidly than thick films. This suggests that thickness has an important role in the plasticization behavior of thin glassy films in the presence of highly sorbing penetrants such as CO₂ [12]. Also Horn et al. [15] observed completely different plasticization behavior of asymmetric polymer membranes compared to thick dense membranes. This behavior could be of significant interest in future studies of the plasticization behavior of filled asymmetric MMMs. As shown in this study the presence of MOF particles increases the plasticization resistance of dense MMMs. It can be expected that MOF particles also improve the plasticization behavior of asymmetric MMMs. Additionally, investigating the effect of temperature upon CO₂ plasticization of asymmetric MOF-MMMs could be useful.

In literature, plasticization behavior of MMMs is often shown in terms of gas permeation experiments. However, gas permeation experiments only provide indirect measurement of morphological change during plasticization. Therefore it is important to explore other techniques e.g. ellipsometry, infrared spectroscopy, positron annihilation lifetime spectroscopy, which could show molecular alterations occurring during plasticization of the polymer and the mixed matrix membranes.

References

- [1] R. Adams, C. Carson, J. Ward, R. Tannenbaum, W. Koros, Metal organic framework mixed matrix membranes for gas separations, *Microporous and Mesoporous Materials*, 131 (2010) 13-20.
- [2] L.M. Robeson, The upper bound revisited, *J. Membr. Sci.*, 320 (2008) 390-400.
- [3] A. Bos, I.G.M. Pünt, M. Wessling, H. Strathmann, Plasticization-resistant glassy polyimide membranes for CO₂/CO₄ separations, *Separation and Purification Technology*, 14 (1998) 27-39.
- [4] S. Basu, A. Cano-Odena, I.F.J. Vankelecom, Asymmetric membrane based on Matrimid® and polysulphone blends for enhanced permeance and stability in binary gas (CO₂/CH₄) mixture separations, *Separation and Purification Technology*, 75 (2010) 15-21.
- [5] G.C. Kapantaidakis, S.P. Kaldis, X.S. Dabou, G.P. Sakellaropoulos, Gas permeation through PSF-PI miscible blend membranes, *J. Membr. Sci.*, 110 (1996) 239-247.
- [6] G. Dong, H. Li, V. Chen, Challenges and opportunities for mixed-matrix membranes for gas separation, *Journal of Materials Chemistry A*, 1 (2013) 4610-4630.
- [7] B. Zornoza, A. Martinez-Joaristi, P. Serra-Crespo, C. Tellez, J. Coronas, J. Gascon, F. Kapteijn, Functionalized flexible MOFs as fillers in mixed matrix membranes for highly selective separation of CO₂ from CH₄ at elevated pressures, *Chemical Communications*, 47 (2011) 9522-9524.
- [8] J.A. Thompson, J.T. Vaughn, N.A. Brunelli, W.J. Koros, C.W. Jones, S. Nair, Mixed-linker zeolitic imidazolate framework mixed-matrix membranes for aggressive CO₂ separation from natural gas, *Microporous and Mesoporous Materials*, (2013).
- [9] J.-R. Li, R.J. Kuppler, H.-C. Zhou, Selective gas adsorption and separation in metal-organic frameworks, *Chemical Society Reviews*, 38 (2009) 1477-1504.
- [10] P.L. Llewellyn, S. Bourrelly, C. Serre, Y. Filinchuk, G. Férey, How hydration drastically improves adsorption selectivity for CO₂ over CH₄ in the Flexible chromium terephthalate MIL-53, *Angewandte Chemie International Edition*, 45 (2006) 7751-7754.
- [11] F. Gul-E-Noor, B. Jee, A. Poppl, M. Hartmann, D. Himsl, M. Bertmer, Effects of varying water adsorption on a Cu₃(BTC)₂ metal-organic framework (MOF) as studied by ¹H and ¹³C solid-state NMR spectroscopy, *Physical Chemistry Chemical Physics*, 13 (2011) 7783-7788.

- [12] J. Xia, T.-S. Chung, P. Li, N.R. Horn, D.R. Paul, Aging and carbon dioxide plasticization of thin polyetherimide films, *Polymer*, 53 (2012) 2099-2108.
- [13] P.H. Pfromm, W.J. Koros, Accelerated physical aging of thin glassy polymer-films - evidence from gas-transport measurements, *Polymer*, 36 (1995) 2379-2387.
- [14] C. Zhou, T.-S. Chung, R. Wang, Y. Liu, S.H. Goh, The accelerated CO₂ plasticization of ultra-thin polyimide films and the effect of surface chemical cross-linking on plasticization and physical aging, *J. Membr. Sci.*, 225 (2003) 125-134.
- [15] N.R. Horn, D.R. Paul, Carbon dioxide plasticization and conditioning effects in thick vs. thin glassy polymer films, *Polymer*, 52 (2011) 1619-1627.

SUMMARY

The main research objective of this work was to develop high-performance mixed matrix membranes (MMMs) based on metal organic frameworks (MOFs) for low and high pressure gas separation applications. MOF-MMMs have the potential to show significantly better performance than membranes made from pure polymers. To successfully employ MOF based MMMs in industrial separations, membranes with good MOF-polymer interfacial adhesion and high pressure stability need to be developed. Fundamental knowledge on the rather complex behavior of plasticization in MOF-MMMs and on the aspect of poor MOF-polymer interfacial compatibility is developed in this thesis.

Processes like natural gas upgrading, enhanced oil recovery and landfill gas cleaning need membranes that can deal with feed streams containing high pressure CO₂. The sorption of CO₂ causes the polymer to swell, which accelerates the permeation of especially the less mobile components (e.g. CH₄, N₂), a phenomenon called plasticization. As a consequence the membrane loses its selectivity. To prevent plasticization, understanding of this phenomenon is necessary. The plasticization behavior of pure polymers is well studied in literature. However, there are only few studies on the plasticization behavior of mixed matrix membranes. In **Chapter 2** of this thesis, pure and mixed gas plasticization behavior of MMMs prepared from mesoporous Fe(BTC) nanoparticles and the polymer Matrimid® is investigated. All experiments were carried with solution casted dense membranes. Mesoporous Fe(BTC) MOF particles showed reasonably good compatibility with the polymer. Incorporation of Fe(BTC) in Matrimid® resulted in membranes with increased permeability and selectivity. At low pressures of 5 bar the MMMs showed an increase of 60 % in CO₂ permeability and a corresponding increase of 29 % in ideal selectivity over pure Matrimid® membranes. It was observed that the presence of Fe(BTC) particles increases the plasticization pressure of Matrimid® based MMMs. Furthermore, this pressure increases more with increasing MOF loading. This delay in plasticization is attributed to the reduced mobility of the polymer chains in the vicinity of the Fe(BTC) particles. Also, at higher Fe(BTC) loadings, the membranes showed more or less constant selectivity over the whole pressure range investigated. The enhanced permeability and selectivity of Fe(BTC)-MMMs were the combined effect of slight rigidification, increased adsorption and diffusivity and reduced CO₂

induced plasticization. The presence of Fe(BTC) particles not only helps in delaying plasticization but also increases the gas transport performance of the MMMs.

Chapter 3 subsequently presented the preparation and plasticization behavior of MMMs based on three distinctively different MOFs (MIL-53(Al) (breathing MOF), ZIF-8 (flexible MOF) and $\text{Cu}_3(\text{BTC})_2$ (rigid MOF)) dispersed in Matrimid[®]. The ideal and mixed gas performance of the prepared MMMs was determined and the effect of MOF structure on the plasticization behavior of MMMs was investigated. The increased density, glass transition temperature and improved degradation behavior of the membranes confirmed a good MOF-polymer interfacial contact. Among the three MOF-MMMs, membranes based on $\text{Cu}_3(\text{BTC})_2$ showed highest selectivity while ZIF-8 based membranes showed highest permeability. The respective increase in performance of the MMMs is very much dependent on the MOF crystal structure and its interactions with CO_2 molecules. Although moderate improvements were shown for the MOF-MMMs over native Matrimid[®] membranes at low pressures, the benefits of MOF incorporation (i.e. high CO_2 permeability and CO_2/CH_4 selectivity) became more significant at higher pressures. All MOF-MMMs showed a comparable delay in plasticization pressure irrespective of the MOF structure.

Chapter 4 described the preparation of Matrimid[®] polyimide (PI)/polysulfone (PSF)-blend membranes containing ZIF-8 particles for high pressure gas separation. Homogeneous blending is an easy way to tune gas separation properties of polymer membranes and it may increase the stability to aggressive feed streams as well. An optimized PI/PSF blend ratio (3:1) was used and performance and stability of PI/PSF mixed matrix membranes filled with different concentrations of ZIF-8 were investigated. PI and PSF were miscible and provided good compatibility with the ZIF-8 particles, even at high loadings. The PI/PSF-ZIF-8 MMMs showed significant enhancement in CO_2 permeability with increased ZIF-8 loading, which was attributed to a moderate increase in sorption capacity and faster diffusion through the ZIF-8 particles. In pure gas measurements, pure PI/PSF blend (3:1) membranes showed a plasticization pressure of ~18 bar while the ZIF-8 MMMs showed a higher plasticization pressures of ~25 bar. Mixed gas measurements of PI/PSF-ZIF-8 MMMs showed suppression of plasticization as confirmed by a constant mixed gas CH_4 permeability and a nearly constant selectivity with pressure but the effect was stronger at high ZIF-8 loadings. Gas separation results of the prepared PI/PSF-ZIF-8 MMMs show an increased commercial

viability of Matrimid® based membranes and broadened their applicability, especially for high-pressure CO₂ gas separations.

For successful implementation of mixed matrix membranes in industrial separations several challenges need to be overcome. These challenges especially include a homogeneous dispersion of particles in the polymer matrix and a defect-free polymer-filler interface. In **Chapter 5**, a novel route for the preparation of mixed matrix membranes via a particle fusion approach was introduced. This approach improved the MOF-polymer interaction and eliminated MOF incompatibility, agglomeration and particle distribution problems, even at high loadings of MOF. Surface modification of the polymer with 1-(3-aminopropyl)-imidazole led to an excellent ZIF-8-Matrimid® interfacial compatibility. The particulate morphology of a mixture of modified polymer particles and filler particles was transformed into a dense membrane structure by keeping the film in a controlled vapor environment. It was possible to successfully prepare MMMs with MOF loadings as high as 30 wt.% without any non-selective defects. Upon increasing the ZIF-8 loading, MMMs showed significantly better performance in the separation of CO₂/CH₄ mixtures as compared to the native polymer. The CO₂ permeability increased up to 200 % combined with a 65 % increase in CO₂/CH₄ selectivity, compared to the native Matrimid®. Gas sorption studies further confirmed that selective gas transport (CO₂/CH₄ selectivity) is mainly governed by the increase in diffusivity selectivity, which is in all cases higher than the solubility selectivity. The ZIF-8 MMMs prepared by this particle fusion technique showed a significant improvement in CO₂ permeability and selectivity compared to literature based MMMs containing identical MOF materials. This study showed that it is possible to increase the gas separation performance of MMMs when challenges associated with the preparation and the formation of defect free MMMs can be overcome. The presented approach provides a simple method to eliminate these challenges. In addition, particle fusion is a very versatile MMM preparation route, not only for this specific ZIF and polymer but for numerous combinations of polymers and MOFs. **Chapter 6** finally discussed the conclusions and directions for future research based on the findings presented in this thesis.

Résumé de la thèse en français

Cette thèse a été réalisée en cotutelle entre trois universités européennes : l'Université de Twente aux Pays-Bas (université hôte), l'Université de Leuven en Belgique, ainsi que l'Université Montpellier 2, devenue entre-temps l'Université de Montpellier, dans le cadre du programme doctoral européen EUDIME. Ainsi le manuscrit de thèse a été rédigé en anglais. Toutefois, dans un souci de clarté, un résumé étendu en français, reprenant les principales découvertes, a été rajouté.

Membranes à matrice mixte Polymère- Réseaux métallo-organiques (MOF) pour des applications en séparation des gaz

La littérature établit clairement l'importance des membranes pour la séparation des gaz et plus particulièrement le besoin de membranes à matrice mixte pour améliorer les performances en séparation mais aussi pour étendre le champ possible des applications membranaires. Toutefois, sans une excellente compatibilité entre le polymère et, dans notre cas, le réseau métallo-organique (MOF), ce type de membranes ne sera jamais viable pour une application industrielle en séparation des gaz. De plus, nous devons remarquer que l'opération de séparation implique souvent l'utilisation de hautes pressions comme dans le cas du dioxyde de carbone (CO_2). A ces pressions d'alimentation, le CO_2 agit comme un agent de plastification et a pour conséquence un gonflement de la partie polymère de la membrane. Ce phénomène de plastification est très bien décrit dans la littérature pour les polymères purs mais il est encore assez délicat de trouver des explications fondamentales à la plastification des membranes à matrice mixte et encore plus incertain de trouver des solutions pour l'éviter.

Ainsi, tout l'objectif de cette thèse est de tenter de répondre à cette problématique.

Le Matrimid® est un polyimide commercial classiquement utilisé dans les études scientifiques traitant de la séparation des gaz en raison de ces bonnes performances observées. Toutefois, la tendance de ce polymère à subir la plastification au CO_2 a jusqu'à présent limité son utilisation commerciale. Dans le **Chapitre 2** de ce manuscrit de thèse, l'impact sur les performances membranaires de l'ajout de MOF à une membrane de Matrimid® a été étudié.

Lors de ce travail, des membranes à matrice mixte (MMM) ont été préparées en incorporant des MOFs de type Fe(BTC) à une membrane Matrimid® et caractérisées en séparation du CO_2 et du méthane (CH_4) sur un large domaine de pressions de sorte à évaluer les phénomènes de plastification. Les propriétés physiques (densité, dégradation thermique, transition vitreuse) du Fe(BTC) ainsi que des MMMs préparées ont été analysées. L'optimisation de la préparation des MMMs via un protocole de suspension des MOFs dans la solution de polymère a permis l'obtention d'une distribution homogène des particules de MOF dans le Matrimid®, comme le montre les clichés de Microscopie Electronique à Balayage (**Figure 1**). Les résultats expérimentaux ont démontré une amélioration de la dégradation thermique du polymère mais aussi une augmentation de la densité de la membrane ainsi

que de la température de transition vitreuse lorsque la proportion de Fe(BTC) a été augmentée jusqu'à 30% en masse. Une amélioration de la perméabilité en CO₂ ainsi que de la sélectivité CO₂/CH₄ a été par ailleurs démontrée. Pour de hautes pressions, le Matrimid® présente un phénomène de plastification comme attendu, mais l'incorporation de MOF semble permettre un certain contrôle sur les propriétés de transport de gaz tout en réduisant la tendance de plastification.

La bonne performance observée pour les membranes contenant des MOFs peut être attribuée à la forte augmentation de la capacité de sorption et de la rigidité des chaînes de polymère via l'interaction avec le Fe(BTC) ce qui tend à amoindrir voir à supprimer le phénomène de plastification. Lors d'une expérience avec un mélange gazeux à 40 bar, les MMMs avec 30% de MOF ont démontré une augmentation de 62% de la sélectivité CO₂/CH₄, alors que la perméabilité est elle aussi augmentée de 30% par rapport à la membrane de Matrimid®.

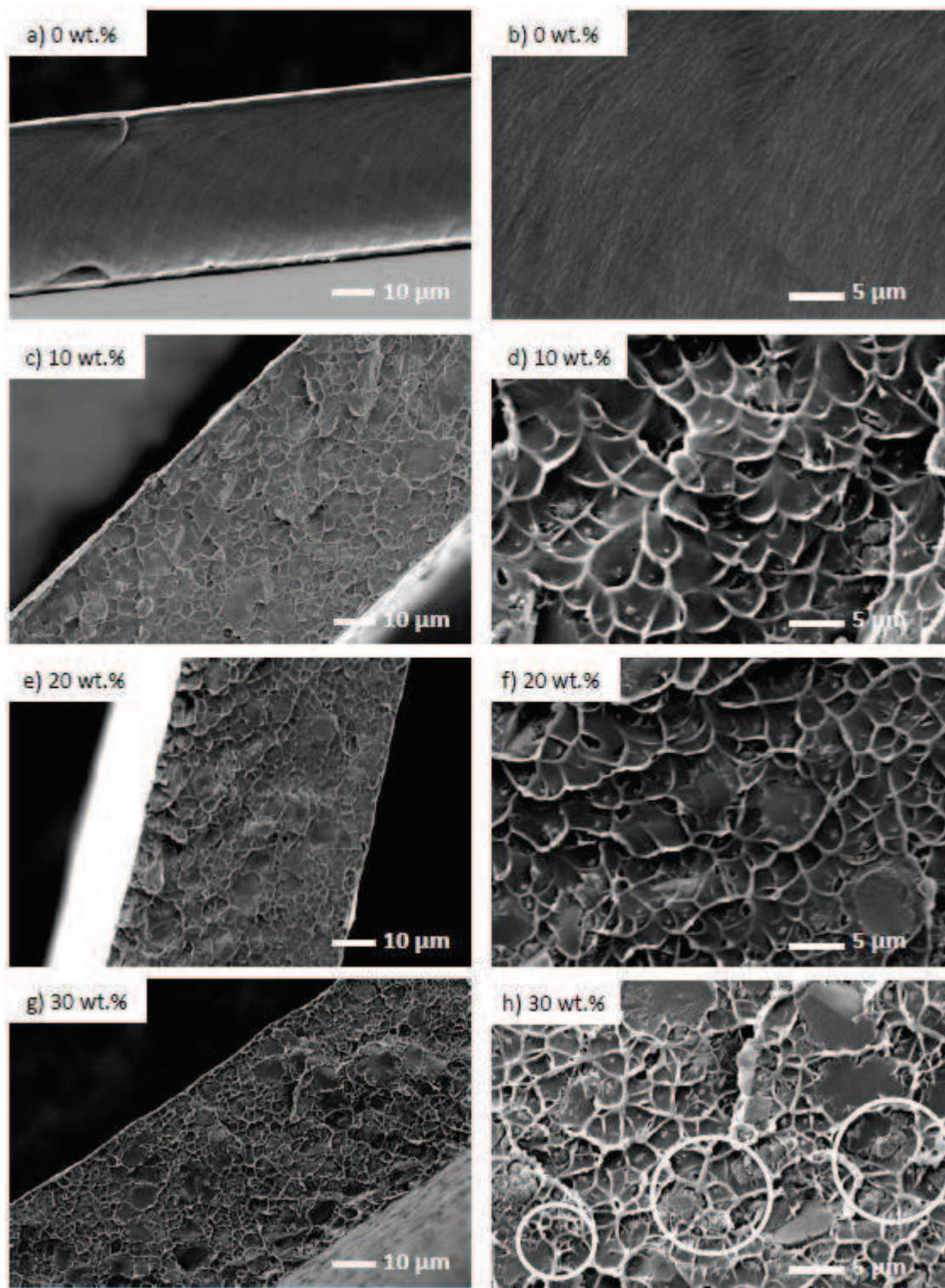


Figure 1. Images MEB des membranes à matrice mixte. a et b : sections transversales d'une membrane Matrimid® ; c et d : sections transversales d'une MMM contenant 10% massique de Fe(BTC) ; e et f : sections transversales d'une MMM contenant 20% massique de Fe(BTC) ; g et h : sections transversales d'une MMM contenant 30% massique de Fe(BTC). (Magnification a ,c, e, g: 1000x; magnification b, d, f, h: 3000x)

Le **Chapitre 3** décrit la préparation de différents MMMs incorporant une diversité de MOFs : MIL 53 (Al) (MOF « respirant »), ZIF-8 (MOF « flexible »), ou Cu_3BTC_2 (MOF « rigide ») toujours dans une matrice de Matrimid®. La performance idéale et en mélange de gaz CO_2/CH_4 des MMMs préparées a été évaluée sur une large gamme de pressions. L'emploi d'un co-solvant moins volatile ainsi que l'ajout d'une étape de recuit thermique ont permis d'optimiser la procédure de préparation des membranes et d'observer une bonne répartition des particules de MOFs dans la matrice de Matrimid®. L'incorporation de MOFs a eu pour effet l'augmentation de la densité et de la température de transition vitreuse, ainsi que l'amélioration de la dégradation thermique témoignant de la bonne compatibilité obtenue entre le polymère et les particules de MOFs. Les séparations gazeuses à faible pression ont montré une amélioration modérée de la perméabilité en CO_2 ainsi que de la sélectivité CO_2/CH_4 des MMMs à comparer aux membranes initiales, mais l'amélioration est devenue plus prononcée avec l'augmentation de la pression. Ainsi, pour de fortes pressions, alors que la membrane de Matrimid® initiale présente un phénomène de plastification, l'incorporation des MOFs permettent, comme dans le cas précédent, de limiter la mobilité des chaînes polymères, supprimant ainsi la plastification au CO_2 et maintenant les facteurs de séparation au plus haut niveau et sur une large gamme de pressions. L'augmentation de performance observée est particulièrement dépendante de la structure cristalline du MOF introduit et de son interaction avec les molécules gazeuses de CO_2 . Parmi les trois MMMs étudiées, les membranes basées sur Cu_3BTC_2 ont présenté les meilleures sélectivités (**Figure 2**) alors que celles avec le ZIF-8 sont celles présentant les meilleures perméabilités (**Figure 3**).

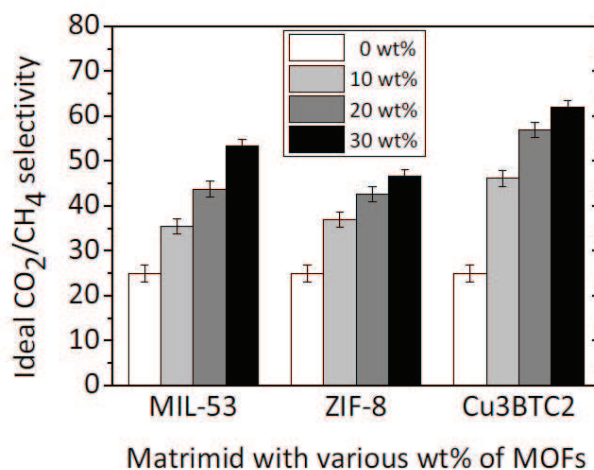


Figure 2. Sélectivité idéale CO_2/CH_4 des MMMs incorporant différentes proportions de MOFs à 5 bar et à 35°C.

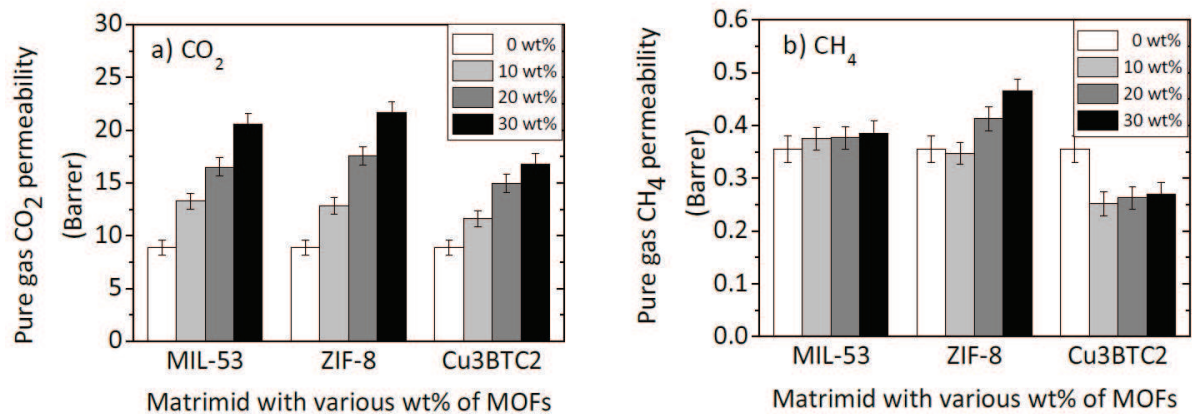


Figure 3. Perméabilité du CO₂ (a) et du CH₄ (b) des MMMs avec 0, 10, 20 and 30 % massique de MOFs à 5 bar et à 35°C

En général, il peut être conclut que la grande perméabilité en CO₂ et la grande sélectivité CO₂/CH₄ des MMMs est la résultante de l'effet combiné d'une augmentation de la sorption, de la sélectivité diffusive et de la plastification réduite. En conséquence, ce travail révèle que les MMMs incorporant des MOFs ont repoussé l'effet de plastification vers de plus fortes pressions et présentent une bonne capacité de séparation, même à hautes pressions, ce qui démontre leur potentiel pour une large gamme d'applications émergentes, notamment dans le domaine de l'énergie.

En se basant sur nos observations révélant la relation entre plastification et taux d'incorporation de MOFs, le **Chapitre 4** rapporte une nouvelle stratégie de préparation de MMS de grande perméabilité et disposant d'une grande résistance à l'effet de plastification. Le mélange de Matrimid® avec de la PSF est ainsi proposé dans le but d'optimiser ces propriétés. Par ailleurs, le ZIF-8 a été choisi comme MOF pour évaluer son impact sur les performances de la membrane obtenue et notamment pour améliorer la perméabilité du CO₂. L'effet de la proportion en ZIF-8 a ainsi été étudié. Les résultats expérimentaux montrent que la perméabilité du CO₂ et du CH₄ augmente avec le taux d'incorporation en ZIF-8 en raison d'une augmentation modérée de la capacité de sorption et d'une diffusion plus rapide à travers les particules de ZIF-8. La sélectivité idéale augmente légèrement, ce qui est principalement attribué à l'augmentation de la sélectivité diffusive et, pour une plus petite part, à l'augmentation de la sélectivité de solubilité correspondante. Pour les gaz purs, les mélanges initiaux de PI/PSF présente une plastification autour de 18 bars, alors que l'introduction de MOFs retarde cette plastification à environ 25 bars pour 30% en masse de MOFs (Figure 4).

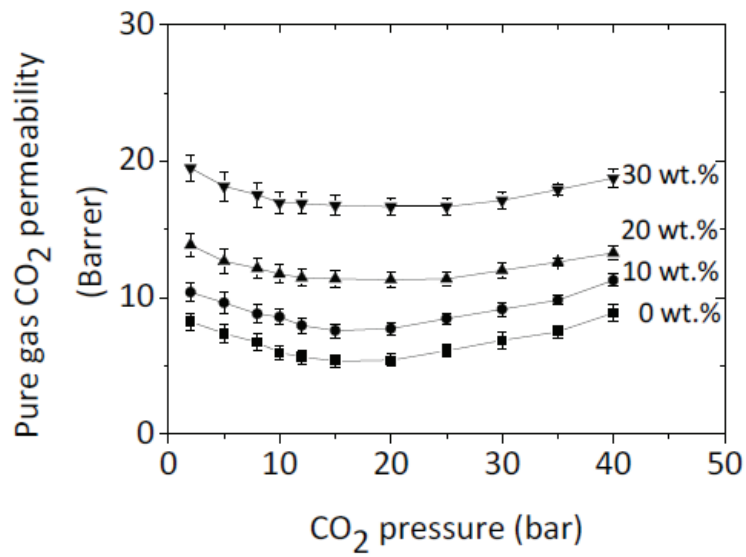


Figure 4. Perméabilité du CO₂ pur en fonction de la pression pour différents taux massiques d'incorporation de ZIF-8 à 35°C.

Lors d'expérience en mélange de gaz, les membranes PI/PSF ainsi que les MMMs ne présentent aucune plastification sur la gamme de pressions évaluées, comme le confirme la perméabilité constante du CH₄ en mélange, la sélectivité étant également pratiquement constante avec la pression (jusqu'à 20 bar de pression partielle en CO₂) (**Figures 5 et 6**).

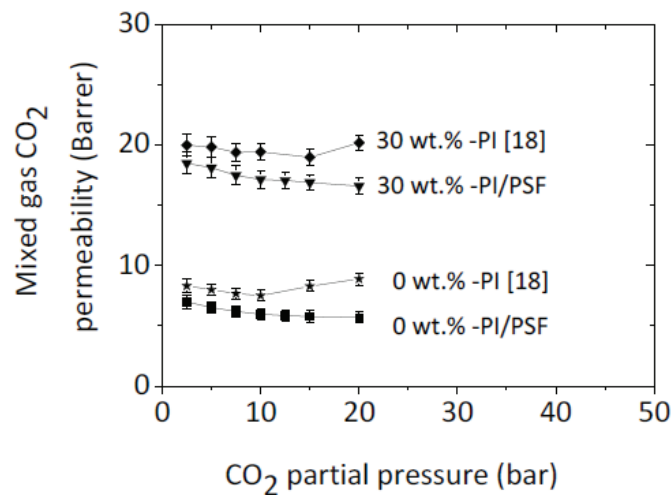


Figure 5. Perméabilités du CO₂ en mélange des membranes de PI [18], et de PI/PSF MMMs en fonction de la pression pour différents taux d'incorporation de ZIF-8 à 35°C.

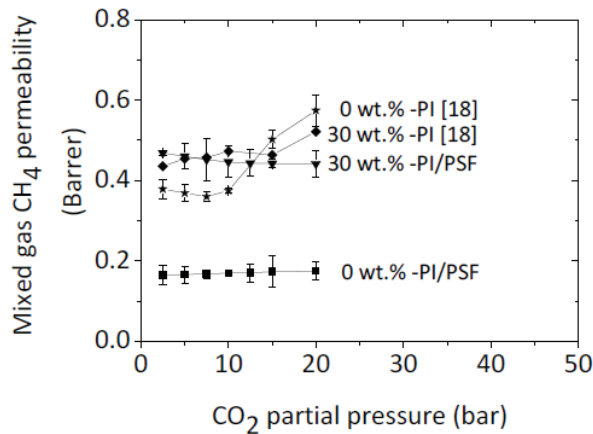


Figure 6. Perméabilités du CH₄ en mélange des membranes de PI [18], et de PI/PSF MMMs en fonction de la pression pour différents taux d'incorporation de ZIF-8 à 35°C.

Les résultats montrent que le simple mélange de polymère (PI et PSF) ou encore l'approche MMM offre une nouvelle voie pour la séparation des gaz évitant les phénomènes de plastification observés à haute pression.

Un des principaux problèmes dans la préparation réussie des MMMs est l'adhésion insuffisante entre la matrice polymère et les particules ajoutées. Ce problème récurrent induit la formation de vides à l'interface particules – matrice polymère, ce qui dégrade les performances des membranes. En plus de la formation de ces espaces vides non-sélectifs, de plus grands taux de MOFs ont pour résultat une agglomération des particules de MOFs avec une distribution inhomogène. De façon à éliminer ces problèmes, une nouvelle méthode de fabrication des MMMs est proposée dans le **Chapitre 5**. Les MMMs sont préparés en partant d'une suspension de particules de ZIF-8 synthétisées in-situ en mélange avec des particules de polymères qui fusionneront par la suite de façon contrôlée pour préparer une matrice dense.

L'interaction polymère-MOF est optimisée grâce à cette stratégie, ce qui permet de réduire voire d'éviter tout problème d'incompatibilité, d'agglomération des particules de MOFs ou encore de distribution inhomogène dans la membrane, en particulier pour de grandes concentrations massiques en MOFs. Les particules de Matrimid® sont dans un premier temps préparées par précipitation d'une solution de polymère dans l'eau (**Figure 7**). La surface de ces particules a ensuite été modifiée pour introduire des groupes imidazole afin de rendre compatible celles-ci avec les MOFs (**Schéma 1**).

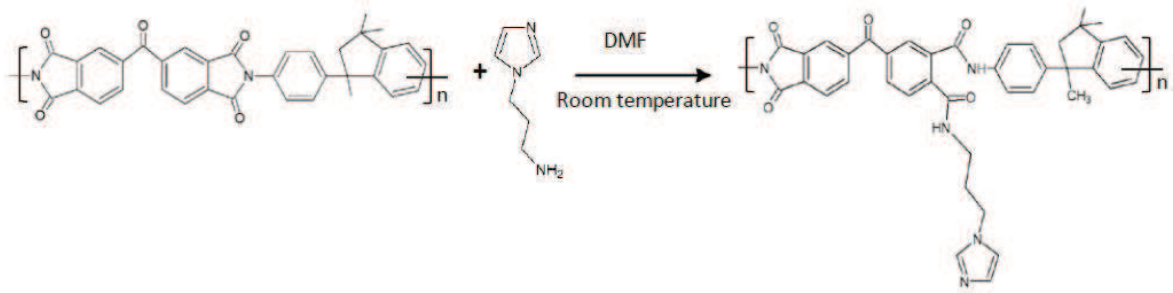


Schéma 1. Greffage du 1-(3-aminopropyl)-imidazole sur le Matrimid®.

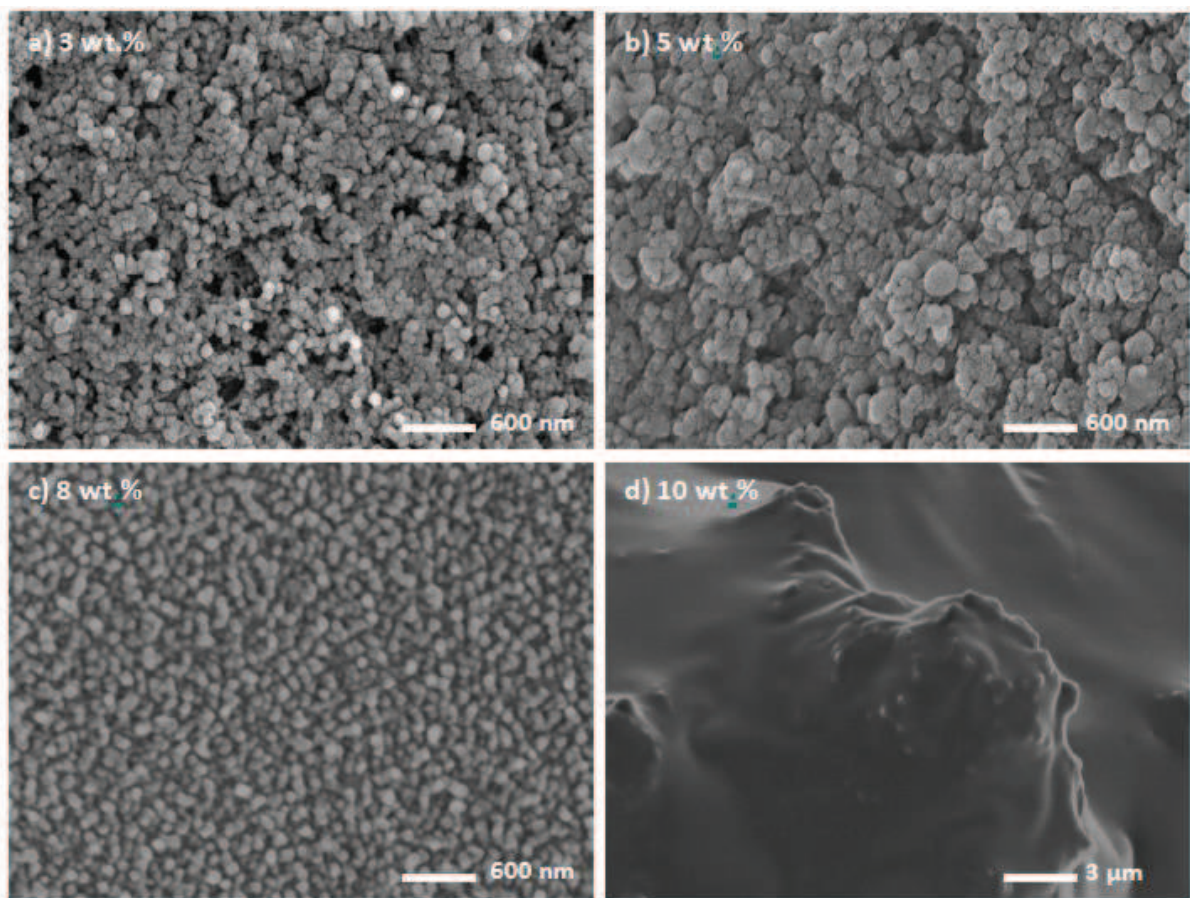


Figure 7. Clichés MEB des particules de polymères préparées à partir de solutions à différentes concentration en Matrimid®. (Magnification: a-c: 50000x and d: 10000x).

Des particules de ZIF-8 ont été synthétisées in-situ au sein de la solution de particules de polymère modifiées par la simple addition du précurseur de synthèse du ZIF-8. La suspension résultante est enfin étalée sur un support jusqu'à évaporation du solvant et recuit par des vapeurs de solvant sélectif du polymère, de sorte à induire la fusion des particules et ainsi produite une MMM de structure dense. Les images de Microscopie Electronique à Balayage (**Figure 8**) montrent une

excellente dispersion des particules de ZIF-8 formant ainsi un réseau percolant sans agglomération des MOFs, même à 40% en concentration massique.

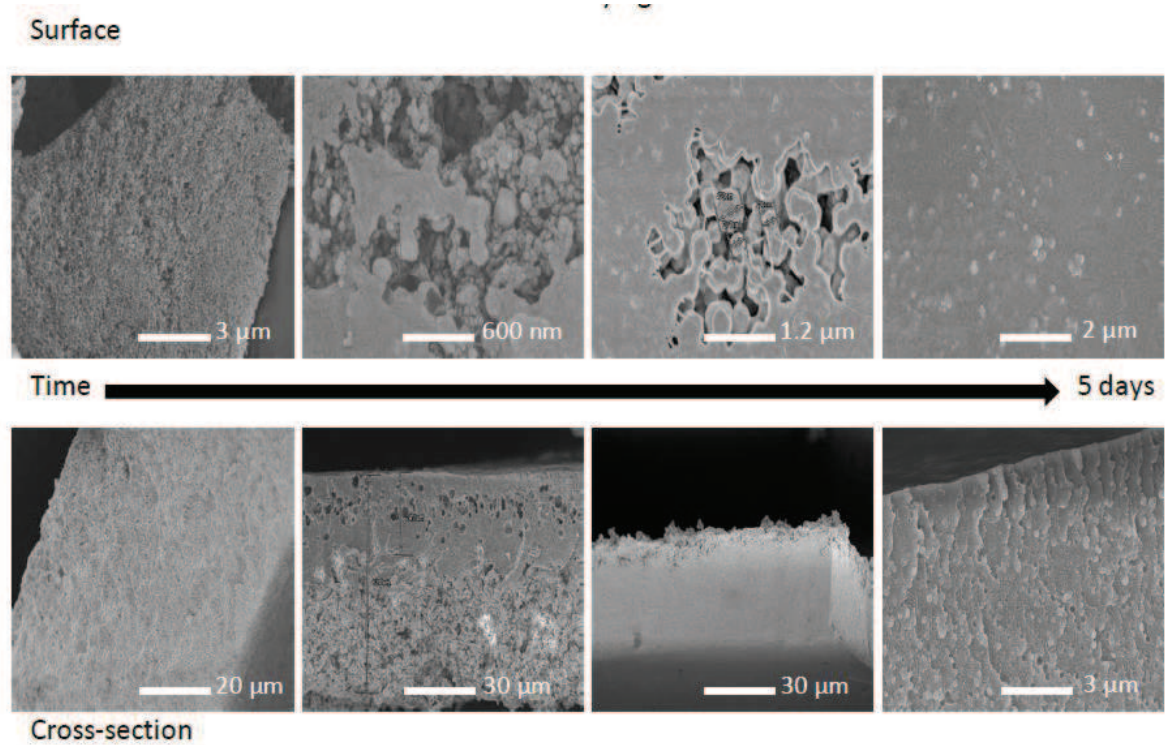


Figure 8. Surface and coupe transversale de la transition entre une forme particulaire des polymères et une forme dense via un recuit aux vapeurs de solvant sur une période de 5 jours.

La bonne dispersion des ZIF-8 et l'excellente adhésion interfaciale entre MOFs et polymère ont eu pour conséquence une amélioration importante à la fois de la perméabilité en CO₂ mais aussi de la sélectivité CO₂/CH₄. La perméabilité en CO₂ a ainsi pu être augmentée de 200% et la sélectivité en CO₂/CH₄ de 65% à comparer au Matrimid® pur (**Figure 9**).

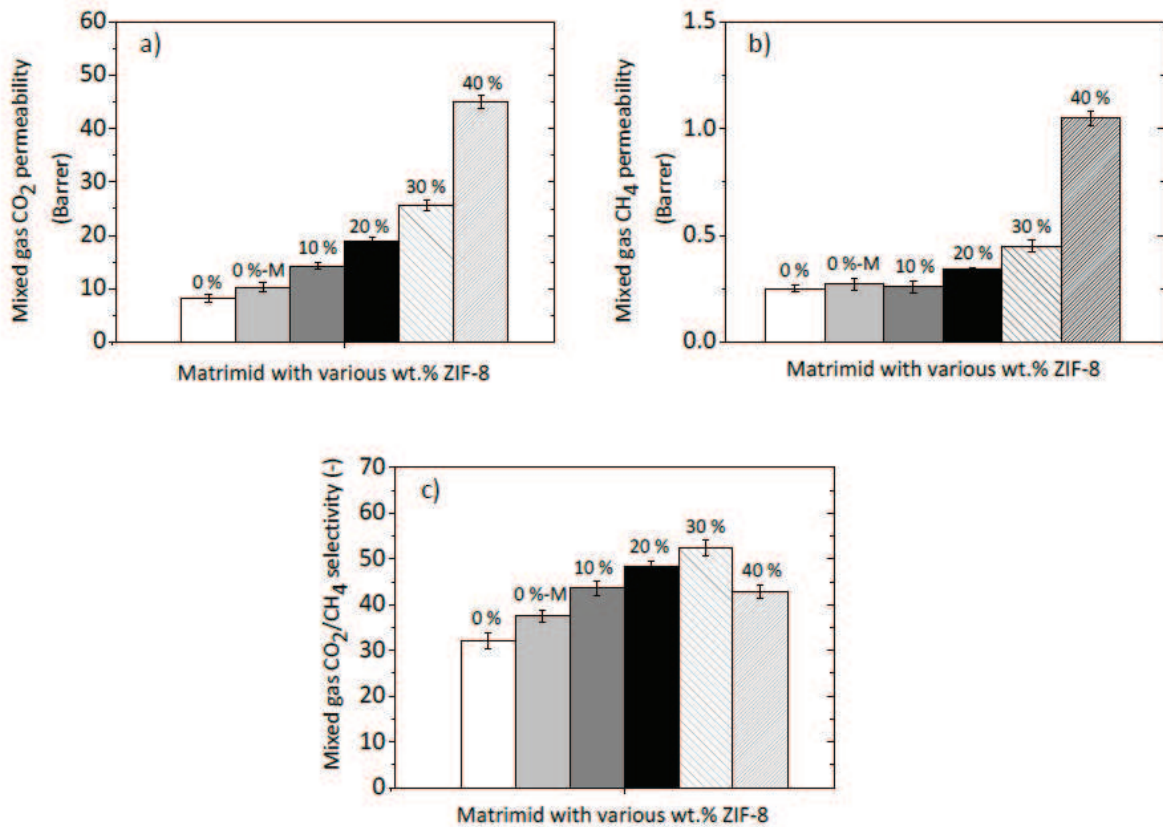


Figure 9. (a) Perméabilité du CO₂ en mélange, (b) perméabilité du CH₄ en mélange et (c) sélectivité CO₂/CH₄ des membranes préparées pour différentes concentrations en ZIF-8 à 5 bars et à 35°C.

Une analyse plus détaillée des performances de transport de gaz des MMMs démontre que la perméabilité en CO₂ et que la sélectivité CO₂/CH₄ sont principalement gouvernées par la diffusivité du CO₂. L'approche présentée pour préparer des MMMs est très versatile et peut être facilement transposée pour d'autres systèmes MOFs – polymères.

Une comparaison des différents systèmes préparés au cours de cette thèse en termes de performance en séparation des gaz est présentée sur le graphique de Robeson (2008) dans la **Figure 10**.

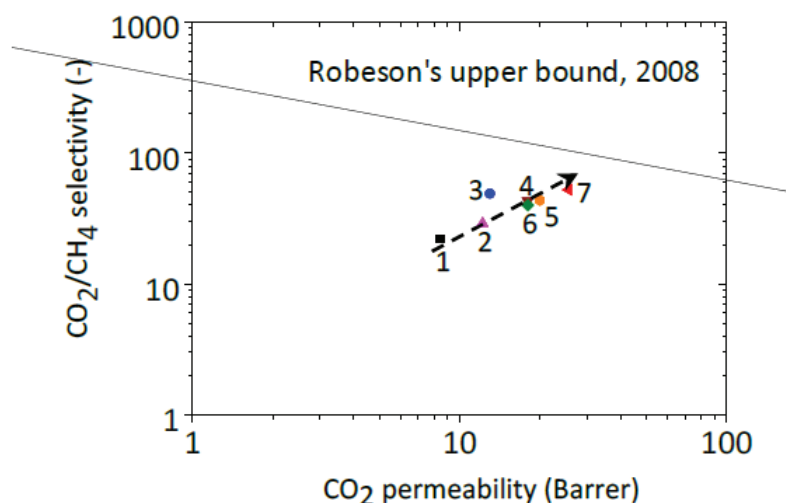


Figure 10. Résumé des résultats obtenus en séparation des gaz des MMMs-MOFs (30% massique) préparés pendant cette thèse et mesurés à 5 bars et 35°C en mélange de gaz. Voir la Table 1 pour les détails sur les différentes membranes présentées.

Table 1. Détails expérimentaux des données présentées dans la Figure 10.

| Code | Membrane | Preparation method |
|------|---------------------------------------|--------------------|
| 1 | PI | Solution casting |
| 2 | PI-Fe(BTC) | Solution casting |
| 3 | PI-Cu ₃ (BTC) ₂ | Solution casting |
| 4 | PI-MIL-53(Al) | Solution casting |
| 5 | PI-ZIF-8 | Solution casting |
| 6 | PI/PSF-ZIF-8 | Solution casting |
| 7 | PI-ZIF-8 | Particle fusion |

*PI Matrimid® 5218

Cette comparaison inclut seulement nos données sur les MMMs-MOFs avec 30% de MOFs à une pression de 5 bar et à 35°C. La **Table 1** présente les détails expérimentaux sur ces membranes. Comme le démontre la Figure 10, une nette amélioration a été obtenue pour les différents systèmes à comparer à la membrane de pur Matrimid®. Indépendamment de la façon de préparer les membranes, l'incorporation de MOFs au sein d'une matrice de Matrimid® permet d'améliorer la perméabilité et la sélectivité du CO₂. Les MMMs basées sur du Fe(BTC) montrent une légère augmentation de la perméabilité et de la sélectivité en comparaison des autres MOFs. Cet effet peut être attribué à une rigidification des chaînes polymères autour des particules de Fe(BTC). En ce qui concerne les autres MOFs, les membranes basées sur le ZIF-8 et le MIL-53(Al) ont présenté une perméabilité améliorée

du CO₂ et une augmentation modérée de la sélectivité, tandis qu'une plus grande sélectivité est obtenue avec Cu₃(BTC)₂. En comparant les méthodes de préparation des membranes, celle préparée par l'approche « fusion des particules » conduit à une amélioration des performances en séparation de gaz par comparaison aux autres voies de synthèse par étalement de solutions. Ceci peut être attribué à une meilleure dispersion des particules de MOFs et à une amélioration de la compatibilité à l'interface MOF-polymère. Cette évaluation globale montre que les MMMs incorporant des MOFs peuvent conduire à de nouvelles opportunités dans la course à l'amélioration de la perméabilité et de la sélectivité. En particulier, une sélection adéquat du réseau métallo-organique, du polymère et de la méthode de fabrication présente un fort potentiel pour dépasser la limite supérieure définie par Robeson.

Thèse EUDIME en cotutelle préparée à l'Université de Twente (Hollande), l'Université de Leuven (Belgique) et à l'Université de Montpellier (France) à l'Institut Européen des Membranes.

Membranes à matrice mixte Polymère- Réseaux métallo-organiques (MOF) pour des applications en séparation des gaz

Mots clés : MOF, polymère, membrane.

Le comportement plastifiant de polymères purs a été bien étudié dans la littérature. Toutefois, il n'y a eu que peu d'études concernant les membranes à matrices mixtes (MMM). Dans ce travail de thèse, le comportement plastifiant de MMM préparés à partir de nanoparticules mésoporeuses Fe(BTC) et du polymère Matrimid® est étudié avec un gaz pur ou en mélange. Les réseaux métaux-organiques (MOF) sous forme particulières ont présenté une relativement bonne compatibilité avec le polymère. L'incorporation de Fe(BTC) dans du Matrimid® a permis d'augmenter la perméabilité et la sélectivité des membranes. Pour de faibles pressions de 5 bars, les MMM ont une perméabilité au CO₂ de 60% plus grande ainsi qu'une sélectivité de 29% plus grande à comparer à la sélectivité idéale de membranes Matrimid®. Le caractère plastifiant des MMMs basées sur trois types de MOFs (MIL-53(Al) (MOF « respirant »), ZIF-8 (MOF « flexible ») and Cu₃(BTC)₂ (MOF « rigide »)) dispersés dans le Matrimid®. Les performances en gaz pur ou en mélange ont été étudiées en fonction de la quantité de MOF introduite. Parmi les trois systèmes MOF-MMM, les membranes avec le Cu₃(BTC)₂ ont présenté la plus haute sélectivité alors que les membranes avec du ZIF-8 ont montré une plus grande perméabilité. Le chapitre 4 décrit la préparation de membranes à base de mélange Matrimid® polyimide (PI)/polysulfone (PSF) contenant des particules de ZIF-8 pour la séparation gazeuse à haute pression. Les MMMs PI/PSF-ZIF-8 ont démontré une amélioration significative de la perméabilité en CO₂ lors de l'augmentation de la concentration en ZIF-8, ce qui a été attribué à une augmentation modérée de la capacité de sorption et à une diffusion plus rapide au travers des particules de ZIF-8. Dans le chapitre 5, une nouvelle voie de préparation des MMMs via la fusion contrôlée de particules a été introduite. La modification du Matrimid® par du 1-(3-aminopropyl)-imidazole a permis d'améliorer considérablement la compatibilité avec les particules de ZIF-8. La perméabilité a augmenté de plus de 200% avec une augmentation de 65% de sélectivité pour le mélange CO₂/CH₄.

Polymer-Metal Organic Frameworks (MOFs) Mixed Matrix Membranes For Gas Separation Applications

Keywords: MOF, polymer, membrane

The plasticization behavior of pure polymers is well studied in literature. However, there are only few studies on the plasticization behavior of mixed matrix membranes. In Chapter 2 of this thesis, pure and mixed gas plasticization behavior of MMMs prepared from mesoporous Fe(BTC) nanoparticles and the polymer Matrimid® is investigated. At low pressures of 5 bar the MMMs showed an increase of 60 % in CO₂ permeability and a corresponding increase of 29 % in ideal selectivity over pure Matrimid® membranes. Chapter 3 subsequently presented the preparation and plasticization behavior of MMMs based on three distinctively different MOFs (MIL-53(Al) (breathing MOF), ZIF-8 (flexible MOF) and Cu₃(BTC)₂ (rigid MOF)) dispersed in Matrimid®. Among the three MOF-MMMs, membranes based on Cu₃(BTC)₂ showed highest selectivity while ZIF-8 based membranes showed highest permeability. Chapter 4 described the preparation of Matrimid® polyimide (PI)/polysulfone (PSF)-blend membranes containing ZIF-8 particles for high pressure gas separation. The PI/PSF-ZIF-8 MMMs showed significant enhancement in CO₂ permeability with increased ZIF-8 loading, which was attributed to a moderate increase in sorption capacity and faster diffusion through the ZIF-8 particles. In pure In Chapter 5, a novel route for the preparation of mixed matrix membranes via a particle fusion approach was introduced. Surface modification of the polymer with 1-(3-aminopropyl)-imidazole led to an excellent ZIF-8-Matrimid® interfacial compatibility. The CO₂ permeability increased up to 200 % combined with a 65 % increase in CO₂/CH₄ selectivity, compared to the native Matrimid®. Chapter 6 finally discussed the conclusions and directions for future research based on the findings presented in this thesis.